LOW TRANSPORT STAGES BY WATER STREAMS OF FINE, COHESIONLESS, GRANULAR AND FLAKEY SEDIMENTS

by

Peter A. Mantz. B.Sc. Hons. (Physics)
M.Sc. (Oceanography)

March 1975

Thesis submitted to the University of London for the Degree of Doctor of Philosophy in the Faculty of Engineering, and to the Imperial College of Science and Technology for the Diploma of Membership

Civil Engineering Department
Imperial College
London S.W.7.

ABSTRACT

Low stages of sediment transport in water streams occur when the applied fluid stress is up to several times in excess of the critical incipient motion stress. The little known details of this transport for fine, cohesionless solids (that is solids whose geometric diameter are less than 150μ say) are reported from an experimental study. The information is used to extend that of coarse sediment research, and is also intended to aid the future study on cohesive sediments.

Closely-graded samples of both fine granular and flakey solids (ranging in median diameter from about 15μ to 80μ) were prepared from a 500Kg. sample of fluvio-glacial sediment. When immersed in direct town-supply softened water, these solids were shown to behave as if cohesionless. Each grade was slowly deposited from suspension in the moving water of a recirculating, straight laboratory flume (10m long by 30cm wide), to give a naturally laid bed. Sediment movement was then observed visually for incrementally increasing applied fluid stresses.

The critical incipient motion stress was measured for each grade, and compared with previous theoretical and experimental studies for coarse sediments. The fine grain results confirmed those from similar experiments made by White, S.J. (1970), and together with the new flake results, they can be used forthwith as an aid towards the engineering design of non-erodible channels which convey natural fine solids of any shape.

For stress increments slightly above the incipient motion stage, the movement of sediment was observed at or near the bed, and contradicted the general supposition that fine solids become suspended at the critical stress. The associated bedform development was shown to differ significantly with solid shape, and also with several aspects of coarse grain bedform development. A new fine granular configuration was observed as isolated primary ripples on an otherwise flat bed; the configuration developed into a secondary ripple system which has been previously reported by Rees (1966). The flake bedforms were primary current lineations only; their development and eventual entry into fluid suspension was studied in the light of recent theories on turbulent boundary layer flow structures.

MEMORANDUM

This thesis entitled "Low transport stages by water streams of fine, cohesionless, granular and flakey sediments" is submitted for the degree of Doctor of Philosophy in the Faculty of Engineering at the University of London.

The thesis is based on independent work carried out by the author, between October 1970 and October 1971 at Southampton University under the supervision of Dr. A.I. Rees, and between October 1971 and October 1973 at Imperial College under the supervision of Professor J.R.D. Francis. The author was sponsored by a Research Studentship Award from the Natural Environment Research Council.

The work described has not previously been submitted for a degree or award at London University or at any other Institution.

Signed P.A. Mantz

March, 1975.

CONTENTS

	PAGE
TABLE OF CONTENTS	(i)
LIST OF PLATES	(vi)
LIST OF FIGURES	(vii)
LIST OF TABLES	(x)
CHAPTER 1. INTRODUCTION	1
1.1. The role of fine sediment transport studies	1
1.2. Major problems associated with fine, cohesionless sediment transport studies	5
1.2.1. Apparatus	5
1.2.2. Estimation of bed shear stress	6
CHAPTER 2. THE PREPARATION OF NEAR UNIFORMLY SIZED FINE SEDIMENT GRADES	9
2.1. Collection of fluvio-glacial fine sediment	9
2.1.1. Location	9
2.1.2. Mineralogy of the bulk sample	10
2.2. Grading of the bulk sample	11
2.2.1. Preliminary grading	11
2.2.2. Aerodynamic grading	11
2.3. Preparation of flake grades	14
2.3.1. Separation of mica component	14
2.3.2. Viscous standard fall diameter	15
2.3.3. Nominal diameter	17
2.4. Cohesion of natural sediments	20
2.4.1. Organic and clay contamination	20
2.4.2. Cohesion by surface forces	21
2.4.3. Constancy of the angle of repose for cohesionless sediments	23

CHAPTER 3. REVIEW OF THE LITERATURE ON THE BEGINNING OF SEDIMENT MOVEMENT 25

3.1. Introduction 25

3.1.1. Historical development 26

3.1.2. Statement of variables for deterministic representations 28

3.2. Velocity representations for turbulent-rough flows 32

3.2.1. Bed-velocity 32

3.2.2. Depth-mean velocity 34

3.2.3. Comparison with the shear stress expression 35

3.3. Definitions for the beginning of sediment movement and the 'transition' region 38

3.3.1. Observational similarity requirements 38

3.3.2. The critical low-transport stress and the nature of a sedimentary bed 40

3.3.3. Low-transport rates over artificial flat beds and the 'transition' region 44

3.4. Turbulent-smooth boundary and viscous flows 48

3.4.1. Previous research 48

3.4.2. The maximum critical detachment stress distribution for idealised coplanar beds 50

3.4.3. The maximum critical detachment stress distribution for natural beds 53

3.5. The probabilistic nature of the beginning of sediment movement 56

3.5.1. Statement of the problem 56

3.5.2. The influence of lift pressure 59

3.5.3. Summary 61

CHAPTER 4. THE LOW-TRANSPORT CRITICAL STRESS FOR NATURALLY-LAID FINE, COHESIONLESS, GRANULAR SEDIMENTARY BEDS 64

4.1. Bed laying procedure 64

4.1.1. Flow conditions 64

4.1.2. Sediment introduction to the flume 67

4.2. Naturally-laid bed properties 70

4.2.1. Bed surface contours 70

4.2.2. The volumetric packing coefficient 72

4.2.3. Angle of repose 74

4.3. Experiments 76

4.3.1. Errors involved in the stress estimate 76

4.3.2. Observation of grain motion 78

4.3.3. Procedure 79

4.4. Interpretation of the results 80

4.4.1. Summary 80

4.4.2. Comparison with previous results 80

CHAPTER 5. THE LOW-TRANSPORT CRITICAL STRESS FOR NATURALLY LAID FINE, COHESIONLESS, FLAKEY SEDIMENTARY BEDS 83

5.1. Previous research on solids of various shapes 83

5.1.1. The orientation influence of bed solids 83

5.1.2. Previous research on coarse solids 85

5.1.3. Summary 87

5.2. Laying a flake bed by natural deposition 90

5.2.1. Flow conditions and sediment concentrations 90

5.2.2. Bed surface contours 91

5.3. Angle of repose 92

5.3.1. Angle of repose for solids of various shapes 92

5.3.2. Measurement for fine flakes 93

5.4. Incipient motion experiments 94

5.4.1. Procedure 94

5.4.2. Observation of flake motion 94

5.4.3. Results 96

5.5. Interpretation of results 97

CHAPTER 6. BEDFORMS ASSOCIATED WITH LOW TRANSPORT STAGES OF FINE, COHESIONLESS, GRANULAR AND FLAKEY SEDIMENTS 99

6.1. Bedforms associated with the movement of coarse granular sediments 99

6.1.1. General description 99

6.1.2. The initiation of bedforms on a flat bed 101

6.1.3. The distinction between ripples and dunes 105

6.2. Bedforms associated with low transport stages of fine, cohesionless granular sediments 109

6.2.1. Previous experiments 109

6.2.2. Limitations of these experiments 112

6.2.3. Observation of bedform development 114

6.2.4. Interpretation 119

6.3. Bedforms associated with low transport stages of fine, cohesionless flakey sediments 122

6.3.1. Flake incipient suspension and bedform experiments 122

6.3.2. Primary current lineations 124

6.3.3. Flake lineation behaviour and viscous sub-layer theory 126

6.3.4. Transverse separation distances between lineations 128

CHAPTER 7. CONCLUSION 132

7.1. The beginning of sediment movement 132

7.2. Bedform development at low transport stages 136

PLATES 137

FIGURES 144

TABLES 188

REFERENCES 202

NOMENCLATURE 211

LIST OF PLATES

1. The four grades of fine, granular sediments

2. The flake faces of the six mica grades

3. The flake edges of the six mica grades

4. Run 1 of the 15 micron grade grain transport experiments

5. Run 2 of the 15 micron grade grain transport experiments

5.5. Transverse primary ripples for the 15 micron grain grade

6. Runs 1 and 2 of the 66 micron grade grain transport experiments

7. Primary current lineations formed during the low stage transport of fine, flakey sediments

LIST OF FIGURES

CHAPTER 1.

1.1. The 10 metre recirculating tilting flume and pumping system

1.2. Flume channel floor contour relative to the horizontal

1.3. Velocity profile development for a high flow Reynolds number

1.4. Velocity profile development for a low flow Reynolds number

1.5. Friction factor curve for a flow depth of 10cm

CHAPTER 2.

2.1. Typical size distribution curves for fluvio-glacial tills and sand-silt rythmites

2.2. A typical fluvio-glacial rythmite sequence (2.5m vertical exposure at Donachton Quarry. Grid Reference number NH 824051)

2.3. The 6 metre recirculating flume used for preliminary grading of the sediment

2.4. Size distribution curves for the preliminary graded sediment

2.5. The Nauta-Hosakawa aerodynamic classifier

2.6. X-ray diffractometer traces for sieved fractions of the medium silt grade

2.7. Standard fall diameter size distribution curves for the mica grades

CHAPTER 3

3.1. Comparison of mean-velocity representations for incipient motion

3.2. Observational similarity conditions for different experiments on incipient motion

3.3. The trend for low transport rates over artificial and natural flat beds

3.4. Low-transport rates plotted on the Shields diagram

3.5. A functional representation for average grain velocities in turbulent rough boundary flows.

3.6. Low transport rate curves for observations over fixed areas

3.7. Force balance for sliding detachment

3.8. Bed surface arrays for different planes of sliding

3.9.1. The rolling condition

3.9.2. The limiting static angle of repose for sliding

3.10. Probability distributions for grain shear resistance

3.11. The maximum angle of rolling for $\alpha_p = 60^\circ$

3.12. Probability distributions for applied shear stress and grain shear resistance

3.13. The Shields curve for geometrically similar flat granular beds at a proposed condition of maximum stability

CHAPTER 4.

4.1. Sedimentary bed surface contours, along the channel centre-line, for the entire channel length (15μ and 66μ granular grades)

4.2. Sedimentary bed surface contours, along the channel centre-line, for the test-section (all 4 granular grades)

4.3. Average water surface gradients for the 30μ granular grade incipient motion experiment

4.4. Average water surface gradients for the 66μ granular grade incipient motion experiment

4.5. Variation of the low transport, normalised, critical stress with depth of flow (30,45 and 66μ granular grades)

4.6. Summary of granular incipient motion empirical data for low Boundary Reynolds number, plotted on a Shields' diagram

4.7. Critical incipient motion stress versus grain diameter for fine, cohesionless silica solids in water at 20°C

4.8. The Shields diagram for flat granular beds of maximum stability, extended to low Boundary Reynolds numbers

CHAPTER 5.

5.1. The Shields diagram for the incipient motion of coarse solids of various shapes

5.2. Sedimentary bed surface contours, along the channel centre line, for the test section (for each of two depositions of the 6 flake grades)

5.3. Average water surface gradients for the 15.5μ flake grade incipient motion experiment

5.4. Average water surface gradients for the 76μ flake grade incipient motion experiment

5.5. Variation of the low transport, normalised, critical stress with depth of flow (for the 6 flake grades)

5.6. Critical incipient motion stress versus fall diameter for grain and flake grades in water at 20°C

5.7. The Shields diagram for flakey solids, using various solid dimensions as a length scale

CHAPTER 6.

6.1. Bed surface contour at the end of Run 2 of the 15μ granular grade bedform experiment

6.2. Incipient motion and suspension critical stress values for the flake grades

6.3. Normalised frequency distributions for the transverse spacings of the flake lineations

LIST OF TABLES

4.1. Bed surface contour measurements, relative to a horizontal datum, for a 30 x 30 cm^2 area (15μ granular grade)

4.2. Incipient motion data for the four grades of fine, cohesionless, granular sediment

4.3. Collected incipient motion data for low boundary Reynolds number grain experiments

5.1. Dimensions and angle of repose measurements for the 6 flake grades

5.2. Incipient motion data for the six flake grades

5.3. Summary of incipient motion data for flakey solids

6.1. Bedform experiments for the 15 micron granular sediment

6.2. Bedform experiments for the 66 micron granular sediment

6.3. Incipient suspension data for fine, cohesionless flakes

6.4. Bedform experiments for fine, cohesionless flakes

6.5. Transverse separation modal distances for flake lineations

6.6. Dimensionless transverse separation modal distances for flake lineations

CHAPTER 1. INTRODUCTION

1.1. The role of fine sediment transport studies

Although the movement of fresh water and sediment from land to sea may occur together, the total transport of each phase differs. In global terms, fresh water transport forms part of a Hydrologic cycle, and evaporation over oceanic surfaces is partially recycled to the land as rainfall. In contrast, sediment transport is non-cyclic; the moving solids are generally changed, both in size and possibly chemistry, on their single route from land to sea. The overall result of sediment transport is therefore a continuous denudation of the Earth's crust, the rate of which has been recently estimated as about 7cm per 1000 years (Holeman 1968). In turn the deep sea floor acts as a sink for fine sediments (which are composed of solids whose geometric size are less than about 150μ say), and deposits of several kilometres thickness have accumulated over recent geological epochs.

The sediment transport route can thus be associated with a solid size decrease. Beginning with large boulders and rocks at mountainous sources, the decrease continues to a limit for individual solids or aggregates of solids (floccules) of geometric size, $D \sim 1\mu$, at the sea bed. (For $D \lesssim 1\mu$, sediments remain suspended in water of normal temperature, by reason of Brownian thermal energy.) An intermediate size can be estimated as that of beach and nearshore sediments; these are typically of medium sand size, $D \sim 200\mu$.

A simple size diminution model needs however further qualification for the case of many rivers. In particular, degradation of solids may sometimes occur at any stage of the rivers progress; the total sediment

load is then transported downstream in two modes, being that of coarse solid rolling or saltation at and near the bed (unsuspended movement) and that of direct transport in fluid suspension. Size determinations for the suspended load indicate that the solids are usually less than about 63μ diameter (Simons 1971), and they may sometimes be designated the 'silt-clay' fraction of the total load. A qualified model for many rivers is therefore that of slow bed-load transport associated with downstream size diminution, together with a faster superimposed water and fine sediment discharge.

The influence of the fine sediment faction of the total load in rivers has recently been reviewed (Schumm 1960). From a data analysis of 36 stable channel reaches, located in the U.S.A. and Australia, it was inferred that the variation in channel dimensions were attributable to changes in the silt-clay fraction of the load; wide and shallow channels were correlated with small silt-clay fractions whilst narrow and deep channels were correlated with large silt-clay fractions. A further analysis also indicated that channels of high silt-clay fraction were subject to higher sinuosity (as defined by the ratio of channel length to valley length) than those of lower fractions (Schumm 1968). Such conclusions therefore begin to establish the importance of fine sediment transport, not only in the seas, but also in many rivers.

Although attention has otherwise been often drawn to the importance of fine sediment transport (since it has, for example, been estimated that on average 90% of the total load enters the sea in fluid suspension), the technical difficulties associated with a systematic study has usually made such work prohibitive. The desired knowledge demanded is not only that for the turbulence characteristics of rivers,

but also that of the mutual interaction between fine solids (which is influenced by the solid surface chemistry and fluid salinity plus pollution condition). The combination of these processes may be such as to give a cohesive sediment for which the subsequent deposition, erosion and transport varies with each local condition that is studied. In contrast, research on the transport of coarse sediments (D >150μ say) has achieved a relative amount of success, owing to the inertness of the solids to the fluid chemical condition. Not only do coarse solids behave as if cohesionless, but their associated weight is such that their motion is usually unsuspended and thus less affected by stream turbulence. Their transport may therefore be directly described by physical laws of mechanics (for example, Bagnold 1966).

In consequence of the above situation, most research has concentrated on coarse solid transport in rivers. Several attempts have however been made towards investigating fine, cohesive sediment movement, but these have been restricted by the particular environmental nature of the solids studied (for example, Partheniades 1965). Because of this restriction, it follows that a new approach to the research must be made using the classical method of limiting the associated variables. Accordingly, Griffiths et al (1960) began laboratory studies on systems of cohesionless, quartz silts (for which D > 10μ), with the particular view to understanding the sedimentary fabric (position and orientation of grains in a sedimentary bed) of fine solids which are deposited in a fluid stream. This work was extended to a first investigation of cohesionless, granular silt bedforms by Rees (1966), and to the estimate of the critical applied fluid stress at a flat bed (a bed whose surface grains are approximately coplanar to within 1 D) for which cohesionless, fine grains begin to move (White, S.J. 1971).

In sequence to the above studies, this thesis reports the further investigation of low stages of cohesionless, fine grain movement from a flat bed laid in a straight laboratory channel, for experimental conditions of a larger scale than those previously employed; the influence of contrasting solid shape on the movement is also investigated for the first time. Although this research is still at an initial, investigatory level, it is hoped that sufficient knowledge will be eventually gained as to extend the study to the movement of more natural cohesive, fine sediments at both low and high flow stages.

1.2. Major problems associated with fine, cohesionless sediment transport studies

Two major practical problems exist towards the study of fine, cohesionless sediment transport. The first is that of preparing large quantities of grades of near uniformly-sized sediment, so that experiments can be conducted with the initial simplest condition of as near equal solids as possible. (The preparation techniques used for this study are described in Chapter 2.) Secondly, there is the major problem of estimating the fluid forces which cause the sediment movement.

Since experiments were to be conducted on flat beds laid in a straight open channel, it was decided to use as near two-dimensional, uniform flow conditions as practicable. The time and spatial average of the fluid forces at a bed could then be expressed as the averaged fluid stress ($\bar{\tau}_o$), and estimated using du Boys (1879) equation

$$\bar{\tau}_o = \rho g \bar{d} \bar{i} \qquad (1.1)$$

where ρ represents the fluid's density, $\bar{d}$ the measured average flow depth and $\bar{i}$ the measured average water surface gradient. ($\bar{\tau}_o$ was thus assumed as equal to the average potential energy decrease per unit area of the flow).

The practical aspects resulting from these two major problems are now considered.

1.2.1. Apparatus

The sediment preparation was both time consuming and expensive, hence only limited amounts of a grade were prepared. It was therefore necessary to use a recirculating laboratory flume apparatus for this

study in order to reduce sediment wastage. An Armfield glass-sided, tilting flume (manufactured at Armfield Engineering Ltd., Ringwood, Hampshire, England) of 20m channel length, 30cm high glass sides and 30cm wide rolled steel channel floor was used in conjunction with a Worthington-Simpson centrifugal pump, which was capable of handling slurries at constant discharge (manufactured at Worthington-Simpson Ltd., Newark, Nottinghamshire, England). Flow regulation was achieved by discharge and feedback valves, and since maximum turbulence was desired in the piping system at all ~~times~~ places (so that no sediment could deposit in the pipeline), the feedback pipeline was designed to be as long as possible (Fig. 1.1.).

The upstream end of the flume (at the main-channel entry) was designed to give as gradual a geometrical transition as possible into the main-channel. The purpose for this was to eliminate the need for conventional, mechanical flow-energy dissipators at the channel entry (such as baffles and 'honey-combs'); such dissipators create disturbances at the flow surface and prohibit the subsequent direct measurement of low water surface gradients. Finally, since a control of fluid chemistry and sediment purity was necessary for the experiments, reinforced P.V.C. pipelines were used throughout, and all painted steel surfaces of the apparatus were frequently maintained.

1.2.2. Estimation of bed shear stress.

The estimate of bed shear stresses involved in fine sediment transport requires the resolution of very low water surface gradients ($\sim$ 1 in 10^5 minimum). To achieve this, it was first necessary to align the channel floor as closely to a single plane as possible, and to check the flume cross-section for rectangularity. (It is shown in Chapters 4 and 5 that fine sediment beds, which are produced by the natural

deposition of solids from the recirculating flow in the channel, follow the channel floor alignment very closely; a flat bed can therefore only be attained with a plane channel floor.) Levelling was made with the aid of a surveyors level and precision block level. The channel floor was accordingly adjusted to be within about $\pm$ 0.2mm of the same plane, with the exception of a 2m. length of floor which had a permanent 'rise' of about 0.5mm (Fig.1.2.). A closer levelling precision than $\pm$ 0.2mm was unwarranted, since both loading and tilting the flume were found to give floor alignment displacements of the same magnitude of a few hundred microns. (A similar maximum precision in levelling was obtained by Tracy and Lester, 1961, for a 24m long flume.) As the solid sizes to be used for the study were less than the levelling accuracy, a flat bed could not be attained for the entire channel length; it was therefore necessary to assume that the time and spatially averaged measurement for the water surface gradient over a test length of the channel represented that for uniform flow over a flat bed.

The measurement of low water surface gradients ($\bar{i}$) was made using 4 precision micrometer screw gauges, each with a least reading of 0.05mm, positioned on the channel centre-line at 4.0, 5.5, 7.0 and 8.5m downstream respectively. Ten consecutive measurements of the moving water surface were made at each of the 4 positions, and the mean of these 10 measurements were used, with stationary water surface measurements at these positions, to calculate $\bar{i}$. With careful dampening of pump vibration, a minimum $\bar{i}$ of 1 in 10^5 could be statistically resolved to within about 20% standard deviation.

The choice of the 4 to 8.5m test length for slope measurement was made with the aid of average velocity profile measurements along the channel. Figs. 1.3 and 1.4 show the transverse flow development (as

measured using a 1cm diameter propeller current meter) along the channel for 2 conditions of high and low channel Reynolds number, $\bar{R}e_m$. ($\bar{R}e_m = \bar{u}_a m/\nu$, where $\bar{u}_a$ represents the transverse sectional average of the longitudinal flow velocity, m the hydraulic radius of the flow and ν the fluid kinematic viscosity.) The profiles were taken for a flow depth of 10cm, with no sediment in the channel. The average, centre-line, vertical velocity profiles (shown as the dotted lines in the figures) appeared to be fairly constant within the test section, and the flow was accordingly assumed to be fully developed. (The velocity defects in the transverse profiles indicated the existence of secondary currents, which could be observed visually by means of dye injection.)

Water surface gradient measurements for a quasi-uniform flow depth of 10cm. (with no sediment in the channel) were compared against those of other workers, by estimating the Darcey-Weisbach friction factor ($f = 8gmi/\bar{u}_a^2$) for various magnitudes of $\bar{R}e_m$ (Fig. 1.5.). A close correspondence was obtained, and the curve in turn was represented by the form of the Blasius equation given by Chow, 1959 ($f = 0.223/\bar{R}e_m^{0.25}$).

It is finally noted that the bed shear stress estimate given by eq. (1.1.) was assumed for two-dimensional flow only. Since a practical range of flow width to depth ratio of 3 to 15 was used for the experiments, it was inevitable that the flow was not always two-dimensional over the major part of the channel transverse section. It followed that a variation in bed-shear stress occurred across the transverse section, for which the maximum (given by eq.(1.1.)) was then assumed for the channel centre-line. Although the assumption was not quantitatively verified, previous experiments, for flows of higher Reynolds number than those used herein, show it to be approximately correct (for example, Chow 1959, Ghosh and Roy 1970).

CHAPTER 2. THE PREPARATION OF NEAR UNIFORMLY-SIZED FINE SEDIMENT GRADES

2.1. Collection of fluvio-glacial fine sediment

2.1.1. Location

Fine sediments are found subaerially in the form of glacial till, glacial stratified drift and loess. It is well known that large areas of fluvio-glacial sediment occur in the Spey Valley in Scotland, and Hamilton (1963) located suitable deposits near to Kingussie, Invernesshire. A field trip was therefore made to this site, in order to collect bulk samples.

The Mid-Strathspey area around Kingussie is particularly suited to accumulations of alluvial material. The gradient of this part of the river course is abnormally low, (Johnston 1966) and the area between Kingussie and Loch Inch (about 5 miles NNE) is in fact a recent alluvial plain with an average breadth of 3/4 mile. The sediment filling this basin is an ablation till deposited from the melt waters of retreating valley glaciers. Typical size distribution curves for this till are shown in Fig. 2.1. (The pipette sedimentation method used for determining the distributions is described in section 2.3.2.; each grade is described by its median diameter (D_{50}) and the Trask geometric quartile sorting coefficient, $S_o = (D_{75}/D_{25})^{1/2}$).

The Kingussie alluvial plain is also flanked by well marked, high level terraces, varying from several hundred yards to more than a mile in breadth. (It has been proposed that these terraces were laid down by marginal glacier lakes. (Hinxman 1915)).

Exposures along the terraces show the sediment to be a glacial stratified drift and a typical stratified rythmite sequence is shown in

Fig. 2.2. The sediment used for these experiments was sampled from the fine sand and silt rythmite layers. About 500 Kg. were collected, and typical size distribution curves are also shown in Fig. 1.

2.1.2. Mineralogy

The glaciated highlands around Kingussie are mainly composed of low grade metamorphic rocks, rich in quartz, muscovite and biotite micas. The rocks belong to the Moine series, and are of three groups: undifferentiated schists and gneisses, siliceous schists and granulites, pelitic gneisses and schists. The area is also noted for a number of large acid igneous intrusions, essentially of a granitic nature, and rich in quartz, feldspars and micas. The mineralogy of the sediments sampled therefore resembled that of its nearby provenance.

Examination of the collected sediment by petrographic microscope showed it to consist mainly of quartz and feldspar grains, together with secondary amounts of muscovite and biotite mica flakes. Further analysis using the powder method of X-ray Diffractometry (Klug and Alexander 1954) showed a small amount of chlorite. A final trace component of heavy minerals such as magnetite was also detected using the technique of heavy liquid separation (Carver 1971).

The sediment therefore consisted of three main components: quartz and feldspar grains, mica flakes, chlorite and possibly illite clay minerals. It was first necessary to remove the clay minerals from the bulk sample, by washing and preliminary grading.

2.2. Grading of the bulk sample

2.2.1. Preliminary grading

The preliminary grading of the bulk sample was made in a small 6m x 30cm recirculating, fixed-channel flume (Fig.2.3.). 5Kg. aliquots of sediment were added slowly during 30 minute periods to the end of the flume channel. The sediment was first disaggregated in the highly turbulent flow within the pumping system, then the fine fraction was elutriated to settle in the main channel, whilst the coarse fraction sedimented in the end column. (The flow condition found most suitable for this separation was $\bar{u}_a$ = 5cm/s with $\bar{d}$ = 15cm). After 10 such additions, the very fine sediment in suspension (which was mainly the clay fraction) was drained from the flume, and the fine fraction deposited at the channel floor was removed for drying (prior to aerodynamic sorting). This process was repeated until the entire 500 Kg. had been preliminarily graded into about 360 Kg. of fine and 140 Kg. of coarse sediment.

Fig. 2.4. shows the size distribution curves for sediment sampled at different positions along the flume, after each preliminary grading. It was seen that the median fall diameter of the coarse fraction was 180μ, and that few grains of less than 10μ were contained in the fine fraction downstream. X-ray diffractometric studies of the fine fraction indicated that the chlorite component had been considerably reduced in quantity.

2.2.2. Aerodynamic grading

It was decided to separate the fine fraction into 5 well-sorted grades of fine, medium and coarse silt, very fine and fine sand. The use of an aerodynamic Micron classifier was investigated and found successful for this purpose. A type MS-1 'Nauta-Hosakawa' classifier (Fig. 2.5.) was kindly made available for use by the Department of Chemical Engineering, Loughborough University.

The operating principle of an air classifier is as follows(Fig.2.5.) A spherical particle of diameter D and density ρ_s circulating with the rotor is subject to opposing forces. A centrifugal force(F_1) acts radially outwards, and is given by

$$F_1 = \frac{\pi}{6} D^3 (\rho_s - \rho_a) \frac{u_\theta^2}{r} \qquad (2.1.)$$

where ρ_a represents the density of air,and u_θ the tangential component of the velocity of the particle.

A centripetal force (R), caused by the air drag force on the particle, acts radially inwards. For small particles, this force can be assumed to obey Stokes Law, and is given by

$$R = 3\pi \mu_a D u_r \qquad (2.2.)$$

where μ_a represents the dynamic viscosity of air, and u_r the radial component of velocity of the particle.

The diameter of a particle (D_c) for which these forces are balanced is

$$D_c = \frac{1}{u_\theta} \left(\frac{18 u_r \mu_a r}{\rho_s - \rho_a}\right)^{1/2} \qquad (2.3.)$$

Particles for which $D < D_c$ are thus entrained towards the centre of the rotor and collected through the outlet duct, whilst oversize particles ($D > D_c$) are rejected from the rotor. The rotor speed in this particular classifier could be adjusted to separate the sediment at any diameter between about 2μ and 125μ.

(It is noted that the air classification technique is very similar to the sedimentation and decantation method of separating small particles in still water, since both methods utilise a balance between fluid drag and solid inertial forces. The former method is however better suited to separating bulk quantities, since the classification is continuous in time. The theoretical separation diameter in both cases is however approximate, due mainly to the effect of 'hindered settling' with increased concentrations of sediment, and the non-spherical nature of the solids.)

The rotor speeds used for these separations were 2,000, 1,000 500 and 250 r.p.m. and the feed supply to the classifier was about 30 Kg. per hour. 5 grades of near uniformly-sized sediment were subsequently obtained, whose statistics were as follows:

$D_{50(\mu)}$	16.5	26	46	82	110
S_o	1.22	1.34	1.27	1.30	1.40
Total weight of grade (Kg)	30	60	60	60	150

2.3. Preparation of flake grades

2.3.1. Separation of the Mica component

The sediment originally consisted of 3 components, namely quartz and feldspar grains, mica flakes and clay minerals. A large amount of the clay minerals were removed during preliminary grading. It was decided to further separate the remaining components of granular and flakey solids, so that experiments could be conducted with grades of each contrasting shape.

Since the 5 grades had been prepared dynamically using the principal of Stokes Law, it was expected that each grade would contain a size distribution of grains whose mean geometric diameter was smaller than the mica face mean geometric diameters. Major fractions of flakes could, on this assumption, be separated from grains by sieving a mineralogically mixed grade at a mesh size near to the grains maximum geometric diameter.

Rectangular sieves, each consisting of a 15 x 30 cm wooden frame and nylon mesh, were used to wet sieve by hand each grade of sediment. A trial separation was first made on the medium silt grade (D_{50}=26μ). Fig. 2.6. shows the X-Ray diffractometric trace of the sieved fractions, and indicates semi-quantitatively the mineral amounts for this separation. It was seen that the > 35μ fraction consisted predominantly of mica flakes, as desired.

The 5 grades were sieved in the same manner, using mesh apertures of 20, 35, 61, 118 and 170μ for the finest to coarsest grade, respectively. Each mica separate was then additionally sieved as necessary at 35, 61, 90, 118, 170 and 250μ, in order to obtain a total of 6 uniformly sized flake grades (Plate 2). Optical slides were made of a sample from each

mica grade, by sedimenting a dispersion of the sample in water onto a slide. The maximum (Fa) and minimum (Fi) face diameters of 200 flakes, selected randomly from each grade, were measured using an optical microscope. Cumulative curves of the number frequency of the flake face diameters $D_G = (FaFi)^{1/2}$ then gave the following values:

Nylon mesh aperture(μ)	20-35	35-61	61-90	90-118	118-170	170-250
D_{G50} (μ)	33	54	70	101	148	205
S_o	1.21	1.15	1.14	1.16	1.14	1.15

It was seen that the optically measured face diameters corresponded closely to the sieve apertures used.

2.3.2. Viscous standard fall diameter

A useful parameter describing the size and behaviour of a sedimenting solid is the 'standard fall diameter' (D_F). This is defined as the diameter of a sphere that has an S.G. of 2.65 and the same terminal fall velocity as the solid in still water of infinite extent at 24°C. (Subcommittee on Sedimentation 1957). The fall diameter for silt sized solids is usually estimated using the pipette-sedimentation method (B.S. 1377. 1967). The technique involves the sedimentation of dilute suspensions of solids and it is assumed that each solid does not influence the movement of any other.. Using water as the liquid medium the method is useful for measuring D_F to a maximum of about 30μ. Larger sized solids have a fall velocity in water which is too great for accurate sampling by this method. The standard fall diameter for larger grains is then found by timing the fall of a single solid in water, or by using large visual accumulation tubes (which are commercially available) to find the size distribution for a sample.

below about 50μ will be unaltered. (Since this correction only applies for perfect spheres, it was necessary to assume that similar differences apply for non-spherical and flakey fine solids, and thus $D_V \simeq D_F$).

The standard fall diameter distributions for the 6 mica grades used for the experiments are given in Fig.2.7. A close correspondence was noted for each grade when liquids of different viscosity were used as the sedimentation fluid.

2.3.3. Nominal diameter

Another parameter which describes the size of a solid is its nominal diameter (D_N). This is defined as the diameter of a sphere that has the same volume as the particle (Subcommittee on Sedimentation 1957). For sand sized and coarser solids, a mean nominal diameter is usually determined from the total weight and density of a group of several hundred counted particles of one sieve fraction. The method is however impractical for fine flakes, and the nominal diameter must be approximated by using the triaxial dimensions of a flake.

Observations of flake faces (Plate 2) and their edges (Plate 3) indicate that it is fairly reasonable to approximate a flake to the shape of a rectangular solid of constant thickness. The volume (V) of the solid is then given by the product of the maximum and minimum face diameters, and its thickness (T), thus

$$V = D_G^2 T$$

$$\text{and} \quad D_N = \left(\frac{6}{\pi} D_G^2 T\right)^{1/3} \qquad (2.5)$$

To measure the thickness of mica flakes, aliquots of each grade were sedimented in resin, to produce a lithified, naturally packed sedimentary bed. Thin sections of each bed (Carver 1971) were then cut in the plane of sedimentation. Microscope examination using oil immersion showed that many exposed edges of flakes were aligned in this plane (Plate 3). It was therefore possible to measure directly the thickness distribution of the flakes for each grade.

(The resin sedimentation techniques involved the use of 1gm aliquots of flakes which were first dispersed, using a magnetic follower, in a 2 x 2 x 6 cm trough containing the resin. Araldite MY 778 and Hardener HY 951 were used, together with 10% by weight of Acetone. The latter was used to lower the resin viscosity and prolong the setting, thus enabling the finest grades to sediment to natural packing.)

The following statistics were obtained from cumulative curves of the number frequency of a 200 flake thickness measurement sample from each grade;

T_{50}(in microns)	1.85	2.5	3.1	4.0	6.2	9.2
S_o	1.35	1.28	1.20	1.20	1.24	1.22

It was seen that S_o was of a similar magnitude to that for the near uniform sizing of the face diameters. The nominal diameters and aspect ratio (D_G/T) for each grade were calculated as:

D_{N50}(in microns)	15.5	24	31	43	64	90
$D_{G/T}$	17.8	21.6	22.6	24.9	23.9	22.2

The estimates thus indicated that a natural mica flake of about 20:1 aspect ratio was mechanically stable.

Six near uniformily-sized grades of mica flakes and five grades of quartz and feldspar grains were thus prepared for these experiments. The subsequent natural deposition of these solids in the laboratory flume involved a variation in grade statistics along the channel, and the new statistics are given in Chapters 4 and 5.

2.4. Cohesion of natural sediments

A natural sediment may be cohesive for 2 reasons; contaminating adhesive particles or organic mucilage may cause the individual solids to combine, or the surface forces of the solids themselves may be mutually attractive. In order to reduce cohesion to a minimum, the following procedures were adopted for the purpose of these experiments.

2.4.1. Organic and clay contamination

A particular reason for using fluvio-glacial sediment for this research was that a minimal amount of organic material would be present; this was due to the cold climate during conditions of original deposition. An estimate for the amount of carbon contained in the fine granular silt grade was made using a chemical analysis adopted from Marshall and Orr (1964). The grade was found to contain less than 0.1% by weight of carbon, and hence a correspondingly insignificant quantity of organic material.

During initial flume experiments, it was found that an added source of organic contamination was a mucilage produced by bacteria and protozoa. (These animals synthesise from the continuous supply of organic debris contained in a city atmosphere.) After several days of eroding fine sediment beds in the laboratory flume, individual solids became enveloped in the mucilage, and flocculated. This problem was reduced by using direct supply town water, filtering and chlorinating the water daily, and covering the flume with a black dust cover throughout long-term experiments.

It was conceivable that colloidal clay solids contained in the sediment may adhere to 2 larger solids, thus causing cohesion. An

initial removal of the clay grade from the sediment was made during the preliminary separation. The ultimate removal of this grade depended however on the successful dispersion of smaller and larger solids.

The standard method for dispersing colloidal clay particles in an aqueous solution involves the addition of a small quantity (about 0.01% weight of sediment) of peptising agent such as sodium hexametaphosphate(B.S. 1377, 1967). Repeated sedimentation and decantation of the grades were therefore made using the peptizer. The clay grade was removed until the decanted solution became clear. As a final test for removal, a sedimentary bed was laid in the flume, and the superimposed water was seen to remain clear.

2.4.2. Cohesion by surface forces

The nature and magnitude of inter-particulate surface forces is a subject of research in the field of Colloid Chemistry. Direct measurement of such forces between small particles are impracticable, but measurements on idealised, macroscopic bodies have yielded much information. In particular, the nature of 3 types of surface forces, existing between mineral dispersions in water, have been recognised. (Kitchener 1969),

They are a mutually attractive London-Van der Waals force, a force between electrical double layers which form at each solid surface, and a steric repulsive force due to the solution of water at the mineral surface. (Little is known about the latter force, and its effect is usually neglected in theoretical considerations.)

The electrical double layer force arises from the fact that most minerals acquire a surface electric charge when immersed in an electrolyte. For the case of dispersions of solids which have the same charge

(such as silica grains in water of normal pH), the force is usually of a repelling nature; it may be of such a magnitude as to overcome the cohesive London-Van der Waals force, and therefore influence the solids to behave as if cohesionless. The repelling interaction energy (V_R) associated with the repelling electrical double layer force has been estimated, for the case of equal spherical solids (of diameter D) separated by a distance (x), by Verwey and Overbeek (1948) as

$$V_R = \frac{eD\phi_o^2}{4} \ln(1 + e^{-Kx}) \qquad (2.6)$$

where e represents the dielectric constant of the fluid medium, ϕ_o the mineral surface potential, and 1/K the 'double-layer thickness' (Shaw 1970) and is given by

$$K = 0.328 \times 10^{10} \left(\frac{cz^2}{\text{mol.dm}^{-3}}\right) m^{-1} \qquad (2.7)$$

It is seen that V_R (and consequently the surface interacting behaviour of the solids) is directly affected by the concentration (c) and charge number (z) of the salts in an electrolyte.

In order to test if these fine, natural grades of sediment were influenced by electrolyte nature, aliquots of the finest (16.5μ) aerodynamic grade (from which the mica component had been removed) were sedimented in direct town-supply hard ($z \simeq 2$) and softened water ($z \simeq 1$). It was considered that a cohesive sediment could be inferred from the measurement of the packing coefficient (defined as the ratio of solids volume to the total volume occupied) of a naturally sedimented bed. When cohesion existed, it was expected that the flocculated solids

would give a lower C than cohesionless solids. The following measurements were recorded.

	SOFT WATER	HARD WATER
Packing coefficient (C)	0.50±0.02	0.41±0.02

The result showed that the inter-solid behaviour was significantly influenced by the electrolyte nature, and that it could be explained in terms of the differing z values and consequent difference in V_R distribution. Since the soft water C value approached that which has been measured for the deposition of coarse granular solids in still water (Kolbuszewski, 1950, obtained C = 0.54), it was concluded that these natural granular sediment grades tended towards a cohesionless behaviour when immersed in direct town-supply softened water. The latter fluid condition was therefore used throughout these following flume experiments.

2.4.3. Constancy of the angle of repose for cohesionless sediments

The cohesive or cohesionless nature of fine sediments can also be investigated by measuring the 'angle of repose' (α) of a mass of the solids. This is usually defined as the maximum angle made with the horizontal by the free surface of a pile formed from the solids. It is to be expected that cohesive solids will exhibit a larger α than cohesionless solids; correspondingly, if the α values for grades of fine sediment are constant and equal to that of similarly shaped coarse sediments, then the grades are cohesionless.

Previous research on α estimates have established that the property varies considerably with the method used for determination. Richards (1966) accordingly classified the property as a 'poured α '

and drained α ', depending on the procedure used for forming the solid pile. Variability still exists however within these classifications. For example, Van Burkalow (1945) considered the poured α to vary with the height and direction of fall of the solids. Furthermore, Richards classified 4 different methods for estimating the drained α , and a summary of collected results gave differing values of a few degrees for each method. (The methods were those of draining grains from a horizontal platform, a circular platform, a long flat ledge and through a circular orifice.)

It appears that if α is to be used as a means for investigating the surface behaviour of solid grades, the same experiment for its determination must be used throughout. Accordingly, White, S.J. (1970) measured the drained α from a flat ledge for 12 grades of fine granular sediment immersed in distilled water (the sediment grains being of a similar mineralogy to those used for these experiments); the grade sizes ranged from 23μ to 170μ. α was then found to be approximately constant at 39° with a maximum scatter of $\pm 4^{\circ}$. It was thus concluded that the fine granular sediments in distilled water were cohesionless.

Since it was shown in the previous section 2.4.2. that the inter-solid behaviour of fine sediments is significantly influenced by the nature of the watery electrolyte, α determinations for these grades of granular and flakey solids were made for the actual flume experimental water condition (direct town-supply softened water). The results are given in Chapters 4 and 5. It is noted that this precaution was not observed by White, S.J., since he showed α to be constant for a different water condition than that actually used during his experiments.It was therefore necessary to repeat several of his experiments for the determination of the critical incipient motion stress for fine, cohesionless granular sediments.

CHAPTER 3. REVIEW OF THE LITERATURE ON THE BEGINNING OF SEDIMENT MOVEMENT

3.1. Introduction

The beginning of sediment movement (or 'incipient motion') from flat granular beds was the first low transport stage problem to be tackled. Despite the apparent simplicity of the description for this initial stage, an unusually large amount of literature (mainly concerned with coarse grains of $D > 150\mu$ say) appears on the subject. This chapter attempts to review and criticise some of the literature on both fine and coarse grains, and in doing so, draws attention to the physical complexity of the problem.

The review begins with a comparison of the traditional deterministic methods employed towards describing coarse grain incipient motion for the case of two-dimensional, turbulent-rough boundary flows (section 3.2.). It is shown that these methods lead to a large range of scatter when empirical results are plotted on a Shields (1936) diagram. One of the reasons for this scatter is the lack of a quantitative definition for the condition, and accordingly, new definitions are proposed in section 3.3. In the light of these, it is then shown that a fall in the Shields diagram, as the turbulent-rough boundary flow becomes transitional, is inevitable if observational similarity criteria are not applied during an experiment.

The theoretically predicted rise in the Shields diagram for the change from turbulent transitional to smooth boundary flows, (which rise is associated in water experiments with a size change from coarse to fine solids) is compared with empirical data from previous fine sediment experiments in section 3.4.; further empirical scatter is shown to exist. The problem of estimating a maximum limiting dimen-

sionless stress (below which any sediment size will begin to move) is also attempted in this section, and this leads to an estimate for the resistance distribution of fine naturally laid sedimentary beds.

Section 3.5. deals with the fact that incipient motion is a problem concerned with both fluid and sediment variable distributions; it is therefore better represented in terms of estimates for these distributions. It is concluded from this that the trend of the Shields curve is better explained by considering it as a fall in dimensionless stress from viscous and turbulent-smooth boundary flows to turbulent-rough flows, rather than the reviewed conventional explanations based on the reciprocal trend.

3.1.1. Historical development

The following literature has been mainly referenced from 4 recent reviews on incipient motion (I.M.), namely the A.S.C.E. Task Force review (1966), Raudkivi(1967), Graf (1971) and Yalin (1972). These reviews have generally been divided into 2 sections, depending on the flow parameter used as a dependent variable to represent the condition. The first parameter used was that of a flow velocity, and the second was bed shear stress. The question has often been raised as to which is the more'fundamental' variable. Such a problem is however needless, since a correct physical model involving either variable will give the same answer.

Repeated references to various authors and experiments indicate the major advances of the problem over the past two centuries. However, considerable doubt surrounds the proposer of the first published expression, which describes I.M. in terms of the average velocity near to a sediment

bed ($\bar{u}_b$). It was attributed to Brahms (1753) by Forcheimer (1914) and to Leslie (1829) by Rubey (1948).

Towards the end of the last century, the shear stress concept was first used. Kreuter (1898) was attributed by Schoklitsch (1914) to be the first person to apply du Boys equation (1879) in the field. In accord with this new approach, Schoklitsch's own laboratory work (1914) was also represented in shear stress terms; he also drew attention to the possible influence of lift forces in turbulent flow. Furthering the lift force idea, Jeffreys (1929) theorised that such forces could exist in viscous flow at a boundary. However, it was not until 20 years later that lift force measurements of any nature were attempted (Einstein and El Samni, 1949).

Despite the advent of the shear stress concept, many workers preferred to use velocity representations. A typical example was that of Hjulstrom (1935), who proposed a chart for the average transverse flow velocities in a water stream which are necessary to start moving solids ranging in size from 10cm gravels to 10μ clays. In 1936, the classic Shields' 'dimensionless shear stress' representation was derived using the Nikuradse(1933) law of flow in sand roughened pipes. A similar representation to that of Shields was also developed analytically by White, C.M. (1940).

Although it was fully recognised by Shields and others that the I.M. problem was one concerned with statistically distributed variables and therefore governable by laws of probability, Einstein (1942) appears to be the first person to develop sediment transport relations based on this concept. The problem could however be approached deterministically provided an idealised model was chosen to reduce the variable distributions. For example, Bagnold (1956) introduced the concept of

a maximum dimensionless shear stress, which was applicable to solid movement by a steady viscous flow over a flat granular bed.

With the development during the past ten years of the hydrogen bubble tracer technique, hot-film anemometry and the Laser-Doppler technique for measuring fluid turbulence characteristics, the probabilistic approach has benefited from a better understanding of flow statistics. The study is however incomplete and little attention has been given to the equally important statistics of the sediment variables. It is the purpose of this chapter to review the I.M. literature, and to finally consider the results in the light of both fluid and sediment variable distributions.

3.1.2. Statement of variables for deterministic representations

Deterministic representations for I.M. rely, for prediction, on the temporal and spatial average (denoted throughout this text by an overbar) of the variables involved. From the various models proposed a dimensional analysis proceedure, similar to that of Yalin (1963) is used below.

The beginning of movement from geometrically similar flat granular beds (i.e. coplanar to within 1D) by a 2-dimensional, quasi-uniform open-channel fluid flow can be considered as a 2-phase problem. The separate phases are the fluid, described by its density (ϱ) and kinematic viscosity (ν), and the solids, described by their density (ϱ_s) and median geometric diameter(D). The fluid motion is described by the quasi-uniform depth ($\bar{d}$), averaged slope ($\bar{i}$), whilst both fluid and solids are subject to body forces caused by the gravitational acceleration (g). Any dependent variable of the 2-phase system may therefore be described by the 7 independent variables

$$\rho, \nu, \rho_s, D, \bar{d}, \bar{i}, g$$

For example, the flat-bed sediment transport rate (submerged weight of solids transported per unit bed-width per unit time, $\bar{Q}_{so}$) which occurs after the beginning of sediment movement, can be expressed as

$$\bar{Q}_{so} = \bar{Q}_{so}(\rho, \nu, \rho_s, D, \bar{\tau}_o, \bar{d}, g) \qquad (3.1)$$

where $\bar{\tau}_o$ has been substituted for $\bar{i}$ by assuming the du Boys (1879) relation, $\bar{\tau}_o = \rho g \bar{d} \bar{i}$. According to the Buckingham-Pi theorem, equation (3.1) may be reduced to 5 dimensionless variables, chosen for their physical utility as

$$\frac{\bar{Q}_{so}}{\rho' g D (\bar{\tau}_o/\rho)^{1/2}} = \bar{G}_o\left(\frac{\bar{\tau}_o}{\rho' g D}, \frac{(\bar{\tau}_o/\rho)^{1/2} D}{\nu}, \frac{\rho_s g}{\rho g}, \frac{\bar{d}}{D}\right) \qquad (3.2)$$

where $\rho' = \rho_s - \rho$, and $\bar{G}_o$ represents a dimensionless low-transport rate term. The dimensionless terms have the following physical meanings.

If the number of moving grains in an area A ($>>D^2$) is represented by P, and the averaged velocity for each grain is $\bar{U}$, then

$$\bar{Q}_{so} = \frac{P}{A} \times \rho' g \gamma D^3 \bar{U} \quad \text{gm./cm.sec.}$$

where γ represents a volumetric shape factor for each grain ($= \pi/6$ for a sphere). If the packing coefficient of a grain layer (ratio of integral solids volume to the total volume of the layer, C_s) is considered with the denominator of $\bar{G}_o$, then $\rho' g D C_s (\bar{\tau}_o/\rho)^{1/2}$ represents

the transport of a surface grain layer (depth D) at a scale velocity $(\bar{\tau}_o/\rho)^{1/2}$. $\bar{G}_o$ is then modified to

$$\bar{G}_o = \frac{P/A \times \rho' g \gamma D^3 \bar{U}}{\rho' g D C_s (\bar{\tau}_o/\rho)^{1/2}}$$

and the modified term represents a transport rate which is measured in proportional units of total surface grain-layer transport.

The first term on the R.H.S. of equation (3.2.) is a dimensionless shear stress, denoted by $\bar{\Theta}_o$. If the denominator is multiplied by C_s, the term represents a shear stress as measured in units of surface grain layer weight. A better physical interpretation is gained if the denominator is further multiplied by the averaged static coefficient of resistance between a surface and adjacent grain layer, $\overline{\tan \alpha_-}$. The term $\bar{\tau}_o/\rho' g D C_s \overline{\tan \alpha_-}$ then represents the ratio of applied fluid shear stress and static bed resistive stress; it is now vectorially correct. The ratio is a drag coefficient, and in analogy to say a solid falling freely in a still fluid, it will be a function of a boundary Reynolds number, given by $(\bar{\tau}_o/\rho)^{1/2} D/\nu$ $(\bar{R}o)$.

The term $\rho_s g/\rho g$ represents the influence of solid and fluid accelerations on the problem. For this particularly defined subject of quasi-uniform flow and averaged flat bed transport, acceleration terms do not appear in the analysis. Finally, the $\bar{d}/D$ ratio represents the fluid depth influence. Since $\bar{Q}_{so}$ represents the transport of solids at or very close to the flat bed (bed-load transport), $\bar{d}/D$ can be disregarded.

Using the above physical considerations and assumptions, equation (3.2) becomes

$$\bar{G}_o = \bar{G}_o(\bar{\Theta}_o, \bar{R}o) \qquad (3.3)$$

from which it is assumed that the flat-bed low-transport rate (measured in proportional units of surface grain-layer transport) depends solely on the applied bed-shear stress (measured in proportional units of surface grain-layer weight) and whether this stress is transmitted to the bed by inertial or viscous fluid forces.

The I.M. condition follows from eq. (3.3) for the case when $\bar{G}_o \rightarrow 0$ and a critical stress ($\bar{\theta}_{oc}$) is then given as

$$\bar{\theta}_{oc} = \bar{\theta}_{oc}\,(\bar{R}o) \qquad (3.4)$$

This expression was proposed by Shields (1936), and accordingly he produced the well known $\bar{\theta}_{oc}$, $\bar{R}o$ diagram by extrapolating $\bar{Q}_{so}$ measurements to zero. (The diagram was subsequently reduced to a curve by Rouse, 1939).

3.2. Velocity representations for turbulent rough flows

3.2.1. Bed velocity representation

As noted previously, both shear stress and velocity expressions should be equivalent, provided the subject is modelled correctly for either case. It will be shown below that this is approximately true for turbulent-rough boundary mean-velocity expressions, but no comparison can be made for other flow conditions.

The relative success towards the understanding of I.M. (as opposed to total sediment transport problems) may be due to the assumed simplicity of the averaged kinematics for 2-dimensional flow. In particular, the clear-water flow may be described by fixed-boundary kinematics, such as the Karman-Prandtl velocity distribution,

$$\frac{\bar{u}}{u_*} = \frac{\bar{u}}{u_*}\left(\frac{u_* y}{\nu}\ ,\ \frac{y}{D}\right) \qquad (3.5)$$

u_* is defined as $(\tau_o/\rho)^{1/2}$, and is chosen as such in order to represent a velocity scale for the flow. The statement of the equation is that the temporal average of the longitudinal velocity ($\bar{u}$) at a perpendicular distance from the bed (y), as measured in u_* units, depends on the dimensionless co-ordinate $y(\nu/u_*)^{-1}$ (where ν/u_* is classically considered as proportional to a viscous sub-layer thickness) for viscous and turbulent-smooth boundary flows; for turbulent-rough boundary flows, the dimensionless co-ordinate becomes y/D.

Equations (3.4) and (3.5) can be considered as simultaneous equations, and accordingly, u_* may be eliminated to give a combined expression

$$\frac{\bar{u}_c^2}{\rho' g D} = \bar{\theta}_{uc}\left(\frac{\bar{u}_c y}{\nu}\ ,\ \frac{\bar{u}_c D}{\nu}\right) \qquad (3.6)$$

Attempts to use this type of I.M. representation for $\bar{u}_c$ near the bed have failed because of non-unique definitions for the position y. In historical order, bed-velocity expressions (where y is assumed to be "near the bed") have been proposed by Brahms (1753), summarised by Forcheimer (1914), proposed by Rubey (1938), summarised by Heyndrikx (1948), summarised from Soviet works by Barekyan (1963) and more recently proposed and summarised by Le Feuvre et al (1966).

The earlier expressions do not specify the y position. Examples are:

Brahms (1753) $\bar{u}_{bc} = kG^{1/6}$ where G = grain weight, k is a dimensional coefficient,

Forcheimer (1914) $\bar{u}^2_{bc} = kD$ in m-s units, where D is grain diameter

and Mavis and Laushey (1948) $\bar{u}_{bc} = 1/2\ D^{4/9}(\frac{\rho'}{\rho})^{1/2}$ in f-p-s units.

Rubey (1938) attempted to define y. He considered that the velocity measured at the position where the turbulent boundary layer meets the viscous sub-layer was appropriate. A universal law cannot however be derived from this definition, since there is no viscous sub-layer in turbulent rough-boundary flows. More recently, Le Feuvre et al (1970) proposed an expression for which $\bar{u}_c$ is measured at a position of 0.6 D above the bed. Although the expression included a drag coefficient which was intended to cover all flow conditions, one wonders how the velocity, for grains of say 100μ and less, was to be measured.

3.2.2. Depth-mean velocity representations

Use of the temporal and spatial average of the longitudinal velocity throughout the flow depth ($\bar{u}_m$) for I.M. automatically defines the position y for which $\bar{u}_c$ is measured, since integration of both the Karman-Prandtl turbulent velocity distribution, and the parabolic viscous flow distribution, gives $\bar{u} = \bar{u}_m$ at $y \simeq 0.4\bar{d}$. Equation (3.6) then becomes

$$\frac{\bar{u}_{mc}^2}{\rho' g D} = \bar{\theta}_{\bar{u}_{mc}} \left(\frac{\bar{u}_{mc}\,\bar{d}}{\nu}, \frac{\bar{u}_{mc} D}{\nu} \right) \qquad (3.7)$$

For turbulent-rough boundary flows, equation (3.7) becomes independent of ν, and thus

$$\frac{\bar{u}_{mc}^2}{\rho' g D} = \bar{\theta}_{\bar{u}_{mc}} \left(\frac{\bar{d}}{D} \right) \qquad (3.8)$$

The drag coefficient is then given as a function of the dimensionless co-ordinate $\bar{d}/D$ only. The co-ordinate is necessary since $\bar{\theta}_{\bar{u}mc}$ is expressed in terms of a velocity scale within the flow depth at $y \simeq 0.4\bar{d}$. (If $\bar{u}$ is alternatively expressed as a velocity scale which can be physically associated with the bed itself (such as $(\bar{\tau}_o/\rho)^{1/2}$ say), then $\bar{d}/D$ becomes redundant, and we have on substitution

$$\frac{\bar{\tau}_{oc}}{\rho' g D} = \text{a constant} \qquad (3.9)$$

which is the Shield's shear-stress representation for turbulent-rough boundary flows.)

Most mean-velocity representations have been proposed for turbulent rough boundary flow conditions only. In historical order, they have been qualitatively summarised by Fortier and Scobey (1926), graphically summarised by Hjulstrom (1935), proposed by Straub (1953), graphically summarised by Lane (1953), proposed by Rottner (1959) and Jarocki (1963), summarised from Soviet works by Goncharov (1964), proposed and summarised by Neill (1967), Bogardi (1968) and Yalin (1972).

Using a different procedure of dimensional analysis, Neill (1967) reduced his observations to the form of equation (3.8). This representation has since become quite popular, and we have examples of

Straub (1953) $$\bar{\theta}_{\bar{u}_{mc}} = 2.22\ (\bar{d}/D)^{1/3}$$

Rottner (1959) $$\bar{\theta}_{\bar{u}_{mc}} = \bar{d}/D\left(\frac{5.50}{(\bar{d}/D)^{2/3} + 4.75}\right)^2$$

$$= 30(\bar{d}/D)^{-1/3} \text{ for large } d/D$$

Neill (1967) $$\bar{\theta}_{\bar{u}_{mc}} = 2.50\ (\bar{d}/D)^{1/5}$$

Bogardi (1968) $$\bar{\theta}_{\bar{u}_{mc}} = 2.89\ (\bar{d}/D)^{1/5}$$

and Garde (1970) $$\bar{\theta}_{\bar{u}_{mc}} = 2.56\ (\bar{d}/D)^{1/4}$$

Although these expressions differ, there is experimental data used for their derivation, which is common to each. For example, the Neill, Bogardi and Garde expressions all use the results of Neill (1967).

3.2.3. Comparison with shear stress representations

It has been shown by Yalin (1972) that mean velocity expressions can be simply considered as power laws which form part of a more general logarithmic relation. If the turbulent-rough boundary conditions of $\bar{\theta}_{oc}$ = a constant and $\bar{u}_m/u_* = 2.5 \ln (11\bar{d}/D)$ are assumed (where the latter expression has been shown to hold by Nikuradse (1933) for $\bar{d}/D > 15$),

then

$$\bar{\theta}_{\bar{u}_{mc}} = \bar{\theta}_{oc} \frac{\bar{u}_{mc}^2}{u_{*c}^2} = \bar{\theta}_{oc} \times [2.5 \ln (11\bar{d}/D)]^2 \qquad (3.10)$$

The above expression, proposed by Yalin, is herein further simplified for purposes of direct comparison, by expressing the logarithmic function as a power law. A plot of equation (3.10) on log-log paper, using the empirical value of $\bar{\theta}_{oc} = 0.06$ then gives

$$\bar{\theta}_{\bar{u}_{mc}} = 4.0(\bar{d}/D)^{1/3} \quad \text{for } 15 < \bar{d}/D < 100 \qquad (3.11)$$

Equation (3.11) indicates that the empirical results for $\bar{\theta}_{\bar{u}mc}$ in section 3.2.2. are lower than that proposed by Shields. This difference may be due to the fact that the 'common' Neill data was compiled for a different observational condition than that of Shields. In contrast to the method of extrapolating low sediment transport rates to zero, Neill recorded $\bar{\theta}_{oc}$ and $\bar{R}o$ values for the observed 'first-movement' of sediment.

It is interesting to numerically compare the Shields result of $\bar{\theta}_{oc} = 0.06$ with that obtained with mean-velocity expressions, since both representations attempt to describe the I.M. condition, without mutual bias. Since the condition for both cases should, ideally, be equivalent, a comparison of the data will give an idea of the scatter to be expected on the Shields curve for turbulent-rough flows.

Figure 3.1. gives a log-linear plot of equation (3.11), together with the mean-velocity expressions, for the same empirical range of $15 < \bar{d}/D < 100$. It is first seen that the Straub expression is closest to that of Shields (which fact is not surprising, since the Straub

expression was originally derived from a combination of $\bar{\theta}_{oc} = 0.06$ and the Manning open-channel resistance formula). Using the turbulent rough logarithmic relation, $\bar{\theta}_{oc}$ values can be calculated from the Neill curve as 0.026 and 0.020 for $\bar{d}/D = 15$ and 100 respectively. It is thus seen that these examples of I.M. estimates have been given for any value within the approximate range of $0.02 \lesssim \bar{\theta}_{oc} \lesssim 0.06$.

Before discussing the transition region of the Shields curve, it is finally relevant to note that another class of representations exist. These attempt to describe the solid resistance to motion in terms of its fall velocity (for example Liu 1973, Yang, 1957). The physical statement of such representations is that the behaviour of a solid in a 2-dimensional shear flow is a function of its behaviour in a 1-dimensional flow. Such a proposition is questionable.

3.3. Definitions for the beginning of sediment movement and the 'transition' region

3.3.1. Observational similarity requirements

It was considered in section 3.2.3. that the considerable experimental scatter associated with $\bar{\theta}_{oc}$, $\bar{R}o$ representations for I.M. could be caused by different methods of observation. In addition, it has often been alluded to in the literature that the scatter is also associated with subjective estimates for the 'amount' of sediment moved at I.M. An attempt is now made to define the physical nature of the I.M. condition, and observational similarity criteria are accordingly presented.

As stated in section 3.1.2., the flow model assumed herein is that of two dimensional, quasi-uniform, open-channel flow over geometrically similar flat beds. The model without further qualification implicitly assumes a bed of infinite length. At any instant of time, the fluid applies a statistical distribution of shear stress (of spatially averaged value $\tilde{\tau}_o$) to the bed, whilst a stastical distribution of maximum resistive stress (of spatially average value $\tilde{\tau}_R$) is associated with the bed grains. For $\tau_o > \tau_R$ at any instant, simultaneous grain detachments occur at the infinite bed. It is therefore this hypothetical condition which is assumed to be represented by 'first-movement' experiments, and for which $\tilde{\theta}_{oc}$ has been estimated.

The condition for observational similarity follows from the above hypothetical experiment as that of spatial similarity. That is, if a comparison is to be made between one experiment and another, values of $\tilde{\theta}_o$ must be compared for equal values of detached grain areas (or volume). If P_A represents the number of grains detached in an

area A at any instant, the condition can be given as

$$\frac{P_A D^2}{A} = \text{a constant} \qquad (3.12)$$

and the critical stress, $\tilde{\theta}_{oc}$, is that value for which the dimensionless bed-load, $P_A D^2/A \rightarrow 0$.

The above idealised condition defines the simplest description of incipient motion, being that for which simultaneous grain detachment at an infinite bed approaches zero (Fig. 3.2.1.). The Shields method of extrapolating transport rates to zero is correspondingly the condition for which continuous grain movement over an infinite flat bed approaches zero. Since solid motion is now considered, the observational similarity condition demands kinematic as well as spatial similarity, and can be stated as

$$\bar{G}_o = \frac{P_{Au_*} D^2}{A} \times \frac{\bar{U}}{u_*} = \text{a constant} \qquad (3.13)$$

where P_{Au_*} represents the number of moving grains in an area A, and $\bar{U}$ the averaged grain velocity expressed in scale units of u_* (Fig. 3.2.2.).

It follows that the critical simultaneous detachment stress is only equal to the critical incipient transport stress when $P_A D^2/A \rightarrow 0$ in the same numerical manner as $\bar{G}_o \rightarrow 0$. A typical case for which this condition is not met is that of bed armouring (Gessler 1965, Grass 1971). During armouring, the least stable grains are detached (P_A finite), then subsequently move to bed positions of greater stability ($\bar{G}_o = 0$). 'First-movement' and 'low-transport'

critical stresses can therefore differ, and it may well be that the scatter on a Shields' diagram is associated with recording both conditions.

It is finally relevant to note that observational similarity requirements have been proposed for the particular experiment of continued grain detachment from finite flat beds. (Neill 1968, Neill and Yalin 1969). Such an experiment then determines a 'sediment removal rate' as opposed to a sediment transport rate' (Fig.3.2.3.). Since grain detachment occurs in both space and time, the observational similarity requirement is that

$$\frac{P_{AT}D^2}{A} \times \frac{\overline{\delta t}}{T} = \text{a constant} \qquad (3.14)$$

where P_{AT} represents the number of detachments in an area A and time T, and $\overline{\delta t}$ the average time taken for a single detachment. It has been proposed by Yalin (1972) that $\overline{\delta t}$ can be associated with the average period of large scale eddies at the bed, which in turn are represented by the flow boundary parameters such that $\overline{\delta t} \sim D/u_*$. Such a proposal is however questionable in the light of recent boundary-layer visualisation studies by, for example, Offen and Kline (1974). These studies indicate that bed shear-stress distributions are significantly influenced by relative fluid movements to and from the superimposed flow; the scale time for boundary macroturbulence need not therefore be described by boundary parameters alone.

3.3.2. The critical low-transport stress and the nature of a sedimentary bed

In summary of the previous section, it is seen that the beginning of sediment movement over flat infinite beds can be considered as a

spatial or a time and spatial condition. The critical stress for which simultaneous detachment begins ($P_A D^2/A \rightarrow 0$) can be termed the "critical detachment dimensionless stress, $\tilde{\theta}_{oc}$", whilst that for the beginning of transport ($\bar{G}_o \rightarrow 0$) can be termed the "critical low-transport dimensionless stress, $\bar{\theta}_{oc}$". Several attempts have been made to estimate $\bar{\theta}_{oc}$ in the light of observational similarity (Shields 1936, Paintal 1971, Taylor and Vanoni 1972), and these have led to various contradictions. It is now proposed that some of the contradictions can be resolved by acknowledging the fact that each set of experiments were conducted for geometrically dissimilar beds (and consequently different τ_R distributions).

The obvious example for the above dissimilarity is that of the Shields experiments. Gessler (1971) stated that "some of Shields' bed load measurements were made under conditions where ripples and dunes prevailed". Accordingly Gessler corrected the Shields turbulent-rough critical stress value to a flat-bed magnitude of $\bar{\theta}_{oc} = 0.05$.

Using an alternative method, Paintal (1971) showed that a turbulent rough $\bar{\theta}_{oc}$ value of 0.05 could be defined by linearly extrapolating relatively high flat-bed transport rates to zero. He estimated that the complete flat-bed transport relation was in fact a power law, which could be given (in terms of the parameters used in this Chapter) as

$$\bar{G}_o = (6.56 \times 10^{18})\bar{\theta}_o^{15.5} \quad \text{for } \bar{\theta}_o < 0.05 \qquad (3.15)$$

Accordingly, he proposed that "there is no single value (of $\bar{\theta}_o$) below which not a single particle will move." The linear extrapolation of eq. (3.15) for $\bar{\theta}_o \sim 0.05$ thus gave $\bar{\theta}_{oc} \simeq 0.05$, whereas the continued extrapolation gave $\bar{\theta}_{oc} = 0$.

It is noted however that eq. (3.15) was derived from experiments for which the flat bed was artificially laid and smoothed. For such conditions, individual grains may take any position and orientation relative to adjacent grains; there is therefore a small probability for a surface grain having almost zero resistance. If instead, a stable bed is laid slowly under natural conditions of shear flow, for which the averaged bed-laying stress is $\bar{\theta}_{ob}$ say, then $\bar{\theta}_R > \bar{\theta}_{ob} > 0$. The Paintal expression therefore represents a limiting relationship which is possibly applicable to natural beds laid for the condition of $\bar{\theta}_{ob} = 0$. (For any other condition, equation (3.15) will either include the $\bar{\theta}_{ob}$ parameter, or some description of the bed fabric.) Fig. 3.3. illustrates this principle, and it is logical that the exponent for $\bar{\theta}_o$ in equation (3.15) increases with $\bar{\theta}_{ob}$, for any finite $\bar{\theta}_{ob} < 0.05$.

Another interpretation for the $\bar{\theta}_{oc} = 0.05$ value was implied by Paintal(1971). He showed that when the bed-load transport data (for $\bar{\theta}_{oc} > 0.05$) of Gilbert (1914), U.S.W.E.S. (1935) and Casey (1943) were plotted logarithmically, they could be approximately represented by the power law

$$\frac{\bar{q}_{so}\rho^{1/2}}{\rho_s g D(\rho' g D)^{1/2}} = 13\,\bar{\theta}_o^{2.5} \quad \text{for } \bar{\theta}_o > 0.05 \qquad (3.16)$$

$$\text{or} \qquad \bar{G}_o = 13\,\bar{\theta}_o^{2} \quad \text{for } \bar{\theta}_o > 0.05 \qquad (3.17)$$

when expressed in terms of the parameters of this chapter. The lower rate of increase in $\bar{G}_o$ with $\bar{\theta}_o$ (as compared with eq. (3.15)) was due to the additional shear stress of bed forms (as alluded to by Gessler). Fig. 3.3. also shows this relation, and it is seen that eq.(3.17) inter-

sects eq. (3.15) at $\bar{\theta}_o \simeq 0.05$. It is thus concluded herein that the amended Shields' $\bar{\theta}_{oc} \simeq 0.05$ value can be considered as the approximate crtical stress for which bedform development begins from a flat bed, and thus it describes a condition of maximum stability for a flat bed.

It is now relevant to discuss the procedure of the fine sediment experiments conducted for this thesis, and the observance of the above principles. Firstly, the experiments were conducted in a long flume, and since D was very small, the bed could be considered infinite. Secondly, the beds were first laid so that bed forms were produced during deposition. $\bar{\theta}_{ob}$ was then incrementally reduced until no bed forms were observed on deposition. The total bed was then laid for this stress condition. $\bar{\theta}_o$ was subsequently recorded under clear water flow conditions for which a minimum and continuous bed-load transport was observed visually. This stress value therefore represented a close approximation to $\bar{\theta}_{oc}$, and the procedure in turn represented an approximation to the Shields condition of maximum flat bed stability. It was therefore relevant to plot the fine sediment $\bar{\theta}_{oc}$ estimates on the original diagram proposed by Shields.

It is noted that although observational similarity was not conducted for these experiments (since $\bar{G}_o$ was not measured), the increase in $\bar{G}_o$ with increased $\bar{\theta}_o$ was so large (compared with artificially laid beds) that visual observation provided a reasonable first order estimate. It will be shown in the next section of this chapter that observational similarity must however be considered for experiments conducted with artificially laid beds.

3.3.3. Low transport rates over artificial flat beds and the 'transition' region

A common acceptance of the I.M. literature is that there exists a fall in the $\bar{\theta}_{oc}$, $\bar{R}_o$ curve for $10 < \bar{R}_o < 100$ say. This $\bar{R}_o$ region is usually denoted as part of a 'transition' region (for which $1 < \bar{R}_o < 100$ say), and its limits have been widely disputed (Yalin 1972).

Several ideas have been proposed for the physical cause of the fall, but the amount of scatter existing for turbulent rough flows (0.02-0.06) does not significantly establish its existence. Recently, Taylor and Vanoni (1971) reported low flat bed transport rate measurements, for natural sands under water flows, which gave a well defined fall. However, when the data of Paintal (1971) are compared with those of Taylor and Vanoni (Fig. 3.4.) the fall again becomes questionable.

Prior to observational similarity attempts at defining an objective transport rate for I.M, over artificially laid beds, most observations were ocular. A commonly applied definition was that due to Kramer (1935). He gave 4 definitions for increasing flat-bed transport as none, slight, moderate and general. For example, the slight movement attempted to signify that "some small, countable number of grains were set in motion at various positions on the bottom." It is noted that such a definition does not include spatial similarity, and it is now shown quantitively that when such observations are made over fixed areas, a fall of $\bar{\theta}_{oc}$ in the transition region will be recorded.

The observational similarity condition for low transport rates over flat beds has been given as

$$\bar{G}_o = \frac{P_{Au_*} D^2}{A} \times \frac{\bar{U}}{u_*} = \text{a constant} \qquad (3.13)$$

The variation of $\bar{U}$ with $\bar{u}_*$ and ρ_s has been empirically studied by Francis (1970, 1973) and Abbott (1974). In particular, Abbott observed the motion of single 'pea-gravel' solids (D = 0.828cm) moved by water flow over fixed, flat beds of the same solids. He obtained the dimensional relation

$$\bar{U} = K\,[u_* - f(\rho_s)] \qquad (3.18)$$

where K was proposed as a constant which depended on solid size and shape. Using an S.G. range for the same solid of 1.20 to 2.57, Abbott further obtained the empirical relation of $\rho_s \propto u_*^2$ for a constant value of $\bar{U}$.

Equation (3.18) is herein expressed as

$$\frac{\bar{U}}{u_*} = K\left[1 - \text{const.} \times \frac{\rho_s^{1/2}}{u_*}\right] \qquad (3.19)$$

A plot of the 'pea-gravel' data using $\bar{U}/u_*$ and $\bar{\theta}_o^{-1/2}$ as axes (Fig.3.5.) then gives the regression line

$$\frac{\bar{U}}{u_*} = 13.2 - 1.61\ \bar{\theta}_o^{-1/2} \qquad (3.20)$$

This first order empirical estimate for turbulent-rough flow can now be combined with the Paintal equation (3.15) to give

$$\frac{P_{Au_*} D^2}{A} = \frac{(6.56 \times 10^{18})\bar{\theta}_o^{15.5}}{13.2 - 1.61\ \bar{\theta}_o^{-1/2}} \qquad (3.21)$$

The above equation is thus proposed for moving-grain area ratios in turbulent-rough flows over artificial flat beds for which $\bar{\theta}_o < 0.05$. (It is restricted to values of $P_{Au_*} D^2/A$ less than about 1%, since it has been shown by Francis (1973) that $\bar{U}$ for a number of moving grains is decreased when this value is exceeded.)

The concept of low transport rates as a countable number of moving grains over a fixed area can now be treated numerically. Fig. 3.6 gives a dimensional representation for low transport in terms of $\bar{\theta}_o$ versus D. The curve proposed by Rouse (1939), from the Shields diagram, has been plotted using $\rho_s = 2.65$ gm/cc. and $\nu = 0.01$ stokes. Superimposed on this curve are horizontal lines of $P_{Au_*} D^2/A$ values, calculated from equation (3.21). (It is seen that equation (3.21) provides a physical meaning to $\bar{G}_o$ values, since for example, a $\bar{G}_o$ of 10^{-3} is associated with a moving-grain area ratio of about 0.003%). If it is now assumed that a fixed observational area (A) is used for the artificial bed experiment, of say $10^3 cm^2$ (about 1 foot by 1 foot), then curves for $P_{Au_*} = 1$ and $P_{Au_*} = 10$ may drawn as shown in the figure. It is thus seen that such an experiment leads to a fall in the Shields curve, and that this fall is of the same magnitude as proposed by Rouse (1939) and others.

It is finally relevant to discuss the most common reason given for the transition fall. Sundborg (1956) stated that for the onset of the transition region:

"the resistance is no longer distributed over all the particles of the uppermost layer, as it was in the turbulent rough region. The turbulence does not extend so far down among the particles. Grains in more shielded positions are not reached by the turbulent flow, and therefore do not offer any shape resistance. The force acting on the

most exposed grains is so much the greater, which explains the decrease....."

In other words, the applied stress is mainly incidental to the few most exposed grains on a flat bed surface, and hence $\bar{\theta}_{oc}$ decreases. Such a reasoning was however given at a time when it was thought that a 'laminar sub-layer' existed adjacent to a transitional (and smooth) boundary, and for which layer the flow was both viscous and steady. Recent boundary layer studies (as summarised in Chapter 6.3) show however that large shear stress fluctuations can exist within the 'laminar sub-layer' and it is accordingly re-named the 'viscous sub-layer'. It follows that such fluctuations may also be incident to the 'least-exposed' grains of a flat bed under transitional flow, hence the Sundborg (1956) speculation becomes questionable.

3.4. Turbulent-smooth boundary and viscous flows

3.4.1. Previous research

There exists several contradictions in the literature for I.M. descriptions under turbulent-smooth and viscous flows. (For such flows, the $\bar{R}o$ region is herein described, for convenience, as $\bar{R}o < 1$ or low $\bar{R}o$). A commonly discussed idea is that due to Shields (1936), who extrapolated the 'transition' region of his results such that

$$\bar{\theta}_{oc} \propto \bar{R}o^{-1} \quad \text{for } \bar{R}o < 10 \qquad (3.22)$$

This extrapolation was without experimental or theoretical justification, yet it was proposed since $\bar{\tau}_o$ was then independent of D. Attempts to physically explain the independence have been made. For example, Sundborg (1956) and Yalin (1972) associate low $\bar{R}o$ values with low D values, and suggest that fine grains then become cohesive and independent of their individuality as described by D. If such is the case, then the extrapolation should not appear on an I.M. representation for cohesionless solids.

White, C.M. contradicted the Shields idea by estimating, from 2 experiments conducted with coarse grains and a highly viscous fluid ($\bar{R}o$ = 0.04 and 0.28), that

$$\bar{\theta}_{oc} \propto \bar{R}o^{o} = \text{a constant} \qquad (3.23)$$

Other dependencies have also been proposed from experiments with

fine-sand sized solids in water. For example, Nagy et al (1959) gave

$$\bar{\theta}_{oc} \propto \bar{R}o^{-0.5} \quad \text{for } 0.5 < \bar{R}o < 11.6 \qquad (3.24)$$

and Grass (1970) proposed

$$\bar{\theta}_{oc} \propto \bar{R}o^{-0.63} \quad \text{for } 0.7 < \bar{R}o < 2 \qquad (3.25)$$

It is thus seen that the whole range from 0 to -1 has been proposed for the $\bar{R}o$ power.

A physical reasoning, again using the 'grain exposure' idea, was proposed by Bagnold (1941) to explain a rise in $\bar{\theta}_{oc}$ for decreasing $\bar{R}o$. The reasoning continues from that of the 'transition fall', and assumes that

"the drag, instead of being carried by the few, more-exposed grains, is distributed more or less evenly over the whole surface. Consequently a relatively greater drag is required to set the first grains in motion".

In the following section 3.5., it is proposed that a $\bar{\theta}_{oc}$ increase is better explained by the decreasing magnitude of applied stress distribution with an $\bar{R}o$ decrease.

In contrast to the idea that $\bar{\theta}_{oc}$ should increase continuously with decreasing $\bar{R}o$, Bagnold (1956) proposed that there should be a maximum value, as $\bar{R}o \to 0$, of $\theta_{oc_{max}} \simeq 0.4$ (see next sub-section). Recent observations to very low $\bar{R}o$ values ($\bar{R}o \simeq 0.03$) for naturally laid beds of silt-sized solids in water (Rees 1966) and both water and oil (White, S.J. 1970) have given $\bar{\theta}_{oc}$ values less than 0.4, thus tending to confirm this limit. It is however proposed overleaf that

$\theta_{oc_{max}}$ depends considerably on the nature of a bed formation, and its average value may well exceed that of 0.4.

3.4.2. The maximum critical detachment stress distribution for idealised coplanar beds

The idea of $\theta_{oc_{max}}$ was proposed by Bagnold to apply for the "ideal conditions of purely laminar fluid flow over a bed of uniform spheres perfectly piled and therefore equally exposed". The reason for postulating this hypothetical condition was that the applied fluid stress could be directly equated to the bed shear resistance. By independently considering the mechanical stability of a coplanar granular bed, the applied stress could thus be predicted as $\theta_{oc_{max}}$. Since "the surface grains of a natural bed are not uniformly exposed, nor under a turbulent fluid is the applied tangential stress steady", it is then expected that for $Ro > 0$, individual solids detach for $\theta_{oc} < \theta_{oc_{max}}$.

The above concept is however limited, for the purposes of prediction, to the particular nature of the coplanar bed considered. An attempt is now made to extend the concept to conditions of various coplanar bed formations. A $\theta_{oc_{max}}$ distribution is thus derived. It is proposed that such a distribution will indicate the magnitude of an actual granular bed shear resistance distribution, in addition to providing an averaged estimate for $\theta_{oc_{max}}$.

The physical statement underlying the definition for a particular $\theta_{oc_{max}}$ was given by Bagnold as:

"The ultimate shear resistance of the bed is that of its topmost layer. If under ideal conditions the whole of this layer were to yield simultaneously, at the plane $y = -D$, the necessary applied tangential

stress τ_{oc} would be expected to be given by

$$\tau_{oc} = \rho' g D \; C_{-} \tan \alpha_{-} \qquad (3.26)$$

where C_{-} and $\tan \alpha_{-}$ are respectively the uniform static values of the grain concentration and of the grain stress ratio within the bed. (The suffices - indicate constant static conditions at the negative plane - y)."

The particular nature of the surface layer of the above model coplanar bed was thus subject to three constraints.

a) The surface spheres were equally exposed. (A symmetrical and equal packing of adjacent layers was therefore implied, and each sphere resisted the same applied force.)

b) The surface layer resisted the whole applied stress. (Together with a) this condition implied that τ_{oc} was a maximum value.)

and c) The surface layer yielded at the plane y = -D.

The balance of forces at detachment could then be postulated, provided it was known whether the movement began by sliding, or by rolling. (It is later considered that τ_{oc} for sliding is always greater than that for rolling, hence $\tau_{oc_{max}}$ is theorised for the former condition only.)

When rigidly applied, the above three constraints can only refer to the case of a bed packed in cubic array (Fig. 3.7.1.). The balance of forces at the plane y = -D are physically interpreted by considering those at the point of contact of each surface sphere. If the applied tangential force ($F = \tau_o D^2$) is considered to act at this point (together with a couple whose magnitude depends on τ_o and its resultant line of action), then sliding detachment occurs for

$$\tau_{oc_{max}} D^2 = \rho' g \, \pi/6 \, D^3 \tan \alpha_F$$

where α_F represents the limiting coefficient of sliding friction between the spheres. Thus

$$\theta_{oc_{max}} = 0.52 \tan \alpha_F \qquad (3.27)$$

If constraint c) is now relaxed, then $\theta_{oc_{max}}$ can be associated with other ideal conditions of bed packing. C must now be replaced by the packing of the surface layer only, C_s (which is the ratio of the volume of integral solids in a surface layer of depth D to the total volume of the layer), and tan α refers to the actual plane of surface and adjacent layer contact, which is at a depth of $y < -D$. Fig. 3.7.2. illustrates this more general condition. The force balance at the point of contact for each sphere is indicated by considering F and G (the sphere's weight force) as a force and couple system. If α_P represents the angle of the plane of contact between the spheres with the horizontal, then sliding detachment occurs for the condition.

$$F \cos \alpha_P = G \sin \alpha_P + (G \cos \alpha_P + F \sin \alpha_P) \tan \alpha_F$$

whence

$$\theta_{oc_{max}} = C_s \tan(\alpha_P + \alpha_F) \qquad (3.28)$$

As particular examples for this more general condition, a bed may be packed with $\alpha_P = 30^\circ$ (Fig. 3.8.1.) for which $C_s = 0.52$, or as shown in Fig. 3.8.2. for which $C_s = 0.35$ and $\alpha_P = 60^\circ$. $\theta_{oc_{max}}$ thus becomes a spatially distributive quantity for coplanar beds composed of ideal spheres which are haphazardly packed.

The fundamental difference between sliding and rolling detachment is that the latter, by definition, is independent of mechanical friction (α_F). Fig. 3.9.1. repeats the model, for the force condition at rolling, which was proposed by White, C.M. (1940). If the constraints a) and b) are maintained, and γ_o is assumed to act at a line vertically displaced above a surface sphere centre, then

$$\theta_{oc} = C_s \tan \alpha_L \quad \text{for rolling}$$

where α_L = the angle for rolling such that $\alpha_L < \alpha_P$ hence

$$\theta_{oc_{max}} \text{ (rolling)} < C_s \tan \alpha_P < \theta_{oc_{max}} \text{ (sliding)}$$

The above considerations for sliding detachment therefore give a $\theta_{oc_{max}}$ magnitude (depending on the bed packing and mechanical friction) which applies to both sliding and rolling.

3.4.3. <u>The maximum critical detachment stress distribution for coplanar beds composed of natural grains</u>

The previous sub-section 3.4.2. has employed a classical approach to problems of nature, by considering specified ideal circumstances. The subsequent step is to use empirical constants for the purpose of extrapolating to a real situation. For this particular case, α_- is estimated as the limiting static angle of repose for natural solids (α_R). The basis for this estimation is illustrated in Fig.3.9.2., from which it is seen that gravitational instability for sliding occurs at the angle

$$\alpha_R = \alpha_P + \alpha_F$$

The possible range for α_R can be estimated from the single grain experiments of Miller and Byrne (1966). A mean and standard deviation for 'nearshore natural sand' was measured as $65^\circ \pm 22^\circ$. Since it is probable that the higher surface layer packing values ($C_s \simeq 0.5$) occur for low α_R, and the lower values ($C_s \simeq 0.35$) occur for high α_R, then $\theta_{oc_{max}}$ ($=C_s \tan \alpha_R$) takes an average value of about 1.0, with standard deviation limits of 0.5 and 6.0 say (Fig. 3.10).

Values of ($\alpha_P + \alpha_F$) for naturally laid beds appear to be even more speculative than those considered above. An indirect estimate can however be made from magnetic remanence studies, such as those by Rees (1961). The direction of the magnetic remanence vector, attained by natural fine sediments deposited in water, has been explained by postulating an averaged 'angle of rolling' (ϕ). This angle has been estimated to be as large as 70°. The rolling theory has also been extended to account for empirical results of the anisotropy of magnetic susceptibility; ϕ was then estimated at about 56°. If it is assumed that a bed surface array similar to that shown in Fig. 3.8.2. exists for these naturally laid beds, then $\phi_{max} \simeq 120^\circ$ (Fig. 3.11.), and $\phi_{min} = 0$. A speculated average value of $\phi_{average} = 60^\circ$ thus approximately agrees with empirical observation. (The implication that $\alpha_P \simeq 60^\circ$ is further corroborated by the low value of natural bed packing, $C \simeq 0.5$, reported in Chap.4). It is therefore speculated that an average, naturally laid bed formation resembles that illustrated in Fig. 3.8.2. and

$$\theta_{oc_{max\ average}} \simeq 0.35 \tan (60^\circ + \alpha_F) \quad (3.29)$$

α_F values between 10^o and 20^o have been recorded (Van Burkalow 1945) for natural solids resting on planes of similar surface roughness. If an average value of say 15^o is assumed, then $\theta_{oc_{max\ average}} \simeq 1.0$. It is therefore probable that θ_{oc} (for steady viscous flow) will be recorded for values less than 1.0.

It is finally proposed that the shear resistance distribution magnitude for single grains contained in the surface layer of a naturally laid bed is indicated by that of $\theta_{oc_{max}}$. The minimum value of shear resistance ($\theta_{R_{min}}$) will of course be determined by the maximum value of bed-laying applied stress ($\theta_{ob_{max}}$). The resulting θ_R distribution will thus be skewed, as indicated in Fig.3.10.

In summary, an attempt has been made in this section to estimate the grain resistive stress distribution for naturally laid beds. The Bagnold (1956) estimate of $\theta_{oc_{max}} = C_- \tan \alpha_- \simeq 0.4$ (using a C_- value of 0.63 which is applicable to the tight packing of natural granular beds in air, and a value of $\tan \alpha_-$ of 0.63 which was derived from a 34^o angle of repose for natural grains in air) has been reconsidered. The following section utilises the θ_R distribution to aid the physical interpretation of the Shields curve.

3.5. The probabilistic nature of the beginning of sediment movement

3.5.1. Statement of the problem

Although Shields (1936) fully recognised that I.M. was governed by the statistical distributions of the relevant variables, it was Einstein (1942) who first developed a sediment transport relation acknowledging this fact. The principle evolved was that grain detachment was better represented in terms of the instantaneous applied bed stress (or lift pressure, as discussed in the next section). The number of grains detached then depended on whether τ_o (for every instant and grain position) exceeded τ_R, and was expressed analytically by assumed laws of probability. (More recently, this probability reasoning has been extended to beds composed of varying grain sizes (Gessler, 1965, Irvine, 1971).)

The simplest exposition of the problem applies for the case of 'simultaneous detachment' from an infinite flat bed. If it is assumed that τ_o and τ_R are the relevant distributions which determine I.M. (Fig. 3.12.1.), then the chance for detachment occurs if these distributions are partially superimposed in space. It is seen that the normalised bed area capable of being detached (A_1) is given for $\tau_R < \tau_{omax}$ as

$$A_1 = \int_o^{\tau_{omax}} P(\tau_R) d\tau_R = f_1(\tau_{omax}, \tilde{\tau}_R) \qquad (3.30)$$

where $P(\tau_R)$ ≡ the normalised frequency distribution for τ_R, and is expressed as a variable about $\tilde{\tau}_R$.

Similarly, the normalised applied stress area which may cause detachment (A_2) is given by

$$A_2 = \int_{\tau_{Rmin}}^{\infty} P(\tau_o) d\tau_o = f_2(\tau_{Rmin}, \tilde{\tau}_o) \quad (3.31)$$

The actual normalised detached area ($P_A D^2/A$ where $A \to \infty$) is therefore given analytically by the probability that part of A_1 is coincident with A_2. (When $\tau_{omax} = \tau_{Rmin}$ (Fig. 3.12.2) $P_A D^2/A \to 0$ and thus $\tilde{\tau}_o = \tilde{\tau}_{oc}$.) In general, the dimensionless functional expression for simultaneous detachment will be given as

$$\frac{P_A D^2}{A} = \frac{P_A D^2}{A} \left(\tilde{\theta}_o, \theta_{omax}, \tilde{\theta}_R, \theta_{Rmin}\right) \quad (3.32)$$

Since it is customary to express the distribution limits in terms of multiplicative factors (a_o and a_R say) of the standard deviations, then

$$\frac{P_A D^2}{A} = \frac{P_A D^2}{A} \left(\tilde{\theta}_o, \frac{a_o \sigma_o}{\tilde{\tau}_o}, \tilde{\theta}_R, \frac{a_R \sigma_R}{\tilde{\tau}_R}\right) \quad (3.33)$$

Part of the problem is thus seen to be that of estimating θ_{omax}. Kalinske (1947) proposed that $\tau_{omax} = 3\tilde{\tau}_o$, but such an estimate can only apply for turbulent flow conditions. (It is to be expected that $\tau_{omax} \longrightarrow \tilde{\tau}_o$ as $\widetilde{Ro} \to 0$).

Most experimental interest has been concerned with estimating σ_o, whilst the 'a_o' value determining θ_{omax} has been left for speculation (for example, Garde 1970). The estimates of Compte-Bellot (1963), Schraub and Kline (1965), Clarke (1968), Grass (1971) and Blinco and Partheniades (1971), for pipe and 'two-dimensional' open-channel boundary layers (for a range of flow Reynolds number from about 7,000

to 50,000) all give the magnitude of $\sigma_o/\bar{\tau}_o \simeq 0.4$ for turbulent-smooth conditions. The instantaneous bed shear stress is usually estimated, for such conditions, from velocity measurements within the viscous sub-layer, such that $\tau_o = \mu_w \frac{du}{dy}$. For the case of turbulent rough flows this procedure can not be used, since an eddy kinematic coefficient and the zero bed level is indeterminate. Instead, $\sigma_o/\bar{\tau}_o$ estimates have been made from direct measurements on solids which form part of a rough bed. For example, Cheng and Clyde (1972) found $\sigma_o/\bar{\tau}_o = 0.6$ to 0.8 for shallow open-channel flow conditions ($\bar{d}/D \simeq 3$)

It thus seems reasonable to assume that $\sigma_o/\bar{\tau}_o$ varies from zero (for $\bar{R}o \to 0$) to about 0.4 for turbulent-smooth boundaries, to a constant magnitude of say 0.8 for turbulent-rough boundaries. It is questionable however whether $\sigma_o/\bar{\tau}_o$ correlates uniquely with $\bar{R}o$ (as implied by the Shields representation). For example, Grass (1971) considered that "an extremely high contribution to the Reynolds stress and hence turbulence production close to the boundary" was caused by fluid inrush and ejection sequences from and to the superimposed flow. (These features of the flow structure were observed for both turbulent-smooth and turbulent rough boundary flows.) For such sequences, $\sigma_o/\bar{\tau}_o$ may become dependent on the superimposed flow condition, which may in turn be described by the flow Reynolds number, $\bar{R}e$. Such an idea was proposed by Gunter (1971), who modified the Shields representation to

$$\bar{\theta}_{oc} = \bar{\theta}_{oc}(\bar{R}o, \bar{R}e) \qquad (3.34)$$

This new idea is however controversial. Gessler (1971) for example stated that the $\bar{R}e$ effect "is minor since the process of incipient motion occurs at the rough wall away from the area of highest velocity.

Any large scale turbulence is greatly damped out before it reaches the area of the rough wall."

It is thus concluded that even the simplest description of I.M., that of simultaneous detachment as described by tangential stress distributions alone, is a complex subject desiring further research on boundary layer flow structures. At present, equation (3.33) can only be solved with assumed laws of probability, assumed values for the coefficients a_o and a_R and empirical estimates for $\sigma_o/\bar{\tau}_o$ and $\sigma_R/\bar{\tau}_R$. The difficulty in postulating a τ_R distribution has been alluded to in section 3.4. of this chapter. The difficulty in postulating a τ_o distribution is further complicated by the possible mutual influence of both $\bar{R}o$ and $\bar{R}e$. An additional complication is now considered, being that of possible lift pressures which act during detachment.

3.5.2. The influence of lift pressure

Although the possible influence of fluid lift pressure (l_o) has often been mentioned in the early literature (for example, Schoklitsch 1914), practical estimates were not made until 1949. By means of pressure measurements at the top and bottom of closely spaced hemispherical roughness elements, Einstein and El-Samni estimated that $\bar{l}_o = 3\bar{\tau}_o$. The estimate was considered by Chepil(1958) to be too large; he estimated $\bar{l}_o/\bar{\tau}_o = 0.85$ both by computing pressure distributions and by making direct force measurements on a single hemisphere situated in a bed whose hemispherical roughness elements (of diameter D) were spaced 3D apart. (The ratio was also found to be constant for the $\bar{R}o$ range from 500 to 7,000.)

It has however been considered by Bagnold (personal communication) that such estimates are significantly influenced by the experimental procedure of using beds of only 0.5D in depth. For such a case, it is

considered that a recorded high pressure at the channel floor plane of y = -0.5D may be caused by the impact of eddies which would otherwise be gradually dispersed in the interstices of a deeper bed. The ratio of 0.85 may thus be a large over-estimate.

In addition to the indeterminacy for $\bar{l}_o$, estimates for $\sigma_l/\bar{l}_o$ vary considerably in the literature. Values range from 0.18 (Cheng and Clyde 1972) to 0.36 (Einstein and El-Samni 1949) to 0.49 (Chepil 1958), for similar turbulent-rough flow conditions. Furthermore, disagreement exists as to the nature of l_o distributions. Einstein and El-Samni (1949) stated that "a careful statistical analysis showed that the frequency of lift pressures or lift forces at the wall follows very accurately the normal error law". Christensen (1965) reviewed the same data, and concluded that it was the velocity fluctuations which were normally distributed.

The existence of lift pressures for turbulent smooth and viscous flows (low $\bar{R}o$) may be postulated from both indirect experimental evidence (Segré and Silberburg 1961) and the theoretical consideration of forces on a sphere moving in a slow shear flow (Saffman 1965). In particular, the lift force magnitude (l), due to small inertial effects on a sphere moving in a steady viscous velocity gradient, was given by Saffman as

$$l = 2\mu V_R D^2 \left(\frac{d\bar{u}}{dy}\right)^{1/2} \nu^{-1/2} \qquad (23.35)$$

where V_R = the relative velocity of the sphere and fluid as measured at the streamline through the particle centre. If the expression is crudely assumed to apply for the case of a singly exposed sphere at the boundary of a viscous shear flow (low $\bar{R}o$), then

$$l = \rho v^2 Ro^3 \qquad (3.36)$$

and thus $l_o/\tau_o = 1.3Ro$. For the case of partially exposed grains at $\bar{Ro} = 0.01$, equation (3.36) then indicates that lift pressures are negligible compared with τ_o. However, for unsteady viscous flow conditions at say $\bar{Ro} = 1$, l_o may become significant.

The above considerations have led several authors to consider l_o as the dominant variable which determines I.M. In fact, complete sediment transport theories have been derived using this assumption (for example Einstein 1942, Yalin, 1963). It still remains however a matter of speculation whether the vertical lift pressure or the tangential bed stress dominates the process. A combination may in fact exist, for which the Shields representation may still be adequate. If the lift pressure distribution is associated solely with the grain resistance distribution (since its effect may be to reduce the grain weight and subsequently the limiting friction opposing sliding detachment), then a modified bed shear resistance distribution can be proposed. The considerations of sub-section 3.5.1. will therefore continue to apply, since the condition can again be described in terms of τ_o and a 'modified' τ_R distribution.

3.5.3. Summary

An attempt has been made to review some of the problems concerned with the I.M. of granular solids by 2-dimensional open-channel flows over a flat bed. The early deterministic approaches have been explained in the light of the 2-phase model proposed by Yalin (1963). The reduction of mean velocity expressions to bed shear stress representations has shown that a scatter of almost one order of magnitude ($\bar{\theta}_{oc}$ = 0.1 to 1.0) exists for turbulent-rough flow conditions. Part of this scatter

was considered as attributable to lack of observational similarity for a particular type of experiment, and part was due to non-reproducible initial bed conditions arising from artificially laid and smoothed beds.

Probabilistic approaches to the problem are at present limited. If the process is considered as one involving grain resistance and applied shear stress distributions alone, then the limitations are caused by a lack of knowledge of these variables. The discussion on I.M. under viscous flows illustrated the present speculative attempts of postulating a τ_R distribution for naturally-laid beds. A major difficulty encountered was in establishing whether detachment began by one or a combination of sliding, rolling or lift mechanisms. This section has further indicated the possible non-uniqueness of the $\bar{\theta}_o$ distribution with $\bar{R}o$ (since $\bar{R}e$ may also be involved), and consequently challenges the original Shields' representation.

It seems that the present available knowledge can be summarised as in Fig. 3.13. The reasoning for this figure will depart from the traditional view of explaining the Shields' diagram from the turbulent rough region and then introducing the concept of 'grain-exposure' to explain the 'transition fall' and subsequent rise with low $\bar{R}o$. Instead, it is first assumed that experiments are conducted on naturally-laid, geometrically similar flat beds, The θ_R frequency distribution is thus indicated at $\bar{R}o = 0.01$ using $\bar{\theta}_R = 1.0$ from section 3.4.3 and $\theta_{Rmin} = 0.4$ (as indicated by the experiments of White, S.J. 1970). In accord with this 'diagramatic'representation, the θ_{oc} frequency distribution is superimposed as a Dirac-delta function at $\bar{R}o = 0.01$, and in accordance with section 3.3.2, the flat bed condition is also assumed as that of maximum stability. For turbulent-smooth boundaries ($\bar{R}o = 1.0$), it is

possible that the θ_R distribution increases with the onset of lift pressures, and it is probable that the θ_o distribution increases with $\bar{R}o$ and $\bar{R}e$. The fall in $\bar{\theta}_{oc}$ between $\bar{R}o = 0.01$ and 1.0 is thus physically inevitable. For $\bar{R}o > 1.0$ say, the traditional speculation for a transition region is denied, and the θ_R and θ_{oc} distributions are assumed constant. $\bar{\theta}_{oc}$ is accordingly an empirical constant at say 0.05.

It is finally emphasised that the Shields curve can no longer be considered universal for conditions of <u>any</u> flat bed. The fine sediment experiments described in the following chapters of this thesis acknowledge this fact, by estimating low-transport critical stresses for flat beds which are at their limit of stability (prior to changing their configuration with increased $\bar{\theta}_o$). The further non-universality of the curve, as implied by a possible $\bar{R}e$ influence, awaits longer-term research into the nature of the turbulence structure in open-channel fluid flows.

CHAPTER 4. THE LOW TRANSPORT CRITICAL STRESS FOR NATURALLY LAID FINE, COHESIONLESS SEDIMENTARY BEDS

4.1. Bed Laying Procedure

4.1.1. Flow conditions

The major experimental difficulty (as alluded to in Chapter 3) for incipient motion (I.M.) experiments is that of achieving reproducibility, since so many variables may operate both locally and simultaneously. The compromise necessary for research is therefore to constrain the system, and the limitations should accordingly be presented in a report. A typical example of this problem was in deciding the initial sediment suspension concentration, C_I (equal to the ratio of the initial volume of solids introduced as a suspension into the flume to the total fluid volume) to use for laying a fine sediment bed by gradual deposition of the solids from the moving flow. It is possible that the bed fabric (position and orientation of the individual grains) and subsequent sediment transport may be affected by varying C_I.

For the purpose of these fine, granular I.M. experiments, C_I was chosen such that the initial averaged linear separation ($\bar{\lambda}$) of the suspended solids was given by

$$\bar{\lambda} > 10 \not{D} \qquad (4.1)$$

This first constraint was chosen in the light of studies on the viscous sedimentation of single solids in a cylinder containing still fluid (for example, Uno and Kintner, 1956). For such a case, it has been shown that the wall influence of increased drag of a sedimenting solid is negligible for $\lambda > 15$ D. It was therefore assumed that for $\lambda > 10$D in

a shear flow, the motion of each solid was minimally affected by that of neighbouring solids. (It was of course possible that C_I would affect the flow properties of the transporting fluid, and consequently the averaged bed laying stress ($\bar{\tau}_{ob}$); this fact therefore necessitated the estimate of $\bar{\tau}_{ob}$ after the bed had been laid, by observing low transport under clear water flow conditions.)

Equation 4.1. can be used to estimate the maximum weight of suspended solids transported by the flow during bed-laying (W). Since $\bar{\lambda}^3 D^3$ represents the average volume occupied by a grain (assumed as a sphere for these rough calculations) in the transporting fluid, then

$$W = \rho_s \frac{\pi D^3}{6} \times \frac{owd}{\bar{\lambda}^3 D^3} \quad \text{gm.wt.} \qquad (4.2)$$

where o represents the overall flume length (=13m), w the channel width of 30cm., and $\bar{d}$ the quasi-uniform flow depth, thus

$$W = 50\bar{d} \text{ gm.wt.} \qquad (4.3)$$

A maximum practical $\bar{d}$ value of 20cm. was chosen for bed laying during these experiments, to aid suspension uniformity by reason of high turbulence. The associated W was therefore about 1kg.wt.

The second constraint imposed on the deposition procedure was that $\bar{\tau}_{ob}$ should be as close as possible to that stress which was necessary to produce bedforms. As an aid to experimental procedure, it was first necessary to express this condition in terms of average flow velocity ($\bar{u}_m$), since the latter was more readily measured than

$\bar{\tau}_{ob}$. An approximation for this 'bed form' stress can be made by assuming the White, S.J. (1970) I.M. stress estimates for a water condition of about 20°C, whence

$$\bar{\tau}_{ob} = 25D^{0.6} \quad \text{c.g.s.} \tag{4.4}$$

and then expressing $\bar{\tau}_o$ in terms of $\bar{u}_m$ with the use of the depth friction factor ($f_d = 8\,\rho g\bar{d}\bar{i}/\ \bar{u}_m^2$) calculated from Chapter 1 ($f_d = 0.033$ for $5{,}000 < Re < 20{,}000$), whence

$$\bar{u}_{mb} = 80D^{0.3} \quad \text{cm/s} \tag{4.5}$$

This second constraint also enabled an estimate to be made for the maximum grain size (D_{max}) which could be deposited to cover the entire channel length. The maximum distance travelled by a grain along the main channel was given approximately by $\bar{u}_{mb}\bar{d}/V_g$ (where V_g is the fall velocity of the solid, and was assumed to take the still water value, given for viscous sedimentation as

$$V_g = 1/18\ \frac{(\rho_s - \rho)gD^2}{\mu_w} = 9000\ D^2 \text{ cm/s for water at about } 20^\circ\text{C} \tag{4.6}$$

D_{max} was then given for the case when the maximum distance travelled was equal to the main channel length (10m), such that

$$\frac{\bar{u}_{mb}\,\bar{d}}{V_g} = 1000 \text{ cm.}$$

Solving for D_{max} using equations (4.5) and (4.6),

$$D_{max} \simeq 80\mu \qquad (4.7)$$

Although this estimate was very approximate, it was ~~in fact~~ found that the very fine sand grade (D = 110μ) could not be laid along the entire channel length.

From the 5 originally prepared grades of fluvio-glacial sediment ($D_{Foriginal}$ = 16.5, 26, 46, 82 and 110μ), only 3 were finally used for these granular experiments. The finest grade was not used, owing to lack of quantity after the micaceous friction had been removed. A 15μ grade, consisting of commercially cleaned crushed silica was therefore used in replacement (Plate 1).

Using equations (4.5) and (4.7), it was seen that $\bar{u}_{mb}$ required to lay the maximum grain size was about 17 cm/s. (The pump capacity was sufficiently large for this discharge requirement, since a maximum $\bar{u}_m$ of 20cm/s could be attained for d = 20cm.) It was finally noted that all depositions were conducted for sub-critical flow conditions, since

$$Fr_{max} = \frac{\bar{u}_m}{(gd)^{1/2}} \simeq 0.12$$

In summary, natural beds of 4 cohesionless, fine sediment grades were each laid by deposition under sub-critical flow conditions from a quasi-uniform suspension which never exceeded a initial average volumetric concentration, C_I, of about 0.05%.

4.1.2. Sediment introduction to the flume

Aliquots of sediment (W) were introduced at the downstream end of the flume. The grains were subsequently dispersed in the high turbulence region of the recirculating pipeline system, and finally

entered the main channel as an initially uniform suspension. For the largest grade used the introduction of sediment to the flume was made continuously in time, since the grains deposited in one channel transit. The sediment introduction rate, G_I, for this grade was then given by

$$G_I = \frac{W}{o} \bar{u}_{mb} = 17 \text{ gm.wt./s} \qquad (4.8)$$

The 3 smaller grades did not totally deposit in one channel transit. The following method of 'interrupted deposition' was therefore used. For one channel transit, the approximate distance of fall for a fine grain was given by $V_g o/\bar{u}_{mb}$. If it was (again very approximately) assumed that the recirculating weight of solids after one transit was then given by $W(1-V_g o/\bar{u}_{mb}\bar{d})$, then the remaining recirculating weight of solids after n transits was

$$sW = W\left(1 - \frac{V_g o}{\bar{u}_{mb}\bar{d}}\right)^n \qquad (4.9)$$

where s represents the fraction of remaining W.

For the purpose of these experiments, a value of s = 0.1 was selected before a successive introduction of W was made. The time scale for deposition could then be roughly estimated for each particular grade. For example, the 15μ grade required about 24 successive transits for s to become 0.1. The time for a 1kg. aliquot deposition was thus estimated as 12 minutes, and the total deposition time for 60kg. was 15 hours. (In practice however, a longer aliquot deposition time was necessary, owing to the feedback system incorporated in the pumping arrangement).

Aliquot depositions were made simply by hand, and the entire flume was covered throughout to reduce the possibility of water contamination from the debris contained in the laboratory atmosphere.

The above considerations for interrupted deposition show that the grades were never completely sedimented. It was therefore necessary to drain the flume slowly, after the near completion of a complete deposition (whilst reducing the discharge so as not to move the bed solids), to a minimum depth of about 2cm. The remaining solids were then removed by flushing the system with new water. The channel was finally re-filled to the first working depth for I.M. experiments.

4.2. Naturally-laid bed properties

4.2.1. Bed-surface contours

Despite the considerable effort taken in levelling the flume channel floor, it was shown in Chapter 1 that a significant rise occurred in the test-section reach of the channel; the floor contour about a single plane was increased to about $\pm 400\mu$ for this reach. It might be expected that this contour would be altered after superimposing a naturally laid bed of about 1cm. thickness. This was not the case. Fig. 4.1. shows the bed surface contour (as estimated from point gauge measurements) relative to the channel floor contour, along the channel centre line, for the finest and coarsest grades. Details of the floor contour were seen to influence that of the bed surface, for both grades. The observation indicated that approximately equal numbers of grains were deposited at every bed position, which inference further implied that a reasonable uniformity of initial suspension concentration had been achieved.

The bed surface contours in Fig. 4.1. are plotted relative to the channel floor, which in turn was kept at a fixed horizontal slope during the entire deposition process. It was seen that aggradation had occurred for the coarsest grade; this was due to the heavier grains of the grade depositing upstream during their first channel transit. The aggradation was less for the finest grade, since the heavier grains of this grade could be transported to any downstream position.

The flume aggradation process showed the necessity for measuring grain statistics at the actual position where I.M. was observed (i.e. at the 6m downstream channel-centre line position). Accordingly, samples were taken from this position at the termination of each experiment, and

the median D_F were recorded as 15, 30, 45 and 66μ; the sorting coefficients were less than those of the original grades, being 1.14, 1.15, 1.18 and 1.21 respectively.

The channel centre-line bed-surface contour over the test-section (4.25m to 8.25m downstream) for each grade, is shown in Fig. 4.2. Again the channel floor influence was significant, and the overall bed flatness condition was similarly about ± 400μ. It was possible that this variable contour could provide an additional form drag to the flow, but such an effect was (for lack of further information) assumed negligible. The linear regression of these bed contours, when drawn from the 4.25m downstream position, was seen to intercept the bed surface within ± 100μ at the 8.25m position. For this reason, the adjustment for quasi-uniform flow depth was made throughout by adjusting the flume slope so that equal depths were recorded at the 4.25 and 8.25m positions.

An additional, more localised estimate on bed flatness was made for the 15μ bed. Sixty-four point gauge measurements of the bed surface (accurate to within ±100μ) were made relative to a horizontal water surface, over a 30 x 30cm^2 bed area near to the end of the channel (Table 4.1.). If it is assumed that the recorded measurements were randomly distributed, then it was probable that 67% of the bed area was flat to within ±100μ, and 95% to within 200μ. (The quantitative estimate of a more localised flatness could not be made with the available equipment.) Close visual observation of naturally laid bed surfaces, by microscope, showed however a local flatness to within ±1D. (Similar estimates were made by Rees (1966), who resolved a flatness condition for 10μ silt beds to within 3D, using an ultrasonic depth gauge).

It was thus concluded that each bed was locally flat (to within ±1D) for areas of several square centimetres only, but not for the entire test section.

4.2.2. The volumetric packing coefficients

It was mentioned in Chapter 3 that the bed packing coefficient, C (equal to the ratio of the volume of solids to the total volume) was of importance in indicating the magnitude of maximum shear resistance of a granular bed. Since the packing properties of granular solids are also of interest to industry a considerable amount of empirical research has been conducted.

The theoretical C for systematic assemblages of equal spheres may take on a range of values. For example, when described in terms of geometrical symmetry, a loose packing for a cubic array gives C = 0.52, whilst a tight packing for a hexagonal array gives C = 0.74 (Graton and Fraser, 1935). Alternatively a mechanically stable packing has been proposed as describable in terms of the number of spheres which touch an individual sphere (the co-ordination number). C then ranges from 0.23 for a co-ordination number of 3 to 0.72 for 11 (Manegold and von Engerhardt, 1933).

Macrae and Gray (1961) have however shown that it is impossible to model regular arrays of spheres, owing to small departures of mechanical solids from equal sphericity and size. The haphazard packing of almost equal spheres thus takes a maximum C of about 0.65 (Brown and Richards, 1970). This maximum value varies considerably with solid shape and size distribution; it decreases to about 0.58 for a fairly uniformly sized sharp sand grade.

If the shape and size distribution of natural sand grades are considered to be roughly constant, it is to be expected that a variability

for natural packing exists with the condition of deposition. Graton and Fraser (1935) suggested that the intensity of deposition, I (defined as the mass of solids deposited per unit time and bed area), and the direction of impact velocity (V_D) of the settling solids were the controlling variables. Kolbuszewski (1950) demonstrated this quantitatively, using a fairly uniformly-sized natural sand grade (So = 1.3). He found that a maximum C of 0.64 was only attained for very low I and high V_D, in still air. For increasing I and any V_D, C asymptoted to a constant minimum value of 0.54. This minimum value was also recorded, for all his experimental I values, when depositions were conducted in still water.

It was further shown quantitively by Kolbuszewski that C for natural sands increased when a fluid shear stress was applied during deposition. It was however probable that during the fine grain deposition of these experiments, the added fluid stress was insufficient to increase C above the still water minimum value (0.54).

Since a grading and shape difference exists between the Kolbuszewski sands and the fine grains used for these I.M. experiments, it was necessary to measure the natural bed packing in situ. The overall bed depth for the 15μ grade, for a 30 x 30cm^2 area at the 9.5m downstream position of the flume channel, was estimated by 64 point gauge measurements; the sediment was subsequently removed by pipette and dried to constant weight. A value of C = 0.50 $\pm$0.1 was recorded, which was similar to that reported in Chapter 2.4.2. for sedimentation in still direct town-supply softened water. (This smaller value than the Kolbuszewski value (0.54) was expected, since these fine sediments were more uniformly sized.) It was thus seen that the packing coefficient for fine, cohesionless solid beds naturally formed in a shear flow, was considerably less than the maximum C of 0.65 for coarse solids in

air. This fact was shown to be of theoretical importance, in Chapter 3.4.3.

4.2.3. Angle of repose

The variability for angle of repose estimates have been discussed in Chapter 2; it was concluded that most results were useful for relative comparison purposes only, since the estimate depended on the method of measurement. The constancy of angle of repose estimates by White, S.J. (1970), was used to infer the cohesionless nature of fine quartz grains in distilled water. This inference was not however verified for the actual fluid condition used for his I.M. experiments. It was therefore necessary to repeat the experiments.

The electrolyte condition used throughout these further I.M. experiments was that of direct town-supply softened water. It was considered necessary to test for the constancy of angle of repose for this actual fluid condition, in order to verify the cohesionless nature of the solids.

The procedure used was that of slowly tilting a flat, sedimentary bed through 90° of arc, and recording the final angle which the free granular surface made with the horizontal (the angle determined was therefore a drained angle of repose, α, as described in Chapter 2). Small quantities of each grade were first naturally sedimented in still, direct town-supply softened water contained in 70cc cylinders of 2.5cm inside diameter. The cylinders were then stoppered, so as to exclude any air, and very slowly rotated through 90°. The final values for α (together with their standard deviations) were recorded as follows:

Sediment grade (microns)	15	30	45	66
α (degrees of arc)	27.5 ± 0.5	28.5 ± 0.5	29 ± 0.5	31.5 ± 1.0

Since these estimates were very close to reported values for coarse solids, it may be reasonably assumed that the fine grades behave as if cohesionless. (The values were however significantly lower than those recorded by White, S.J. (1970), who used a different technique and found α to be constant at about 36° for this size range.)

4.3. Experiments

4.3.1. Errors involved in the critical stress estimate

When an averaged critical stress is recorded directly, a systematic error may occur. This is because the averaged stress can only be applied incrementally, and I.M. may occur at a stress within the limits of this increment. For the case of recording the I.M. stress under gradually increasing stress increments (such as the technique used herein), the result will be significantly higher than the true mean value. Correspondingly, for the case of recording the I.M. stress for gradually decreasing stress increments, the result will be significantly lower. Accordingly, the experimental procedure should involve both methods. This may be possible for artificially-laid beds, but it cannot be so for naturally-laid beds, since bed forms develop for $\bar{\theta}_o > \bar{\theta}_{oc}$.

Owing to the low stresses involved in these experiments, the very small stress increments ($\delta\bar{\tau}_o$) were difficult both to apply and record. An increment of about 10% was found possible for the finest grades (which involved the lowest stress magnitudes). If it is roughly assumed as in section 4.1., that $\bar{\tau}_o \propto \bar{u}_m^2$, then the associated averaged velocity increment was given by

$$\frac{\delta\bar{u}_m}{\bar{u}_m} = \frac{\delta\bar{\tau}_o}{2\bar{\tau}_o} = 5\%$$

Since $\bar{u}_m$ was directly measurable using a propeller current meter, 5% increasing velocity increments were applied to the bed until the I.M. condition was observed. The averaged critical stress was then estimated by water depth and surface slope measurements. The average value for an infinite number of critical stress estimates, using 10% stress increments, will have a 5% high systematic error. It was therefore

only necessary, in practice, to take a sufficient number of estimates which would reduce the presumed random errors to about the same magnitude of 5%. The recorded average of these estimates thus corresponded to a finite magnitude of very low bed-load transport, which was accordingly approximated to $\bar{\theta}_{oc}$.

The measurement error associated with an individual shear stress estimate ($\bar{\tau}_o = \rho g \bar{d} \bar{i}$) was given by the sum of each associated error for $\bar{d}$ and $\bar{i}$. It was shown in Chapter 1 that very low slope measurements ($\sim$1 in 10^5) were in error of a few per cent. The depth measurement involved a further error, since it was determined by point gauge measurements, at each end of the test-section, of $\pm$0.01 cm resolution. An approximate idea incurred by this error was obtained by assuming the gradually varied flow equation

$$\bar{\tau}_{og} = \rho g \bar{d} \bar{i} \pm \rho \bar{u}_m^2 \delta \bar{i} \qquad (4.10)$$

where $\bar{\tau}_{og}$ represents the stress value associated with gradually varied flow due to the maximum non-alignment (denoted by the slope increment $\delta \bar{i}$) between the averaged water and bed surface. The error in the uniform depth value of $\bar{\tau}_o$ was then given approximately by

$$\frac{\delta \bar{\tau}_o}{\bar{\tau}_o} = \frac{\bar{u}_m^2}{g \bar{d}} \frac{\delta \bar{i}}{\bar{i}} = Fr^2 \frac{\delta \bar{i}}{\bar{i}} \qquad (4.11)$$

If the maximum slope error, $\delta \bar{i}/\bar{i}$, is considered as that due to depth measurement ($\pm$ 0.02cm) over the test-section of length 400cm, then

$$\frac{\delta \bar{\tau}_o}{\bar{\tau}_o} = Fr^2 \times 5 \times 10^{-5}$$

from which it was seen that the error was negligible compared with $\bar{i}$ errors of a few percent.

4.3.2. Observation of grain motion

All observations were made at the 6m. downstream position of the channel centre-line, using a travelling microscope of 15 times magnification. The apparent size of a 10μ grain was thus magnified to about 0.15mm, and proved difficult to resolve visually. An alternative procedure for I.M. determination was thus conducted for the 15μ grade (section 4.3.3.). The field of view for observation was constant at $2cm^2$, and the criterion used for deciding I.M. was that a minimum but consistent number of grains were in continuous motion.

The minimum number of moving grains at I.M. was estimated to vary from about 5 to 50, depending on the stress increment above $\bar{\theta}_{oc}$. The smaller number of moving grains were associated with the larger grades, and the range of moving-grain area ratio ($P_{Au_*} D^2/A$) varied from about 0.1 to 1.0%. (It is noted that a very large number of grains ~~areas~~ were being observed in the field of view, being about 10,000 for 15μ grains to 500 for 66μ grains). As expected, large increases in the moving-grain area ratio were observed for small stress increments above $\bar{\theta}_{oc}$.

The motion of individual grains of the larger grades was clearly visible. It took place near the bed, and trajectories were often interrupted, by settlement to the bed itself. This 'near the bed' motion contradicted the general supposition that fine grains become suspended in the entire fluid flow after they have been detached. It seems therefore that the motion takes place within the viscous sub-layer associated with a hydrodynamically smooth boundary. (Vertical turbulent velocity fluctuations, which may influence the upward motion of a saltating grain,

have been shown to be minimum within this layer.) Trajectory lengths could occur for distances of several millimetres, but no estimate could be made for their height.

4.3.3. Procedure

Five I.M. stress estimates were recorded for each grade (except the finest 15μ grade) using averaged flow depths adjusted incrementally from 2 to 10 cm. (Table 4.2). The flow was always fully turbulent for these conditions, the minimum Reynolds number ($\bar{R}e$) being about 4,500. ($\bar{R}e$ was estimated using $\bar{R}e = \bar{u}_m \bar{d}/\nu$, and $\bar{u}_m$ was measured at the channel centre-line using the propeller current meter at a depth of $y = 0.4\bar{d}$.)

As a test for reprducibility, the averaged I.M. stress estimate for the 5 observations was made three times, for 3 different bed depositions of the 66μ grade. Values of $\bar{\tau}_{oc} = 1.47 \pm 0.12$, 1.28 ± 0.13 and 1.38 ± 0.14 dynes/cm^2 were recorded, and these did not differ significantly at the 95% level of confidence.

Owing to the difficulty of visual resolution, the 15μ grade I.M. was estimated using a different procedure. After bed laying, the flow depth was adjusted to 6cm, then stress increments were applied for 6 hour periods until a transported load was observed to collect at the downstream end of the flume. It is seen from Table 4.2 that no motion was recorded for an absolute stress value of $\bar{\tau}_o = 0.52$ dynes/cm^2, but the next stress increment gave an observable collected bed-load which co-existed with the development of many, small scale scattered bed forms. Since these bed forms contributed to the shear resistance for this final stress condition ($\bar{\tau}_o = 0.69$ dynes/cm^2 after 6 hours), the I.M. stress was estimated as 0.56 ± 0.04 dynes/cm^2.

4.4. Interpretation of the results

4.4.1. Summary

These experiments were conducted for a very small range of viscosity, and a large range of flow Reynolds number (4,500 to 22,000).

The relative differences between bed-contour and I.M. water surface gradients are illustrated in Fig.4.3. and 4.4. (The vertical scale of these figures are very exaggerated, and the bed relief is in fact very low.) The local bed-relief was seen to be of the same order and sometimes larger than that of the superimposed water surface gradients; the concept of local uniform flow could not therefore be considered as established over the entire test-length.The hypothetical depth of a viscous sub-layer ($\delta = 7\,\nu/u_*$) is also plotted in the figures, using the same relative scale. This depth varied from about 60D for the finest grade to about 10D for the coarsest grade, and thus the flow boundary could be considered as turbulent-smooth throughout.

The $\bar{d}/D$ ratios were much larger than those usually associated with coarse sediment experiments; they covered a range from 300 to 3,000. Fig. 4.5 gives a plot of each I.M. estimate, normalised with the respective average value of the 5 estimates. ($\bar{\tau}o_5$), against the respective depth at measurement. It was seen that there was no obvious correlation. A similar result was noted by White, S.J. (1970), for a set of about 10 I.M. estimates for each of 16 grades, conducted for the range of $\bar{d}$ from 2 to 6cm.

4.4.2. Comparison with previous results

Fig. 4.6 summarises the published data for I.M. at low $\bar{R}o$ (referred to in Chapter 3.4.1.), together with the results of these further experiments, using the Shields' $\bar{\theta}_{oc}$, $\bar{R}o$ representation. The White, S.J. (1970) data has been recalculated using the depth alone in du Boys equation (since the hydraulic radius was originally used

instead of depth, for the shear stress estimate). It was seen that these further experiments confirmed the White, S.J. data (with consideration for the experimental scatter), together with his assumption for negligible cohesion with the sediment-electrolyte systems used.

With the exception of two grades of ballotini used by White,S.J. (of S.G. 2.90) and one grade of glass beads used by Vanoni (1964), the sediment types of Fig. 4.6. were those of natural silica sands. In contrast, there existed a large range of kinematic viscosity for the collected data, varying from 1.6. stokes to 0.01 stokes. Considering the subjective estimates for the I.M. condition, the large range of experimental equipment and fluid conditions, and the smaller range of sediment properties, the $\bar{\theta}_{oc}$, $\bar{R}o$ representation appeared to correlate the data fairly well.

As an approximation, the regression of $\bar{\theta}_{oc}$ on $\bar{R}o$ may express the functional relationship for $0.03 < \bar{R}o < 1.0$. The data of Table 4.2., together with that of White, C.M. and White, S.J. (Table 4.3) give the relationship as

$$\bar{\theta}_{oc} = 0.098\ (\pm 0.05)\bar{R}o^{-0.31(\pm 0.03)}$$

$$\text{hence} \qquad \bar{\theta}_{oc} \simeq 0.10\ \bar{R}o^{-0.3} \qquad (4.12)$$

(It is noted that the results for oil experiments are included in this regression for $\bar{\theta}_{oc}$ of naturally laid beds. Although the oil-grain beds were not laid under conditions of natural shear flow, their surfaces were naturally levelled by surface tension. Since the subsequent results agreed closely with the water experiments, they have been arbitrarily included).

A comparison of the data which is more relevant for field studies is given in Fig. 4.7. Here, the collected data for the I.M. of silica solids (density 2.65) under water at 20°C is given on a $\bar{\tau}_{oc}$ versus D logarithmic plot.

The above regression for fine grains then becomes

$$\bar{\tau}_{oc} = 25D^{0.6} \quad \text{c.g.s. for } 10\mu < D < 100\mu \quad (4.13)$$

in contrast to that for coarse grains ($\bar{\theta}_{oc} = 0.05$)

$$\bar{\tau}_{oc} = 80D \quad \text{c.g.s. for } D > 300\mu \text{ say} \quad (4.14)$$

These collected results are finally plotted in Fig. 4.8. with the original data used by Shields (1936) and the recent results of Paintal (1971), using the Shields parameters. It is reminded that the coarse grain data were obtained by extrapolating bed-load transport curves to zero, and that the extrapolated condition approximated to the shear stress necessary for the beginning of bed form development from a flat bed. (The Kramer (1932) data appearing in the original Shields diagram is therefore omitted in Fig. 4.8., since it was not obtained using the extrapolation procedure). It follows that, if the existence of a 'transition' region is denied, then the critical low-transport shear stress for naturally laid flat beds of maximum stability may occur, for different values of $\bar{R}_o$, within the dashed lines shown in the figure. It is finally noted that the empirical scatter associated with the low $\bar{R}o$ data is similar to that for $\bar{R}o > 10$ say.

CHAPTER 5. THE LOW-TRANSPORT CRITICAL STRESS FOR NATURALLY-LAID FINE, COHESIONLESS, FLAKEY SEDIMENTARY BEDS

5.1. Previous research on solids of various shapes

The first part of this Chapter reviews the literature on the incipient motion (I.M.) of various shaped solids other than the natural grain shape considered in the previous two Chapters. It is shown that coarse solids which depart slightly from a natural grain shape do not give a significantly different critical stress; such differences have however been recorded for extreme solid shapes such as two-dimensional slates or flakes. Accordingly, this research on low transport stages was extended to studying the extreme shape difference of fine mica flakes, and the experimental details for their initial stage of movement is reported in the remainder of this Chapter.

There are many occurrences of various shaped solids in nature. Fluvial examples are sharp-cornered granites, flints and two-dimensional shales and slates. Fluvio-glacial examples are gravels which have become faceted during glacial transport. Large quantities of non-granular, fine solids also exist, typical of which are the flaked micas used for these experiments.

5.1.1. The orientation influence of bed solids

Few detailed experiments have been conducted towards understanding the influence of particle shape at the beginning of sediment movement. The variable has however been usually acknowledged in theoretical proposals, both explicitly in the form of dimensionless coefficients, and implicitly in the form of 'angle of repose' and other terms. Perhaps the most comprehensive speculation on shape influence was given by Shields (1936). The frictional resistance of a single bed solid was

equated to the fluid force acting upon it, thus

$$\rho' g \gamma_1 \gamma_2 D^3 = f_{\gamma 5}[\mathrm{Rof}_{\gamma 4}(\mathrm{Ro})](\gamma_3 D^2) \frac{\rho u^2}{2}[f_{\gamma 4}(\mathrm{Ro})]^2 \qquad (5.1)$$

where γ_1, γ_2, γ_4, represent implicit shape variables and $f_{\gamma 3}$, $f_{\gamma 4}$ are explicit, since:

γ_1 = the bed porosity

γ_2 = a dynamic friction coefficient

$\gamma_3 D^2$ = an exposed normal area of the solid to the flow

$f_{\gamma 4}$ = a function determining the nature of the superimposed velocity distribution

and $f_{\gamma 5}$ = a function determining the drag coefficient of the solid

Despite the above complexity, ~~the author~~ Shields reduced the above equation to the well known form

$$\frac{\rho u_*^2}{\rho' g D} = f_\gamma(\mathrm{Ro}) \qquad (5.2)$$

and thus shape influence was only considered to enter the problem as a single functional variable.

It is however noted that equation 5.1. contains a term $\gamma_3 D^2$, which represents the normal incident area of a solid to the fluid flow. It follows that for non-spherical solids, not only will the coefficient γ_3 depend on shape, but also on the solid orientation. Meaningful experiments can therefore only be conducted if the orientation is controlled.

It is a feature of the following experiments using fine flakes that an orientation control was attempted. This was because the solids were deposited naturally from a water stream, and it is well known that a preferred orientation or 'imbrication' then exists (as shown, for example, by Rusnak, 1957). The following reviewed literature on coarse sediments show however that such precautions have not been previously adopted, since beds have been laid and smoothed artificially.

5.1.2. Previous research on coarse solids

Much of the early work on sediment transport has been summarised in the works of Schoklitsch (1914) and Forcheimer (1914). In particular, the former author considered that Kreuter (1898) was the first person to apply the du Boys estimate for shear stress to river beds of varying sediment type. Kreuter's field results indicated that the critical shear stress was larger for flat sediments (slates) than for rounded gravels. This result was however too vague for any physical principle to be deduced, since neither sediment size nor density were determined.

In accord with the above observations, Schoklitsch (1914) carried out laboratory experiments in a 10cm. wide flume, and recorded a similar shape influence. (It is considered that these series of experiments by Schoklitsch were classic. Not only did ~~the latter~~ he investigate the shape effect, but also the incipient motion of movable solids which were of a different size to fixed bed solids, and the movement of fully exposed spheres on a fixed rough bed). Schoklitsch concluded that the shear stress required to erode solids of equal volume (V) and density(ρ_s) was higher for flakey shapes than granular, and he gave the relation

$$\overline{\tau}_{oc} = (0.00385\,[\rho'\rho_s]\,\gamma_s V)^{1/2} \quad gm/cm^2 \qquad (5.3)$$

where γ_s represents a shape factor varying from 4.4 for slates, 3.1 for sharp edged grains, 1.26 for natural sand, to unity for spheres. These experiments were however conducted on artificially laid and levelled beds, over which there was no reproducibility of flake orientation or bed roughness (the significance of the latter is referred to later).

When the original data of Schoklitsch is plotted on a Shields diagram, using the nominal diameter D_N as the solid length scale, the results appear as in Fig. 5.1. This shape influence was also proposed by Shields (1936), who concluded that "the points for rounded grains and sharp-edged grains lie somewhat higher than those for angular grains".

A detailed study on 'elongate' grains was reported by Chang (1939) who proposed a different trend to that of both Shields and Schoklitsch. From experiments using 8 sieved sand grades (ranging from 8mm to 0.1mm. average geometric diameters) in gradually varied water flow, Chang estimated the uniform flow critical condition as

$$\bar{\tau}_{oc} = 0.009\left[\frac{e'}{e} D \gamma_c^{1/3}\right]^{\beta} \quad \text{lb/ft}^2$$

where D represents the average grain diameter in mm., and γ_c a shape factor equal to the ratio of the average longest and shortest geometric diameters of each grade. (The exponent β was found to take on values of 1 or 1/2 depending as to whether the ratio $\frac{e'}{e} D \gamma_c^{1/3}$ was greater or less than unity.) It was then considered that natural sand grains took a value of γ_c equal to 1.75, whereas spherical grains had γ_c equal to unity. The above relation thus indicated that natural sand grains had a greater critical stress than spherical grains, in contrast to

the Schoklitsch and Shields results.

A particular criticism of the Chang study is that the shape effect was not investigated independently. (Values of Υ_c decreased from 3.2. for the coarsest grade, almost monotonically to 1.37 for the finest grade.) Finally, it is again noted that artificially laid and smoothed beds were used for the experiments.

Not only has the 'elongate' or 'natural' granular shape effect been contradicted in the literature, but the extreme shape effect of 2-dimensional solids (flakes and slates) has undergone different experimental interpretation. A comprehensive study of slate movement was presented by Pang (1939). Five grades of sediment, varying in geometric face size from 6.28mm to 2.0mm were studied in water; the average aspect ratio (geometric flake face diameter divided by flake thickness) of the grades was about four. The I.M. results, when plotted on a Shields diagram using a dimension almost equal to the median face geometric diameter, were interpreted by Pang as being above the Shields curve. (It is noted however that the Shields curve given by Pang was significantly lower than the original curve given by Shields). A re-analysis of the Pang data, using the nominal diameter as the length scale, is given in Fig.5.1. It was then seen that the Pang flake data for 'weak' sediment motion was significantly lower than that of Schoklitsch and Shields. It is finally noted that Pang's experiments were once again conducted using artificially levelled beds.

5.1.3. Summary

As a tentative conclusion from coarse solid research, it appears that for solid shapes which depart slightly from a spherical form (and for which it appears reasonable to describe in terms of a single geometric length dimension), the shape effect on I.M. is undetectable amidst the

scatter caused by the other variables involved during the experiments. Such shapes are considered to be sharp edged grains, slightly elongate grains and model spheres.

For the case of extreme shape differences, such as two-dimensional slates, there appears to be significant differences between both grain results (when D_N is used to represent the solid length scale) and the results of different observers. (Fig.1). Although the contributions to the latter may be the different subjectives estimates of initial movement, together with different sediment aspect ratios, it is considered that individual particle orientation may have considerable effect. Since nothing is known about the surface roughness of artificially laid flake beds (caused by flake orientation) nothing is known of the real length dimension (L) which might possibly be associated with a surface layer of flakes. Since L appears in the dimensionless shear stress, $\bar{\theta}_o = \bar{\tau}_o/(\rho_s - \rho)gL$, there can be no physical interpretation for the slate experiments. It may in fact be the case that if the Schoklitsch and Pang results were calculated using their real surface roughness scales, the $\bar{\theta}_{oc}$ values would be identical.

With these conclusions in mind, it was decided to investigate the critical stress for grades of <u>flakey</u> solids. It has been shown that the behaviour of fine, cohesionless <u>granular</u> solids departs markedly from that which was presupposed (Chap.4). It was therefore expected that a two-dimensional shape influence may also be significant.

The above hypothesis was first tested for naturally-laid, <u>mixed</u> sediment beds, consisting of an original grade of fluvio-glacial sediment (Chap.2, 26μ grade) in the form of quartz and feldspar grains, and mica flakes under water. The fluid stress was slowly increased until movement began. It was observed that the mica flakes first

collected in quantity at the end of the flume; their incipient motion stress was thus lower than grains of the same fall diameter, for the natural roughness condition of this test. Experiments on flakey sediments alone were then conducted, and are described in the remainder of this Chapter.

(It is noted that the above observation of selective transport in mixed sediments is also of interest to geologists, and is termed as sediment bypassing (Eaton 1929).)

5.2. Laying a sedimentary bed by natural deposition

5.2.1. Flow conditions and sediment concentration

As with grains, the flow condition and sediment concentration during flake deposition would affect the bed fabric; the incipient motion condition and subsequent flake transport would likewise be influenced. To ~~enable~~ allow comparison, the bed laying procedure was similar to that used for grains, and similar for each flake grade.

The flume was first adjusted to the horizontal, and filled to 20cm. depth with softened, direct town-supply water. A small quantity of flakes (sufficient for a bed of several flake layers) was added to the recirculating flow at the end of the channel. The aliquot was well mixed in the recirculating pipeline system, and entered the main channel as an apparently uniform suspension, prior to sedimentation along the channel. During deposition, the fluid shear stress at the bed was slowly increased, by increasing the discharge, until bed forms began to develop. The discharge was then reduced by small increments, until bed form development ceased, and the remainder of the sediment was then slowly deposited for this condition.

The settling of fine sediment was discussed in Chap.4. Similar concentration criteria were applied for flakes, namely that their minimum linear separation, if uniformly dispersed in the channel, would be about 10 times the flake face diameter. The desired concentration was achieved by slow addition of 300g. aliquots at the end of the channel. (Ten such additions were required to lay the 3kg. total weight of each grade.) Each aliquot was allowed to sediment completely between additions, thus ensuring that the initial concentration was a maximum. The average bed thickness attained was about 1mm, and if the flakes were assumed to lie flat, then the bed would contain about 500 layers of the finest grade,

and about 100 layers of the coarsest grade.

5.2.2. Bed surface contours

It was shown for flume deposited grains that the bed contour was influenced by the channel floor contour. This effect was more pronounced for flakes than grains, since the bed thicknesses were only 1mm. as compared with the 1cm. granular bed thicknesses. Fig. 5.2. shows the bed contour from the 4.0 to 8.5 metre downstream positions at the channel centre-line for each flake bed. The reproducibility between each of two depositions of each grade and also between different grades was qualitatively apparent. The channel floor centre-line contour is also shown, and its influence on bed topography was noted.

The dashed lines in Fig. 5.2 represent the linear regressions of the bed contour, and are drawn from the bed contour at the 4.25m position. It was seen that the lines intercepted the bed contour near to the 8.25m. position, for almost every curve. This observation was used to facilitate the alignment of average bed slope with the flowing water surface. It was only necessary to adjust for similar depths at the 4.25m and 8.25m positions, in order to achieve average uniform flow.

The regression values for each of the flake bed contours, together with the channel floor slope showed that aggradation had taken place throughout. As with grains, this was probably due to the larger sizes in a flake grade being deposited upstream. Size analyses were conducted for the flakes at the position of incipient motion observation (6 metres downstream at the channel centre-line). The results are summarised in Table 5.1., together with the original data for each grade, as obtained before flume deposition. The original median fall diameters for each grade were seen to be larger than the 6 metre flume sample, as expected.

5.3. Angle of repose

5.3.1. Angle of repose for solids of various shapes

In similarity with the fine grain experiments, it was necessary to establish the cohesionless nature for the grades of fine flakes. This was done by again using an 'angle of repose' technique. The latter was applied in the light of previous α determinations for coarse solids of varying shapes, a brief review of which is now given.

General agreement exists in the literature concerning an increased angle of repose (α) with increased angularity or surface roughness of solids. Van Burkalow (1945) noted the increase with angularity alone, from a survey of six different literature sources. From his own experiments he recorded values of the 'drained α' ranging from 16° to 54°, for various wooden shapes (ranging respectively from spheres of 2.5cm diameter to cubes ~~with octahedral faces and~~ of similar size). In contrast to the above large range of values, Lane (1953) concluded, for a limited number of laboratory determinations together with observations of gravel stock piles, that the range for 2.5cm solids of increasing angularity was only between 32° and 39°. It was furthermore proposed that the α magnitude and range was dependent on solid size, and became 18° to 32° for 0.5cm sized solids.

A large difference in observation is therefore apparent. It is considered however that this is inevitable, since the natural occurrences of differing solid shape, surface roughness, size, density, deposition condition and subsequent bed fabric are infinite. Furthermore, the general proposal that α increases with angularity is questionable. For example, if two dimensional flakey solids are deposited so as to lay flat, their angle of repose may well be less than that for grains, of equal surface roughness.

5.3.2. Measurement for fine flakes

It might be expected that the gravitational instability condition for flakey solids (as determined by an angle of repose technique) is similar for beds of similar flake arrangement and orientation. This idea was tested for the naturally laid flakey beds used in these experiments.

Part of each grade was deposited in similar flow conditions to that described in section 5.2.1., onto 4 glass plates (30cm by 5cm) laid on the channel floor near to the 6 metre downstream observation point. With the flume water stationary, the plates were then very slowly raised by their upstream edges, until avalanche of the flakes began. The angle of the plate at this position, with the horizontal, was recorded as the 'limiting static angle of repose'. (The surface of each plate was permanently roughened by coating with 150μ sand, thus ensuring that flake shear did not take place at the smooth glass surface.) Avalanche sometimes began over several areas of the plate, but the determination was repeated in circumstances where it began near the plate edges.

The results are recorded in Table 5.1. It was seen that the limiting static α was fairly constant at about $40^{\circ} \pm 2^{\circ}$, with the exception of the finest grade. It was therefore concluded that the associated bed fabric was similar throughout. The observed constancy of α for the larger grains was also used to infer that these solids behaved as if cohesionless (in accord with the grain experiments), whilst the increase for the finest grade indicated that it was weakly cohesive for the particular water chemistry of this test.

5.4. Incipient motion experiments

5.4.1. Procedure

The experimental procedure for each flake sediment grade was similar. Visual observation of the incipient motion condition was made throughout, using the same criteria as that described for the grain experiments (Chapter 4). Likewise, bed stress increments were applied and estimated as per the previous grain experiments, so their detail is omitted in this Chapter.

Ten critical stress estimates were made for each grade; they consisted of 5 measurements each for the same bed. Observations were first made using water depths varying incrementally from about 10 to 8, 6, 4 and 2cm. The grade was then re-deposited and the observations repeated. This procedure was a test for reproducibility. Since the bed contours measured for each deposition have been shown to be similar (Fig.5.2), it was expected that the average critical stress would not show any significant difference between depositions.

5.4.2. Observation of flake motion

The initial movement of fine flakes was easier to detect visually than that of grains, due to the high intensity of reflected incident light from the smooth flake faces. It was possible to visually resolve every grade, since the minimum flake face diameter, on magnification of 15 times, was about 0.5mm size to the eye.

A small transport of flocculated material sometimes occurred prior to the incipient motion of individual flakes; the flocs probably consisted of the inevitable residual fines which remained in the flow after deposition of the grade. For each occurrence, the fluid stress was maintained until floc transport had ceased. (The eroded flocs collected at the downstream end of the bed, and did not become resuspended by the flow due to flume geometry.) It was of interest to note that the critical stress for these

flocs was normally less than that of the individual solids; an idea of the stress was obtained from the finest grade, since floc transport began slightly below (about 10%) the stress required to erode individual flakes of this grade.

The movement of individual flakes could be observed quite clearly for the larger grades. Some flakes appeared to 'glide' above the bed before coming to rest; others were seen to overturn during transport, whilst a combination of both overturning and subsequent gliding could also exist. These motions are similar to those of coarse graded flakes in water. A translation of Pang (1939) describes flake movement as follows:

"For low values of average velocity, flat sediment moves principally by large, gliding jumps, and sometimes turns about a horizontal axis in the glide level (during which the full flake surface faces the flow). For larger values of average velocity, more particles move and rotate."

Unsteady flow conditions during incipient motion were easily discernable, since flake erosion then alternated with no flake motion. Such conditions were avoided by allowing suitable time durations (about 15 to 30 m) between the application of stress increments. For the finest 3 grades however, observation at the shallowest depth were made in the transition region between laminar and turbulent channel flow ($\overline{Re} \simeq 2500$). Irrespective of the time duration allowed, the flakes moved discontinuously. It appeared that for the same discharge, the channel flow could alternate from a laminar condition (for which no flakes moved) to a turbulent smooth boundary condition (for which flakes moved continuously). Although the averaged stress estimate was recorded for this condition, the result was not included in the final

average of the remaining 8 results for each of the finest 3 grades.

5.4.3. Results

Figures 5.3 and 5.4 give examples of 5 water surface gradients (for the smallest and largest grades) which were measured for a single bed deposition. The particular bed contour is shown on the same scale, together with the proposed thickness of the viscous sub-layer($7\nu/u_*$). The flows were thus hydrodynamically smooth for all the turbulent flow experiments. As with grains, it was assumed (for lack of further detailed information) that the averaged bed stress around the 6m. channel centre-line position of observation was equal to the time and spatial average over the 4.5m measurement section.

Table 5.2 gives the complete results of the experiments. For the whole series, temperatures varied from 20 to 24°C, depths from 2 to 10cm., and depth Reynolds numbers from 2,000 to 16,000.

Fig. 5.6 shows a plot of the critical stress for each observation, normalised with the respective average of the 8 or 10 results for each grade, against the particular flow depth at measurement. It was seen that the results for each deposition corresponded fairly closely (36 of the 54 results corresponded within the limits of their respective standard deviations). The line through the mean of each stress indicated that there was no significant correlation of critical stress with depth.

5.5. Interpretation of results

The low transport critical shear stresses for the flake grades ~~is~~ are plotted in Fig. 5.6, using the median fall diameter (D_F) to describe each grade. It was seen that the trend for decreased $\overline{\tau}_{oc}$ with D_F was not followed by the finest grade, since the latter had been shown to be weakly cohesive for the particular water chemistry of these experiments. The regression of $\overline{\tau}_{oc}$ on D_F gave

$$\overline{\tau}_{oc} = 16.3\, D_F^{0.65} \text{ c.g.s. for fine flakes} \quad (5.4)$$

which was noted to be significantly lower than that for fine grains given in Chapter 4 as

$$\overline{\tau}_{oc} = 25 D_F^{0.6} \text{ c.g.s. for fine grains} \quad (4.13)$$

The result shows that fine grains and flakes which behave similarly in a still fluid (so as to have a similar fall velocity) do not behave the same at the beginning of transport under a shear flow. The generally accepted use of fall diameter, for describing the transport of any shaped solid in a shear flow, therefore needs modification.

As noted at the beginning of this Chapter, it is difficult to assign any single length dimension to two-dimensional solids, with the view to describing the physical roughness associated with the bed. This problem is illustrated in Fig.5.7., in which the Shields representation is plotted using different length scales (D_G, D_N and T) associated with each grade. No physical comparison could therefore be made between the non-dimensionalised grain and flake data.

The coarse solid flake results of Schoklitsch (1914) and Pang (1939) are summarised, together with these fine flake results, in Table 5.3.

The coarse solid results are also plotted in Fig. 5.7, in an attempt to produce a design curve for the critical stress of all cohesionless flakey solids. With regard to the difference between fine and coarse flake experiments of bed laying procedures and different solid aspect ratios, the design curve, using the nominal diameter D_N as a convenient length scale, is proposed.

It is finally noted that the procedure of representing the roughness of loose boundaries composed of two-dimensional mobile solids is the same as that for fixed boundaries of varying shape and spaced roughness elements. A convenient (though physically inadequate) empiricism to the fixed boundary problem has been made by defining an "equivalent sand roughness" scale (Schlichting, 1968). In like manner, an "equivalent grain critical roughness" length scale may be defined, for which the flake incipient motion curve superimposes on the grain incipient motion curve. For these fine solid results the "equivalent grain critical roughness length" for flakes was calculated from Fig. 5.7 as $L_E = 0.32\ D_N$.

CHAPTER 6. BEDFORMS ASSOCIATED WITH LOW TRANSPORT STAGES OF FINE, COHESIONLESS, GRANULAR AND FLAKEY SEDIMENTS

6.1. Bedforms associated with the movement of coarse granular sediments

This Chapter reports the low transport stages of fine cohesionless solids, from the incipient motion stage to that for which the solids enter fluid suspension. Particular attention is paid to the bedforms associated with the transport, and since these are compared with coarse grain ($D > 150\mu$ say) bedforms, a general description of the latter is first given (together with major associated problems). The second section of this Chapter then deals explicitly with fine granular sediment research, whilst the final section details experiments using the fine flake grades.

6.1.1. General description

A rough description of the sectional geometry (in a plane parallel to the flow and normal to the bed) of bedforms was given by Du Buat (1786). It was that of a triangle whose upstream slope was gentle, and whose downstream slope was steep and sheltered from the fluid's action (the downstream slope was thus recognised as an angle of repose). Deacon (1894) carried out flume experiments and described bedform development from a flat bed in terms of the water surface velocity ($\bar{u}_s$). He observed their initial development with increased $\bar{u}_s$, and noted a subsequent change to irregularity of the features (this was presumably a change from low triangular forms which extended across the flume width and which will be referred to as transverse or two-dimensional forms, to three-dimensional forms which do not extend across the flume width). With further increases in $\bar{u}_s$, the forms disappeared to leave a flat bed with grain transport (which occurrence has commonly become known as bedform 'transition').

The Deacon experiments were repeated by Blasius (1910) and the bedform development was then described according to the flow's average Froude number, $\bar{F}r = \bar{u}_m/(g\bar{d})^{1/2}$. Transition was observed for $\bar{F}r = 1$, and a different configuration was observed for $\bar{F}r > 1$. This new configuration was later described in detail by Gilbert (1914), and named 'antidunes'. (In contrast to $\bar{F}r < 1$ bed forms which migrate downstream, antidunes could migrate upstream by a process of erosion from their downstream faces; their profiles were also seen to be in phase with the water surface.)

In summary to 1914, bed-forms were thus classified from the beginning of movement, as transverse and three-dimensional triangular forms, a flat bed with sediment motion at $\bar{F}r = 1$, and antidunes for $\bar{F}r > 1$. Recent research has been applied to further subdividing the triangular forms into 'ripples' and'dunes', and the $\bar{F}r > 1$ forms into sinusoidal, wavy and other geometrical forms (for example, Guy et al 1965). In accord with such subdivisions, attempts have been made (usually using dimensional analysis), to describe the associated flow conditions. For example, in analogy to the deterministic representation for the beginning of sediment movement, it may be proposed that $\bar{F}r$ be introduced into equation 3.2, such that a bed form type, B_F, is given by

$$B_F = B_F(\bar{\Theta}_o, \bar{R}o, \frac{\bar{d}}{D}, \frac{\rho_s}{\rho}, \bar{F}r) \qquad (6.1)$$

Many two-dimensional graphical attempts have been made for predicting B_F, using combinations of the above parameters. These have been recently summarised by Simons and Richardson (1971), and it was concluded that a 2-parameter representation alone was insufficient for accurate prediction.

In contrast to the above idea, it has been proposed by Yalin (1972) that antidune forms say, can be solely predicted by $\bar{F}r$. This proposal stemmed from the work of Binnie and Williams (1966), who showed that for $\bar{F}r > 0.5$ a geometric discontinuity at a channel bed could cause surface waves whose wavelength increased with $\bar{F}r$. Their observations were extended by Yalin to $\bar{F}r = 1.1$; he also proposed that the surface wave geometry was independent of the causal bed discontinuity. It was then estimated that the surface wavelengths, for given $\bar{F}r$, agreed with antidune wavelengths at the same $\bar{F}r$. Yalin thus concluded that the sole cause of antidunes was surface waves, which were in turn propagated by any independent discontinuity at the bed.

The above contradiction of ideas, for antidune formation say, permeates throughout the literature for almost any aspect of bedform mechanics. Typical of these aspects are the causes for initial bedform occurrence, and the proposed distinctions between ripples and dunes.

6.1.2. The initiation of bed forms from a flat bed

There appears to be two types of ideas proposed for the instability mechanism which causes initial bed form occurrence from a flat bed; these are classified herein as 'layer theories' and 'grain-pile discontinuity theories'. The latter type appears to be the most favoured in recent literature.

The layer theories may be further subdivided into single-layer and double-layer classes. For example, a double-layer type was based on the Helmholtz (1888) instability which considered that two adjacent fluids of different densities, moving with different velocities, were subject to interfacial waves. Baschin (1899) proposed the instability

to apply for sand beds, with the layers being respectively that of a moving sand-fluid mixture, and the superimposed clear fluid. An alternative way of proposing this idea was given by Darwin (1883), who stated that

"the layer of transition between 2 currents of fluid is dynamically unstable, but if a series of vortices be interpolated, so as to form friction rollers as it were, it probably becomes stable."

A double-layer instability mechanism was also proposed by Bagnold (1956), by analysing the stress equilibrium at the base of a statistical, coplanar, immobile grain surface layer and a superimposed moving grain-fluid layer. A non-equilibrium condition was considered to exist for the case when the dynamic coefficient of resistance of the moving layer exceeded its static coefficient of resistance by a given amount; if this occurred, an additional resistance created by bedforms was necessary to achieve equilibrium. In a recent publication however, (Bagnold 1973), the quantitative estimate for these coefficients of resistance have been reconsidered; the quantitative estimate for the instability mechanism therefore remains questionable.

A further double-layer instability mechanism was postulated by Liu (1957). For the case of turbulent-smooth boundary flow, the layers were those of the stationary bed and a hypothetical 'laminar sub-layer'. The instability mechanism of Helmholtz was assumed to operate for this condition, and the subsequent onset of bed-forms was proposed to be represented by the 2 parameter system u_*/V_g and $\bar{R}o$ (where V_g represents the fall velocity of the solid). As noted in Chapter 3 however, it is doubtful that any aspect of solid behaviour in a 2-dimensional flow can be successfully described in terms of the solid behaviour in a one-dimensional flow (as implied by the use of Vg).

Single layer instability mechanisms for the initiation of bed forms may be visualised by considering some spatially cyclic variation in sediment transport rate, which in turn gives alternate erosion and deposition at the bed. Two main ideas have been proposed for the cause of such variations, both of which attribute it to superimposed flow movements. Velikanov (1936) and Tison (1949) considered that the flow movements were large scale turbulent velocity fluctuations, whereas Anderson (1953) considered that they were caused by the influence of free surface waves. (This latter idea re-introduces the concept of $\bar{F}r$ being directly correlated with B_F, and accordingly, lengthy mathematical models have been developed from this assumed physical principle, for example by Anderson (1953), Kondratev (1962), Kennedy (1963)). As noted by Liu (1957) however, the influence of free surface waves cannot explain the observations of ripple formation under deep flow conditions for which $\bar{F}r \ll 1$.

Finally, recent attention has been focused on the grain-pile discontinuity theories. This idea was described by Vanoni and Brooks (1958) as

"when an eddy sweeps down to the bed, particles on the bed are disturbed. Where the particles are piled a few grains higher than the initial surface a small wake develops which makes the particles immediately downstream more likely to be entrained.....with a regular ripple pattern developing from a random turbulent motion."

A chance grain pile is thus formed by fluid turbulent motions, and the single discontinuity leads to bedform propagation downstream. Raudkivi (1963) added to this idea, by proposing that the discontinuity could be caused by sheltering (during which the relative velocities of moving particles may be such that they group by chance), by the non-movement of larger more resistant grains, as well as by turbulent fluid

motions. He also considered the downstream wake of the form to be similar to that of flow over a 'negative step'. In particular, the main flow separates from the crest or top of a discontinuity and reattaches at a point downstream; the increased turbulence at the reattachment point causes excavation of more material, hence another form is developed and the process is propagated downstream.

An alternative mechanism for grain pile formation has been proposed by Williams and Kemp (1971). The initial grain transport over a flat bed was observed to be in finite lanes of solids moving parallel to the flow (a bedform commonly referred to by Geologists as 'primary current lineations'). Sometimes, the leading edge of one lane coalesced with that of another, and the grain pile discontinuity was formed.

A usual argument for and against the validity of layer-type and grain-pile discontinuity type theories is that the former should occur instantaneously whereas the latter is time dependent on the propagation downstream of the discontinuity; the argument is usually associated with observation. For example, Liu (1957) proposed his layer theory since "ripples appeared suddenly at the bed at certain flow conditions", whereas Mercer (1964) observed that

"the flow was increased to well above the level of incipient motion without ripple development occurring. A very small bed disturbance began at a point where two of the glass wall panels abutted, and from this point ripples spread out downstream".

Such observations are however insufficient proof of any particular mechanism proposed. For example, a grain-pile discontinuity may in fact be formed from a localised double or single layer instability. Alternatively, the chance piling of grains may occur simul-

taneously at several or many positions on a flat bed. The problem as to how bedforms are initiated from a flat bed therefore remains open.

6.1.3. The distinction between ripples and dunes

The subdivision of low $\bar{F}r$ bedforms into ripples and dunes has also been a subject of much controversy. Generally, a distinction is made on the basis that ripples are geometrically smaller bedforms than dunes. A typical observation with increased $\bar{F}r$ above I.M. is that of small scale forms (ripples), then large scale forms (dunes) upon which the small scale forms may be superposed. For example, Inglis (1949) stated that

"In the case of a ripple there are no secondary ripples on the upstream slope, whereas small secondary ripples appear at times on the upstream slope of dunes."

These observations were endorsed in detail by Guy et al (1965), and it was further observed (as proposed by Bagnold 1956) that small scale forms do not occur in water flows for solid sizes > 0.7mm. The latter observation has led to the general idea that ripple statistics are governed by solid size, whereas dune statistics may be governed by depth of flow (since their size may be assumed to grow indefinitely until limited in an open-channel by reason of flow continuity). For example, Allen (1970) gave a relation for the average ripple wavelength ($\bar{\lambda}_r$) and average dune wavelength ($\bar{\lambda}_d$) from the data of Guy et al (1966) as

$$\bar{\lambda}_r = 1000\ D \qquad (6.2)$$

and

$$\bar{\lambda}_d = 5\bar{d} \qquad (6.3)$$

Similar empirical relations were also given by Yalin (1972) from a larger source of data. It is seen that the above relations form part of eq. (6.1); it was considered by Simons and Richardson (1971) however that 2 parameter representations were inadequate.

A further proposed distinction between ripples and dunes is that of their plan geometry, namely whether they appear two or three dimensional. Typical of the contradictions which arise over this distinction are:

"Ripples form irregularly, whereas the crest of a dune stretches across a considerable width of the bed" by Inglis (1949).

"Ripples are two-dimensional to the extent that an individual ripple can be traced for some distance normal to the flow" whereas for dunes "their two-dimensional characteristics are less pronounced, as they seldom extend laterally a distance greater than their length" by Mercer (1971), and

"A ripple configuration can vary from an irregular array of three-dimensional peaks and pockets to a regular array of continuous parallel crests and troughs" by Kennedy (1966).

Several ideas have been proposed to explain these differences in plan geometry. The most common appears to be the influence of the laboratory flume width. There is no doubt that a bedform will appear two-dimensional if the flume width is less than the average bedform width. However, two-dimensional ripples can occur on very large natural scales (Allen 1968), for which the boundary width is seemingly infinite.

Alternatively, it has been proposed by Yalin (1972) that the three dimensionality of forms depended on whether the superimposed flow could meander. Such a meandering was considered probable for the slower flows for which ripples propagate. The idea thus implied that ripples were

three-dimensional, whereas dunes were two-dimensional; it does not therefore explain the observation of three-dimensional dunes.

In contrast to the above descriptive and empirical distinctions which seemingly influence bed form types, physical instability mechanisms were proposed by Bagnold (1956) as providing the distinctions. The ripple form was first subdivided into a primary and secondary system. The primary system was initiated by reason of the double-layer frictional instability mechanism, and a"first and minor secondary effect" for an increase in applied fluid shear stress, "should be a general rounding of the ripple cross section" from its triangular profile. At some critical state however,

"with increase in the up-tilt of the ripple faces, the fluid flow close over the alternate down and up faces must become appreciably diverging and converging, and its turbulence should therefore be alternatively stimulated over the hollows and suppressed over the up-slopes. Once scouring occurs in the hollows, these will tend to deepen."

A new and secondary ripple system is therefore developed, whose form drag considerably exceeds that of the primary system. (It follows that the increased bedform resistance is associated with a reduction in bed-load transport rate, and this was demonstrated by Bagnold, using the data of Gilbert (1914) and U.S.W.E.S. (1935).) It therefore seems probable that any change from two-dimensional to three-dimensional ripple forms will be associated with this secondary instability mechanism caused by local scour.

Dune formation was also considered by Bagnold as the result of a different physical mechanism. In similarity with the single layer instabi-

lity mechanism, dunes were assumed to form as a result of cyclic changes in sediment transport rate. The initial cause for a change was any local increase in bed slope (β). A lag distance was then considered to exist between the position of increased β and the eventual deposition of sediment downstream. Since the deposition further increased β, dunes were built up whose length scale was determined by the lag distance.

In summary therefore, it appears that most observers are agreed on a general, qualitative subdivision of low $\bar{F}r$ bedforms, (for $D <$ 0.7mm in water) into small scale ripples and larger scale dunes. The initiation of ripples is not yet understood, but their subsequent change from transverse to three-dimensional appearance is possibly caused by a secondary instability of localised scour. With increased sediment transport, the dune form develops and attains a maximum size which is determined by the overall flow condition (which demands continuity).

It is finally considered that much of the confusion arising from bedform studies is due to the fact that the subject is not examined explicitly. Most observations are made as subsidiary to general experiments on sediment transport. It may be possible that many contradictions may be overcome by comprehensive investigations using varying solid size, shape and density, varying fluid viscosity and density, for both open-channel and conduit flows. As a prelude to such investigations, the bed-forms resulting from low transport stages of granular and flakey fine solids are now presented.

6.2. Bedforms associated with low transport stages of fine, cohesionless granular sediments

6.2.1. Previous experiments

There appears to be only one previous investigation into bedforms associated with cohesionless, fine sediments, namely that by Rees (1966). A uniformly sized 10μ fluvio-glacial granular silt was used for this study; the silt mineralogy was similar to that used for the experiments of this thesis. (The laboratory water used was of very low salt content, hence it was reasonable to assume that the system was cohesionless.) Naturally laid beds were formed in a recirculating flume (similar to those described in Chapter 4), and the subsequent development of bedforms was observed with increased fluid stress.

Two major limitations were however inevitably incurred during the course of the above investigation. Firstly, the recirculating flume was short (2.5m in length), so the sediment could not be totally deposited at the channel floor within a practical time duration of several hours. The subsequent development of bedforms could not therefore be observed continuously by direct visualisation; and an ultrasonic depth gauge was used for their assessment. Secondly, the fluid slopes encountered during the experiment were very small ($\sim$1 in 10^5) and they could not be estimated accurately for so short a flume. The bed shear stress was thus approximated by assuming the Karman-Prandtl logarithmic law of flow together with the measured average flow velocity. It is seen therefore that although the shear stress records subsequently reported were considered constant, for an experiment of constant discharge, it was inevitable that $\bar{\tau}_o$ increased with bedform development.

The first observation by Rees was that primary ripples could form at $\bar{\theta}_o = 0.1$, provided an excess amount of suspended solids was maintained in the flow. This observation apparently contradicts the experiments reported in Chapter 4. For the latter case, a sediment bed was initially formed, under slow deposition at constant averaged stress, from a suspension of solids; the critical stress for primary rippling was then estimated as the I.M. critical stress, being $\bar{\theta}_{oc} = 0.23 \pm 0.02$ for 15μ grains. There exists however a difference between these two experiments. For the Rees experiment, an initial bed was formed by depositing the sediment under conditions of the lowest stress attainable ($\bar{\theta}_{ob} \ll 0.1$); this stress was subsequently incrementally increased to $\bar{\theta}_o = 0.1$ whilst further sediment was added to the flow. For such a case, the continuously depositing bed was unstable to the incrementally increased stresses, and it was possible that such instability influenced the subsequent ripple development to occur for a lower critical stress than $\bar{\theta}_{oc} = 0.23$. (Such an explanation may however be one of many. For example, the excess concentrations of sediment introduced in the flow were higher in the Rees experiments ($\bar{\lambda} \simeq 5D$); this may lead to increased bed load movement for lower relative stresses. Alternatively, the difference may be partially caused by the different methods of stress estimation).

Following the determination of I.M. stress, the development of primary ripples was observed by Rees for two conditions of constant fluid discharge (for which the initial flat bed stress was estimated as $\bar{\theta}_o = 0.20$ and $\bar{\theta}_o = 0.26$). When an excess of sediment was continuously added to the flow for a period of about 20 hours, the original, very small, irregular array of primary ripples developed into transverse primary ripples whose crests extended across the entire flume width of

17cm. However, when the excess sediment supply was terminated for both these runs, the ripples surprisingly disappeared after a period of about 10 hours, leaving an almost flat bed surface covered with erosional markings.

A final constant discharge run, for which the initial flat bed stress was estimated as $\bar{\theta}_o = 0.39$, produced two new sets of bedforms. The first configuration was identified as secondary ripples, and these resulted after a period of 8 hours erosion without addition of sediment to the flow; their maximum height was about 1mm. (Although these secondary features appeared transverse in the small width flume, it is possible that they would appear three dimensional in a wider flume.) The second configuration was observed with the further addition of sediment over a period of 19 hours. Since the maximum height of their associated bedforms was considerably greater than secondary ripples (being about 6mm), it was probable that their size was governed by the flow depth and the limitation of sediment bed depth. Small transverse ripples appeared to be present on the upstream faces of these largest features, and it seems that the form was of the 'ripple on dune' type.

In summary, these fine silt experiments for low $\bar{F}r$ have tended to confirm the idea of a secondary ripple form, as proposed by Bagnold (1956). It appears that for conditions of low constant discharge and excess sediment load, primary ripples can develop; they are subsequently eroded when the excess sediment load is terminated and $\bar{\theta}_o$ does not exceed an initial, flat bed value of the run which was somewhere between $\bar{\theta}_o = 0.25$ and 0.39. When this value is exceeded however, secondary ripples develop which can not be eroded to leave a flat bed. In the light of these observations, it was decided to conduct similar experiments at low $\bar{F}r$, using both the 15μ and 66μ granular grades, in order

to extend the above work.

6.2.2. Limitations of these experiments

By use of a long 10m flume, the two major limitations to the Rees experiments could be overcome. The deposition of fine sediment beds has been described in detail in Chapter 4, whilst the estimation of low applied shear stress was given in Chapter 1.

Since both the 15μ and 66μ grades were deposited so as to leave a clear water flow it was possible to observe initial bedform development visually. The condition of clear water flow precluded however the opportunity of establishing a true bedform equilibrium condition, which was in turn applicable for a bed of infinite length. This was because the usual procedure for re-introducing eroded sediment, from the downstream end of the channel to the upstream end, was not followed. Had such a procedure been adopted, the reintroduced sediment would then obscure the bed. The developing bed forms during these experiments were therefore associated with the constraint of restricted bed-load transport, and their observation was accordingly interpreted. It was considered however that for the initial low transport stages, the constraint was not completely restrictive towards extrapolating observation to that of an equilibrium condition.

A second constraint imposed on these qualitative observations (and similar to that of the Rees experiments) was that an experimental 'Run' was conducted for the condition of constant discharge. An averaged depth of 6.0±0.2cm. was used throughout, whilst constant discharges were applied for about 24 hour periods (to constitute a 'Run'). Again, it was considered that the observed bedforms were not necessarily equilibrium states. This was because the usual procedure for producing an equilibrium condition involves the reduction of fluid discharge (for example Brooks, 1955, Raichlen and Kennedy 1965) with bedform development,

such that the fluid surface slope (and consequently the total bed shear resistance) remains constant for a given bedform. An equilibrium condition, for clear water flows, can thus be considered to exist for the condition of constant fluid power ($\bar{\tau}_o \bar{u}_m$), whereas these experiments were such that the fluid power changed with the bedform. It was found during the experiments however that $\bar{\tau}_o$ varied minimally for certain development stages and an equilibrium state could accordingly be speculated.

It is finally noted that two major difficulties exist for any bedform observation experiment, and these are not always acknowledged in the literature. The first is the influence of flow disturbances at the channel entry on the subsequent bedform development. Many different procedures have been used to minimise this effect. For example, Liu (1957) completely removed that part of the bed near to the channel entry (thus creating a new flow disturbance at the downstream start of the displaced bed). Other workers have 'solidified' that part of the bed near to the channel entry. It is inevitable however that some flow discontinuity must exist or develop from the entry of a channel of finite length. It follows therefore that only a compromise can be achieved in reducing the flow disturbance magnitude. For these experiments on naturally laid beds, the compromise was that of protection from channel entry erosion by natural selective deposition. (The latter was caused by the upstream deposition of the larger solids in a grade). Although the channel entry was designed to encourage a uniformly accelerating flow into the main channel, an entry discontinuity remained. The influence of localised channel entry erosion was therefore particularly noted; it was however subsequently confirmed that the initial stages of bedform development were totally unaffected by entry conditions.

The second difficulty for bedform experiments is that of having a sufficient sediment supply. This was found to be the case for these experiments (since an initial bed depth of about 1cm was used), and the final equilibrium state of bedform development was determined by this constraint.

6.2.3. Observation of bedform development

A summary of the experimental details, together with bedform observations (including those at the channel entry) is given in Tables 6.1. and 6.2. Plan view photographs of the bed for various stages of development, covering a 45cm x 30cm area at the 6m downstream position, are given in Plates 4, 5 and 6. The bedform types of both the grades were similar, and the 15μ grade bed development is now described in detail. In accord with Francis (1973), the bedform development is described as the bedform 'stage'; this is herein defined quantitatively by the ratio of applied shear stress to the incipient motion shear stress, and is further qualified as the'stress-stage'.

The discharge for Run 1 was set such that the stress-stage was initially slightly greater than 1.0. After 2 hours, a primary ripple system of very small forms, covering the entire bed area of the test section, had developed (Plate 4.1). The bed configuration was similar to that observed by Rees, for the first development of ripples when sediment was continuously added to the flow to give an excess concentration of total load. It seems therefore that this configuration was independent of any excess concentration of sediment load. Associated with the primary ripple system was a significant increase in total bed shear stress resistance to almost double the incipient motion stress (stress-stage = 1.8). It was also noted that the

qualitative observation of equal size for these forms implied that they had all developed at about the same time.

By a process of coalescense, the many scattered primary forms developed into larger and fewer isolated primary ripple forms. These isolated forms closely resembled the shape of desert Barchan dunes which are formed by wind-movement, as described by Bagnold (1941). (A confusion in nomenclature is thus seen to arise, but the conventional description of isolated primary ripples will be used herein). After several hours, this bed development was associated with a reduction in total bed shear resistance to almost the initial value; the reduction indicated the decreased form drag of the fewer roughness elements on an otherwise flat bed (Plates 4.2., 4.3.).

During a further 18 hours, the isolated primary ripples continued to coalesce, and increased in size to a height of about 1mm. (Plates 4.4., 4.5.). The associated total shear resistance increased slightly throughout, thus indicating a possible equilibrium state for any stage of this bedform development. It was also noted that the form drag for these stages accounted for about 15% of the total shear resistance.

At the end of the Run, the eroded bed-load, which had collected at the downstream end of the flume, was dried and weighed. An average bed-load transport of 1.7×10^{-5} gm.cm.$^{-1}$s.$^{-1}$ was estimated. If it is crudely assumed that the laws for fine solid bed-load transport are similar to those for coarse-solid transport in turbulent-rough flows (Eq. 3.2.1.), then the averaged bed load transport for this run was equivalent to an average moving grain area ratio (ratio of area of moving grains to total bed area)of about 0.01%. Such a low value therefore suggested that the flat bed, which co-existed with the isolated primary ripples, had become armoured.

The main observations for the Run were therefore the initial development of small scale primary ripples, and their subsequent development to larger scale isolated primary ripples which migrated downstream on an otherwise flat bed. (It is noted that similar small scale primary forms were observed during the experiments of Rees, but their plan geometry after several hours of a Run became transverse; this was probably due to the continuous introduction of sediment and consequently excess bed-load transport during a Run.) A further major observation was that no suspended load was visually observed during this Run; the individual solid movement therefore occurred near the bed. From this, it was inferred that the maximum trajectory height reached by a solid was less than the viscous sub-layer thickness (since vertical velocity fluctuations are least in this layer). This inference further implies that the viscous sub-layer remained established over the isolated primary ripple forms.

With the discharge increase for Run 2 to the stress-stage of 1.9, bedform development occurred more quickly (Plate 5.1). Isolated ripples grew in size, and there differing migration rates were such that they eventually coalesced to span the entire channel width in places. A transverse primary form was thus created, which in turn appeared to accelerate the development of other transverse forms (Plate 5.2., 5.3.). The associated change in total shear resistance was one of continual increase, and hence a non-equilibrium state was observed throughout.

After about 20 hours of this run (stress-stage = 3.0), the onset of a secondary instability was noted. This was manifest by the visual observation of solids entering fluid suspension from a position near the ripple crest, local scour on the ripple downstream slope (in both

the upstream and downstream directions from the flow reattachment point), and the beginning of a change to three-dimensional forms. The amount of suspended load was however insufficient for direct measurement (by sampling the fluid), and the bed was not obscured. The total bed-load transport for the Run was estimated as 3 times that of Run 1, whilst the form resistance of the features (whose average height was about 4mm.) accounted for about 50% of the total shear resistance.

The bed surface contour at the channel centre-line, for the end of this Run, is given in Fig. 6.1. It was seen that an equilibrium bed form profile did not exist, and the ripple size generally increased with distance downstream. (This latter fact provides evidence that bedform development was not influenced by channel entry flow disturbances.) The average upstream slope of this configuration was 0.057, but a repetitive trend occurred in upstream slope variation from one form to another. It was seen that the slope increased gradually, from about 0.03 to 0.09 say, for cycles of 3 or 4 ripple forms. (The start of each cycle is given by numbering the ripple of least slope in Fig. 6.1.) The ripples of least slope were of less height above the channel floor than those of steeper slope. For some critical stage of slope and/or size development, the small slope ripple was either eroded or starved of bed-load; it therefore disappeared (see ripples number 28 and 38). The disappearance was in turn associated with a larger scale, local fluid motion which may be associated with the observed secondary instability. It was finally noted that the scale length of these cyclic slope increases may possibly be associated with the scale length of dunes, which may further develop with unlimited sediment supply.

The discharge increase for Run 3 which gave a stress-stage increase to 3.9 accelerated the change from transverse to three-dimensional forms. Photographic details were no longer recorded, due to the increasing concentration of suspended load. The change was however also influenced by limitation of total sediment used for the experiment, and the consequent exposure of the channel floor at a few positions of the bed. The total shear resistance again increased for this Run, and the averaged bed-load transport was twice that for Run 2. An equilibrium state was finally reached in Run 4, which was inferred from the constancy of stress-stage ($\simeq$ 7.5). This state was no doubt principally determined by the limitation of sediment used for the experiment.

A similar set of observations ~~were~~ Was made for the 66μ grade (Table 6.2 and Plate 6), with the notable exception that transverse primary ripples did not develop. A particular difference for the development of isolated primary ripples was noted with the discharge increase of Run 2 (Plate 6.3, stress stage 1.5). It was seen that the flat bed was no longer stable for this stage, and primary ripples developed continuously with time (as noted by their different sizes). This state of non-equilibrium persisted such that the secondary instability began at the area of maximum applied stress (around the channel centre-line), before a transverse development could take place (Plate 6.4).

Plates 6.5 and 6.6 show the finally developed secondary ripple system (of constant stress-stage $\simeq$ 5.1) which had again reached an equilibrium state by reason of limited sediment supply. It was noted that the average width of these three-dimensional secondary ripples was about 12cm. Since the Rees experiments gave transverse secondary forms for a flume of 17cm width, it might be speculated that his forms

would appear three-dimensional in a wider flume.

6.2.4. Interpretation

The bedform development at low $\bar{F}r$, with increased discharge increments from an initial stress-stage of unity, has been observed for 15μ and 66μ cohesionless silt grades. The developing configurations were those of many, small scale, scattered primary ripples to fewer, larger scale, isolated primary ripples which migrated downstream over an otherwise flat bed. Transverse primary ripples were then formed for the finest grade only, whilst both beds finally developed to three dimensional, secondary ripple forms which covered the entire channel. It is possible that a ripple on dune and dune configuration may then develop for an unlimited sediment supply, but this was not verified for these experiments.

The persistence of a flat bed after isolated primary ripple development may be indicative of bed armouring, or of a stable flat bed with low sediment transport. It seems probable that the former condition applied. Observations for coarse grains (Einstein and Chien 1955, Bagnold 1941) have shown that a sorting process can occur as bed forms migrate. This was considered to arise from the avalanche of the largest grains in a grade into the ripple troughs, where they remained after the form had migrated. The aspect is however demanding of future research.

The development of isolated forms has been described in detail by Bagnold (1941), for the case of sub-aerial Barchan dunes. It was considered that "in a strong sand-laden wind a uniform drift of sand over a uniform rough surface has a transverse instability, so that sand tends to deposit in longitudinal strips". (This transverse instability was "the effect of the higher resistance offered to the wind

by sand motion over a sand surface compared with that offered to the motion over an immobile surface".) It was then probable that one or more of these strips built up to such a thickness as to develop into a chain of dunes. When the dune chain existed, "the increased surface drag along the line of the chain must be much more pronounced because we have now not only the drag due to the moving sand, but also the permanent 'form drag' due to the large scale irregularities of the dunes themselves". The transverse instability thus became more pronounced and so the bordering sand drifted towards the dunes, and added to their form.

The first development of isolated forms under water was observed to differ from the above description. Form building was by the simple process of continued form coalescence; it was however impossible to determine the initial instability which caused the initial small scale, primary ripples. Plate 6.1 confirms however that the growth of isolated forms from longitudinal strips can take place in water; it is considered that the transverse instability mechanism may also be additionally influenced by the large scale secondary circulations in the open-channel flow.

It was also particularly noted that the isolated ripple form did not propagate other forms immediately downstream; this observation contrasted with ripple development observations from "grain pile discontinuities", for coarser grains. (The observation therefore suggests that the separating flow from the ripple crest does not subsequently alter the stability condition of the flat bed at the reattachment point).

Transverse primary ripples were formed by coalescence of isolated forms. This contrasted with the Rees experiments, for which

transverse ripples were formed during the continuous introduction of sediment into the flume during a Run. It seemed possible that if an experiment were conducted from a flat bed condition, which began with a stress-stage considerably in excess of unity, transverse primary ripples would develop in place of isolated ripples. Such a test was made for the 15μ silt (Plate 5.5, stress-stage = 2.0), and verified the fact that transverse primary forms were associated with excess bed-load transport.

The observation of the onset of suspended load, together with local scour and a change in bedform appearance to three dimensionality, confirmed the existence of a secondary ripple system. It seems possible that one or more of these instabilities may occur, for coarse solids in transitional or turbulent-rough flow conditions, immediately after the incipient motion stage. (For example, the ripple initiation mechanism propagating from a 'grain-pile discontinuity' is associated with the instability of local scour). If such is the case, the previous contradictions on ripple descriptions (section 4.1.3) may be possibly resolved, since two ripple configurations can exist.

In summary, these preliminary qualitative observations on fine grain bed-form development have added to those of Rees, and further confirmed the postulation by Bagnold of two distinct ripple systems. An equilibrium primary ripple configuration exists as isolated bed forms migrating over an otherwise flat bed. These forms are geometrically similar to the Barchan dunes of desert regions, and it appears that this is the first report of their observation in water flows over cohesionless, silt beds. The secondary form is of a larger three dimensional scale, and covers the entire bed. Transverse primary forms can exist for conditions of excess bed-load transport, whilst transverse secondary forms appear only in narrow channels.

6.3. Bedforms associated with low transport stages of fine, cohesionless flakey sediments

6.3.1. Flake incipient suspension and bedform experiments

It appears that there have been no bedform experiments specifically concerned with flake transport. However, flake behaviour in stream flows may well differ from that of grains, especially since a different coefficient of inter-solid friction may operate during transport. The following experiments were therefore conducted using the 6 grades of flakes previously described in Chapter 5.

A first investigation was conducted in conjuction with the I.M. experiments. It is recalled that 2 depositions of each flake grade were made, and the I.M. stress was recorded 5 times for each deposition. Following each set of these 5 stress estimates, the flow depth was adjusted to 6cm, and the fluid stress very slowly increased in increments above the I.M. stress. For all flake grades a continuous transport was observed but the individual solids grouped into well defined 'lineations' which in turn moved slowly downstream in a direction parallel to the flow. (As with fine grains, it was noted that the flakes did not become suspended by the flow for these low transport stages).

With increasing applied stress to a stress-stage of about 2.0, the transport increased and the associated lineations became more numerous across the flume width. The average transverse distance ($\bar{\lambda}_1$) between each lineation was greater than the actual lineation width, whilst each lineation could be up to about 30cm. in length. With a further stress increase, to a stress-stage of 3-4 depending on flake size, part of a lineation was seen to oscillate transversely; the bedform was accordingly described as a 'wandering-lineation'. The transverse amplitude of the oscillations was such that it did not exceed a distance $> \bar{\lambda}_1$.

The occurrence of oscillatory movement began at haphazard positions at the bed, and increased continuously with applied stress. A critical stress was finally reached for which individual flakes began to enter suspension. The wandering lineation at this stage appeared like the free end of a rope which has been oscillated in a plane normal to its lengthwise direction. The stress for the onset of suspension was named the "critical stress for incipient suspension", ($\bar{\tau}_{os}$). It could be estimated quite consistently, and 2 measurements for each grade (one for each bed deposition) are given in Table 6.3. Fig. 6.2 gives a dimensional plot of the flake grade nominal diameter (D_N) against $\bar{\tau}_{os}$ and $\bar{\tau}_{oc}$. It was seen that $\bar{\tau}_{os}$ increased with D_N in the same manner as $\bar{\tau}_{oc}$. The regression for these values on D_N was given by

$$\bar{\tau}_{oc} = 21.5\ D_N^{0.67}\ \text{c.g.s.} \qquad (6.4)$$

$$\bar{\tau}_{os} = 135\ D_N^{0.71}\ \text{c.g.s.} \qquad (6.5)$$

and these curves were also nearly parallel to that of $\bar{\tau}_{oc} \simeq 25\ D_N^{0.6}$ for the incipient motion of grains (eq. 4.13 using $D = D_N$).

The stress-stages for incipient suspension (I.S.) are given in Table 6.3, and these do not differ significantly at the 95% level of confidence. It seems therefore that the I.S. stress-stage is approximately constant at about 4.8 ± 1.2 standard deviation.

Following the I.S. experiments, bedform experiments using 3 flake grades (D_N = 23.5, 41.5 and 76μ) were conducted in order to investigate the lineations more closely. In general, lineation configurations were observed at two values of constant applied fluid stresses; these values were those which gave 'parallel' and 'wandering' lineations (Table 6.4).

The duration of each run at the higher stress value was terminated by the eventual erosion of the otherwise flat bed to the channel floor. Each parallel and wandering lineation run was repeated for the smallest and largest grades, as tests for reproducibility; plan photographs were taken for each stage, at the channel 6m downstream position (Plate 7). Since the analysis of the data was made with a view to examining existing theories on lineation occurrence, a literature review is now presented.

6.3.2. Primary current lineations

Lineations of the type observed in these flake experiments have been documented quite frequently in the geological literature, but mainly in respect to granular material. Sorby (1859) reported such features occurring in Carboniferous sandstones, and he conducted experiments which gave a configuration that he called "graining in the line of the current." He suggested that lineations occurred at flow "intensities" both higher and lower than that appropriate for the formation of ripples. Casey (1935) suggested that lineations developed through transverse flow components which were set up in the fluid.

The observation of lineation structures in sandstones has sometimes led to their being termed as 'parting lineations' (Crowell 1955), since the features appear when a rock is split or "parted" along a bedding plane. However, the usual geological term used is that given by Stokes (1947) as "primary current lineations". He suggested that the features only formed "in shallow water of moderate velocity 'marked' by laminar flow but free of turbulence other than on a minute scale". Such an idea contradicts the original 'high and low intensity' proposition by Sorby. The latter idea was extended by Allen (1964), who

concluded from flume experiments using a 450μ sand that lineations which occurred prior to bed rippling were unstable bedforms, whereas stable lineations could occur at a higher flow stages given by $\bar{F}r > 0.75$. The above experiments with flakes indicate however that the bedform can be stable for low $\bar{F}r$. (It is interesting to note that Allen also reported that 'clastic mica' is often concentrated on the lineation surfaces of the bedding planes of Devonian sandstones found in the Anglo-Welsh Basin).

There appear to be 3 main ideas for the cause of the lineation bedform. Firstly, they may arise in response to small scale, transverse flow instabilities as proposed by Casey (1935) and Bagnold (1941); the cause for the transverse instability was described in section 6.2.4 as that of the moving grain influence on the local bed shear stress. Secondly, they may arise in direct response to secondary circulations within the flow (Vanoni 1946). In particular, large scale secondary circulations exist in open-channel flows, and these may in turn propagate smaller scale circulations near the bed. (It is noted however that lineations have been observed on the upstream faces of large scale dunes, hence the postulation of an initial large scale secondary circulation may not be necessary). Finally, the most recent idea has arisen from studies on the structure of turbulent-smooth boundary flows. It has been proposed (Runstadler et al 1963) that 'streaks' or lanes of transversely alternate high and low momentum fluid can exist within the viscous sub-layer. Associated with each streak therefore is a transverse velocity gradient which may give rise to forces which move the bed solids into the lanes of low momentum fluid. Visual estimates of the average transverse 'streak' spacing has given a value of approximately $100\nu/u_*$; this value was also found to be roughly independent

of the flow velocity. Since the average transverse spacing of grain lineations, $\bar{\lambda}_l$, have given similar values to $100\nu/u_*$ (for example, Grass 1971 obtained this value for 100μ grains moving over a fixed smooth boundary), the cause of the bedform has been attributed to viscous sub-layer streaks. The lineation spacings for the above flake experiments were therefore analysed in the light of these recent ideas.

6.3.3. Flake lineation behaviour and viscous sub-layer theory

Prior to considering the flake lineation spacing results, it is worthwhile to consider the literature on turbulent-smooth boundary flows, to see if the reported turbulence structures can explain the flake lineation behaviour with stress-stage.

The physical model of fluid motion near to such boundaries has been gradually built up over the past 20 years, since the advent of instantaneous velocity measurements using hot wire and hot film anemometry (Klebanoff 1954, Laufer 1954). From such measurements, it was proposed by Townsend (1957) that an eddy structure, consisting of low momentum fluid issuing from the boundary region, could exist.

A series of detailed visualisation studies, using the hydrogen bubble and dye-injection techniques, were subsequently conducted at Stanford University (Runstadler et al 1963, Schraub and Kline 1965), and the results summarised by Kline et al (1967). It was considered that a turbulent-smooth boundary flow with zero streamwise pressure gradient could be subdivided into two main regions, as described by the dimensionless distance, $y^+ = y(\nu/u_*)^{-1}$, normal to the boundary. A 'wall' region was considered to exist for $y^+ = 80$-200 (depending on the flow Reynolds number), which in turn could be subdivided into 3 layers as follows:

a viscous sub-layer (V.S.L.), $0 < y^+ < 7$ for which the average velocity gradient was linear,

a buffer layer, $7 < y^+ < 30$ for which the maximum production and dissipation of turbulent energy occurred,

a logarithmic layer, $30 < y^+ < 80\text{-}200$ for which the averaged velocity profile was described by the Karman-Prandtl velocity distribution law, as amended by Clauser (1956).

(For $y^+ > 80\text{-}200$, a 'wake' region was defined for which the averaged velocity profile departed from the logarithmic law.)

Associated with the wall region were well-defined fluid motions. In the V.S.L., low speed 'streaks' were observed (whose streamwise dimension was greater than the other two dimensions), which alternated transversely with high speed streaks. The low-speed streaks interacted with the outer portions of the flow by slowly rising until they became suddenly oscillatory in the buffer layer; they appeared to 'burst' at about $y^+ = 30$, producing intense, chaotic velocity fluctuations which were in turn considered to dominate the process of turbulence production in the entire boundary layer.

More recent visualisation studies have usually confirmed and added to the above model by Kline et al. For example, Corino and Brodkey (1969) noted that the V.S.L. was also disturbed by fluid elements "which penetratrated into the region from positions further removed from the wall". A model of intermittent high momentum fluid inrush towards the boundary, and low momentum fluid ejection from the boundary, was subsequently proposed by Grass, 1971 (and considered also to apply for the case of turbulent rough boundaries). Offen and Kline (1974) proposed that the fluid inrush and ejection phases constituted a cycle of events, which was initially triggered by a 'burst'. In summary, it appears that an understanding of well-defined flow structures appears to

be emerging, but many problems of detail have yet to be answered.

It is now speculated that the observed behaviour of flake lineations may be a direct result of V.S.L. flow structures. In particular, parallel lineations are formed by the transverse stresses set up by high momentum 'streaks', and the subsequent wandering may be caused by the low momentum fluid ejection and sudden oscillation (bursting). For the wandering lineation stage, the flake weight and possible dampening of turbulence by moving flake layers must overcome the upward stress, and the form remains in a position at or near the bed. For higher stages, the bursting is associated with a high upward stress which is sufficient to lift the flakes into suspension. If this model is correct, it is to be expected that the initial flake lineation separations are similar to those observed for the 'streak' spacings of turbulent-smooth fixed boundary flows.

6.3.4. Transverse separation distances between lineations

Several methods have been used by previous workers to estimate 'streak' transverse spacings in hydrodynamically smooth fixed boundary flows. The simplest and most subjective was first made by Runstadler and Kline (1963). They counted the number of streaks (as observed by dye injection at a boundary wall) in a transverse section of the flow, and found $\bar{\lambda}_1$ to correlate with the wall parameter, ν/u_*, such that $\bar{\lambda}_1(\nu/u_*)^{-1} = \bar{\lambda}_1^+ = 70\pm30$ standard deviation; $\bar{\lambda}_1^+$ was also found to be independent for a range of free-stream velocities from about 6 to 24cm/s. This value was later amended to $\bar{\lambda}_1^+ = 100 \pm 10$, using the visual count method on 'streaks' observed with the hydrogen bubble technique (Schraub and Kline 1965). (In this later work, $\bar{\lambda}_1^+$ was also shown to be roughly independent of local streamwise pressure gradients at the boundary.)

A more objective spatial spectral analysis procedure, applied to the transverse profile of the instantaneous streamwise velocity, was also used for the Schraub and Kline (1965) data. When the procedure was applied to individual photographs (which represented the instantaneous streak spacings for a transverse flow traverse of about 10cm.) a frequency distribution was obtained for λ_1^+ which in turn showed several distinct modes. A combined frequency distribution of the modes, for about 30 photographs of instantaneous spacings, gave further well-defined modes. Such modes are herein calculated from the Kline et al data (1967, p.762) as

$$\bar{\lambda}_m^+ = 46,\ 81,\ 115,\ 154,\ 187 \text{ and } 248$$

(This fine structure for λ_1^+ has also been observed by Corino and Brodkey (1969) who estimated that a spacing of about 1/10 $\bar{\lambda}_1^+$ could exist). In contrast to the modal frequency distributions of the above data, the ensemble frequency distribution (consisting of a total sample of about 300cm. of transverse traverse representing both time and spatial variations in λ_1^+) gave a single mode of $\bar{\lambda}_1^+ = 133$. Similar ensemble average values have also been objectively obtained by Eckelmann et al (1972).

In the present experiments, plan photographs of lineations were analysed. Since the edges of the flake lineations could be observed quite clearly on projection of photographic negatives, λ_1 was simply measured visually. Approximately 400 measurements corresponding to a total transverse flow traverse of 200cm, were made for each of the two stress-stages. The measurements were taken from 5 transverse traverses, spaced about 8cm apart, on a negative which represented 45 by 20cm bed area; 200 measurements were therefore made on a single negative, and

these were repeated on a second negative of the same bedform stage. (For the case of the 23.5μ and 76μ flake grades, the second negative was that taken during a repeated experiment, whereas the second negative was taken at a different time for the 41.5μ grade experiment.)

The normalised frequency distribution for λ_1, corresponding to each of the 6 ensembles, is given in Fig. 6.3. It was first noted that at least 4 modes could be distinguished for each distribution; this result contrasts with the similar space-time ensemble average of Kline et al (1967), for which only a single mode was observed. However, since modality was observed for instantaneous profiles over a fixed boundary, it appears that a loose boundary can 'retain the history' of instaneous streak development. (It may of course also happen that flake lineations, once formed, influence the subsequent development and scale-size of'streaks').

The modal values for each curve were objectively estimated by assuming a random distribution about the 3 points locating each peak. The standard deviations were further estimated graphically by measuring the half-width for each mode at 0.6 of the modal height. Table 6.5 gives tha first 4 modal values and associated standard errors for each experiment. It was seen that a possible correlation of λ_m with D_N and stress-stage might exist. For the case of D_N, 10 out of 15 comparisons (67%) for λ_m show a significant increase (at the 95% level of confidence) with increased D_N; for the stress-stage, 7 out of 11 (64%) comparisons for λ_m show a significant decrease with stress-stage.

In accord with Kline et al (1967), the lineations modal spacings were scaled with ν/u_* (Table 6.6.). Since the absolute data showed λ_m to mainly decrease with increased stress-stage, it was to be expected that each pair of modal values, for each grade and mode, became more equal.

Accordingly, it might be tentatively postulated from the results that λ_m correlated directly with ν/u_*, and was otherwise independent of the stream conditions. An average λ_m^+ was calculated for each pair of values, and the trend for increased $\bar{\lambda}_m^+$ with D_N was better observed. (A possible reason for this increase might be due to an increased physical width of flake lineations with grain size, together with a constant separation distance between consecutive lineation edges).

Although $\bar{\lambda}_m^+$ for flake lineations and fixed boundary streaks did not agree exactly (Table 6.6.), it might be inferred that the similarity in modality and first modal values was sufficiently close as to postulate that flake lineations were a direct result of smooth boundary flow structures. Further physical speculations from the results were also attempted. For example, Table 6.6. gives the differences between the adjacent modal averages of each grade; the total average was calculated as $\Delta\bar{\lambda}_m^+ = 16 \pm 3$ standard deviation. Accordingly, the transverse scale size of high momentum streaks might be postulated as $\bar{\lambda}_s = (16 \pm 3)\nu/u_*$. (The fixed boundary data gave a similar average of modal differences as $\bar{\lambda}_s = (36 \pm 4)\nu/u_*$). It was therefore interesting to note that both loose and fixed boundary values gave approximately even multiples of the V.S.L. thickness, $7\nu/u_*$. It might therefore be speculated that a fundamental streak spacing equal to $7\ \nu/u_*$ existed, and that the transverse velocity component of a streak was that of a secondary circulation within the sub-layer.

Finally, the dimensional linear regression of $\bar{\lambda}_l^+$ on D_N will give an approximate idea of the variation in minimum lineation separation distances to be expected for varied fine flake sizes in various flow conditions. This relation was calculated from the data of Table 6.6. (giving a standard deviation for the empirical coefficients of about 5%) as

$$\bar{\lambda}_l^+ = 0.36\ D_N + 30 \text{ where } D_N \text{ is in microns} \qquad (6.6.)$$

CHAPTER 7. CONCLUSION

Experiments on the low transport stages by water streams of fine, cohesionless sediments have been conducted. The sediments consisted of 3 near-uniformly sized grades of natural granular solids (of median fall diameters, D_F = 30, 45 and 66μ), 1 grade of artificially prepared grains (D_F = 15μ), and 6 near-uniformly sized grades of natural flakey solids (of nominal diameter, D_N = 15.5, 23.5, 32.5, 41.5, 52.5 and 76μ). Particular attention was paid towards the initial stage of beginning transport for these solids (the incipient motion condition) and to the bedforms which developed with increased applied fluid stress up to the transport stage for which the solids became suspended by the fluid. Both the quantitative incipient motion data and the qualitative bedform observations were compared with previous experimental and theoretical considerations for coarse grains (of geometric diameter, D > 150μ say); they were therefore used to extend the latter research. It was found that the cohesionless behaviour of these fine solid grades depended considerably on the water chemistry; future controlled experiments on cohesive sediments may therefore be conducted using this fact. A summary and interpretation of the experimental results together with their immediate application to sediment transport problems is now given.

7.1. The beginning of sediment movement

The incipient motion (I.M.) condition has been defined as the beginning transport of solids over a flat bed (that is, a bed which is coplanar to within 1D) which is caused by a two-dimensional quasi-uniform flow. It has been shown however, using an ideal flat bed model composed of equal spheres (Chapter 3.4) that the individual solid resistive stress to erosion (τ_R) can take on any value, depending on the particular flat-bed fabric.

A flat bed definition for the I.M. condition is therefore non-unique, and accordingly, a large range of empirical scatter has been experimentally recorded (Chapter 3.2 gave almost one order of magnitude in estimates for the critical incipient motion stress, $\overline{\tau}_{oc}$). In particular, it has been proposed (Paintal 1970) that $\overline{\tau}_{oc}$ can be of almost zero magnitude for flat beds which have been artificially laid and smoothed. (Such a proposal is explained by the fact that τ_R can be almost zero for such artificial conditions). It follows therefore that $\overline{\tau}_{oc}$ is a variable depending on the particular flat-bed configuration chosen for an experiment.

Attempts have been made during these fine sediment experiments to simulate nature. Accordingly, stable flat beds (that is, beds which were locally flat for an area determined by the extreme difficulties of flume channel-floor levelling (Chapter 1.3)) were laid under natural conditions of deposition from a shear flow. The subsequent critical I.M. stress was therefore finite, and depended on the bed shear stress during deposition ($\overline{\tau}_{ob}$) such that $\overline{\tau}_{oc} \simeq \overline{\tau}_{ob}$. Since $\overline{\tau}_{ob}$ can be varied in nature, a unique condition was chosen so that $\overline{\tau}_{oc}$ could be uniquely defined for a natural flat bed. The condition was that $\overline{\tau}_{ob}$ was slightly below the applied stress which was necessary to produce bedforms during deposition. Accordingly, the flat bed was one of maximum stability, prior to a bed configuration change with increased applied fluid stress.

The critical I.M. stress for flat coarse granular beds of maximum stability was shown in Chapter 3.3 to be approximately represented by the collected data of Shields (1936). These new fine, granular I.M. data were therefore added to the recalculated data of White, S.J. (Table 4.3), and plotted together with the Shields' data on a Shields' diagram (Fig.4.8). The empirical scatter alluded to in Chapter 3.2 was then considerably reduced, and was seen to be similar for both coarse (for which the Boundary

Reynolds number, $\bar{R}o$ was > 1 say) and fine grain experiments. In accord with Shields, this empirical observation for a close correlation of dimensionless applied critical fluid stress, $\bar{\theta}_{oc}$, with $\bar{R}o$ (for a larger range of $\bar{R}o$ than plotted by Shields) indicated that the I.M. condition could be reasonably described in terms of these two parameters only.

It was shown in Chapter 3.5 however, that the analytical details for the I.M. condition was a problem of great complexity. It demanded a knowledge of at least the probability distributions for the dimensionless shear stress and grain resistance, θ_o and θ_R. An attempt was made in Chapter 3.4 to quantify the θ_R distribution for these fine, flat granular beds of maximum stability. It was then speculated that a similar distribution existed for the maximum stability of any flat granular bed. Based on this speculation, Fig. 3.13 was proposed to explain the empirically observed extended Shields' diagram of Fig. 4.8. Since it is physically inevitable that the θ_o distribution increased with $\bar{R}o$ (and associated $\bar{R}e$), a fall in the $\bar{\theta}_{oc}$ curve from very low $\bar{R}o$ (=0.01) was explained. Finally, with consideration for the empirical scatter shown in Fig. 4.8, it was considered that a hypothetical 'transition' region was not significantly established, and $\bar{\theta}_{oc}$ could be considered as empirically constant for $\bar{R}o$ > 10 say.

In summary, the Shields curve has been reinterpreted in the light of these fine, granular studies. The traditional speculations involving laminar sub-layers, grain exposure and the nature of the forces acting on a single grain have been replaced by the single speculation on the maximum stability condition for any flat granular bed. The extended Shields curve was then simply considered as a single fall from $\bar{R}o$ = 0.01 to $\bar{R}o$ = 10, after which it became empirically constant.

The extension of the above ideas to natural flakey beds was made with the caution that little physical meaning could be deduced using the Shields

representation. This was inevitable since the scale-length (L) of the bed surface roughness was unknown. However, this caution did not detract from the fact that an empirical condition for the I.M. of 2-dimensional solids could be graphically represented. Accordingly, the length scale of the flakey grades was arbitrarily chosen as the flake median nominal diameter, and a tentative design curve for the I.M. of both fine and coarse flakes was proposed as in Fig. 5.7.

Turning now to the actual use of these I.M. data for designing non-erodible channels which may carry any cohesionless material, it is implicitly assumed that a coarse solid-transporting channel (operating with $\bar{\theta}_o$ slightly less than $\bar{\theta}_{oc}$) will deposit solids to achieve the condition of maximum bed stability. In other words, the channel will become "armoured", until the stress is reached whereby the bed changes configuration; this armouring condition has been shown to operate for these experiments using fine, cohesionless solids. It is also noted that the extended Shields curve for both grains and flakes can be considered as a minimum stress condition for cohesive solids which do not flocculate. (It was shown in Chapter 5.4, that $\bar{\tau}_{oc}$ for flocculated solids was much less than that for the individual solids.) The design curves are therefore of some use in designing non-erodible channels which transport slightly cohsive sediments. Finally, since most natural sediment shapes vary between the extremes of 1 and 2 dimensionality as exhibited by grains and flakes (the occurrence of needle shaped solids of $D > 10\mu$ are rare), the I.M. curve of Fig.5.7 (which uses D_N as a length scale, and falls below the grain curve which in turn may also be approximately described in terms of D_N) can be considered a minimum for most sediments of <u>any</u> natural shape.

7.2. Bedform development at low transport stages

The ultimate purpose for bedform studies is a general recognition and classification of equilibrium states; these may in turn be associated with a particular fluid dynamical condition, and aid the derivation of sediment transport laws. The bedforms associated with low transport stages of the 15μ and 66μ granular grades have been recognised during these experiments as primary and secondary ripples; they confirm similar bedform observations by Rees (1966) for a 10μ granular grade. (In addition, a new bed configuration was observed as isolated primary ripples migrating over an otherwise flat bed.) When it is considered that it has taken over 100 years for the general recognition and acceptance of coarse grain bedforms, the correspondence of these recent fine grain observations are encouraging.

An immediate engineering application can be pursued from the fine granular studies, by further examining the movement of isolated primary forms. Since the forms were geometrically similar to isolated wind-driven dunes of a much larger scale, the latters' movement may be possibly predicted from small scale flume studies using water and fine grains. Such knowledge is desirable since isolated wind dune movement can be catastrophic to adjacent civilisation.

The bed configuration observed during fine, cohesionless flake transport exhibited a major difference to those of grains. A single flake bedform was observed throughout as that of primary current lineations. It is speculated that this difference was due to the difference in inter-solid dynamic friction between moving grains and moving flakes. (The result of say a higher friction between moving grains may cause the solids to "pile-up" more easily than flakes.) The flake lineation behaviour was examined in the light of recent viscous sub-layer ideas on fixed boundaries.

In turn, they could be considered to add to such ideas. For example, the concept of a high velocity "streak" spacing of about 100 ν/u_* ($\sim$1cm for the flows used in these experiments) seems without physical explanation. However, the measured flake lineation spacings showed that a fine structure could exist, which in turn was speculated as being associated with the actual viscous sub-layer thickness. Accordingly, a qualified model for a high velocity boundary layer "streak" was proposed as that of a streamwise orientated fluid motion having a transverse circulation, and whose transverse scale size was equal to the viscous sub-layer thickness, 7 ν/u_* say.

These bedform studies are of immediate use to geologists. It has in the past been generally supposed that fine solids are always cohesive. The existence of cohesionless fine solids has been demonstrated, and the associated mineralogical and water chemical conditions described. Accordingly, the observation of fine solid bedforms in sedimentary sequences will indicate the water chemistry existing at the time of formation. Furthermore, the flow direction and associated bed shear stress for palaeocurrents can be estimated by comparison with the bedform data reported herein.

This thesis began with a statement of the problem facing the research engineer, towards understanding the laws of natural, fine cohesive sediment transport. The work reported has reduced the problem to that of the low transport stages of fine, cohesionless solids of extreme shapes. It is obvious that the research endeavour sequential to this study should be applied to the behaviour of fine, cohesionless solids at high transport stages, and to chemically controlled experiments on fine, cohesive sediments.

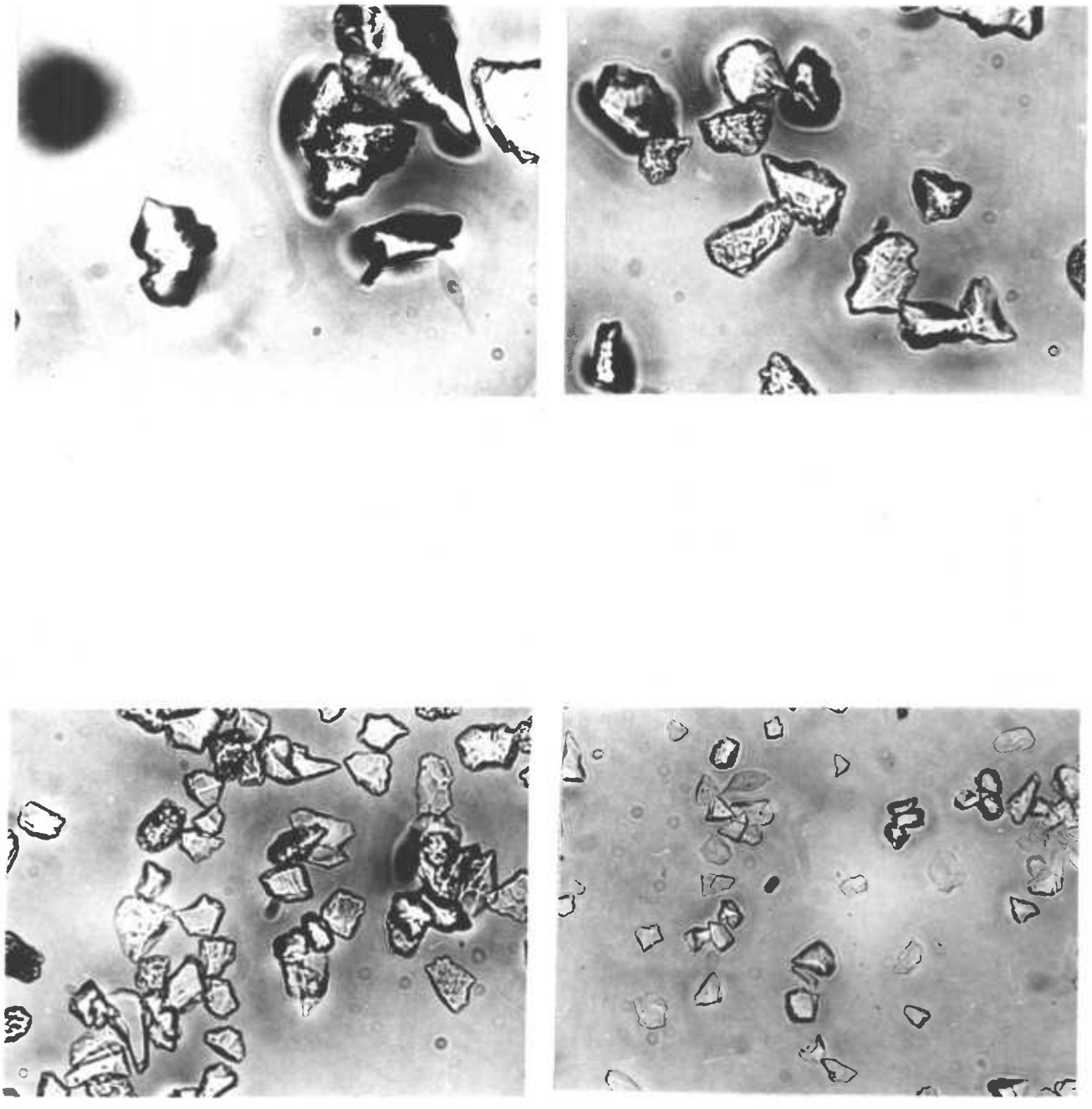

PLATE 1. THE FOUR GRADES OF FINE, GRANULAR SEDIMENT.

(Area of photograph 450 x 300 microns; median grade diameters are 15, 30, 45 and 66 microns)

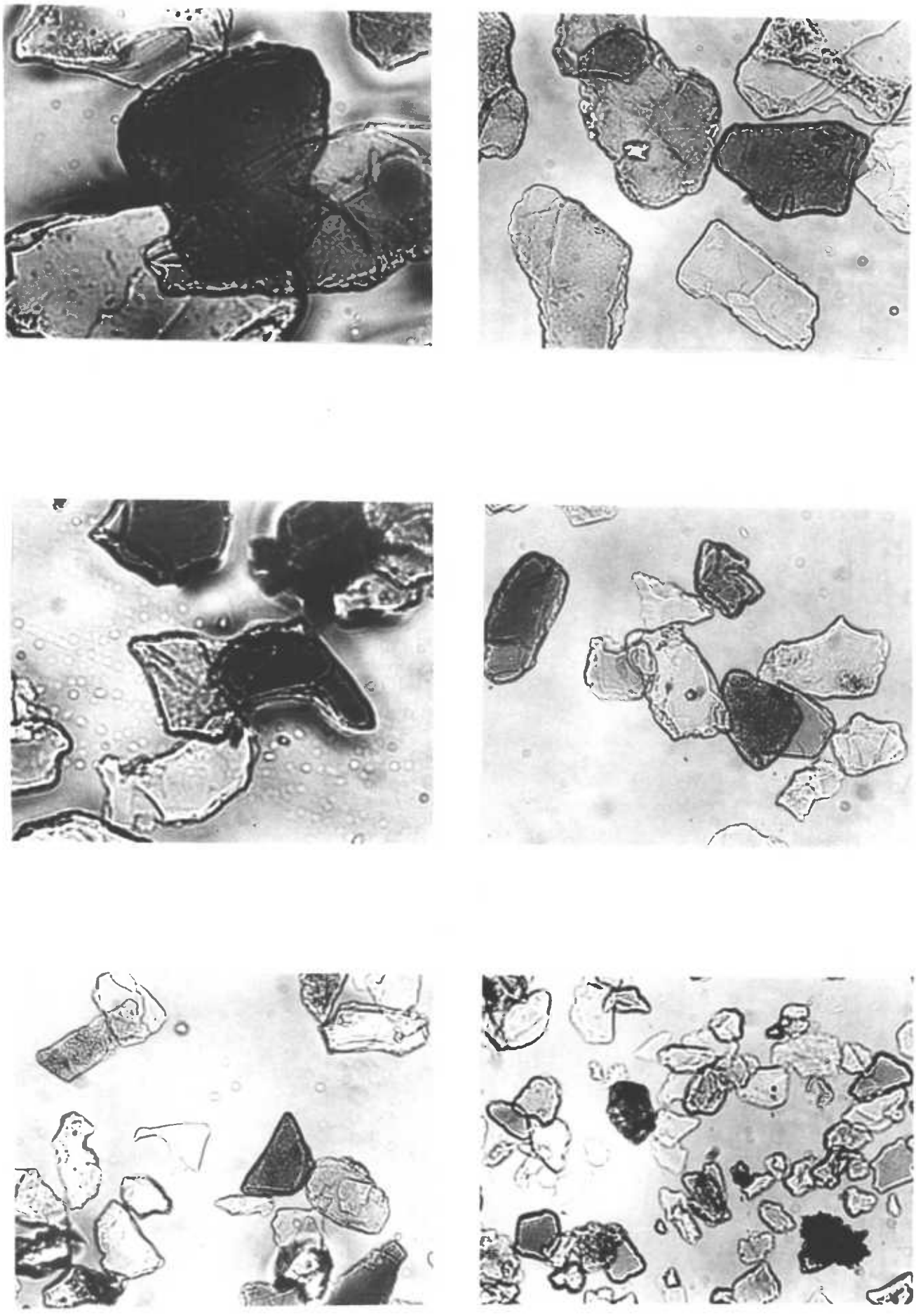

PLATE 2. THE FLAKE FACES OF THE SIX MICA GRADES.
(Area of photograph 450 x 300 microns; median grade face diameters are 33,52,75, 98,120 and 172 microns)

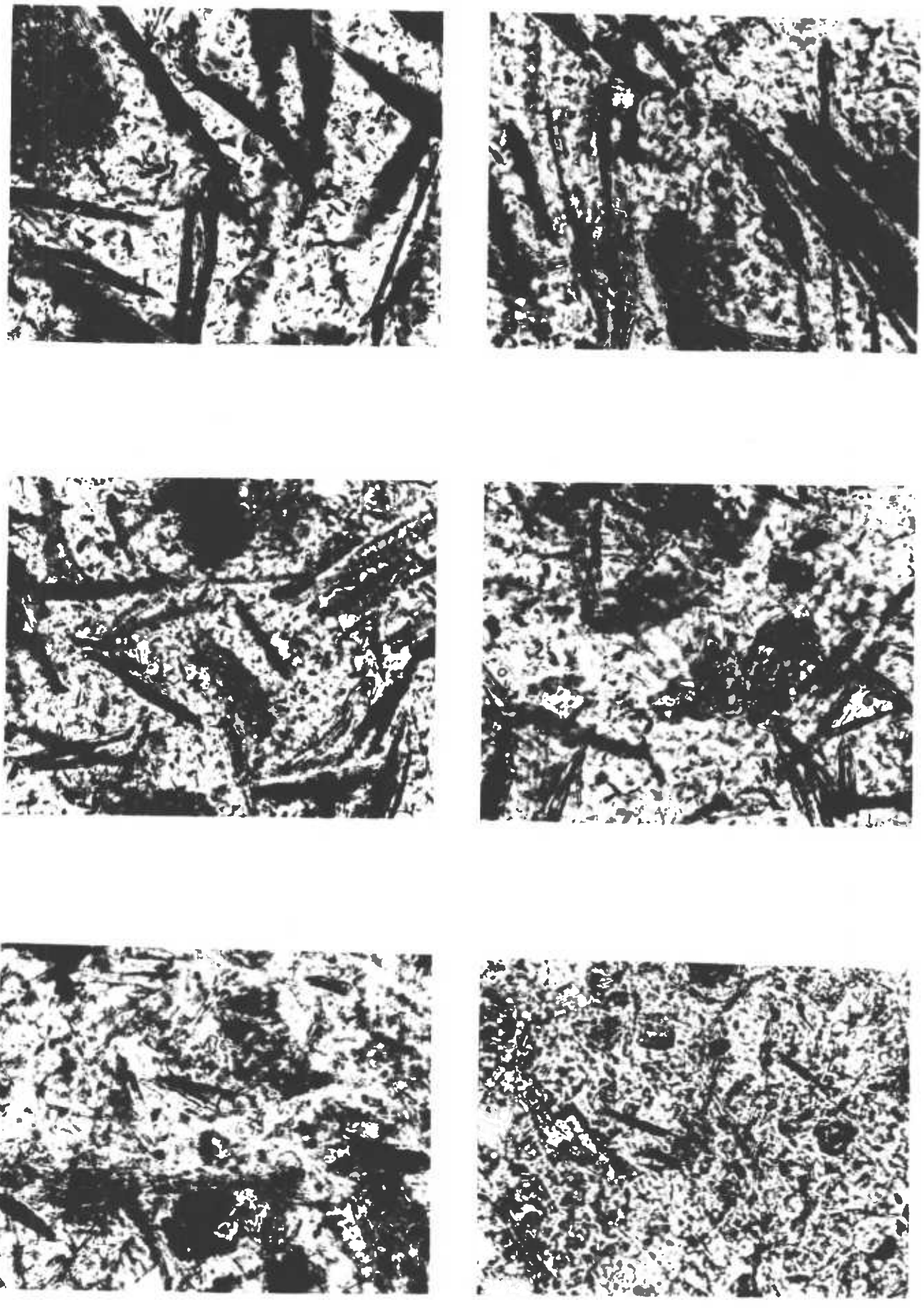

PLATE 3. THE FLAKE EDGES OF THE SIX MICA GRADES.
(Area of photograph 450 x 300 microns; median grade thicknesses are 1.85,2.5,3.2, 4.0,5.0 and 7.8 microns)

4.1. After 2h. erosion, $\bar{\tau}_o / \bar{\tau}_{oc} = 1.8$

4.2. After 4h. erosion

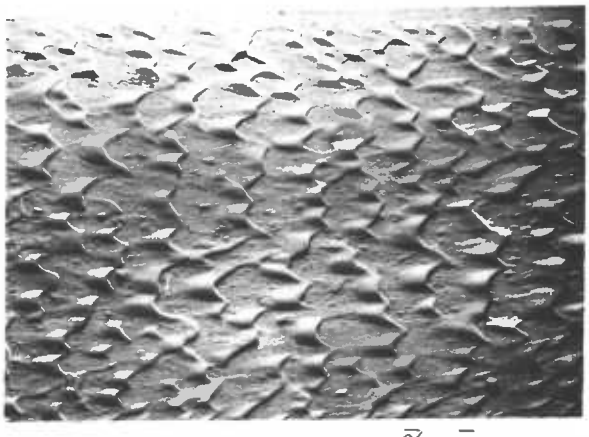

4.3. After 6h. erosion, $\bar{\tau}_o / \bar{\tau}_{oc} = 1.3$

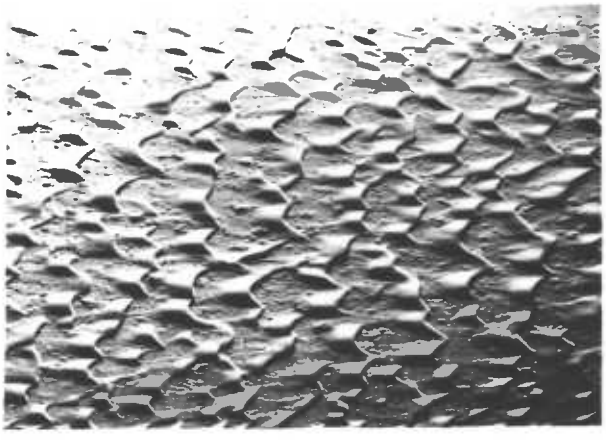

4.4. After 9h. erosion

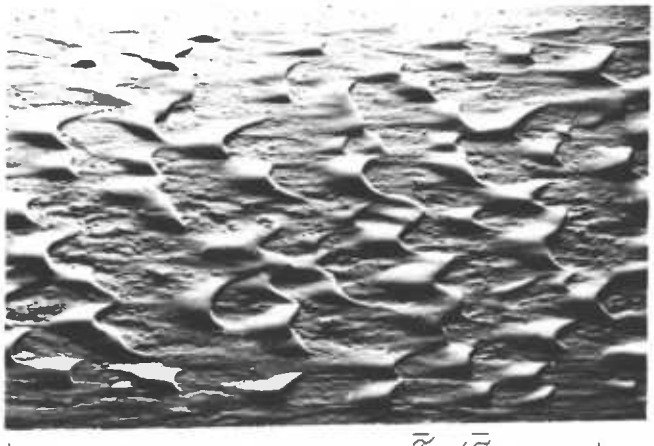

4.5. After 22h. erosion, $\bar{\tau}_o / \bar{\tau}_{oc} = 1.4$

PLATE 4. RUN 1 OF THE 15 MICRON GRADE GRAIN TRANSPORT EXPERIMENT.
(Plan view of 45 x 30cm^2 bed area at 6m downstream; flow left to right)

5.1. Beginning of run, $\bar{\tau}_o / \bar{\tau}_{oc} = 1.9$

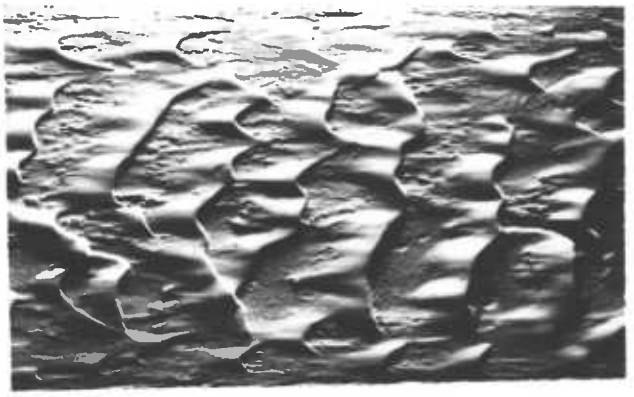

5.2. After 6h. erosion $\bar{\tau}_o / \bar{\tau}_{oc} = 1.9$

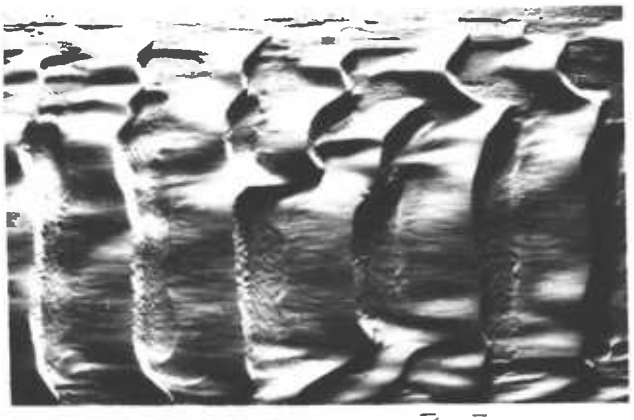

5.3. After 20h. erosion, $\bar{\tau}_o / \bar{\tau}_{oc} = 3.0$

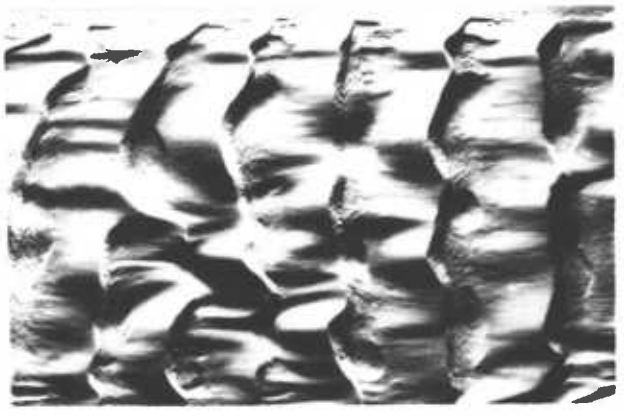

5.4. After 24h. erosion, $\bar{\tau}_o / \bar{\tau}_{oc} = 3.7$

PLATE 5. RUN 2 OF THE 15 MICRON GRADE GRAIN TRANSPORT EXPERIMENT

(Plan view of 45 x 30cm^2 bed area at 6m downstream; flow left to right)

PLATE 5.5. TRANSVERSE PRIMARY RIPPLES FOR THE 15 MICRON GRADE ($\bar{\tau}_o / \bar{\tau}_{oc} = 2.0$)

6.1. After 20h. erosion; $\bar{\tau}_o / \bar{\tau}_{oc} = 1.0$

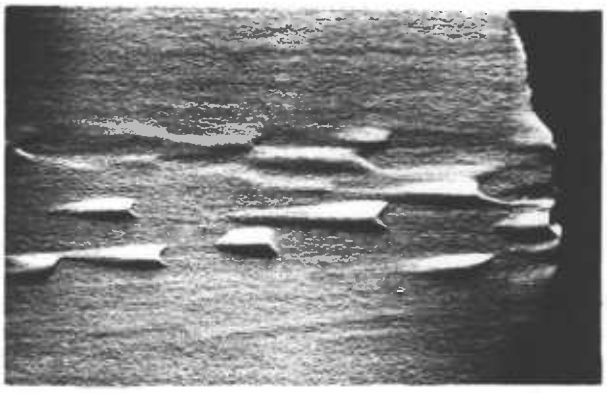

6.2. After 20h. erosion; $\bar{\tau}_o / \bar{\tau}_{oc} = 1.0$

RUN 1 (End of bed, 9.5m downstream of channel entry)

6.3. After 1h. erosion; $\bar{\tau}_o / \bar{\tau}_{oc} = 1.5$

6.4. After 7h. erosion; $\bar{\tau}_o / \bar{\tau}_{oc} = 2.2$

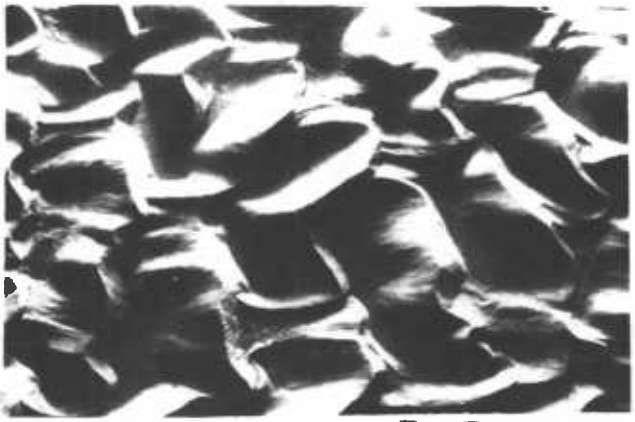

6.5. After 9h. erosion; $\bar{\tau}_o / \bar{\tau}_{oc} = 5.0$

(Channel floor exposed in places)

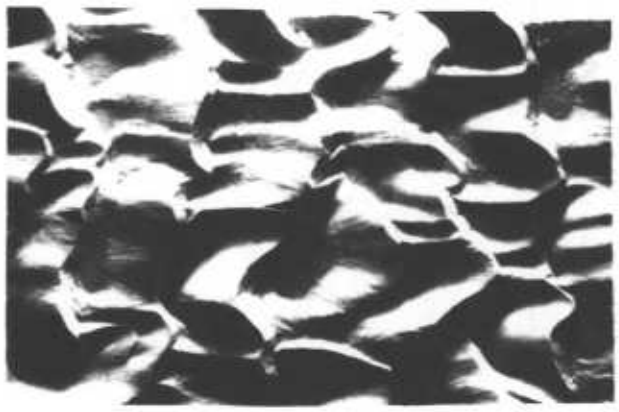

6.6. After 20h. erosion; $\bar{\tau}_o / \bar{\tau}_{oc} = 5.2$

(Channel floor exposed in places)

RUN 2

PLATE 6. RUNS 1 AND 2 OF THE 66 MICRON GRADE, GRAIN TRANSPORT EXPERIMENT.
(Plan view of bed area 45 x 30cm at 6m downstream; flow left to right)

$\bar{\tau}_o / \bar{\tau}_{oc} < 1.0$

Flat bed

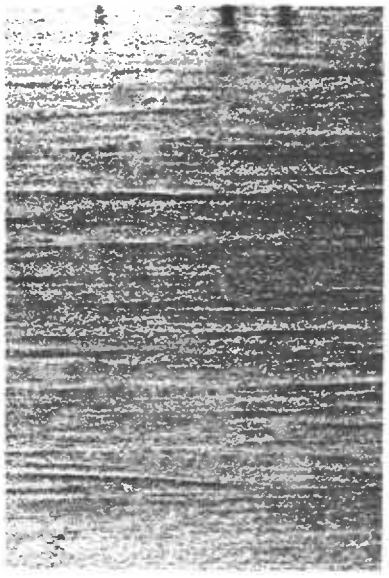

$\bar{\tau}_o / \bar{\tau}_{oc} = 2.9$

Lineations

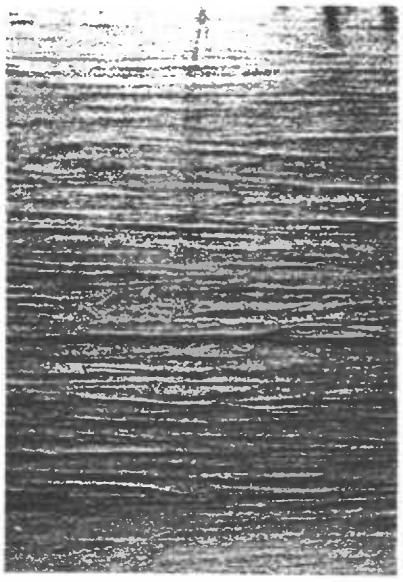

$\bar{\tau}_o / \bar{\tau}_{oc} = 3.8$

Wandering lineation

Flake nominal diameter 23.5μ

$\bar{\tau}_o / \bar{\tau}_{oc} < 1.0$

Flat bed

$\bar{\tau}_o / \bar{\tau}_{oc} = 1.6$

Lineations

$\bar{\tau}_o / \bar{\tau}_{oc} = 2.6$

Wandering lineations

Flake nominal diameter 76μ

PLAT 7. PRIMARY CURRENT LINEATIONS FORMED DURING THE TRANSPORT OF FINE, FLAKEY SEDIMENT

(Plan view of bed area 20 x 30 cm at 6m downstream; flow direction from left to right)

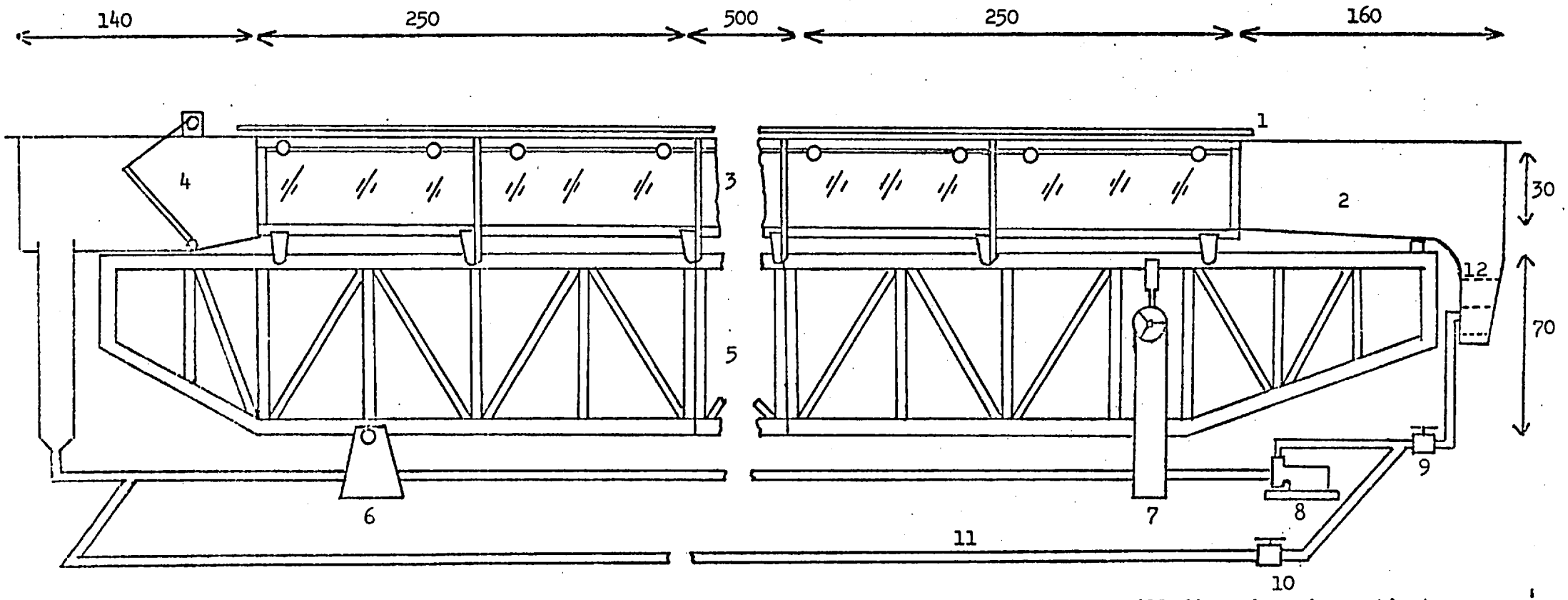

1. Depth gauge carriage rails
2. Channel entry
3. Main channel
4. Adjustable weir
5. Support frame
6. Pivot pedestal
7. Jack assembly
8. Pump
9. Discharge valve
10. Feedback valve
11. Three inch diameter durapipe
12. Perspex baffles

All dimensions in centimetres

Figure not to scale

Figure 1.1. The 10 metre recirculating flume and pumping system

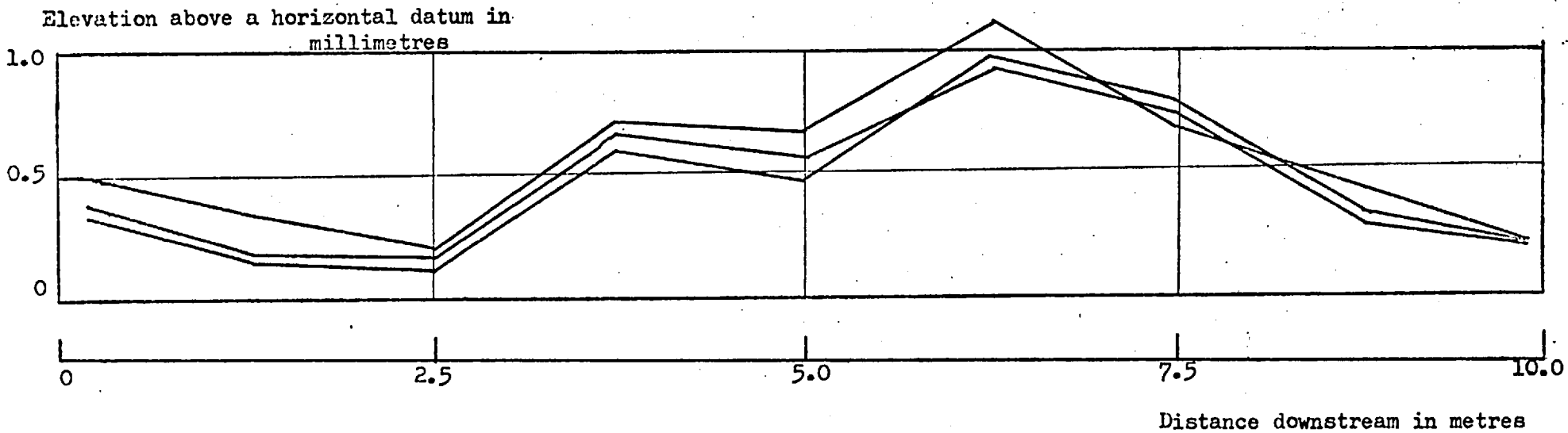

Figure 1.2. Flume Channel-floor contour relative to the horizontal

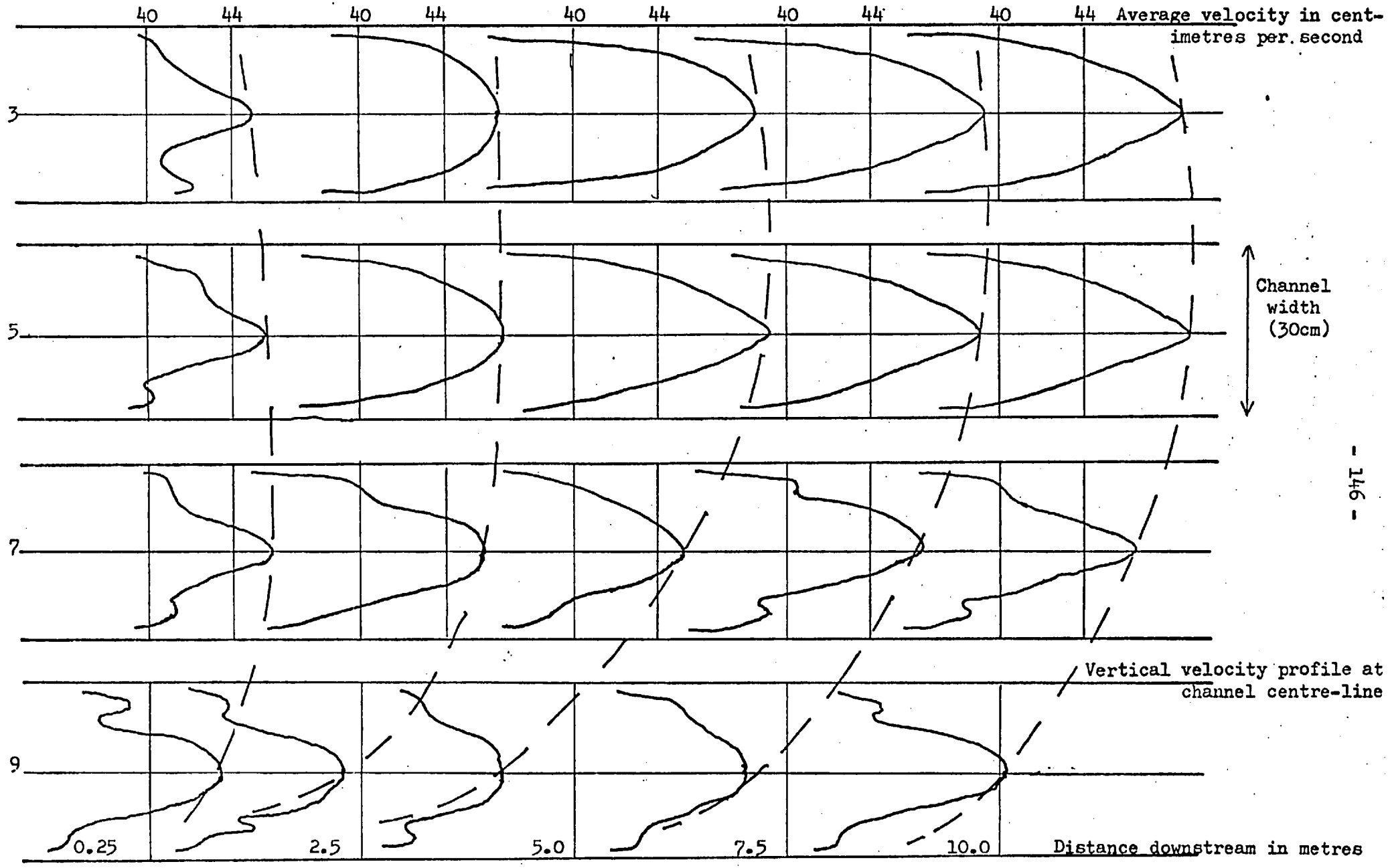

Figure 1.3. Velocity profile development for a high flow Reynolds number (Re_m = 25,000, each individual profile is transverse)

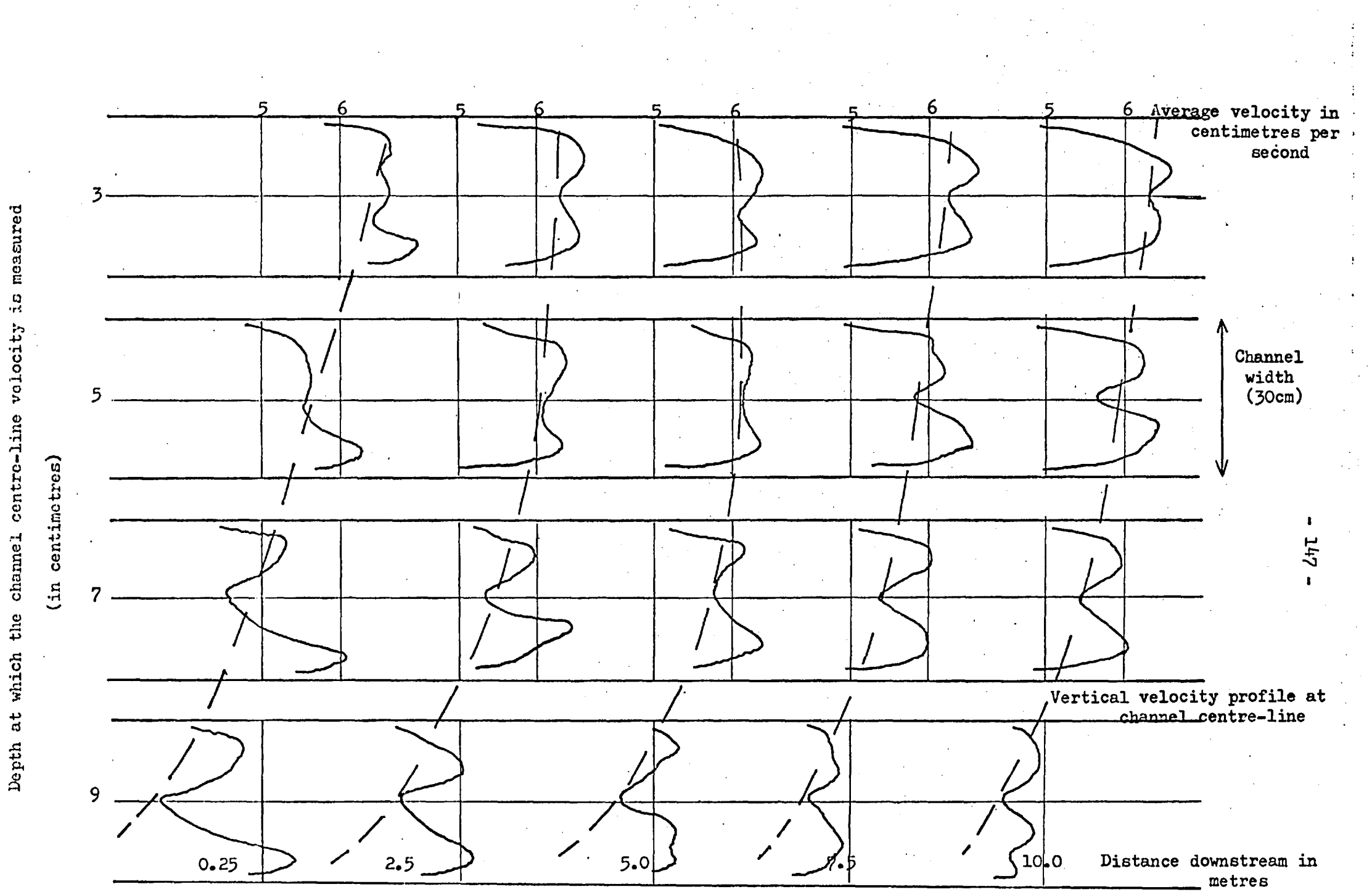

Figure 1.4. Velocity profile development for a low flow Reynolds number (Re_m = 3,000, each individual profile is transverse)

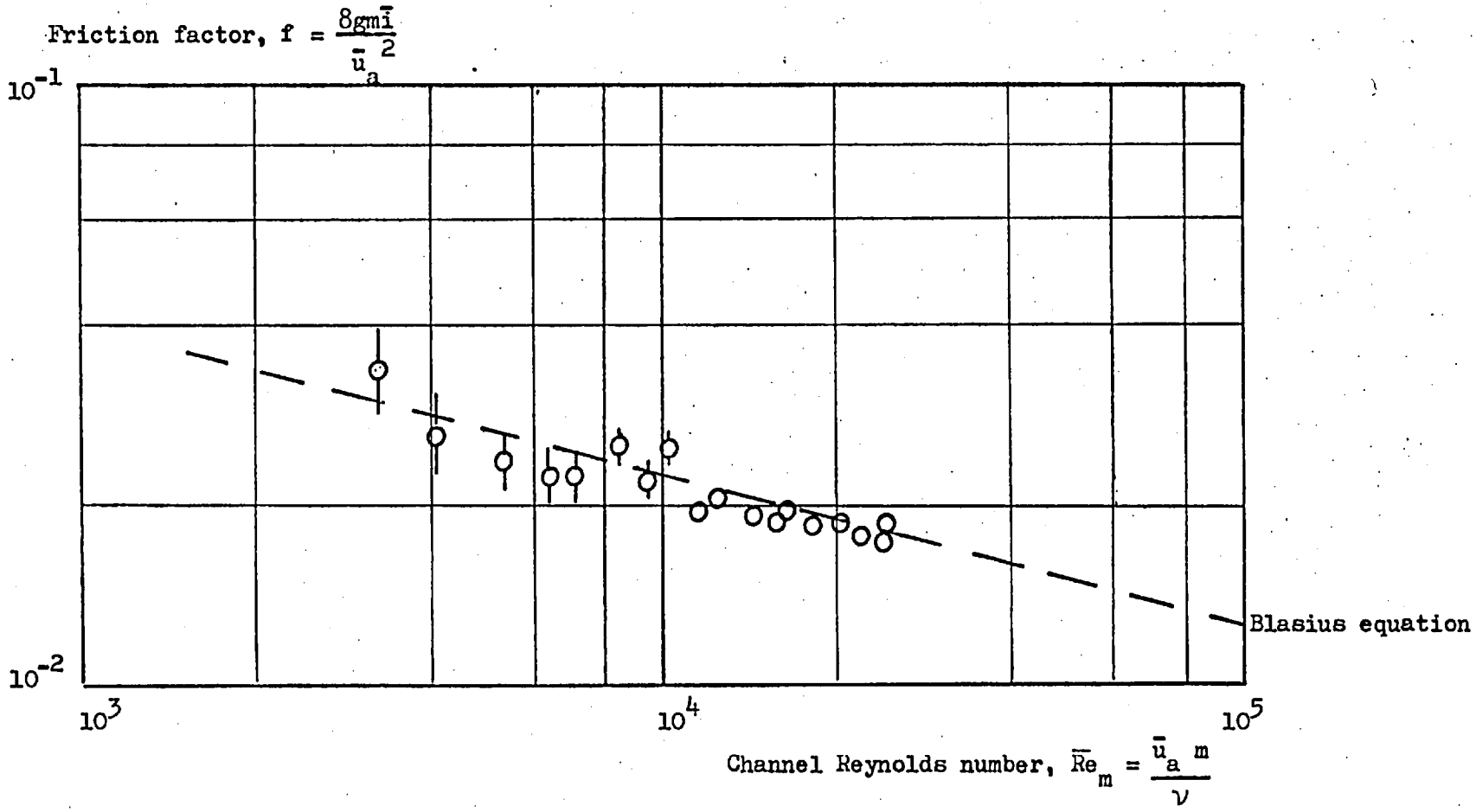

Figure 1.5. Friction factor curve for a flow depth of 10cm.

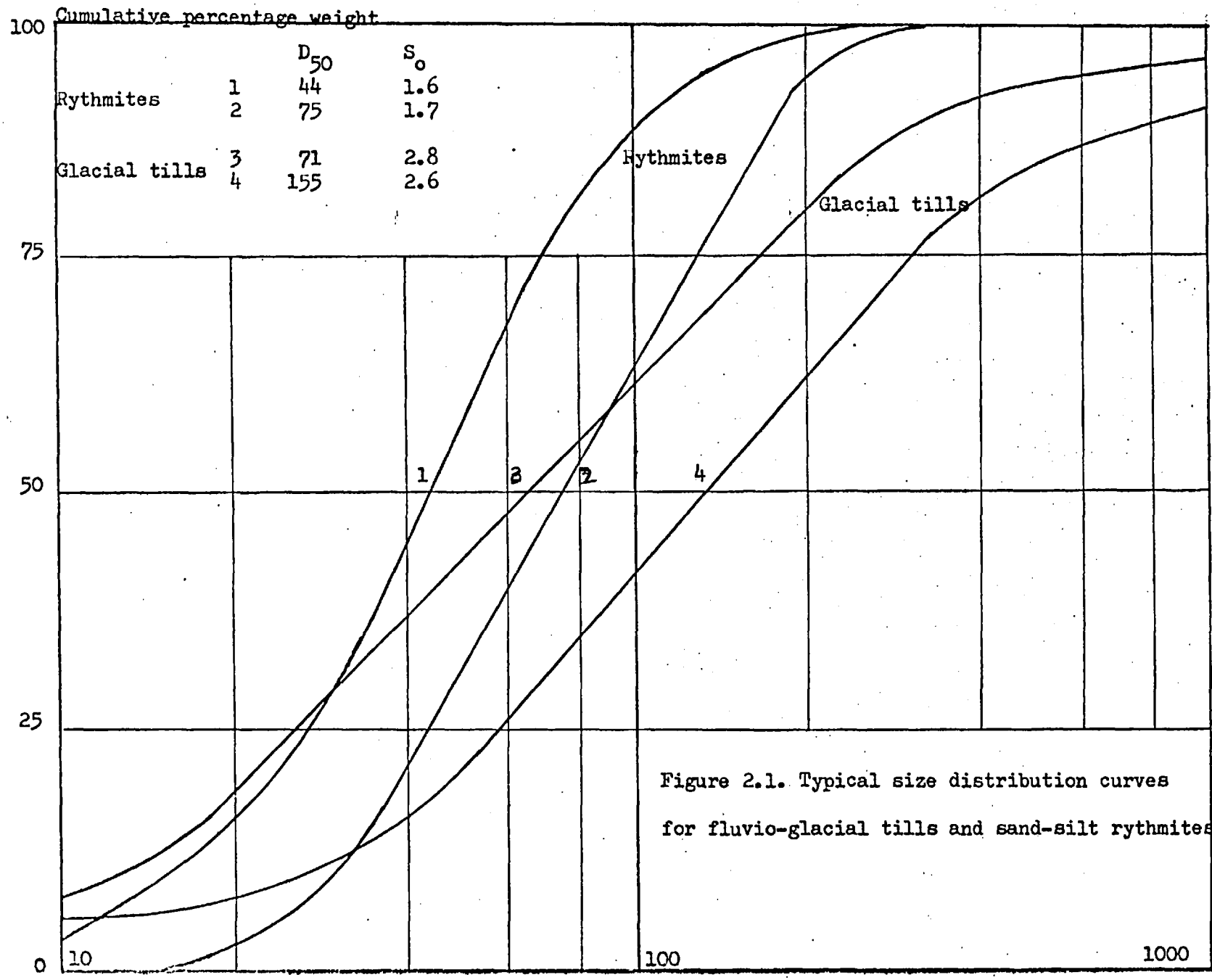

Figure 2.1. Typical size distribution curves for fluvio-glacial tills and sand-silt rythmites

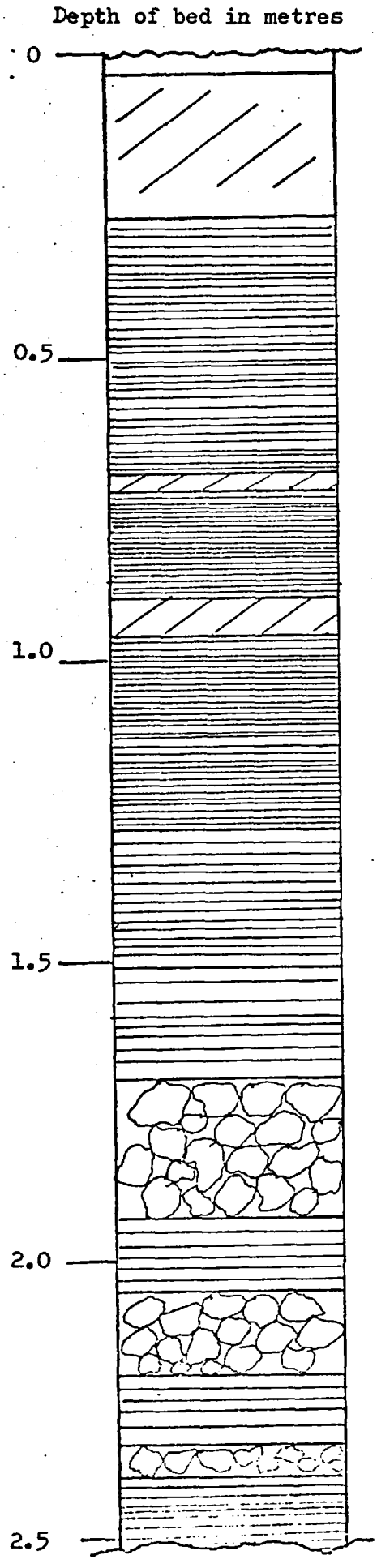

Figure 2.2. A typical fluvio-glacial rythmite sequence (2.5m vertical exposure at Donachton Quarry. Grid Reference number NH 824051)

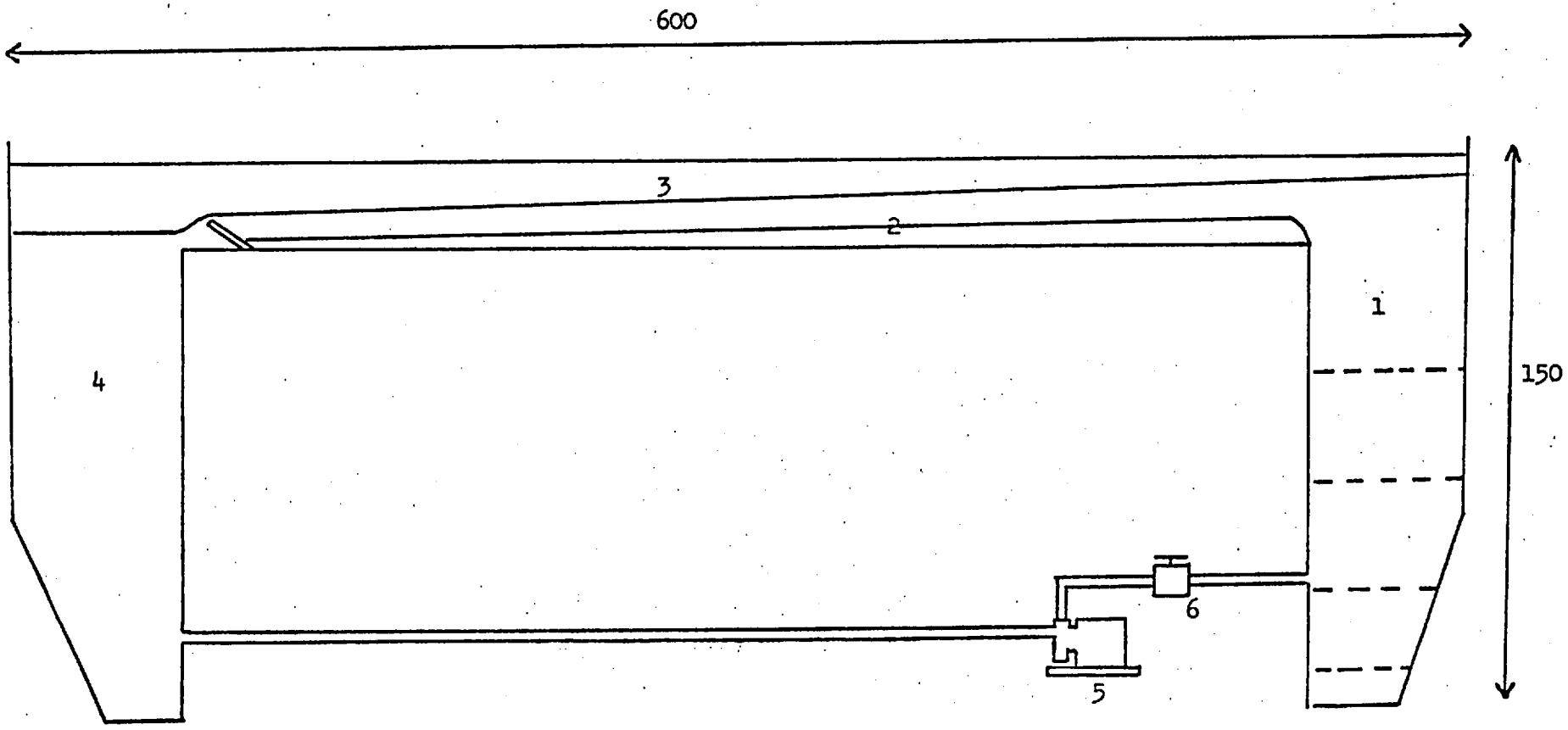

1. Channel entry column
2. Sediment bed
3. Main channel
4. Channel end column
5. Pump
6. Discharge valve

All dimensions in centimetres

Figure not to scale

Figure 2.3. The 6 metre recirculating flume used for preliminary grading of the sediment

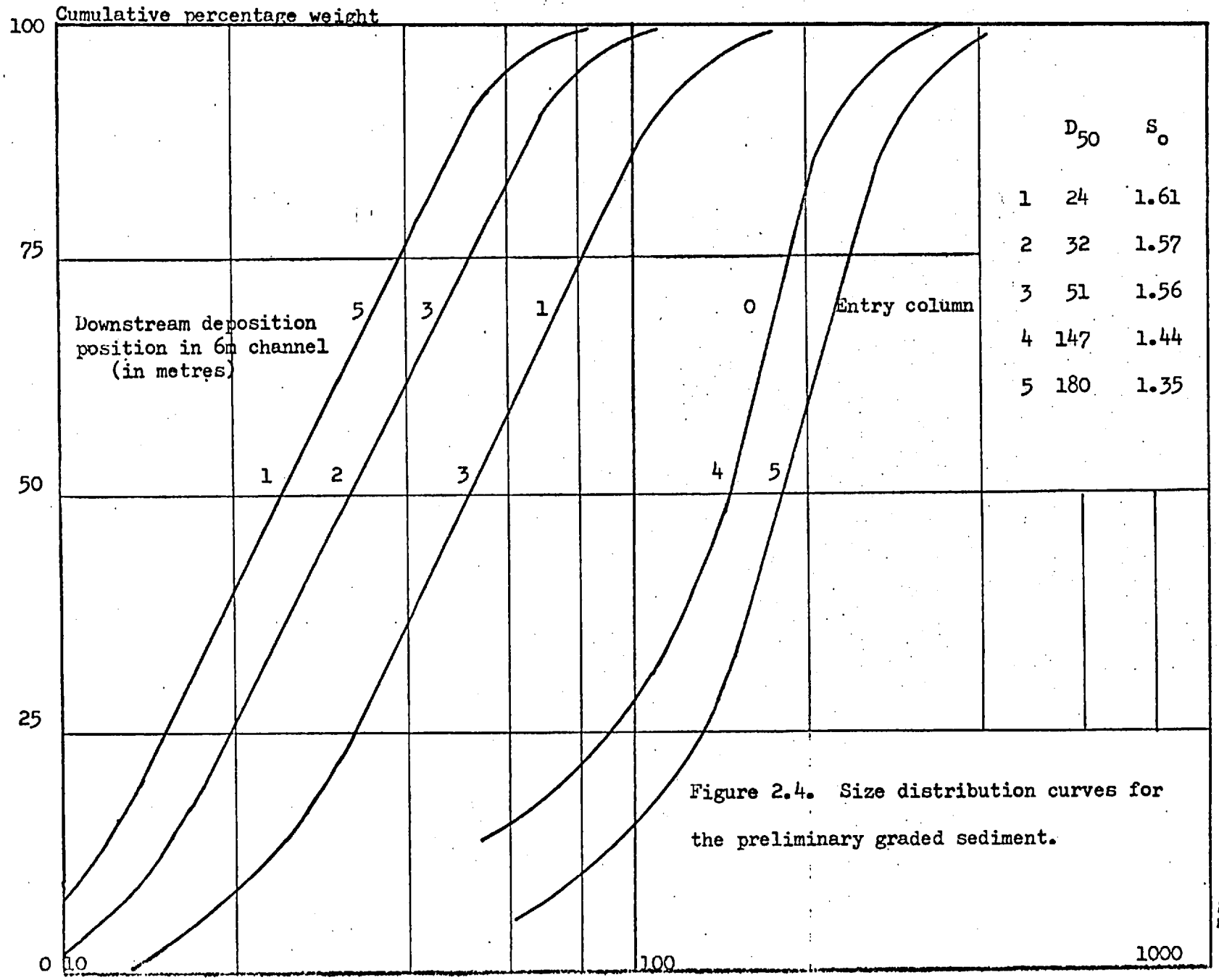

Figure 2.4. Size distribution curves for the preliminary graded sediment.

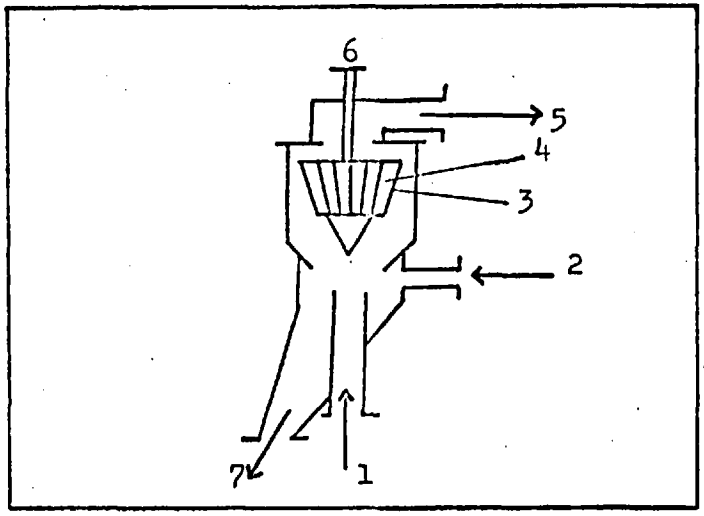

Structure of the Nauta Hosakawa Classifier

1 Conveyor pipe for solids
2 Secondary air inlet pipe
3 Rotor
4 Rotor blades
5 Outlet duct for fine solids
6 Rotor shaft
7 Outlet duct for coarse solids

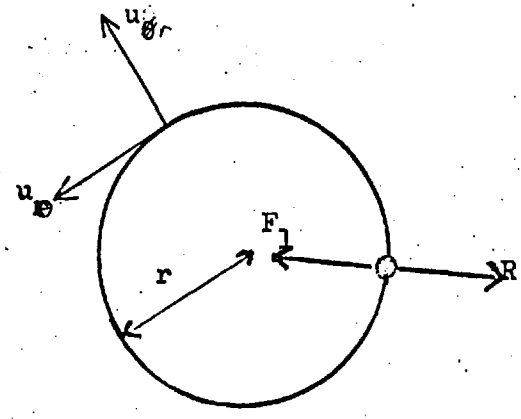

Operating principle of an air classifier

(transverse section of the rotor)

Centripetal air drag force on a solid, $R = 3\pi \mu_a D u_r$

Centrifugal inertial force on a solid, $F_1 = \frac{\pi}{6} D^3(\rho_s - \rho_a)\frac{u_\theta^2}{r}$

Figure 2.5. The Nauta-Hosakawa aerodynamic classifier

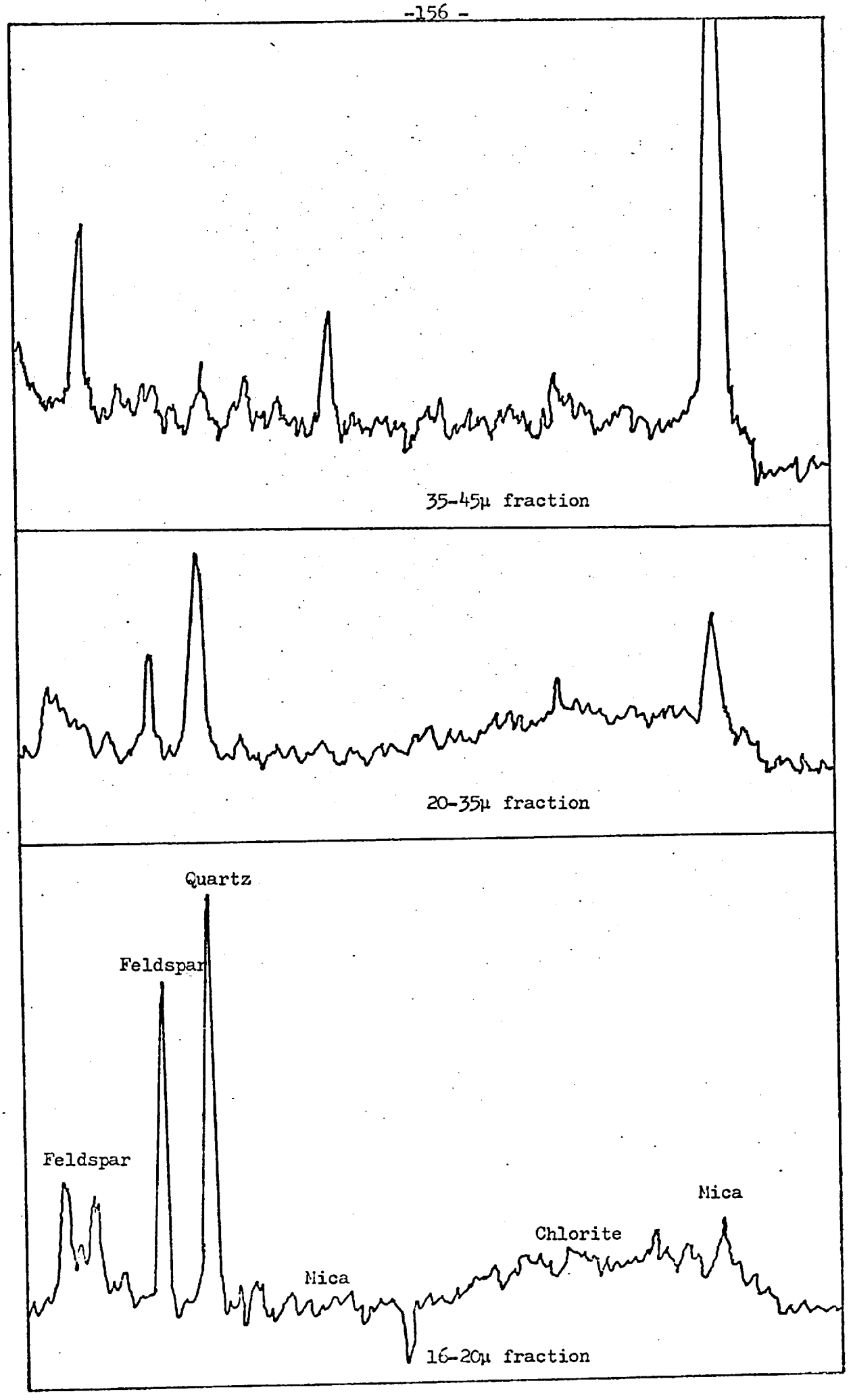

Figure 2.6. X-ray diffractometer traces for sieved fractions of the medium silt grade. (D_{50} = 26μ)

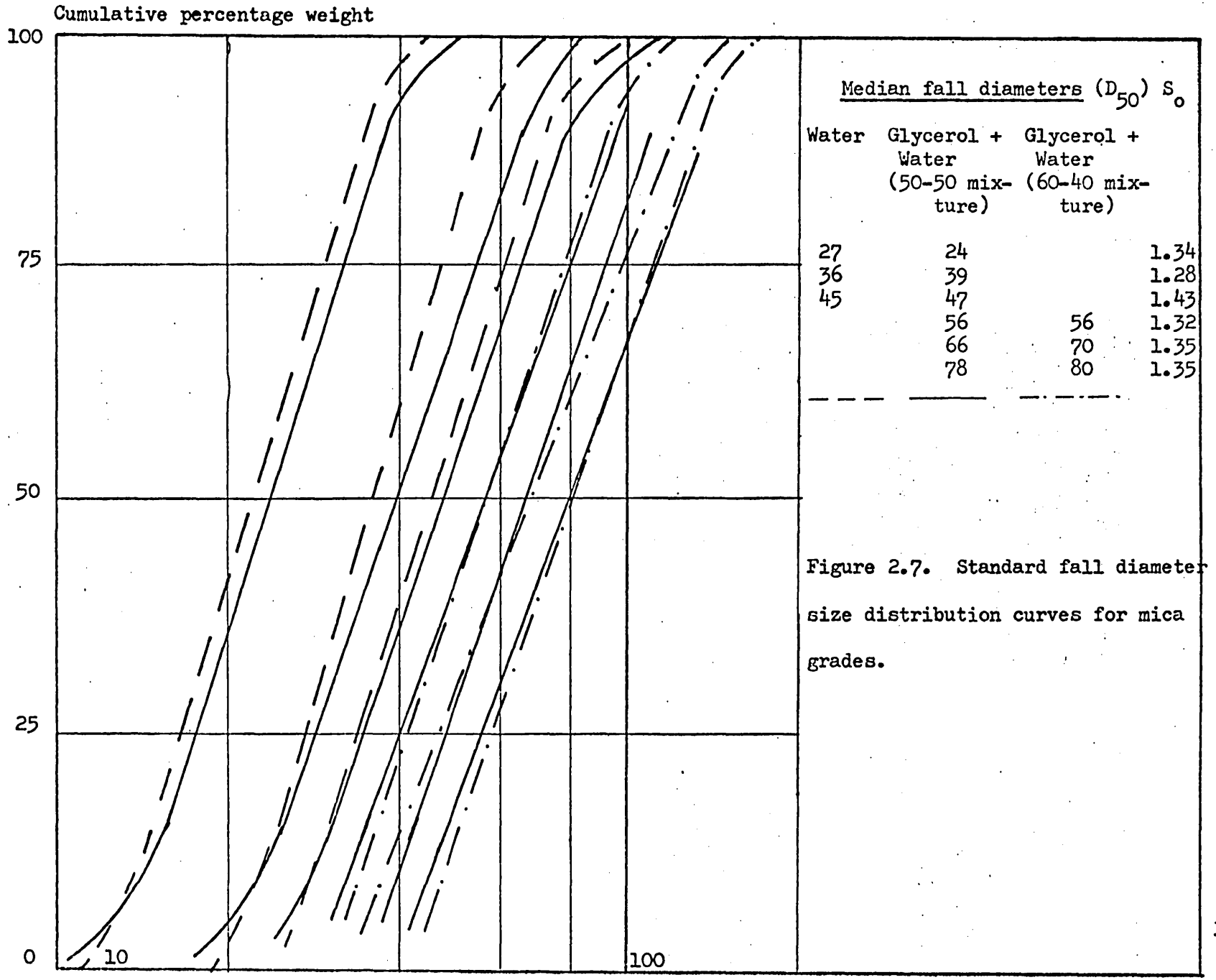

Median fall diameters (D_{50}) S_o

Water	Glycerol + Water (50-50 mixture)	Glycerol + Water (60-40 mixture)	
27	24		1.34
36	39		1.28
45	47		1.43
	56	56	1.32
	66	70	1.35
	78	80	1.35

Figure 2.7. Standard fall diameter size distribution curves for mica grades.

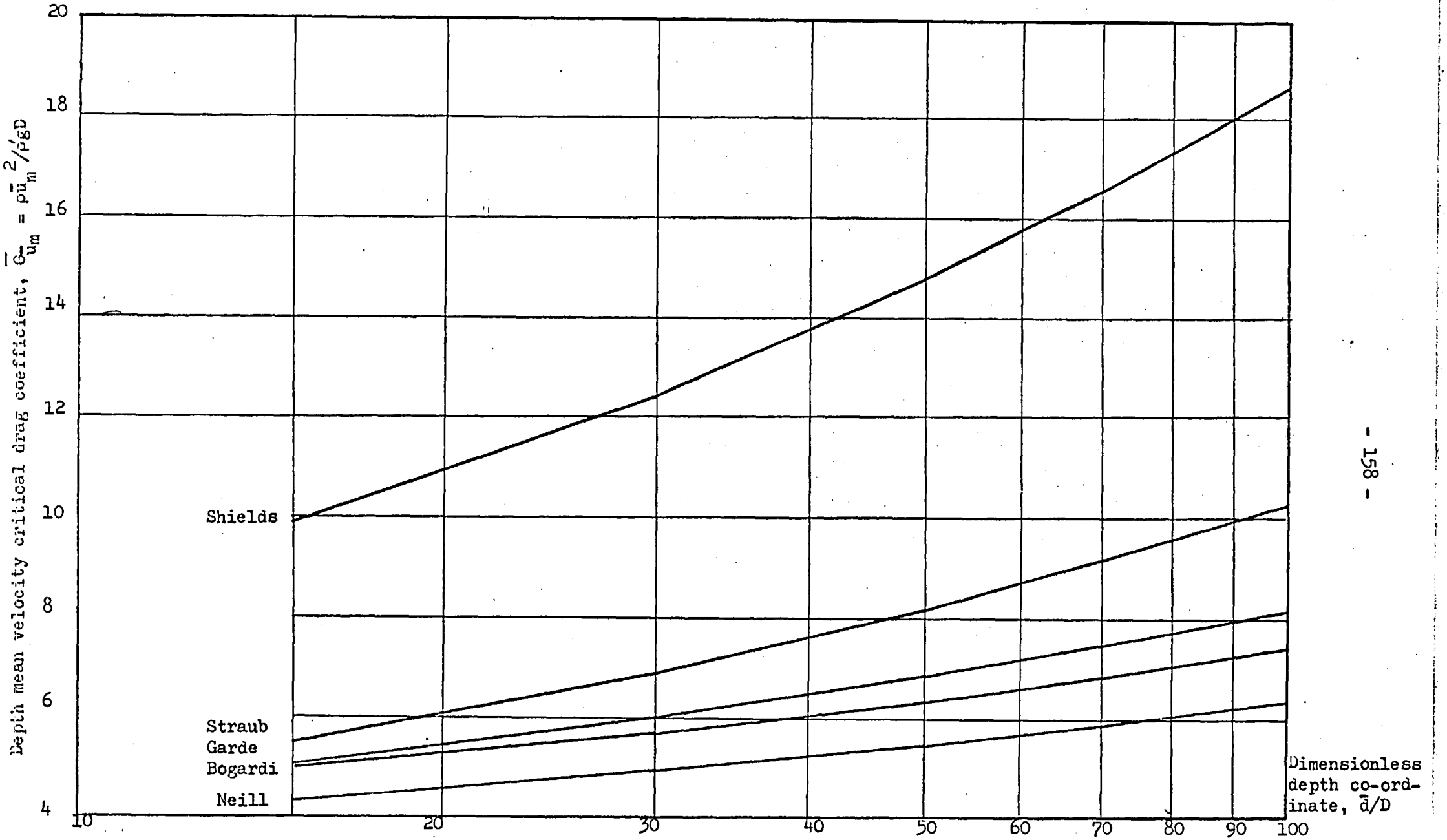

Figure 3.1. Comparison of mean-velocity representations for incipient motion

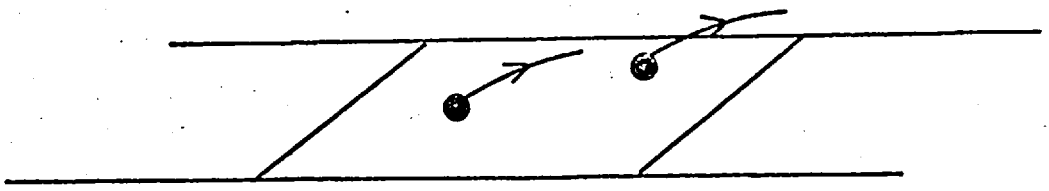

Scale area (A) of bed

Spatial similarity condition is $\frac{\text{area of detachment}}{\text{scale area}}$ = a constant

$$\frac{P_A D^2}{A} = \text{a constant}$$

3.2.1. Simultaneous detachment

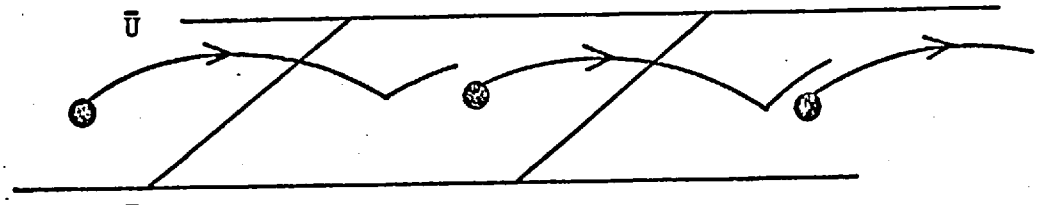

$\bar{U}$ represents average grain velocity

Spatial and kinematic similarity condition is $\frac{P_{Au_*}D^2}{A} \times \frac{\bar{U}}{u_*}$ = a constant

3.2.2. Low-transport rate

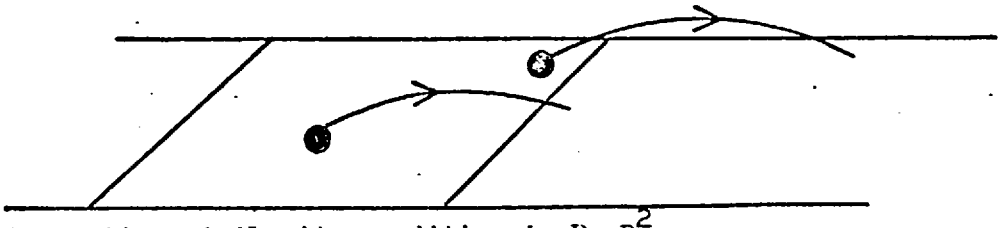

Space-time similarity condition is $\frac{P_{AT}D^2}{A} \times \frac{\overline{\delta t}}{T}$ = a constant

3.2.3. Low removal rate

Figure 3.2. Observational similarity conditions for different experiments on incipient motion

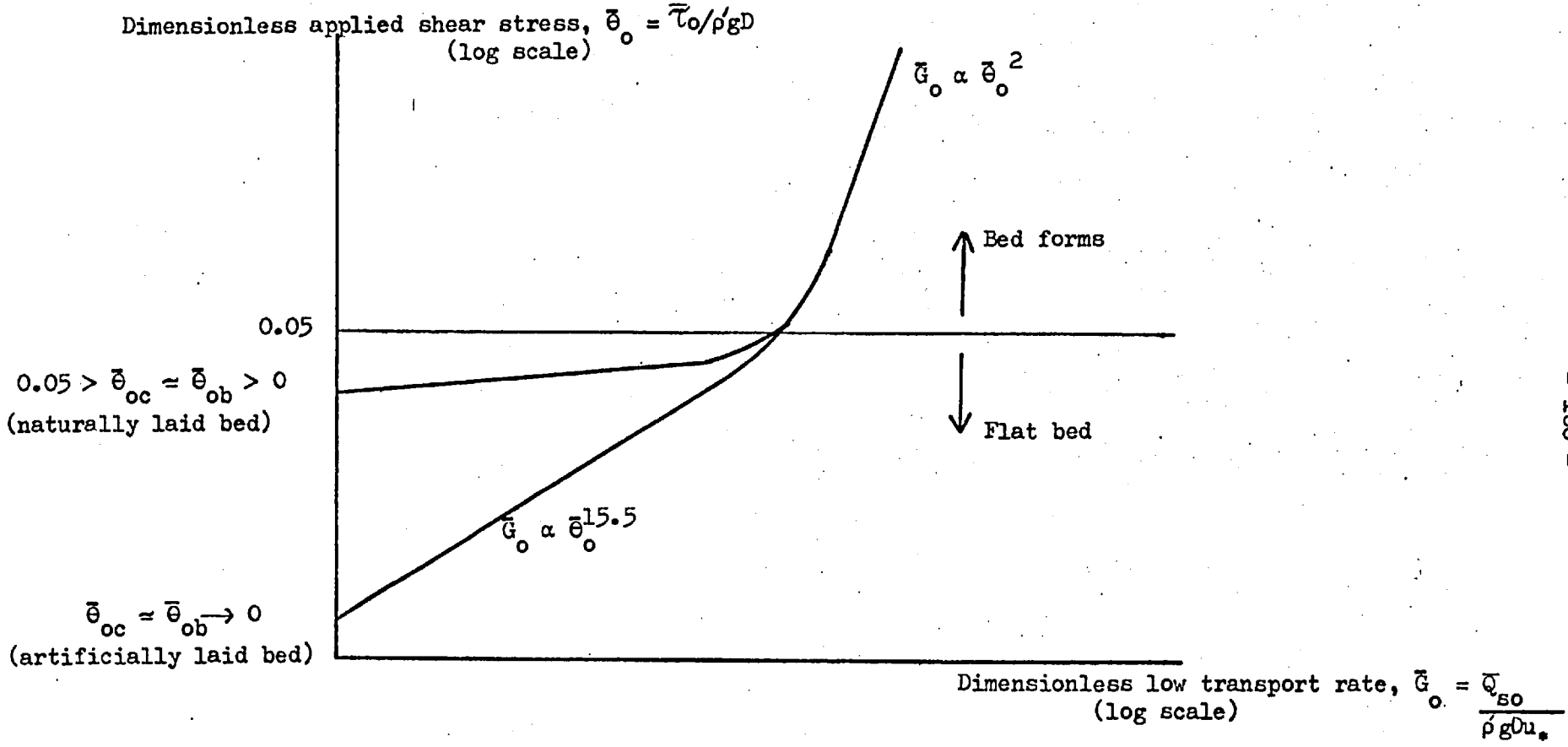

Figure 3.3. The trend for low transport rates over artificial and natural flat beds

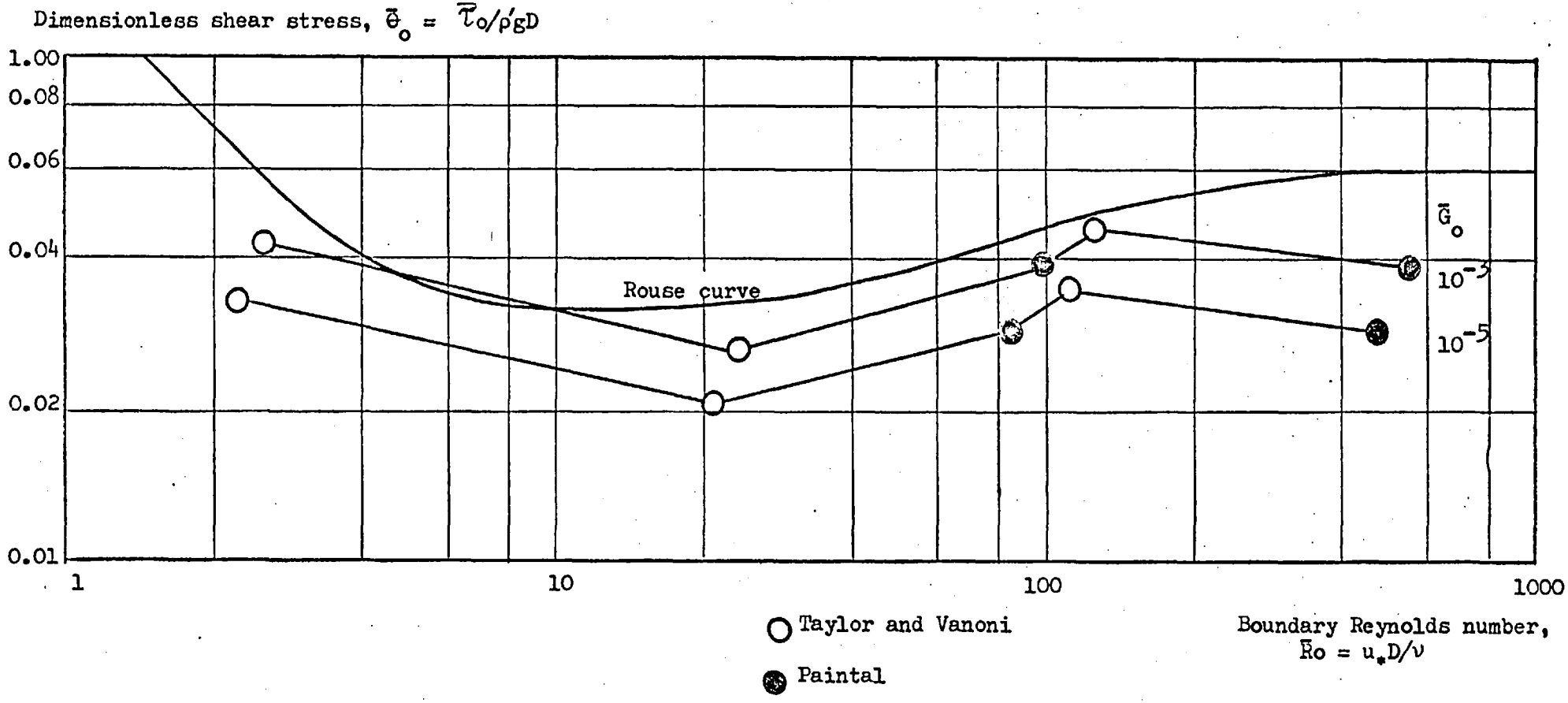

Figure 3.4. Low transport rates plotted on the Shields diagram.

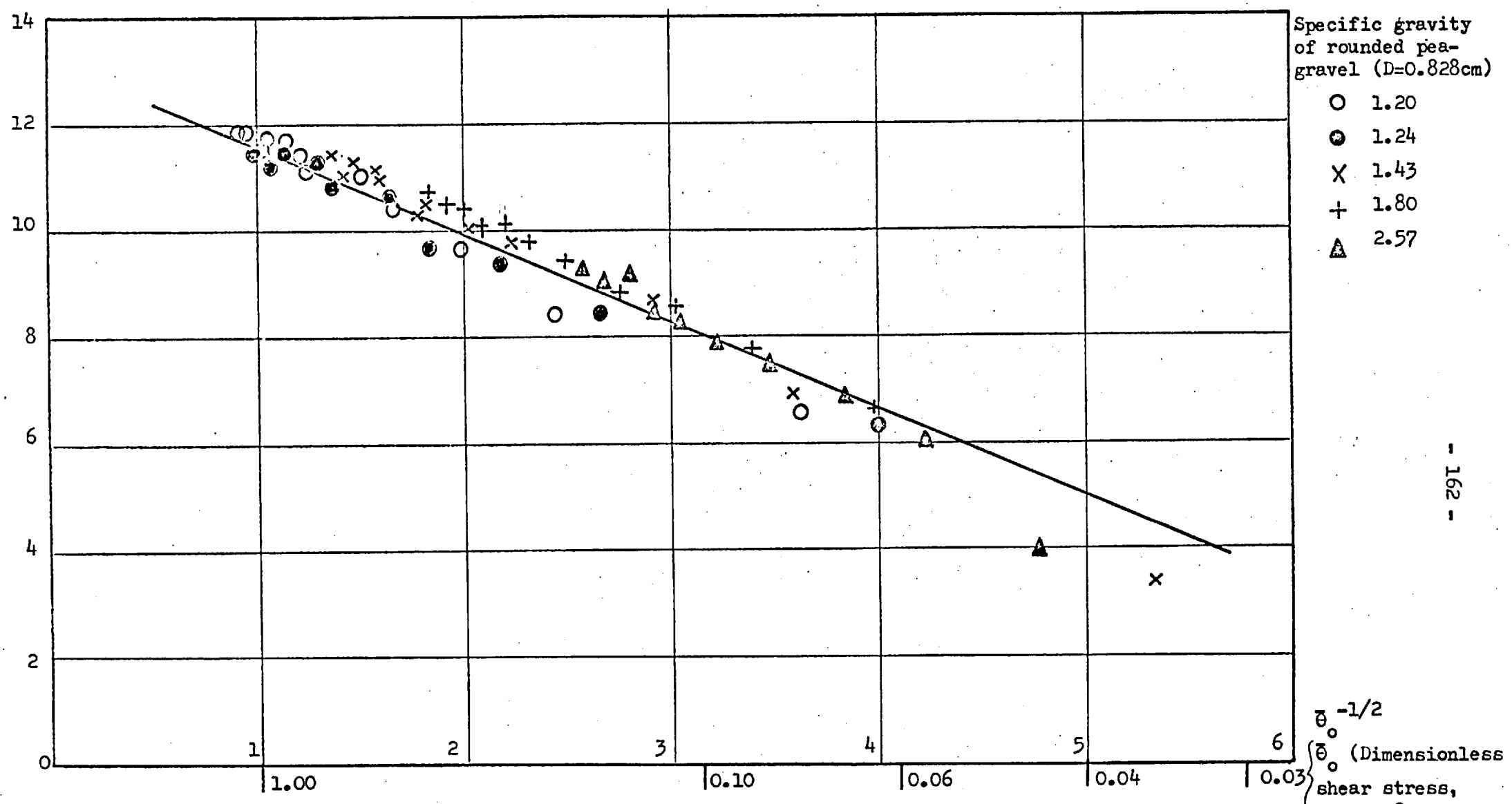

Figure 3.5. A functional representation for average grain velocities in turbulent rough boundary flows.

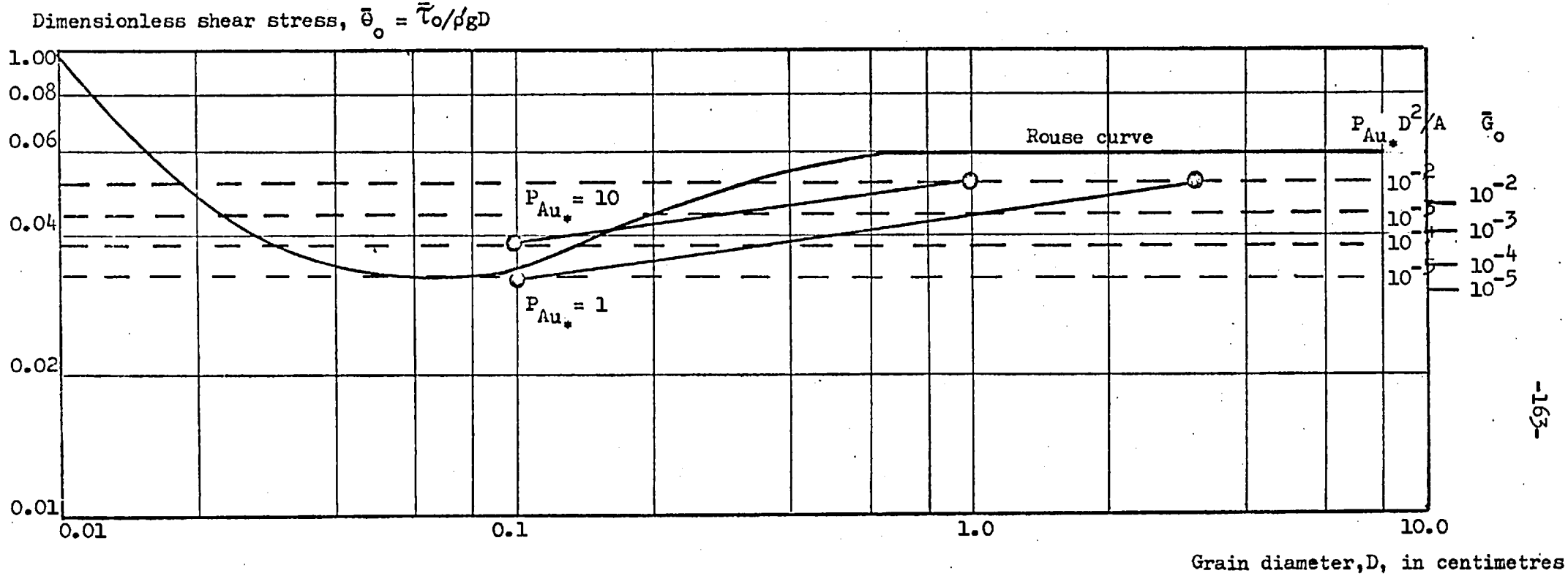

Figure 3.6. Low transport rate curves for observations over fixed areas.

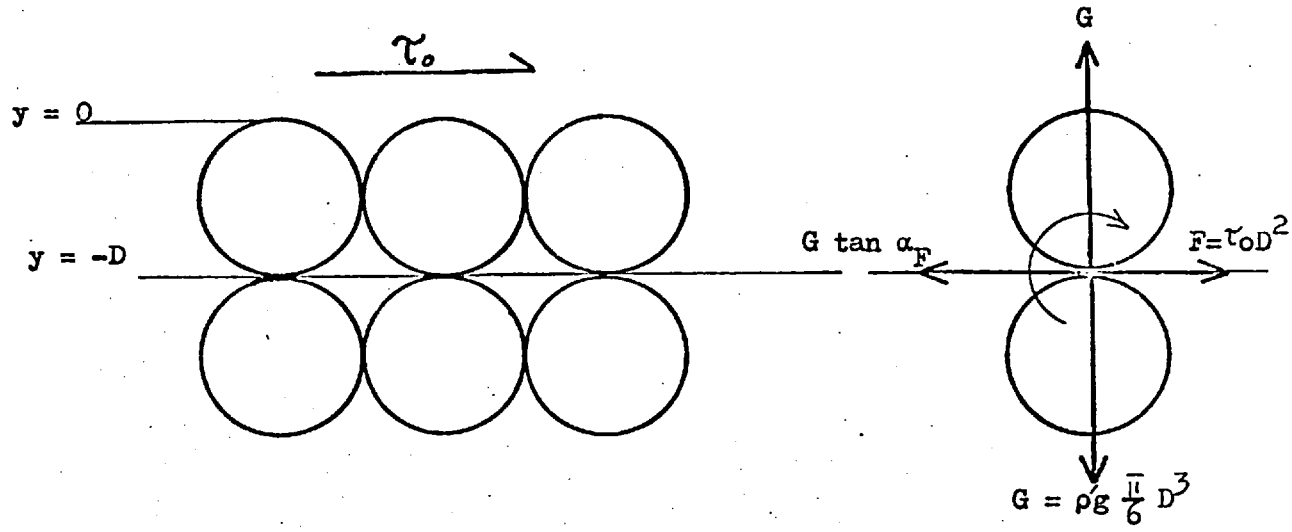

3.7.1. A cubic array of bed spheres

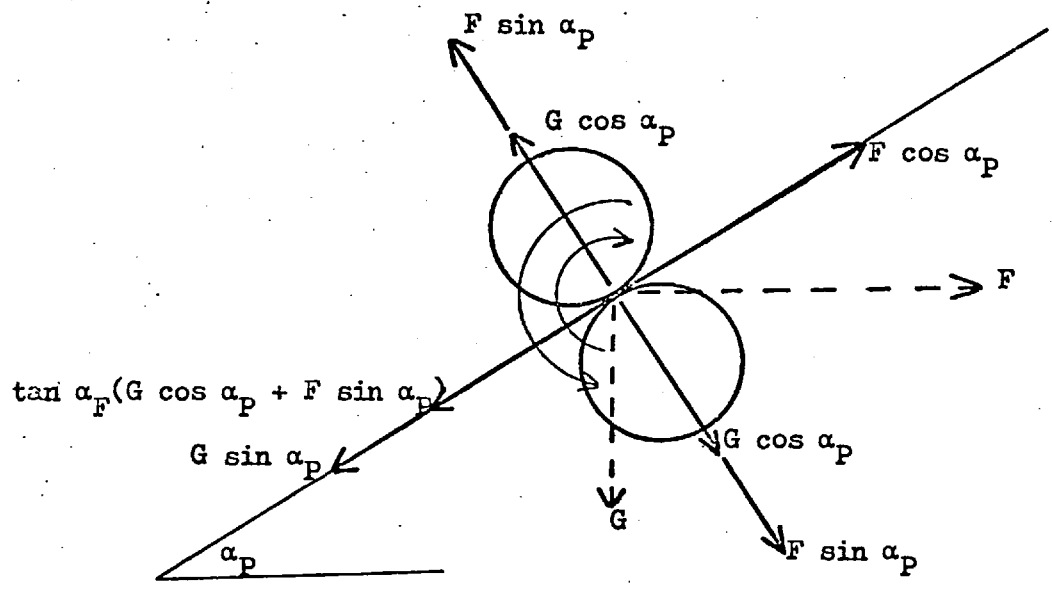

3.7.2. A more general array of bed spheres

Figure 3.7. Force balance for sliding detachment

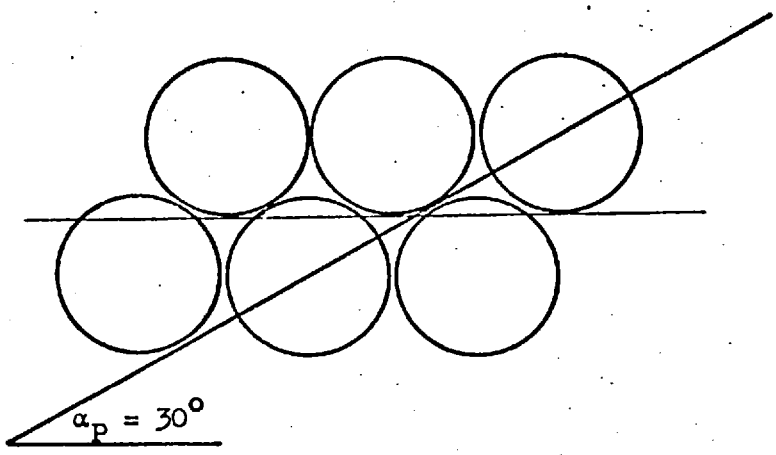

Side elevation through an XY plane

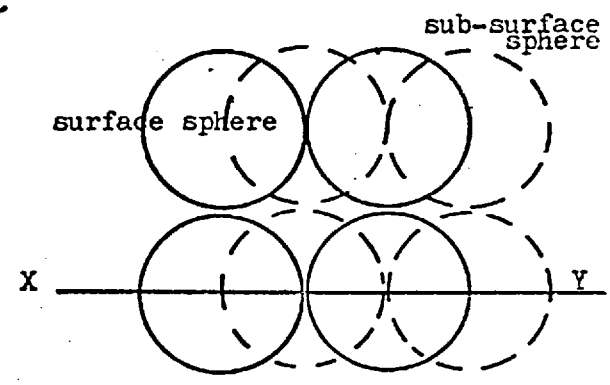

Plan elevation

3.8.1. $\alpha_p = 30^\circ$

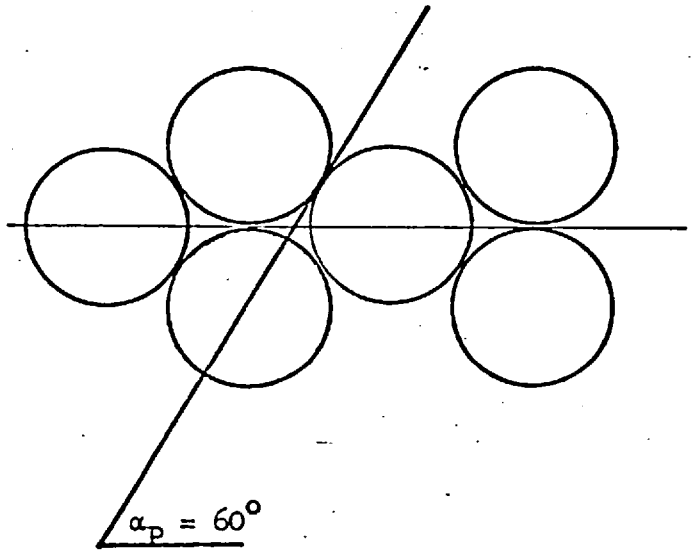

Side elevation through an XY plane

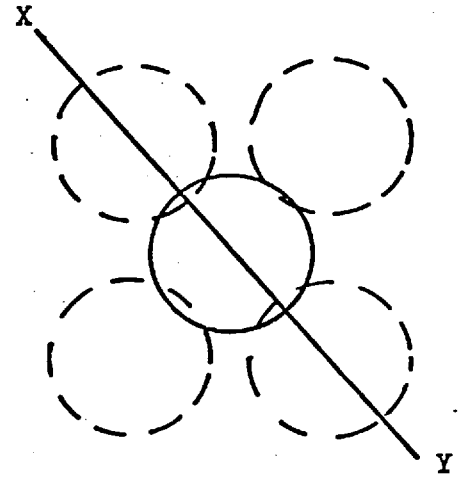

Plan

3.8.2. $\alpha_p = 60^\circ$

Figure 3.8. Bed surface arrays for different planes of sliding

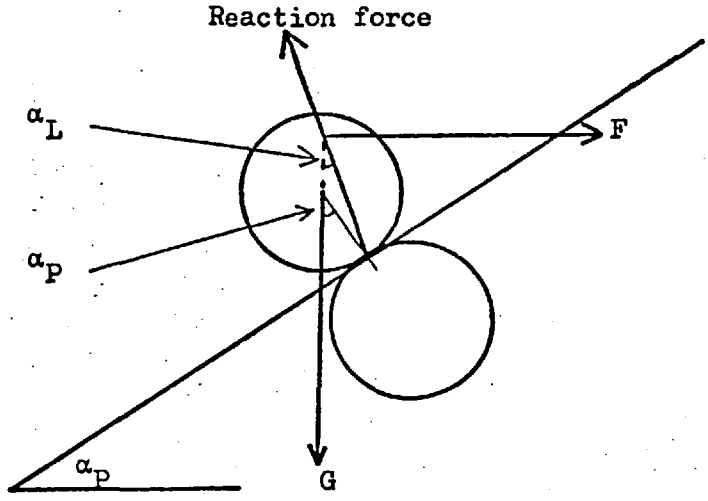

3.9.1. The rolling condition

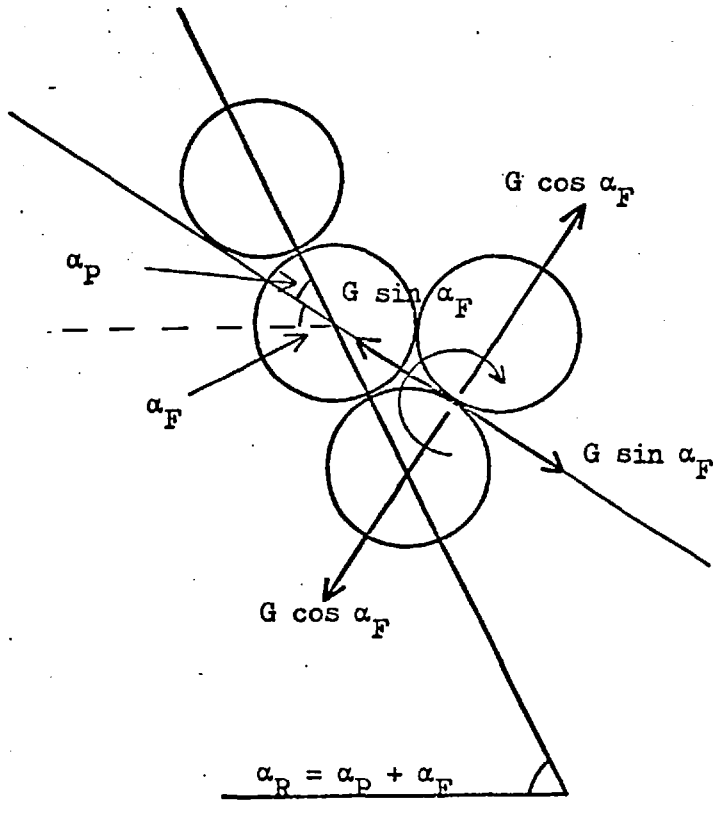

3.9.2. The limiting static angle of repose for sliding

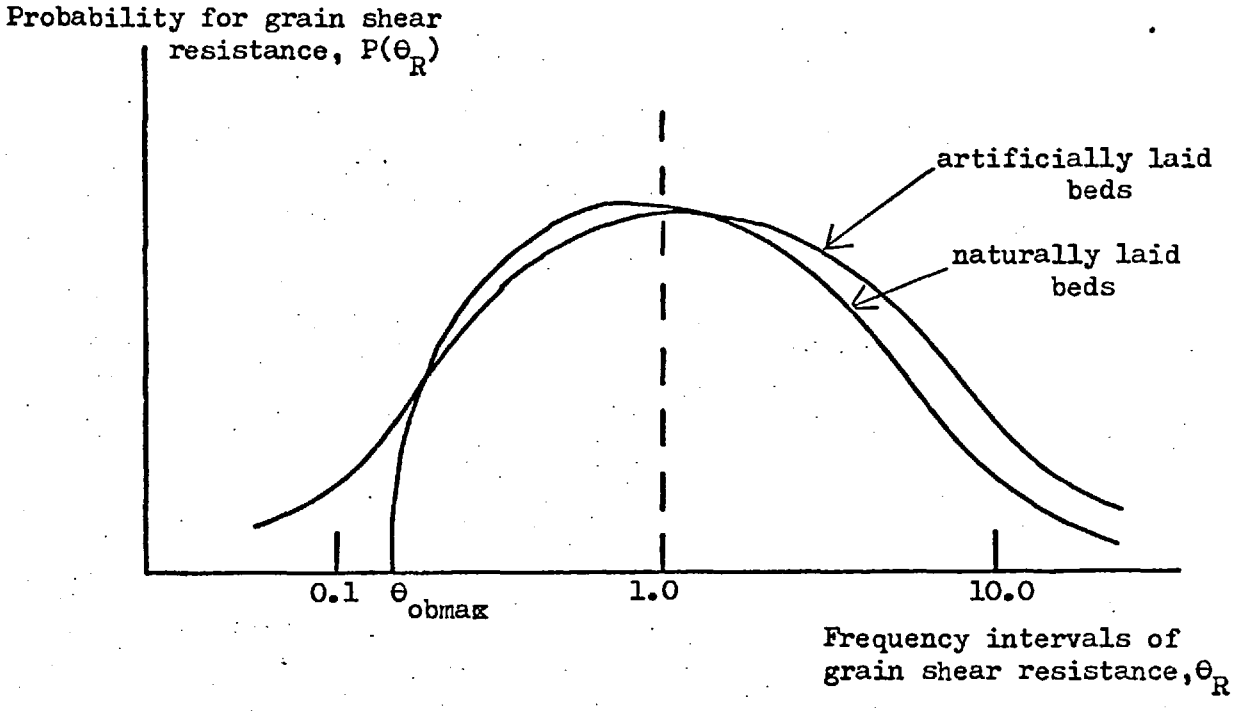

Figure 3.10. Probability distributions for grain shear resistance.

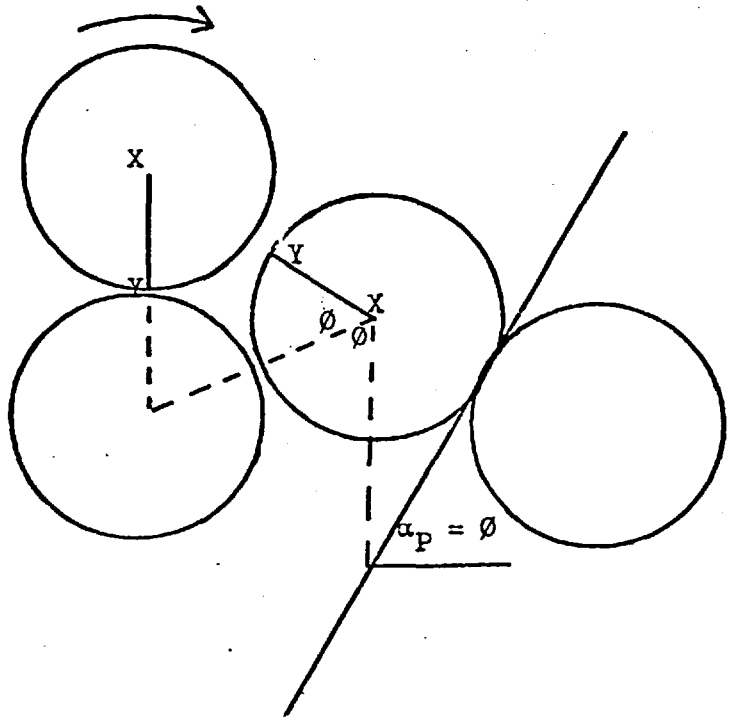

Figure 3.11. The maximum angle of rolling for $\alpha_p = 60^o$

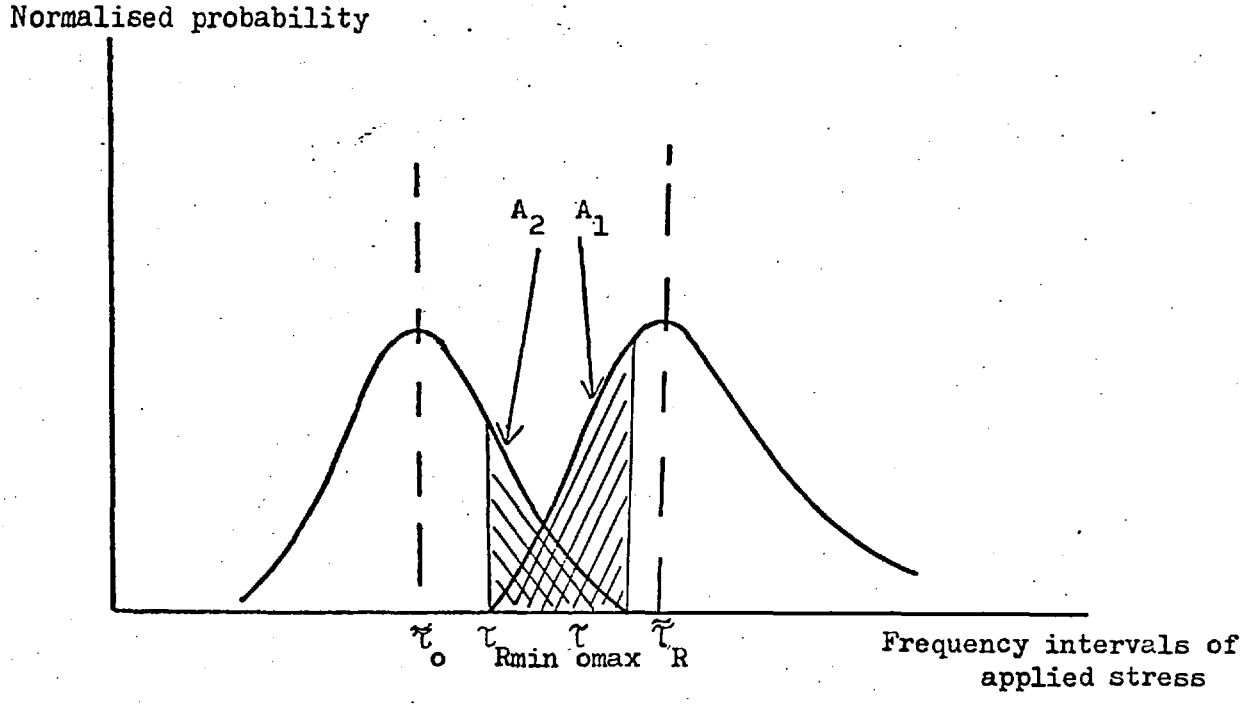

3.12.1. The general case

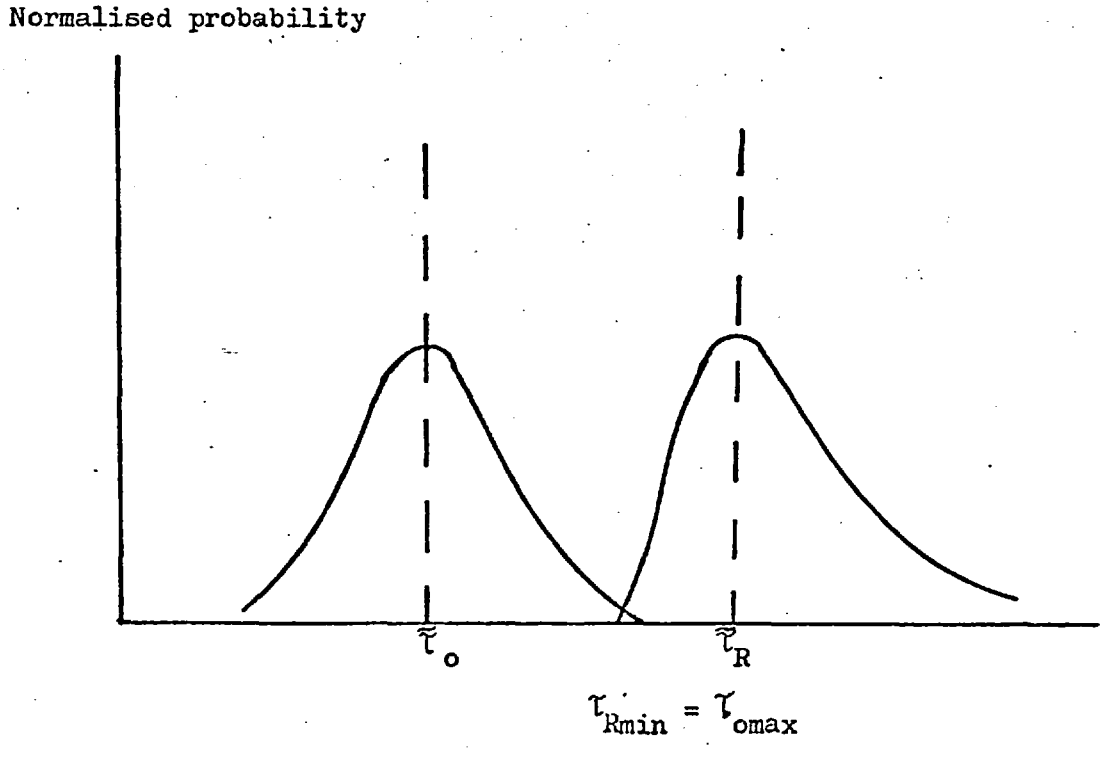

3.12.2. The critical case

Figure 3.12. Probability distributions for applied shear stress and grain shear resistance

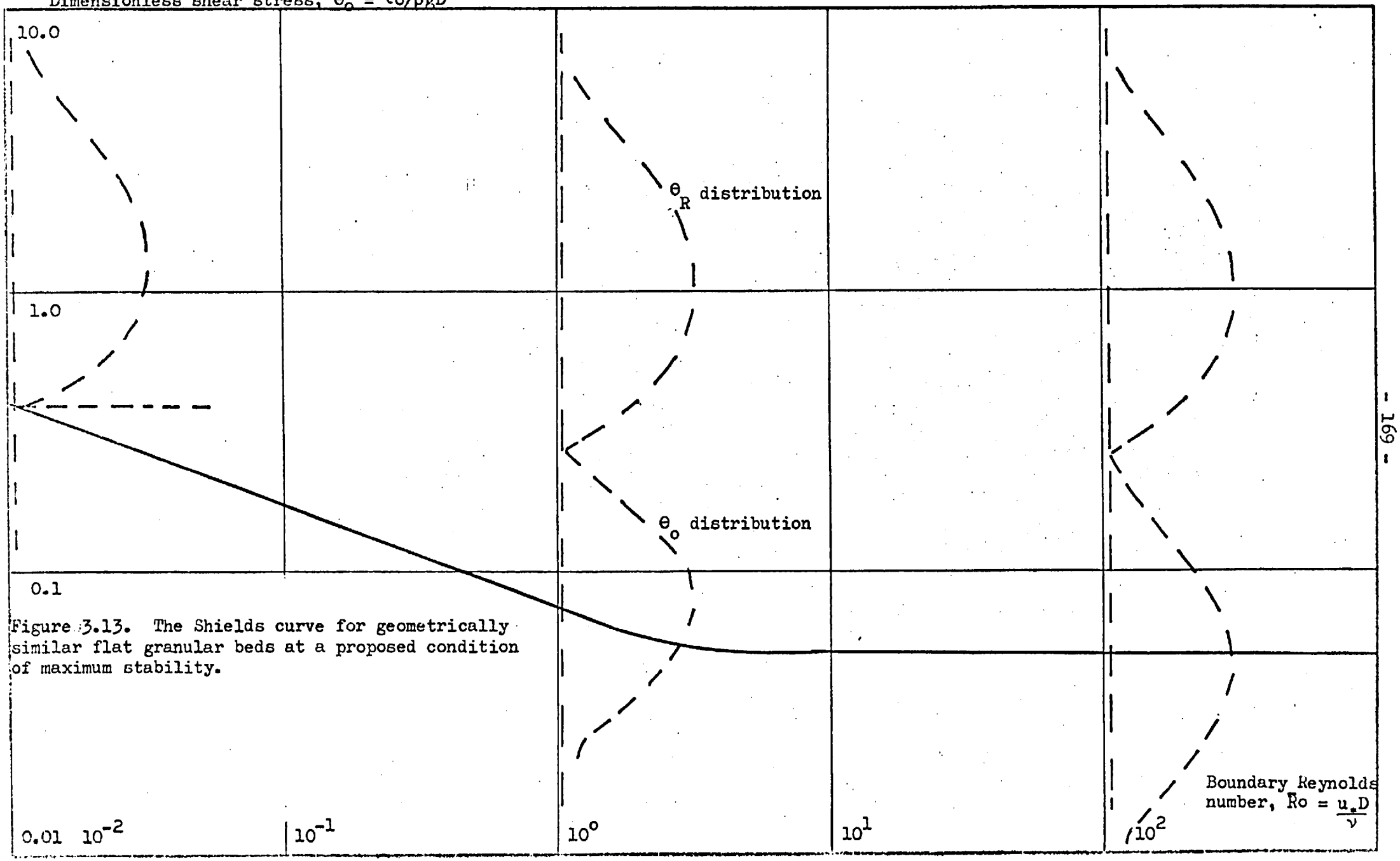

Figure 3.13. The Shields curve for geometrically similar flat granular beds at a proposed condition of maximum stability.

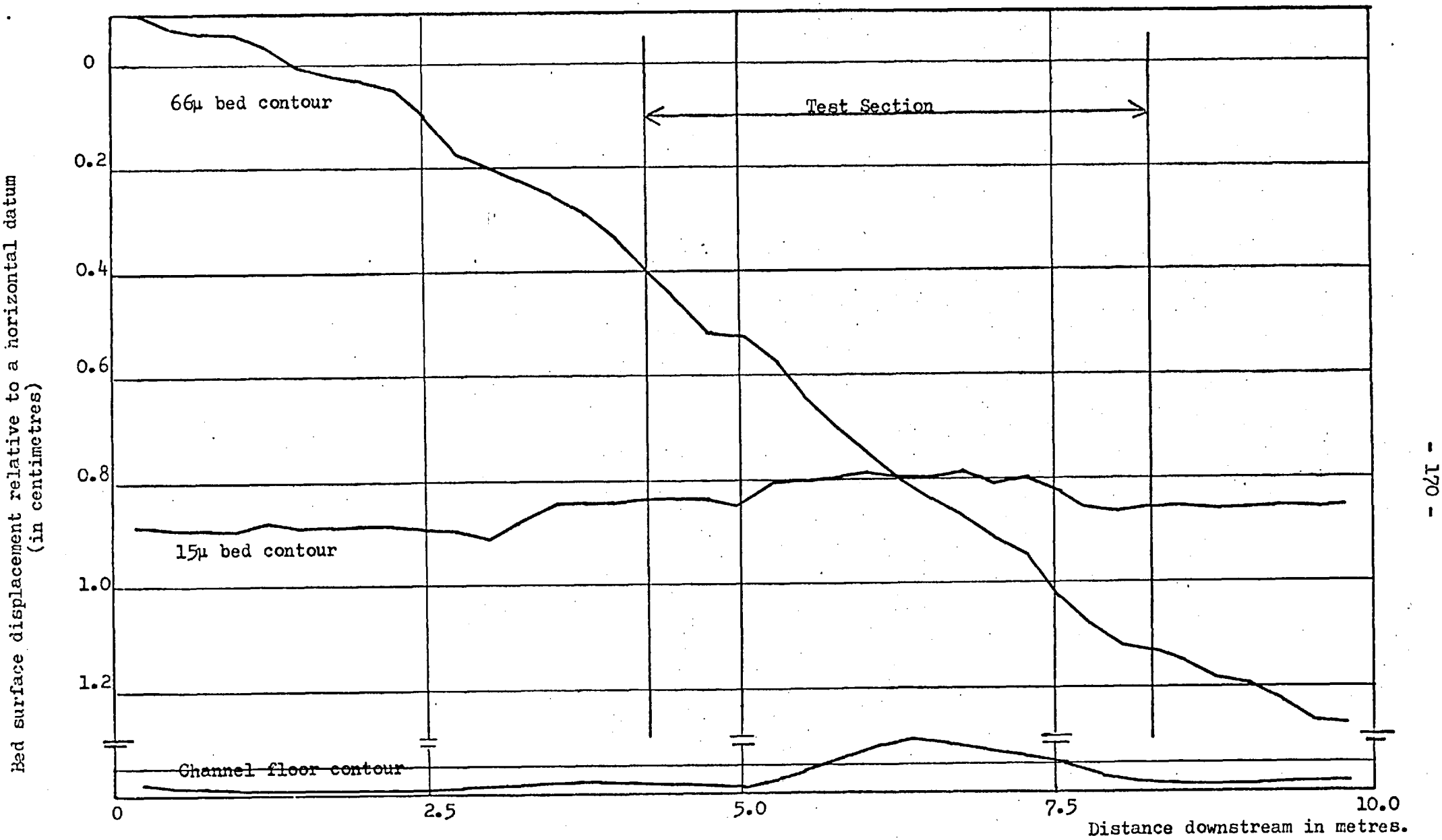

Figure 4.1. Sedimentary bed surface contours, along channel centre-line, for the entire channel length (15μ and 66μ granular grades)

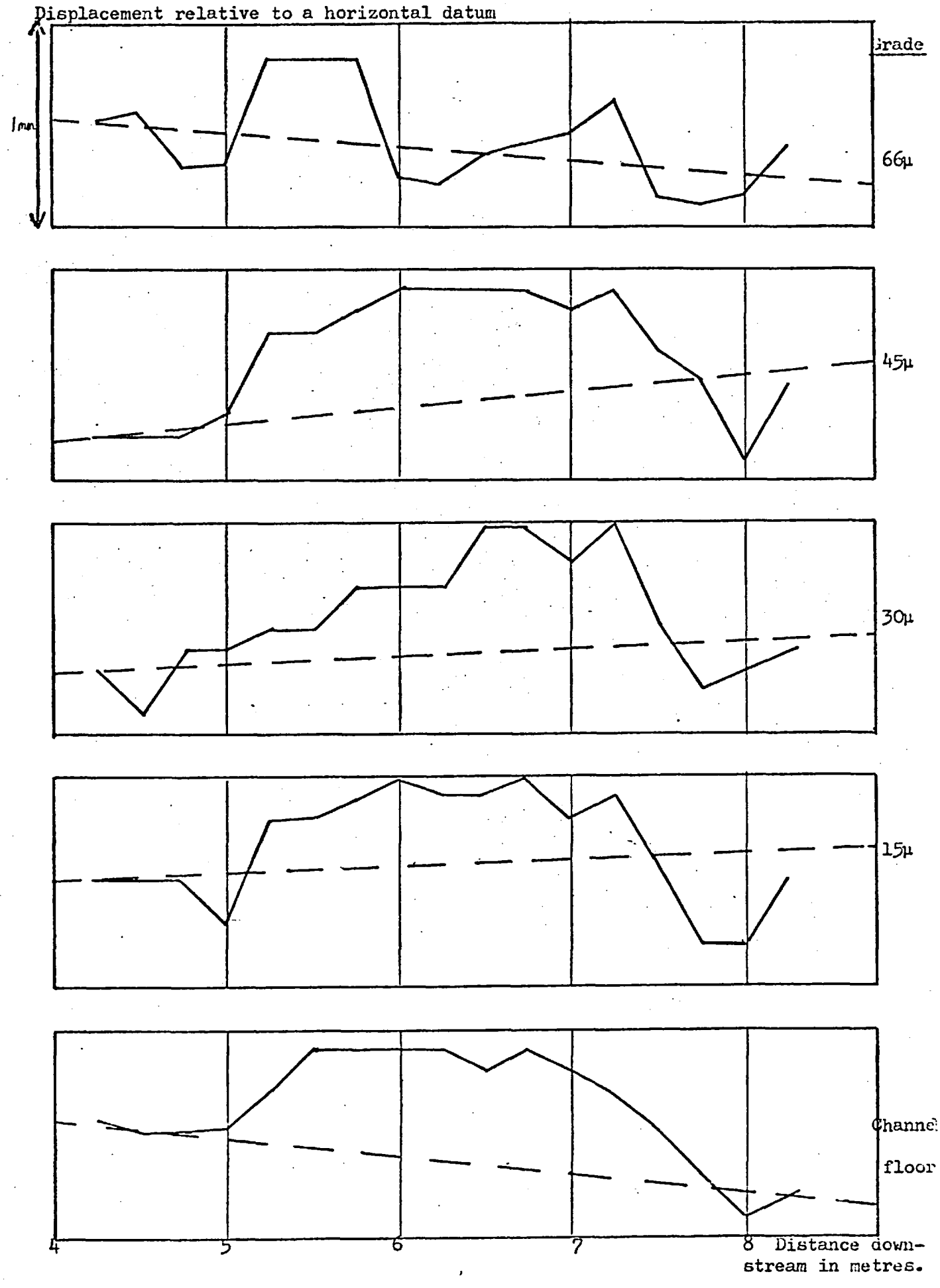

Figure 4.2. Sedimentary bed surface contours, along the channel centre-line, for the test-section (all 4 granular grades).

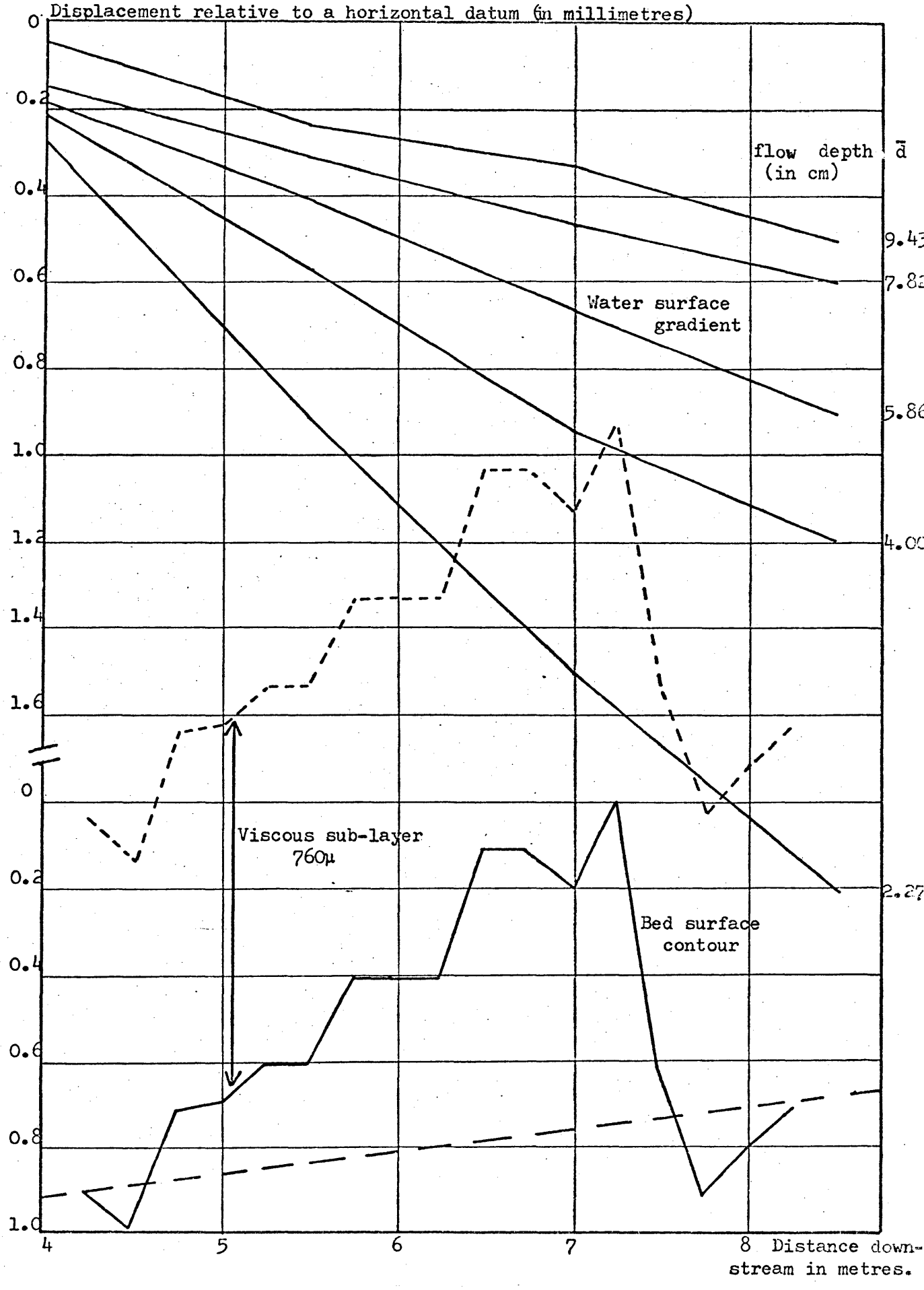

Figure 4.3. Average water surface gradients for the 30μ granular grade incipient motion experiment

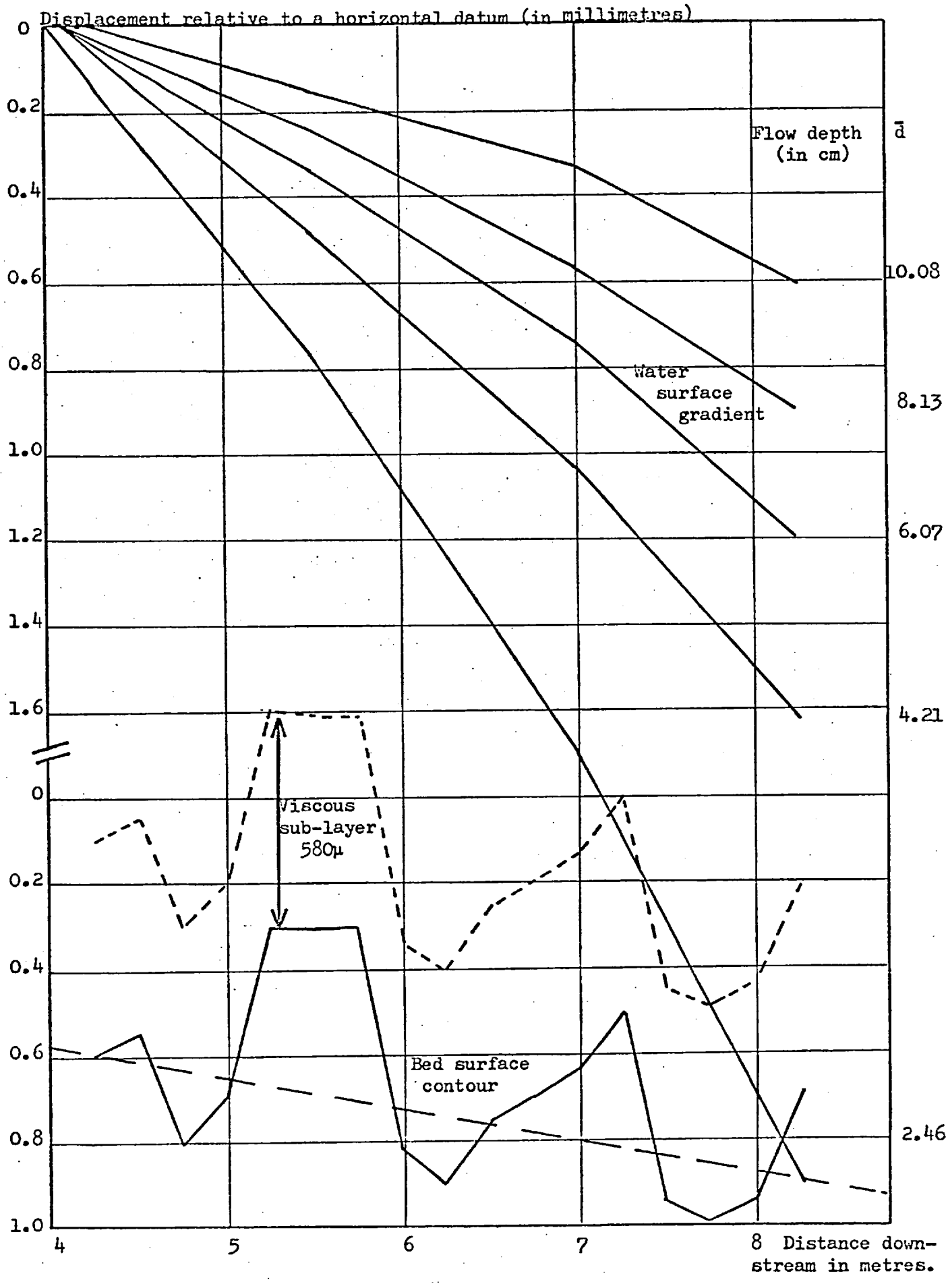

Figure 4.4. Average water surface gradients for the 66μ granular grade incipient motion experiment.

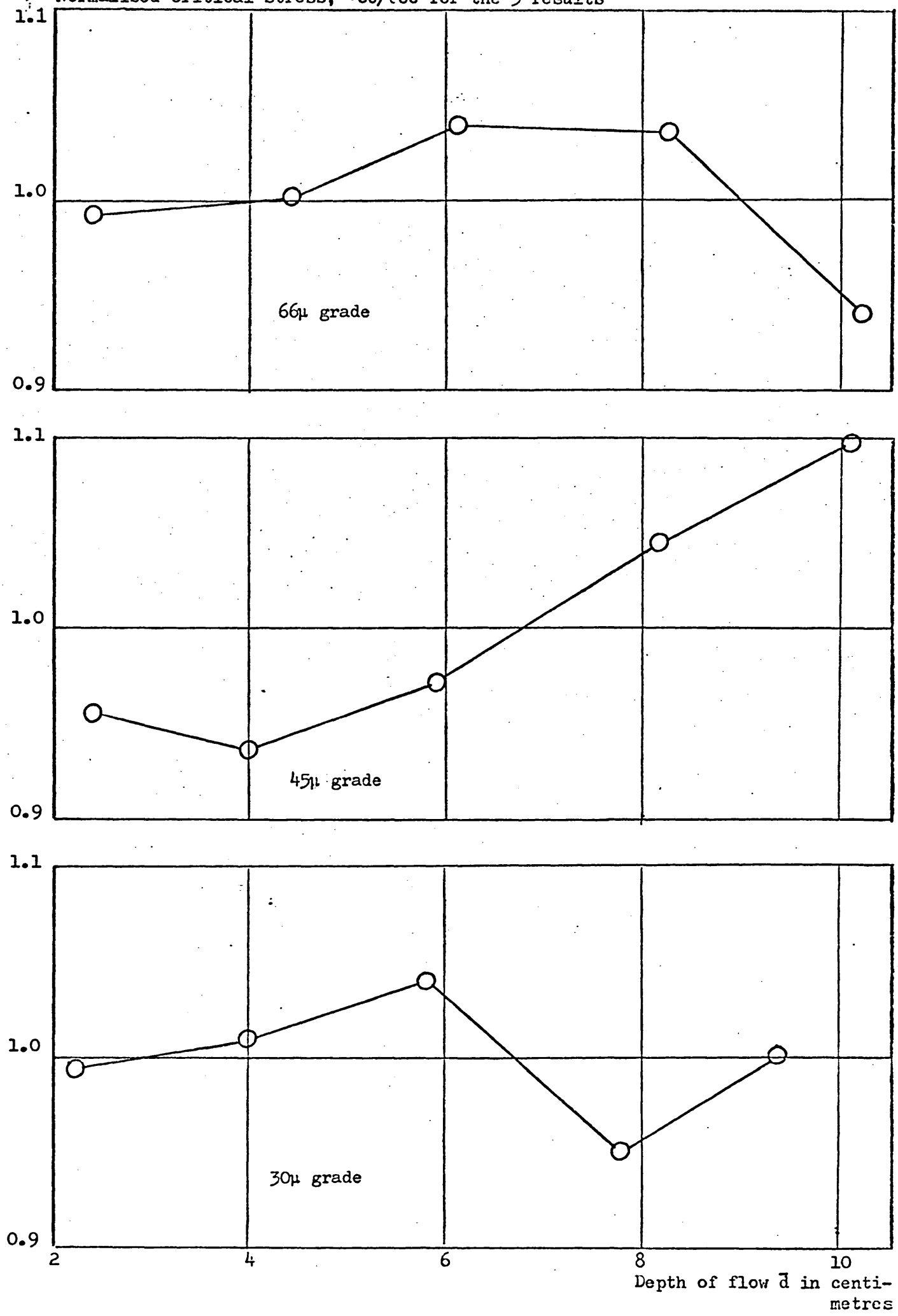

Figure 4.5. Variation of the low transport, normalised, critical stress with depth of flow (30,45 and 66μ granular grades)

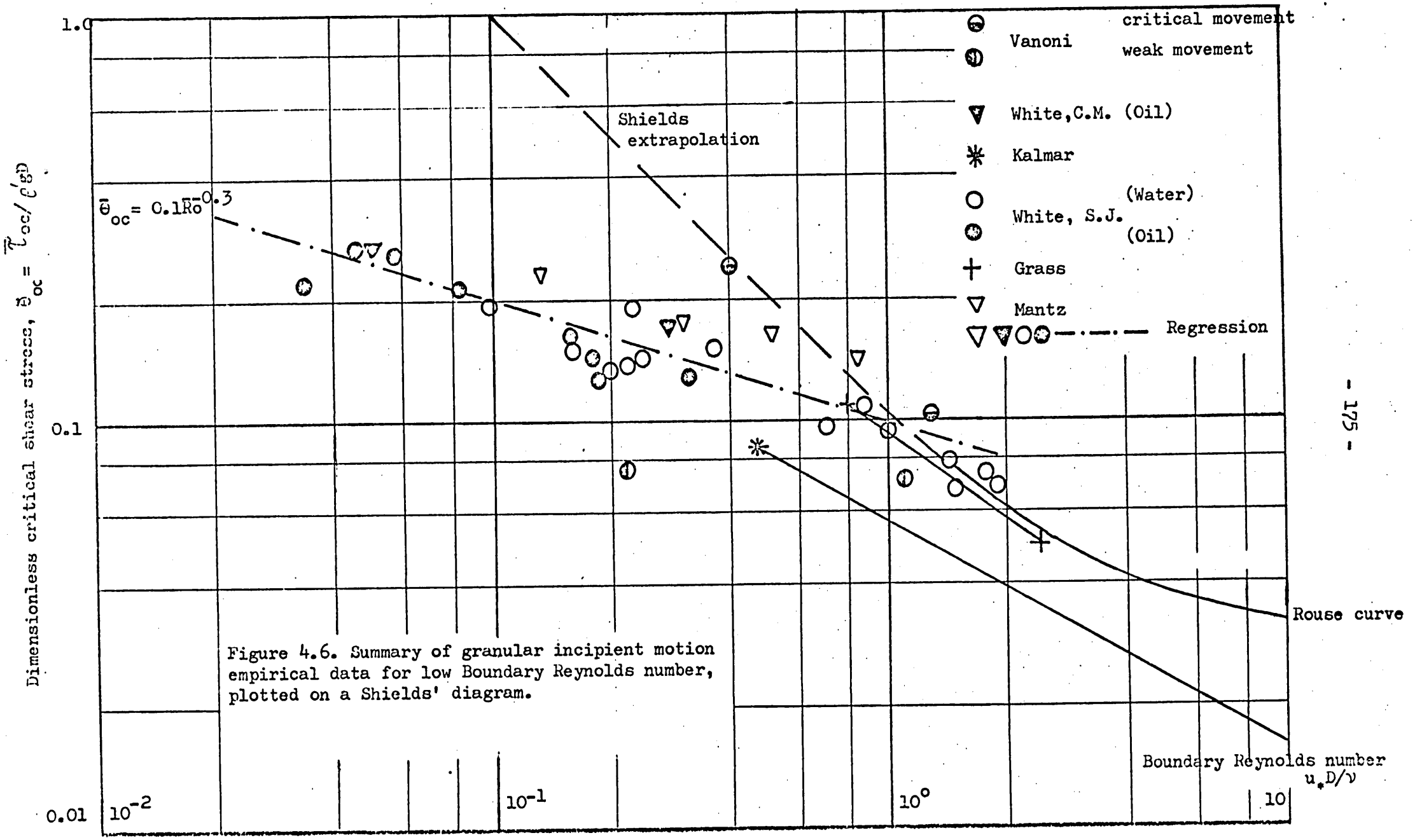

Figure 4.6. Summary of granular incipient motion empirical data for low Boundary Reynolds number, plotted on a Shields' diagram.

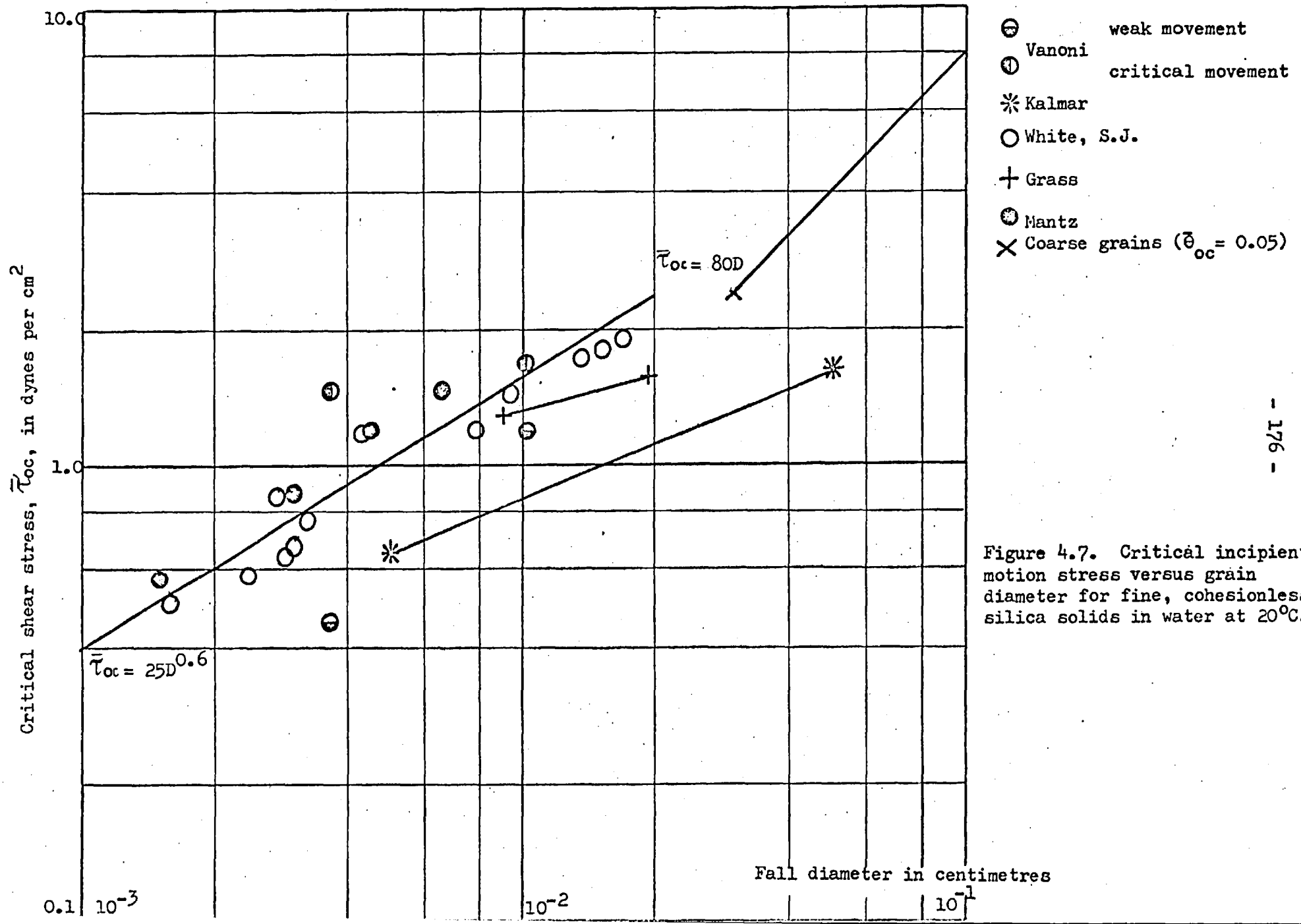

Figure 4.7. Critical incipient motion stress versus grain diameter for fine, cohesionless silica solids in water at 20°C.

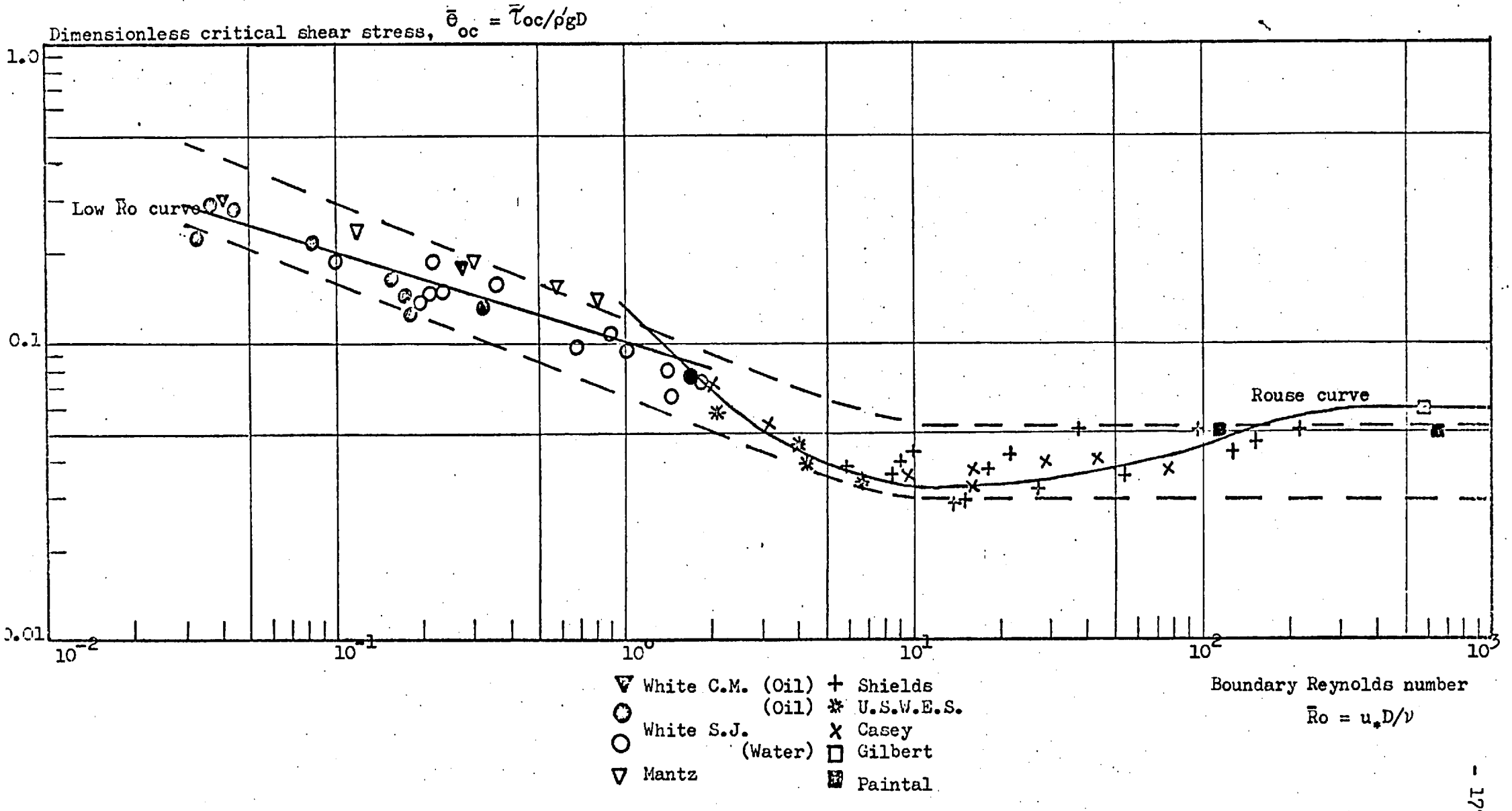

Figure 4.8. The Shields diagram for flat granular beds of maximum stability, extended to low Boundary Reynolds numbers.

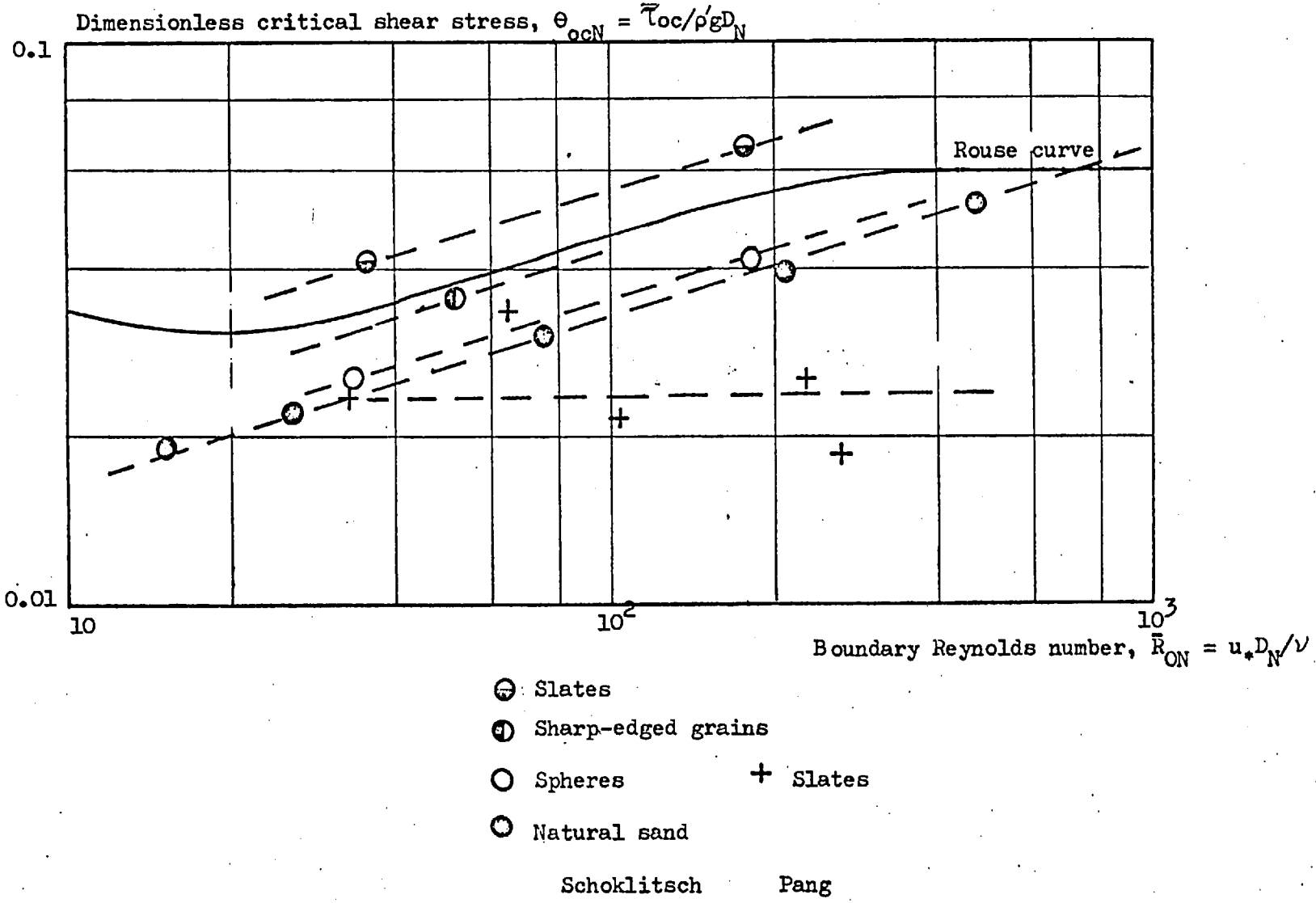

Figure 5.1. The Shields diagram for the incipient motion of coarse solids of various shapes.

Figure 5.2. Sedimentary bed surface contours, along the channel centre line, for the test section(for each of two depositions of the 6 flake grades)

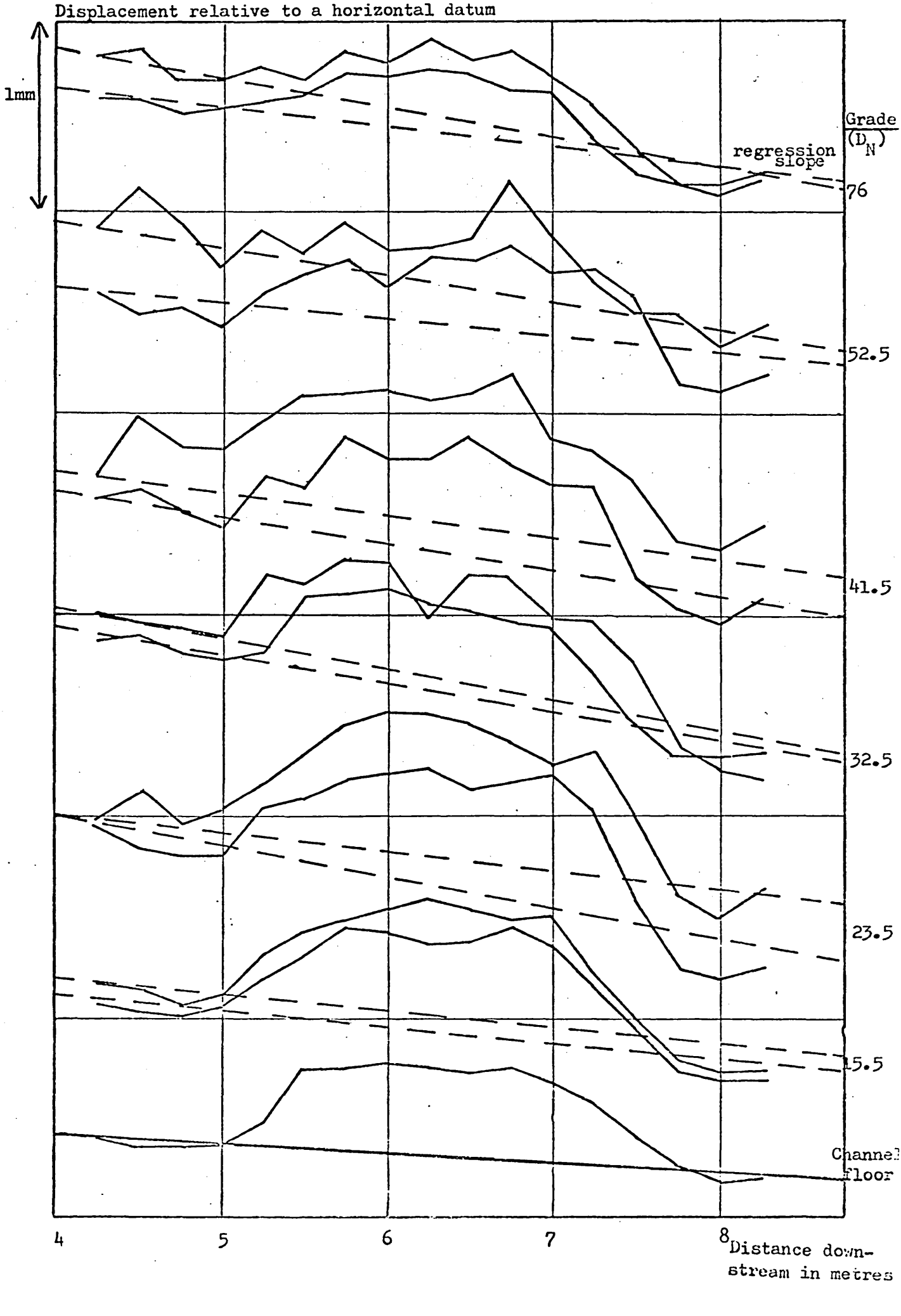

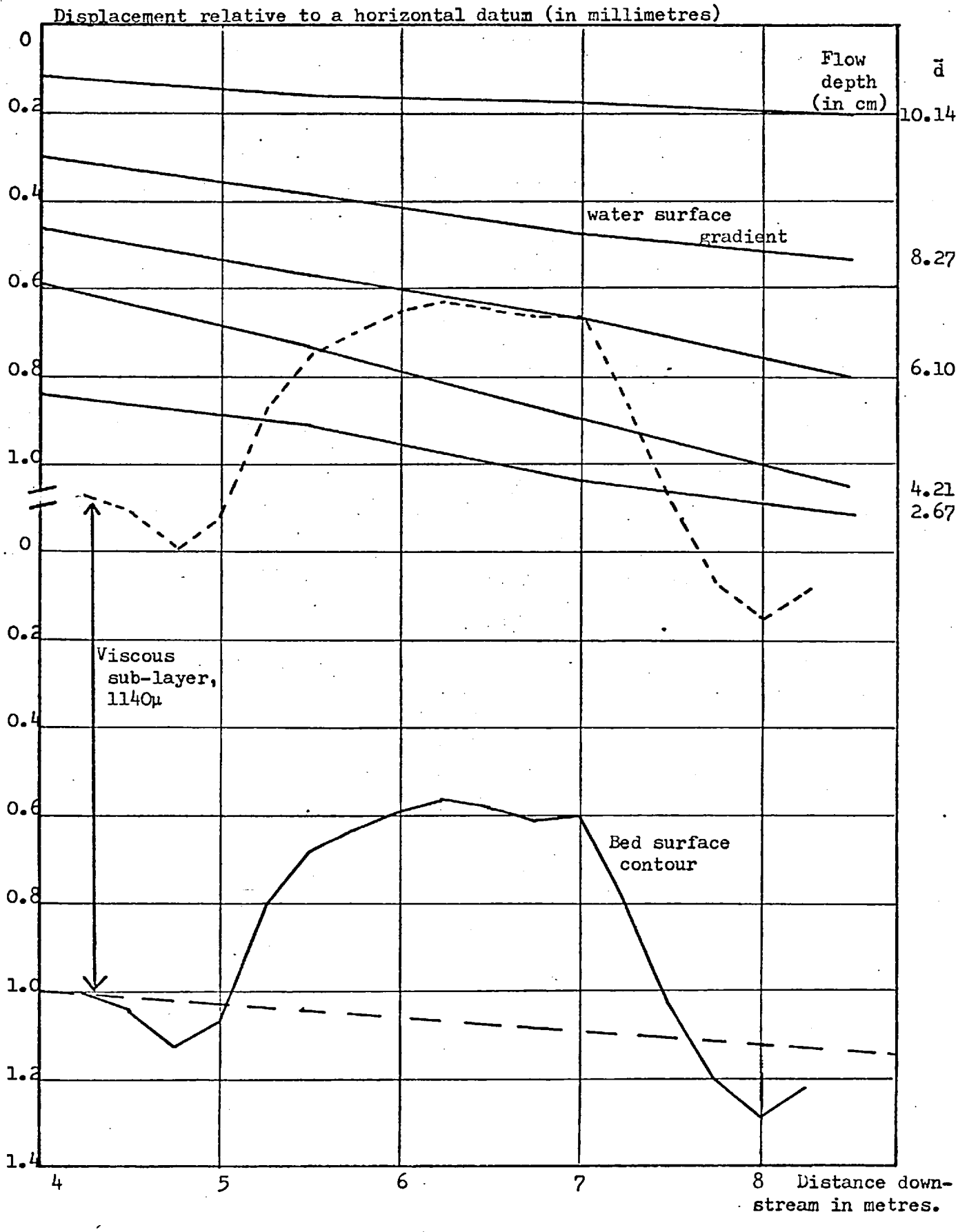

Figure 5.3. Average water surface gradients for the 15.5μ flake grade incipient motion experiment

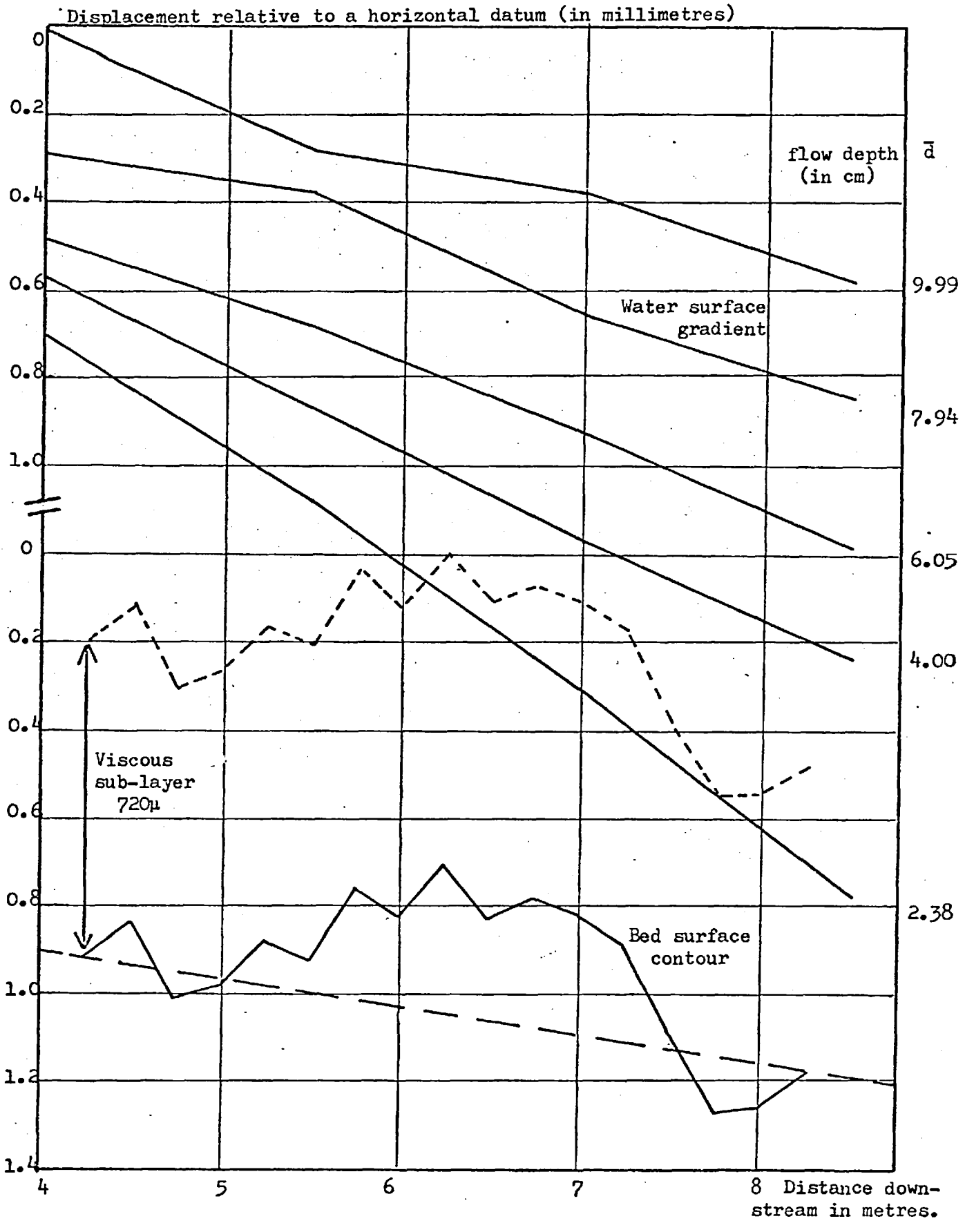

Figure 5.4. Average water surface gradients for the 76μ flake grade incipient motion experiment.

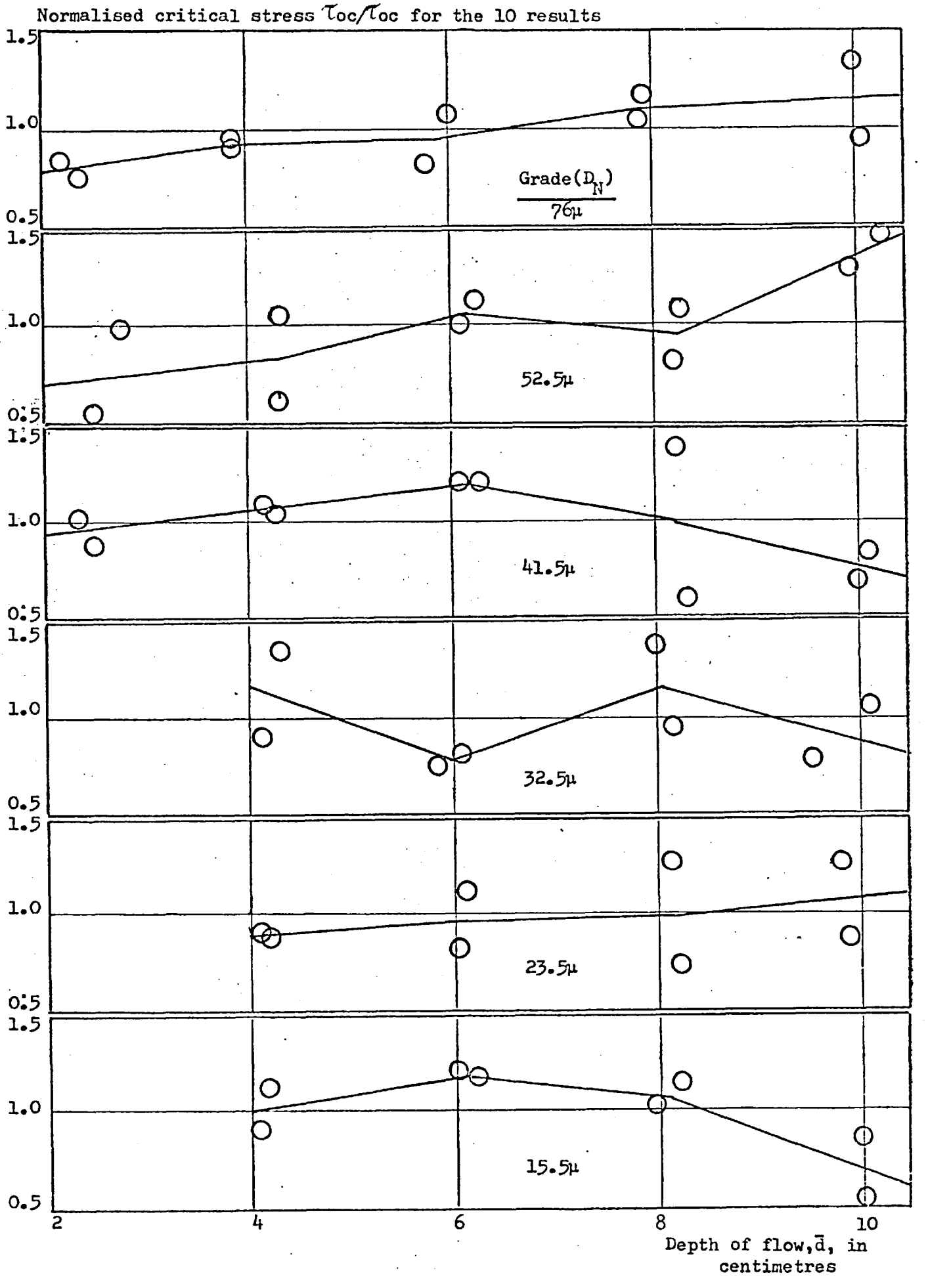

Figure 5.5. Variation of the low transport, normalised, critical stress with depth of flow (for the 6 flake grades).

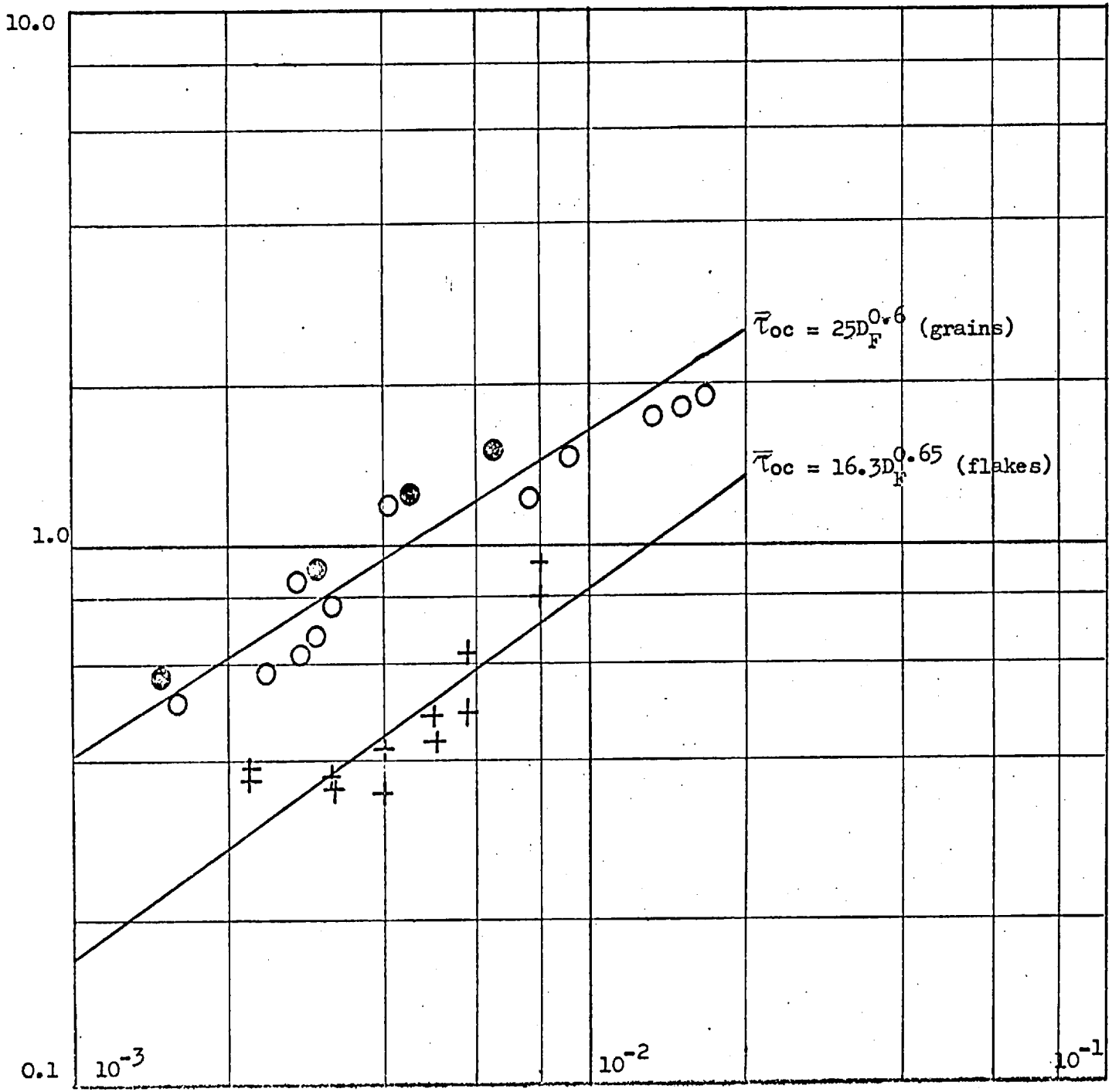

Figure 5.6. Critical incipient motion stress versus fall diameter for grain and flake grades in water at 20°C.

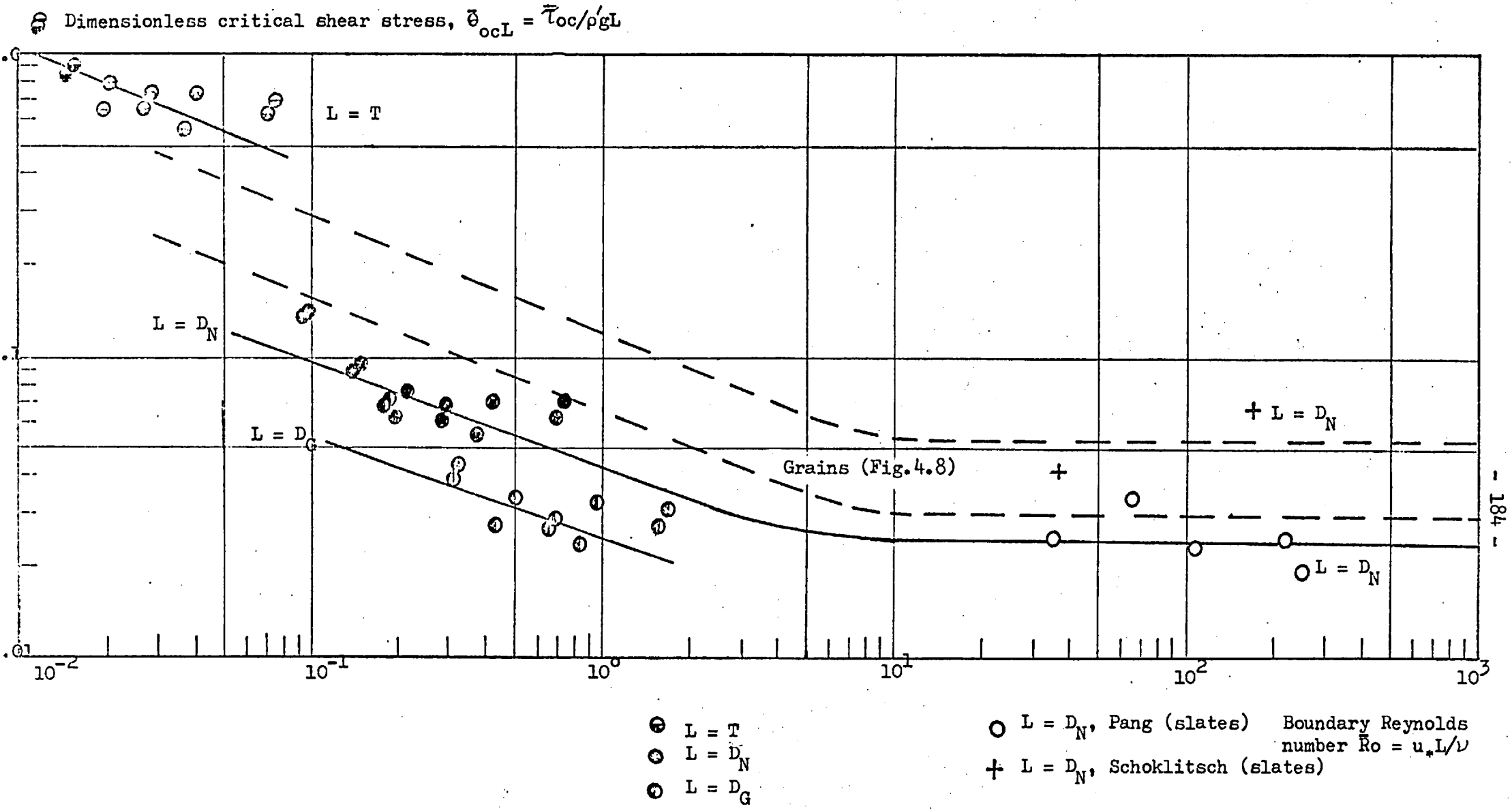

Figure 5.7. The Shields diagram for flakey solids, using various solid dimensions as a length scale.

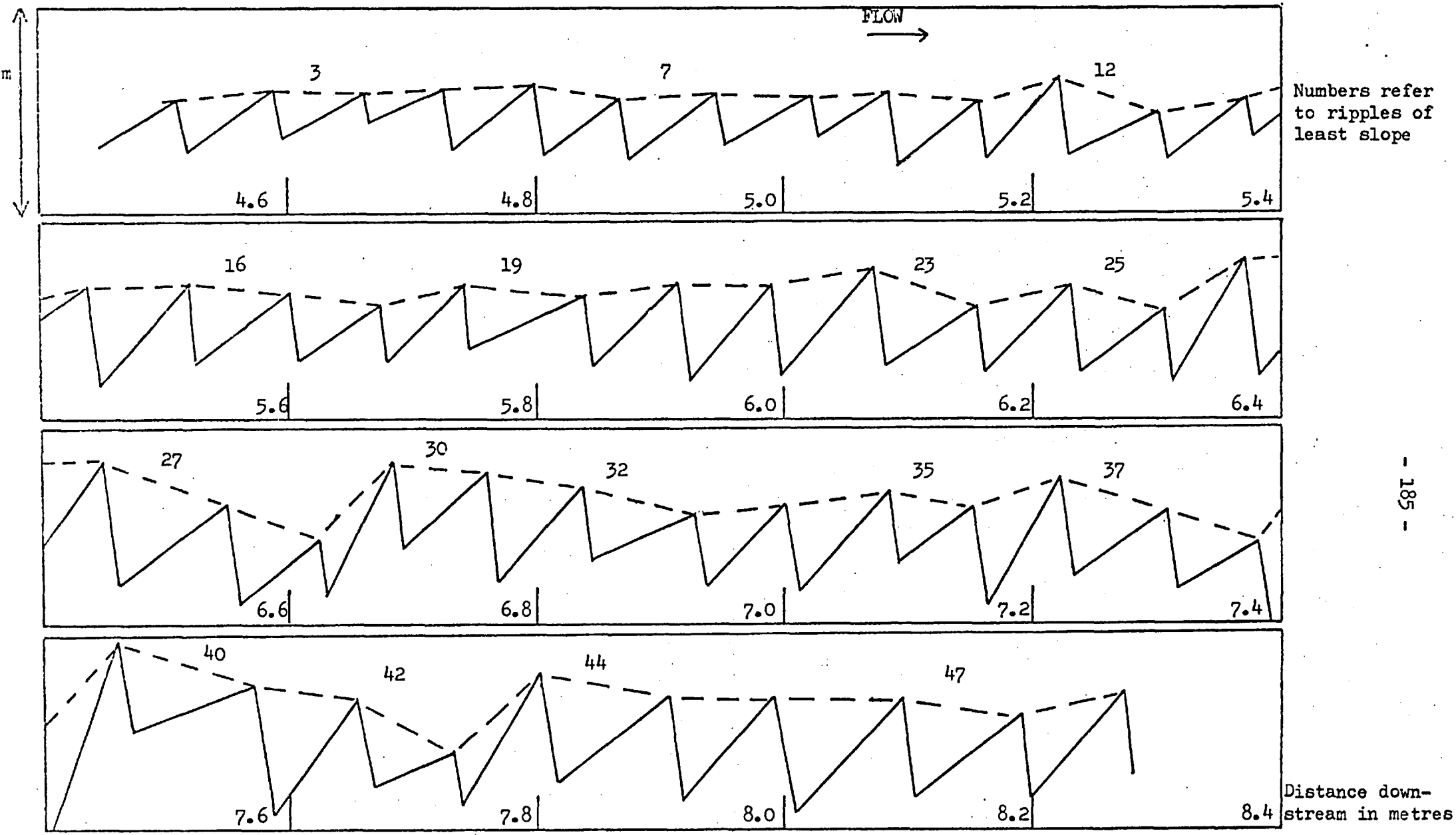

Figure 6.1. Bed surface contour at the end of Run 2 of the 15μ granular grade bedform experiment

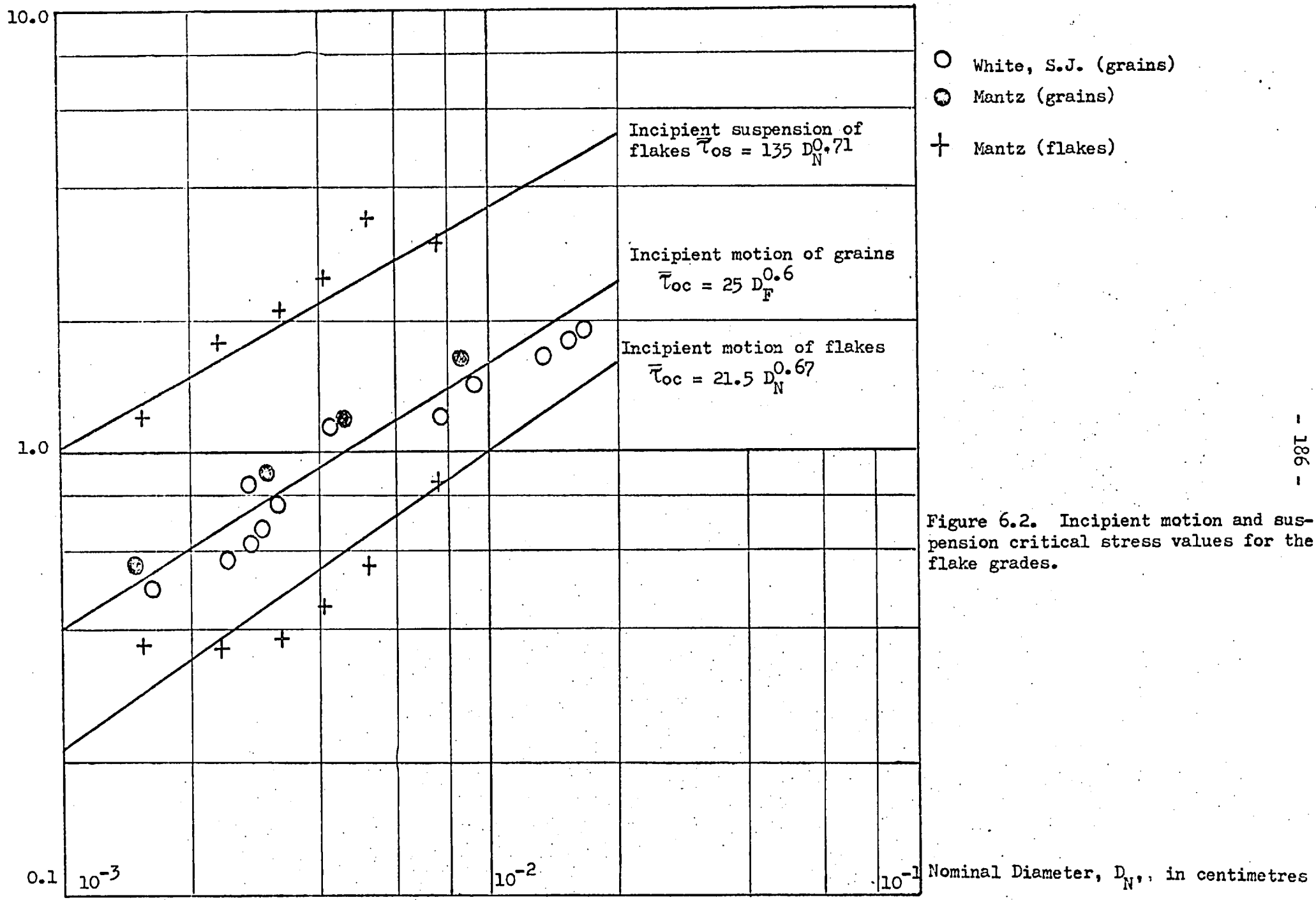

Figure 6.2. Incipient motion and suspension critical stress values for the flake grades.

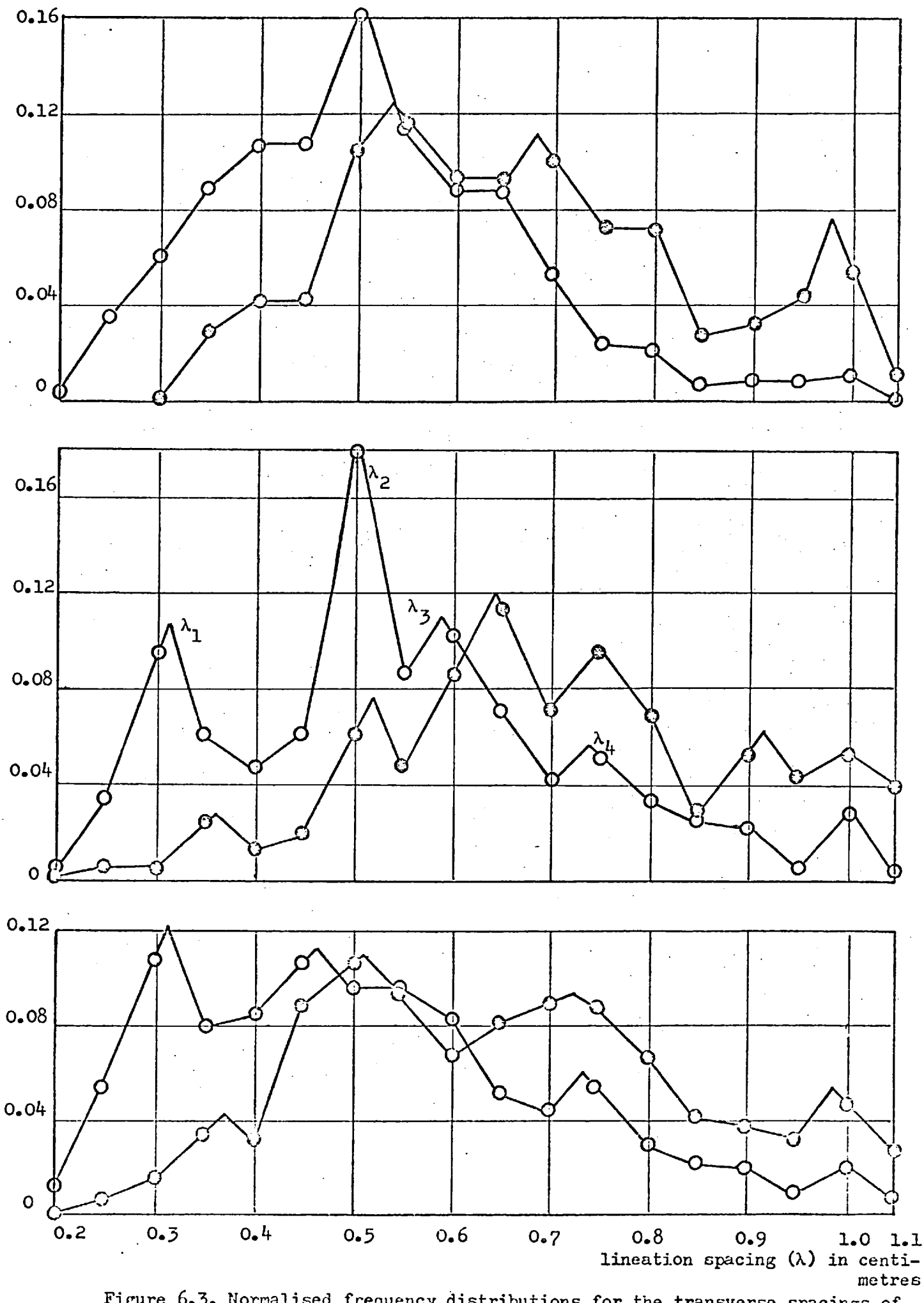

Figure 6.3. Normalised frequency distributions for the transverse spacings of the flake lineations.

Distance across channel width in centimetres		1	5	9	13	17	21	25	29
Distance downstream in channel in metres	9.51	7.5	7.5	7.5	7.5	7.5	7.6	7.4	7.4
	9.55	7.5	7.5	7.5	7.5	7.5	7.5	7.4	7.4
	9.59	7.3	7.5	7.5	7.6	7.6	7.6	7.4	7.5
	9.63	7.4	7.5	7.6	7.5	7.6	7.5	7.5	7.3
	9.67	7.3	7.6	7.6	7.6	7.5	7.5	7.4	7.5
	9.71	7.5	7.5	7.5	7.5	7.5	7.4	7.5	7.4
	9.75	7.3	7.5	7.6	7.6	7.6	7.6	7.4	7.4
	9.79	7.4	7.5	7.5	7.5	7.5	7.6	7.5	7.4

Bed surface measurements in millimetres

TABLE 4.1. BED SURFACE CONTOUR MEASUREMENTS, RELATIVE TO A HORIZONTAL DATUM, FOR A 30 X 30 CM^2 AREA (15 MICRON GRADE).

Median grain diameter (D) in microns, Density (ρ_s) in grams per cubic centimetre	Kinematic viscosity (ν) in square centimetres per second	Average flow depth ($\bar{d}$) in centimetres	Average water surface gradient ($\bar{i}$)	Bed observation	Critical shear stress ($\bar{\tau}_{oc}$) in dynes per square centimetre	Dimensionless critical shear stress, $\bar{\theta}_{oc}$	Boundary Reynolds Number, $\bar{R}_o$
66	0.0095	10.08	0.000131	Incipient	1.30	0.121	0.79
	0.0095	8.13	0.000197	bed-load	1.57	0.147	0.87
2.65	0.0095	6.07	0.000267	transport	1.59	0.149	0.88
	0.0095	4.21	0.000356		1.47	0.137	0.84
	0.0095	2.46	0.000597		1.44	0.135	0.83
Average ± standard deviation					1.47±0.12	0.14±0.01	0.84±0.04
45	0.0100	10.04	0.000147	Incipient	1.45	0.199	0.54
	0.0100	8.08	0.000164	bed-load	1.30	0.178	0.54
	0.0098	5.96	0.000194	transport	1.13	0.155	0.49
2.65	0.0098	4.00	0.000265		1.04	0.143	0.47
	0.0098	2.43	0.000457		1.09	0.150	0.48
Average ± standard deviation					1.20±0.17	0.16±0.02	0.50±0.03
30	0.0090	9.43	0.000093	Incipient	0.86	0.177	0.31
	0.0090	7.82	0.000101	bed-load	0.77	0.158	0.29
	0.0093	5.86	0.000161	transport	0.93	0.191	0.31
2.65	0.0093	4.00	0.000223		0.88	0.181	0.30
	0.0095	2.27	0.000383		0.85	0.175	0.29
Average ± standard deviation					0.86±0.06	0.18±0.02	0.30±0.01
15	0.0085	5.73	0.000077	No transport	0.52	0.214	0.116
2.65	0.0085	6.01	0.000117	&scattered low bedforms	0.69	0.284	0.146
Average ± standard deviation					0.56±0.04	0.23±0.02	0.13±0.01

TABLE 4.2. INCIPIENT MOTION DATA FOR THE FOUR GRADES OF FINE, COHESIONLESS, GRANULAR SEDIMENT.

TABLE 4.3. INCIPIENT MOTION DATA FOR LOW BOUNDARY REYNOLDS NUMBER GRAIN EXPERIMENTS, COLLECTED.

Description of sediment	Density (ρ_s) in grams per cubic centimetre	Median grain diameter (D) in microns	Kinematic Viscosity (ν) in square centimetres per second	Critical Shear stress ($\overline{\tau}_{oc}$) in dynes per square centimetre	Dimensionless critical shear stress $\overline{\theta}_{oc}$	Boundary Reynolds Number $\overline{R}_o$	Range of flow Reynold Number $\overline{R}_e$	Number of observations
White, C.M.(1940) 1m long x 5cm wide fixed-slope flume, naturally levelled beds in oil.								
Natural grains	2.65	900	1.63	26.0	0.17	0.04	1.80	1
Natural grains	2.65	210	1.63	9.5	0.27	0.28	0.15	1
White, S.J.(1970) 6m long x 30cm wide fixed-slope flume, naturally levelled beds in oil.								
Natural grains	2.65	133	Various,	3.07	0.129	0.32	650-2000	7
Natural grains	2.65	93	depending	2.07	0.124	0.19	350-1200	8
Lead glass spheres	2.90	88	on ambient	2.54	0.142	0.18	500-1700	10
Natural grains	2.65	77	temperature	2.22	0.161	0.16	500-1400	7
Natural grains	2.65	46	around 20°C	1.75	0.212	0.083	600-1200	6
Natural grains	2.65	33	$\nu = 0.080$	1.49	0.251	0.058	300-1400	10
Natural grains	2.65	30	$\rho = 0.820$	1.42	0.263	0.049	300- 900	9
Natural grains	2.65	25		0.97	0.216	0.034	200- 700	8
White, S.J.(1970) flume as above, naturally sedimented beds in water.								
Natural grains	2.65	170	Various,	1.85	0.067	1.91	5500-8000	6
Natural grains	2.65	153	depending	1.80	0.073	1.78	5000-9000	10
Lead glass spheres	2.90	137	on ambient	1.71	0.067	1.50	5500-9000	10
Natural grains	2.65	133	temperature	1.71	0.079	1.45	5000-9000	10
Natural grains	2.65	93	around 20°c	1.45	0.096	0.97	6000-9500	11
Lead glass spheres	2.90	88		1.73	0.105	0.89	6000-9000	11
Natural grains	2.65	77		1.20	0.096	0.70	5000-9500	10
Natural grains	2.65	44	$\nu = 0.010$	1.18	0.153	0.37	6000-9500	12
Crushed silica	2.65	33	$\rho = 1.000$	0.76	0.142	0.24	3000-7500	10
Natural grains	2.65	30		0.66	0.163	0.20	2500-6000	10
Natural grains	2.65	29		0.63	0.134	0.22	2500-7500	11
Natural grains	2.65	28		0.85	0.188	0.23	2500-8500	10
Natural grains	2.65	24		0.57	0.147	0.16	2500-6500	10
Crushed silica	2.65	16		0.50	0.193	0.10	1500-5500	10
Yantz, (Table 4.2) 10m long x 30cm wide tilting flume, naturally sedimented beds in water								
Natural grains	2.65	66	0.0095	1.47	0.14	0.84	4500-22000	5
Natural grains	2.65	45	0.0100	1.20	0.16	0.50	4000-19000	5
Natural grains	2.65	30	0.0093	0.86	0.18	0.30	3500-17000	5
Crushed silica	2.65	15	0.0085	0.56	0.23	0.13	7000	1

Grade dimensions before introduction to flume					Grade dimensions at 6 metres downstream in flume channel					Angle of repose measurements (α) in degrees of arc				Mean $\alpha \pm$ standard deviation
Standard fall diameter, D_F in microns	Sorting co-efficient S_o	Geometric, face diameter D_G, in microns	Geometric thickness T in microns	Nominal diameter D_N in microns	D_F	S_o	D_G	T	D_N					
25.5	1.34	33	1.85	15.5	22	1.36	33	1.83	15.5	58	67	63	68	65 ± 5
37.5	1.28	54	2.5	24	32	1.29	52	2.5	23.5	38	37	38	41	38 ± 3
46	1.43	70	3.1	31	40	1.29	75	3.2	32.5	38	39	37	41	39 ± 3
56	1.32	101	4.0	43	50	1.29	98	3.9	41.5	40	41	42	46	42 ± 4
68	1.35	148	6.2	64	58	1.28	120	5.2	52.5	36	40	41	41	41 ± 4
79	1.35	205	9.2	90	80	1.35	172	7.8	76	42	46	41	40	42 ± 4

TABLE 5.1. DIMENSIONS AND ANGLE OF REPOSE MEASUREMENTS FOR THE SIX FLAKE GRADES

Nominal diameter (D_N) in microns	Kinematic viscosity (ν) in centimetres per second	Average flow depth ($\bar{d}$) in centimetres	Average water surface gradient ($\bar{i}$)	Critical shear stress ($\bar{\tau}_{oc}$) in dynes per square centimetre	Dimensionless critical shear stress $\bar{\theta}_{ocN}$	Boundary Reynolds number $\bar{R}_{oN}$
76	0.0097	9.99	0.000119	1.17		
	0.0097	7.99	0.000130	1.02		
First deposition	0.0095	6.05	0.000156	0.93		
	0.0095	4.00	0.000215	0.84		
	0.0095	2.38	0.000284	0.66		
Average ± standard deviation				0.92 ± 0.19	0.070 ± 0.016	0.77 ± 0.17
76	0.0093	10.09	0.000084	0.83		
	0.0093	7.97	0.000116	0.91		
Second deposition	0.0093	5.83	0.000126	0.72		
	0.0091	3.99	0.000205	0.80		
	0.0093	2.19	0.000339	0.73		
Average ± standard deviation				0.80 ± 0.08	0.062 ± 0.06	0.71 ± 0.07
52.5	0.0093	9.78	0.000075	0.72		
	0.0095	8.18	0.000058	0.47		
First deposition	0.0093	6.25	0.000097	0.59		
	0.0093	4.37	0.000082	0.35		
	0.0093	2.56	0.000128	0.32		
Average ± standard deviation				0.49 ± 0.17	0.055 ± 0.018	0.39 ± 0.13
52.5	0.0093	10.29	0.000083	0.84		
	0.0093	8.27	0.000074	0.60		
	0.0093	6.13	0.000094	0.57		
	0.0095	4.61	0.000133	0.60		
	0.0095	2.72	0.000209	0.56		
Average ± standard deviation				0.63 ± 0.12	0.070 ± 0.014	0.44 ± 0.08

Flake density (ρ_s) = 2.74 grams per cubic centimetre.

TABLE 5.2. INCIPIENT MOTION DATA FOR THE SIX FLAKE GRADES

D_N	ν	$\bar{d}$	$\bar{i}$	$\bar{\tau}_{oc}$	$\bar{\theta}_{ocN}$	$\bar{R}_{oN}$
41.5	0.0097	10.15	0.000039	0.39		
	0.0097	8.33	0.000034	0.28		
First deposition	0.0095	6.10	0.000091	0.55		
	0.0095	4.28	0.000115	0.48		
	0.0095	2.36	0.000200	0.46		
Average ± standard deviation				0.43 ± 0.10	0.061 ± 0.015	0.29 ± 0.05
41.5	0.0095	10.05	0.000032	0.32		
	0.0093	8.28	0.000077	0.63		
Second deposition	0.0095	6.32	0.000089	0.55		
	0.0095	4.21	0.000118	0.49		
	0.0093	2.58	0.000163	0.41		
Average ± standard deviation				0.48 ± 0.12	0.068 ± 0.016	0.30 ± 0.06
32.5	0.0095	10.15	0.000039	0.39		
	0.0097	8.20	0.000046	0.37		
First deposition	0.0097	5.94	0.000049	0.29		
	0.0097	4.17	0.000086	0.35		
	0.0100	2.36	0.000217	0.50		
Average ± standard deviation (first 4 results only)				0.35 ± 0.04	0.063 ± 0.006	0.20 ± 0.02
32.5	0.0095	9.51	0.000032	0.30		
	0.0093	8.00	0.000067	0.53		
	0.0093	6.13	0.000052	0.31		
	0.0093	4.34	0.000121	0.52		
	0.0095	2.22	0.000088	0.19		
Average ± standard deviation (first 4 results only)				0.42 ± 0.13	0.076 ± 0.019	0.22 ± 0.05

TABLE 5.2. CONTINUED.

D_N	ν	$\bar{d}$	$\bar{I}$	$\bar{\tau}_{oc}$	$\bar{\theta}_{ocN}$	$\bar{R}_{oN}$
23.5	0.0097	9.82	0.000049	0.47		
	0.0097	8.23	0.000035	0.28		
First deposition	0.0097	6.13	0.000068	0.41		
	0.0100	4.20	0.000077	0.32		
	0.0097	2.57	0.000167	0.42		
Average ± standard deviation (first 4 results only)				0.37 ± 0.09	0.092 ± 0.018	0.15 ± 0.03
23.5	0.0095	9.93	0.000032	0.32		
	0.0093	8.11	0.000058	0.46		
Second deposition	0.0095	6.07	0.000051	0.30		
	0.0093	4.10	0.000081	0.33		
	0.0095	2.57	0.000106	0.27		
Average ± standard deviation (first 4 results only)				0.35 ± 0.07	0.087 ± 0.017	0.15 ± 0.03
15.5	0.0095	10.14	0.000018	0.18		
	0.0097	8.27	0.000053	0.43		
First deposition	0.0097	6.10	0.000075	0.45		
	0.0095	4.21	0.000103	0.43		
	0.0095	2.67	0.000063	0.17		
Average ± standard deviation (first 4 results only)				0.37 ± 0.13	0.140 ± 0.04	0.10 ± 0.03
15.5	0.0095	10.16	0.000032	0.32		
	0.0095	8.01	0.000050	0.39		
	0.0097	6.26	0.000071	0.44		
	0.0097	4.13	0.000083	0.34		
	0.0097	2.41	0.000117	0.28		
Average ± standard deviation (first 4 results only)				0.37 ± 0.05	0.140 ± 0.02	0.10 ± 0.01

TABLE 5.2. CONTINUED.

Description of sediment	Density (ρ_s) in grams per cubic centimetre	Nominal diameter (D_N) in microns	Geometric face diameter (D_G) in microns	Aspect ratio D_G/T where T is thickness in microns	Kinematic Viscosity (ν) in square centimetres per second	Critical shear stress $\bar{\tau}_{oc}$ in dynes per square centimetre	Critical dimensionless shear stress $\bar{\theta}_{ocN}$	Boundary Reynolds Number $\bar{R}_{oN}$	Range of flow Reynolds number	Number of observations
Schoklitsch (1914)	10 cm wide flume - artificially levelled beds in water.									
Natural slates	2.7	3060	-	-	Assumed as	34.08	0.066	176	-	10
Natural slates	2.7	1240	-	-	0.01	8.80	0.041	37	-	10
Pang (1939)	16 m long x 40 cm wide tilting flume - artificially flattened beds. Extremely to very weak movement of bed-load									
Natural slates	2.66	6710	6480	4	0.0115	20.50	0.0184	265	44000-68000	2
with	2.66	5710	6050	2	0.0123	23.54	0.0248	225	38,000	1
accessory	2.70	3260	4140	5	0.0110	11.82	0.0213	102	33000-40000	2
grains	2.49	2210	3640	4	0.0115	11.14	0.0339	65	17000-31000	2
	2.45	1630	1780	5	0.0117	5.74	0.0243	33	12000-16500	
Mantz(Table 5.2.)	10 m long x 30 cm wide tilting flume - naturally sedimented beds in water.									
Natural	2.74	76	172	22	0.0097	0.92	0.070	0.77	3000-16000	5
	Experiment repeated after relaying bed				0.0093	0.80	0.062	0.71	3000-16000	5
Mica	2.74	52.5	120	23	0.0093	0.49	0.055	0.39	3000-14000	5
	Experiment repeated				0.0094	0.63	0.070	0.44	3000-14000	5
Flakes	2.74	41.5	98	25	0.0097	0.43	0.061	0.29	3000- 1100	5
	Experiment repeated				0.0094	0.48	0.068	0.30	3000- 1100	5
	2.74	32.5	75	23	0.0098	0.35	0.063	0.20	4000- 9000	4
	Experiment repeated				0.0094	0.42	0.076	0.22	4000- 9000	4
	2.74	23.5	52	21	0.0098	0.37	0.092	0.15	3500- 8000	4
	Experiment repeated				0.0094	0.35	0.087	0.15	3500- 8000	4
	2.74	15.5	33	18	0.0097	0.37	0.140	0.10	4000-10000	4
(Weakly co-hesive grade)	Experiment repeated				0.0095	0.37	0.140	0.10	4000-10000	4

TABLE 5.3. SUMMARY OF INCIPIENT MOTION DATA FOR FLAKEY SOLIDS.

Run Discharge Q in litres per second	Time after start of Run in hours	Applied shear stress ± standard deviation in dynes per sq. centimetre ($\bar{\tau}_o$)	Stress stage $\bar{\tau}_o/\bar{\tau}_{oc}$	Dimensionless applied stress $\bar{\theta}_o$	Observations	Plate number
Run 1	0	0.69±0.08	1.2	0.28	Flat bed	
Q=2.52	2	0.82±0.05	1.8	0.41	Primary ripple(beginning about 1m downstream of channel entry	4.1
R_e=3,400	4				Fewer and larger primary ripples	4.2
R_r=0.18	6	0.74±0.07	1.3	0.30	Isolated ripples of constant width on otherwise flat bed	4.3
V_m=14cm/s	9				Isolated ripples increase in size	4.4
	22	0.79±0.06	1.4	0.33	Isolated ripples~1mm height.Transverse ripples at channel entry	4.5
	24				End of run. Average bed load transport 1.7×10^{-5}g/cm.s	
Run 2	0	1.05±0.02	1.9	0.43	Isolated ripples become fewer and larger	5.1
Q=3.06	6	1.05±0.02	1.9	0.43	Ripples becoming transverse	5.2
R_e=10,000	20	1.71±0.07	3.0	0.70	Transverse ripples~2mm height.Transverse ripples at channel entry change to isolated forms at 1m downstream, then to transverse ripples at 6m downstream.	5.3
R_r=0.22						
V_m=17cm/s	24	2.04±0.10	3.7	0.84	Secondary ripples begin to develop. Suspended load beginning.	5.4
					End of run. Average bed load transport = 5.2×10^{-5}g/cm.s.	
Run 3	0	2.16±0.08	3.9	0.90	Channel floor exposed in several places downstream	
Q=3.6	6	2.34±0.12	4.2	0.96	Channel entry ripples becoming 3-dimensional	
R_e=12,000	22	3.09±0.12	5.5	1.27	Secondary ripples over entire channel. Floor exposed in many places.	
R_r=0.26						
V_m=20cm/s					End of run. Average bed load transport = 2.2×10^{-4}g/cm.s. Average suspended load transport = 0.25g/l	
Run 4	0	4.03±0.17	7.2	1.66	Bed obscured by suspended load	
Q=4.32	6	4.48±0.12	8.0	1.84		
R_e=14,000	22	4.14±0.14	7.4	1.70	End of run. Secondary ripples overall. Average bed load transport = 8.7×10^{-4}g/cm.s. Average suspended load transport =0.5g/l	
R_r=0.31						
V_m=24cm/s						

TABLE 6.1. BEDFORM EXPERIMENTS FOR THE 15 MICRON GRANULAR SEDIMENT.

Run Discharge Q in litres per second	Time after start of Run in hours	Applied shear stress ± standard deviation in dynes per sq. centimetre ($\bar{\tau}_o$)	Stress stage $\bar{\tau}_o / \bar{\tau}_{oc}$	Dimensionless applied stress $\bar{\theta}_o$	Observations	Plate number
Run 1	0	1.38±0.1	1.0	0.13	Flat bed	
Q=3.96	13	1.37±0.04	1.0	0.13	Isolated ripples. No channel entry forms.	6.1
R_e=13,000	16	1.34±0.06	1.0	0.13	Isolated ripples increase in size, having constant width, and migrate downstream. Plate shows the end of the bed, 9.5m downstream.	6.2
U_m=22cm/s Fr=0.28	20	1.35±0.05	1.0	0.13	Isolated ripples extend downstream from the 4m position. (No channel entry forms) Average bed load transport rate = 1.05 X 10^{-5}g/cm.s.	
Run 2	0	2.08±0.10	1.5	0.19	Primary ripples of varying size develop over entire channel	6.3
Q=4.63	2	3.00±0.25	2.2	0.28	Largest isolated ripples have onset of suspended load, and local scour.	6.4
R_e=16,000 Fr=0.34 U_m=26cm/s	9	6.77±0.37	5.0	0.66	Secondary ripples overall with channel floor exposed	6.5
	17	6.89±0.21	5.2	0.67		
	20	6.82±0.22	5.2	0.67	End of run. Secondary ripples ~2cm height. Suspended load is insufficient to obscure the bed.	6.6

TABLE 6.2. BEDFORM EXPERIMENTS FOR THE 66 MICRON GRANULAR SEDIMENT.

Flake nominal diameter, D_N in microns / Number of deposition	Kinematic viscosity, ν in square centimetres per second	Average water depth, $\bar{d}$, in centimetres	Average hydraulic gradient $\bar{i}$	Incipient suspension shear stress, $\bar{\tau}_{os}$ in dynes per square centimetre	Incipient suspension friction velocity in centimetres per second u_{*s}	Incipient suspension shear stress, $\bar{\tau}_{os}$ in dynes per square centimetre (Average ± standard deviation)	Stress Stage $\bar{\tau}_{os}/\bar{\tau}_{oc}$	Incipient suspension dimensionless stress $\bar{\theta}_{os,N}$	Flow Reynolds Number $\bar{R}_e$ (approx)	Flow Froude Number $\bar{F}_r$ (approx)
15.5										
First	0.0098	6.03	0.000221	1.31	1.14					
Second	0.0098	5.85	0.000188	1.08	1.04	1.2 ± 0.2	3.2±0.8	0.45	11,000	0.23
23.5										
First	0.0100	5.89	0.000342	1.98	1.40					
Second	0.0100	5.93	0.000278	1.62	1.27	1.8 ± 0.2	5.0±1.2	0.45	13,000	0.28
32.5										
First	0.0100	5.94	0.000345	2.01	1.42					
Second	0.0100	6.00	0.000382	2.25	1.50	2.1 ± 0.1	5.4±1.1	0.38	14,000	0.31
41.5										
First	0.0098	6.00	0.000510	3.00	1.73					
Second	0.0098	6.12	0.000350	2.10	1.45	2.6 ± 0.5	5.7±1.6	0.37	16,000	0.34
52.5										
First	0.0095	5.95	0.000547	3.19	1.78					
Second	0.0095	5.90	0.000634	3.67	1.92	3.4 ± 0.3	6.2±2.0	0.38	17,000	0.36
76										
First	0.0096	5.90	0.000564	3.26	1.80					
Second	0.0096	5.84	0.000463	2.65	1.62	3.0 ± 0.4	3.5±0.7	0.23	17,000	0.36
						Mean ± standard deviation	4.8±1.2			

TABLE 6.3 INCIPIENT SUSPENSION DATA FOR FINE, COHESIONLESS FLAKES

Flake nominal diameter, D_N in microns	Bed shear stress, $\bar{\tau}_o$ in dynes per square centimetre	Friction velocity in centimetres per second u_*	Stress stage $\bar{\tau}_o/\tau_{oc}$	Duration of run	Comment	Flow Reynolds Number $\bar{Re}$ (approx)	Flow Froude Number $\bar{Fr}$ (approx)	Viscous sub-layer thickness scale, ν/u_* in microns
23.5								
Incipient motion	0.36	0.60	1.0		From Table 5.3			167
	1.05	1.03	2.9	15m	Lineations parallel	9,000	0.18	97
	1.38	1.18	3.8	15m	Lineations begin to oscillate	10,000	1.22	85
	1.06	1.03	2.9	10m	Repeated experiment			
	1.40	1.18	3.8	10m	Repeated experiment			
Incipient suspension	1.80	1.34	5.0		From Table 6.3	13,000	0.28	75
41.5								
Incipient motion	0.46	0.68	1.0		From Table 5.3			147
	1.54	1.24	3.3	50m	Lineations parallel	13,000	0.29	80
	2.10	1.45	4.6	10m	Lineations begin to oscillate	15,000	0.32	69
Incipient suspension	2.60	1.61	5.7		From Table 6.3	16,000	0.34	62
76								
Incipient motion	0.86	0.93	1.0		From Table 5.3			107
	1.34	1.16	1.6	10m	Lineations parallel	12,000	0.26	85
	2.23	1.49	2.6	5m	Lineations begin to oscillate	15,000	0.32	67
	1.46	1.21	1.7	15m	Repeated experiment			
	2.27	1.51	2.6	5m	Repeated experiment			
Incipient suspension	3.00	1.73	3.5		From Table 6.3	17,000	0.36	58

Kinematic viscosity, $\nu = 0.01 cm^2/s$. Average flow depth, $d = 6.0cm$.

TABLE 6.4. BEDFORM EXPERIMENTS FOR FINE, COHESIONLESS FLAKES.

Flake Nominal Diameter, D_N, in microns	Stress-stage $\bar{\tau}_o / \bar{\tau}_{oc}$	Lineation separation distance First mode λ_1, inmillimetres	λ_2	λ_3	λ_4
23.5	2.9	3.7±0.1	5.1±0.1	——	7.3±0.1
	3.8	3.1±0.1	4.6±0.05	5.0±0.1	7.3±0.05
41.5	3.3	3.6±0.05	5.2±0.05	6.4±0.05	7.5±0.05
	4.6	3.1±0.1	5.0±0.05	5.9±0.05	7.4±0.05
76	1.6	4.2±0.1	5.4±0.05	6.8±0.05	7.8±0.05
	2.6	4.2±0.1	5.0±0.05	6.3±0.05	7.8±0.1

λ given as mean ± standard error.

TABLE 6.5. TRANSVERSE SEPARATION MODAL DISTANCES FOR FLAKE LINEATIONS.

Flake Nominal diameter, D_N, in microns	Stress stage $\bar{\tau}_o / \bar{\tau}_{ow}$	Dimensionless lineation separation distance, first mode, λ_1^+	Average $\bar{\lambda}_1^+$ ± standard deviation	λ_2^+	Average $\bar{\lambda}_2^+$	λ_3^+	Average $\bar{\lambda}_3^+$	λ_4^+	Average $\bar{\lambda}_4^+$
23.5	2.9 3.8	38 36	37±1	53 54	53±1	-- 59	59±1	75 86	80±7
41.5	3.3 4.6	45 45	45±1	65 72	68±5	80 86	83±4	94 107	100±8
76	1.6 2.6	49 63	56±10	64 75	70±7	80 94	87±10	92 116	104±16
Kline et al (1967) results for fixed boundary flow.			46		81		115		154

	$\bar{\lambda}_2^+ - \bar{\lambda}_1^+$	$\bar{\lambda}_3^+ - \bar{\lambda}_2^+$	$\bar{\lambda}_4^+ - \bar{\lambda}_3^+$	
23.5	16	6	21	Average = 14
41.5	23	15	17	Average = 18
76	14	17	17	Average = 16
				Total average = 16±3 (standard deviation)
Kline et al (1967) results for fixed boundary flow.	35	34	39	Average = 36±4 (standard deviation)

TABLE 6.6. DIMENSIONLESS TRANSVERSE SEPARATION MODAL DISTANCES FOR FLAKE LINEATIONS

REFERENCES

Abbott, J.E. (1974) "The dynamics of a single grain in a stream". Ph.D. Thesis. Imperial College, London.

Allen, J.R.L. (1964) "Primary current lineation in the lower Old Red Sandstone (Devonian);Anglo-Welsh Basin". Sedimentology. 3 No. 2 89-108.

Allen, J.R.L. (1968) "Current Ripples". North-Holland. Amsterdam.

Allen, J.R.L. (1970) "Physical Processes of sedimentation". Allen and Unwin Ltd. London.

Anderson, A.G. (1953) "The characteristics of sediment waves formed by flow in open channels". Proc. of the Third Midwestern Conference in Fluid Mechanics. Minneapolis.

Barekyan, A.S. (1963) "Method of determining permissible velocities". Soviet Hydrology. (Am. Geophys. Union) No.3.

Baschin, O. (1899) Zeitschrift Gesellschft..Erdkunde. Bd. XXXIV.

Bagnold, R.A. (1941) "The physics of blown sand and desert dunes". Chapman and Hall. Great Britain.

Bagnold, R.A. (1954) "Experiments on a gravity free dispersion of large solid spheres in a Newtonian fluid under shear". Proc. Roy. Soc. London Phil. Trans. 225A.

Bagnold, R.A. (1956) "Flow of cohesionless grains in fluids". Proc. Roy. Soc. London Phil. Trans. 249A No. 964.

Bagnold, R.A. (1966) "An approach to the sediment transport problem from general physics". U.S. Geol. Survey.P.P. 422-I.

Bagnold, R.A. (1973) "The nature of saltation and of bed-transport in water". Proc. Roy. Soc. London. A.332. 473-504.

Binnie, A.M. and Williams, E.E. (1966). "Self induced waves in a moving open channel". J.Hydr. Res. 4 No.1.

Blasius, A. (1910) Zeitschrift fur Bauwesen. Jgg. LX

Blinco, P.H. and Partheniades, E. (1971) "Turbulence characteristics in free surface flows over smooth and rough boundaries". Jo. Hyd. Res. 9 No.1. 43.

Bogardi, J.L. (1968) "Incipient sediment motion in terms of critical mean velocity". Acta Technica Academiae Scientiarum Hungaricae. Tomus 62. (1-2) Budapest.

Brooks, N.H. (1955) "Mechanics of streams with movable beds of fine sands". Proc. A.S.C.E. Proc-separate No. 668.

Brown, R.L. and Richards, J.C. (1970) "Principles of powder mechanics". Pergamon Press. International series of monographs in Chemical Engineering 10.

B.S. 1377 (1967) "Methods of Testing Soils for Civil Engineering Purposes."

B.S. 188 (1957) "Methods of Measuring the Viscosity of Liquids".

Carrigy, M.A. (1970) "Experiments on the angle of repose of granular materials". Sedimentology 14 147-158.

Carver, R.E. (1971) "Procedures in Sedimentary-Petrography." Wiley New York.

Casey, H. (1935) "Uber Geschiebebewegung". Mitteillungen der Preussischen. Versuchsanstalt fur Wasserban und Schiffbau.(VWS) Berlin. Heft 19.

Chang, Y. (1939) "Laboratory investigations of flume traction and transportation". Trans. A.S.C.E. 104 1246-1284.

Cheng, D.H. and Clyde, C.G. (1972) "Instantaneous hydrodynamic lift and drag forces on large roughness elements in turbulent open-channel flow". From "Sedimentation" Ed. Shen H.W. Fort Collins, Colorado, U.S.A.

Chepil, W.S. (1958) "The use of evenly spaced hemispheres to evaluate aerodynamic forces on soil surfaces". Trans. Am. Geophys. Union 39 No.3.

Chow, V.T. (1959) "Open-channel hydraulics." McGraw Hill.

Christensen, B.A. (1965) "Discussion of Erosion and Deposition of Cohesive Soils" by Partheniades, E. Proc. A.S.C.E. 91 No.HYS 301.

Clarke, J.A. (1968) "A study of incompressible turbulent boundary layers in channel flow." Trans. A.S.M.E. Jo.of Basic Engineering. March.

Compte-Bellot, G. (1963) "Coefficiente de dessymetrie et d'aplatissment, spectres et correlations en turbulence de conduite". Journal de Mechanique. II No. 2.

Corino, E.R. and Brodkey, R.S. (1969) "A visual investigation of the wall region in turbulent flow". J.F.M. 37 pt. 1. 1-30.

Crowell, J.C. (1955) "Directional-current structures from the Prealpine flysch." Bull. Geol. Soc. Am. 66 1351-1384.

Darwin, G.H. (1883) "On the formation of ripple marks". Proc. Roy. Soc. London.

Deacon, G.F. (1894) Proc. Inst. of Civil Eng. CXV111 47-189.

Du Boys, P. (1879) "Etudes du regime du Rhone et l'action exercee par les eaux sur un lit a fond de graviers indefinement affouillable". Annales de ponts et chausees ser 5.18 141-195.

Du Buat, P. (1786) "Principes d'Hydraulique". 2nd Ed. De L'Imprimerie de Monsieur. Paris.

Eaton, J.E. (1929) Am.Ass. Petrol. Geol. Bull. 13 713.

Eckelmann, L.D. Fortuna, G. and Hanratty, T.J. (1972). "Drag reduction and the wavelength of flow-orientated wall eddies". Nature. Phys. Sci. 236 April 94-96.

Einstein, H.A. (1942) "Formulas for the transportation of bed-load". Trans. A.S.C.E. 107.

Einstein, H.A. and El Samni, E.S. (1949) "Hydrodynamic forces on a rough wall". Rev.Mod. Phys. 21 No. 3.

Einstein, H.A. and Chien, N. (1958) Disc. of Brooks, N.H. "Mechanics of streams with movable beds of fine sands". Trans.A.S.C.E. 123 Paper No. 2931. 553.

Forcheimer, P. (1914) "Hydraulik". 1st ed. Teubner. Leipzig. Berlin.

Fortier, S. and Scobey, F.C. (1926) "Permissible canal velocities". Trans. A.S.C.E. 89.

Francis, J.R.D. (1970) "Solitary particle movement in a rough-bedded stream". South African Mech. Eng. 20 72.

Francis, J.R.D. (1973) "Experiments on the motion of solitary grains along the bed of a water-stream". Proc. Roy. Soc. A 332. 443

Garde, R.J. (1970) "Initiation of motion on a hydrodynamically rough surface-critical velocity approach". Irrigation and Power. July Vol. 27.

Gessler, J. (1965) "The beginning of bed load movement of mixtures investigated as natural armoring channels". Translation T-5 W.M. Keck Laboratory. Cal. Inst. Tech. California.

Gessler, J. (1971) Chapter 7 in "River Mechanics" Volume 1 Ed. and Published by H.W. Shen. Fort Collins, Colorado, U.S.A.

Ghosh, S.N. and Roy, N. (1970) "Boundary shear distribution in open channel flow".

Gilbert, G.K. (1914) "Transportation of debris by running water". U.S.G.S. Prof. Paper No.86.

Goncharov, V.N. (1964) "Dynamics of channel flow". Israel programme of scientific translations. Jerusalem.

Graf, W.H. (1971) "Hydraulics of sediment transport". McGraw Hill,USA.

Grass, A.J. (1970) "Initial instability of fine bed sand". Proc.A.S.C.E. 96 No. HY3.

Grass, A.J. (1971) "Initial instability of fine bed sand". Discussion Closure. Proc. A.S.C.E. 98. No. HY10.

Grass, A.J. (1971) "Structural features of turbulent flow over smooth and rough boundaries". J.F.M. 50 233.

Graton, L.C. and Fraser, H.J. (1935) "Systematic packing of spheres with particular relation to porosity and permeability". Jo.Geol. 43 785-909.

Griffiths, D.H., King, R.F., Rees, A.L. and Wright, A.E. (1960) Proc. Roy. Soc. A.256. 359.

Gunter, A. (1971) "Force d'entrainment moyenne critique avec prise en considerations des flucuations dues a la turbulence". I.A.H.R. Proc. 14th Congress, Paris.

Guy, H.P., Simons, D.P., Richardson, F.V. (1965) "Summary of alluvial channel data from flume experiments". U.S. Geol. Survey. P.P.464.L:

Hamilton, N. (1963) "The magnetic properties of some fine grained sediments". Ph.D. Thesis. University of Birmingham.

Helmholtz, H. (1888) Sitzber. Konigl. Preuss. Akad. Wiss. Berlin.

Heyndrikx, G.A. (1948) "Het transport van bodemmaterial dour stromned water". Drukkery, G.I.G. Brussels.

Hinxman, L.W. (1915) Geol. Survey. "The Geology of Mid-Strathspey and Strathdearn". HMSO. Edinburgh.

Hjulstrom, F. (1935) "The morphological activity of rivers". Geol.Inst. Uppsala. 25. Chap. III.

Holeman, J.N. (1968) "The sediment yield of major rivers of the world". Water Resources Research. 4 No.4 737-747.

Inglis, C.C. (1949) "The behaviour and control of rivers and canals (with the aid of models)." Central Water-Power, Irrigation and Navigation Research Station, Poona, India. Res. Pub. No.13 Pt.II.

Irvine, H.M. (1971) "A probabilistic approach to the initiation of movement of non-cohesive sediments in alluvial channels". M.S. Thesis. University of Canterbury, Christchurch, New Zealand.

Jarocki, W. (1963) "A study of sediment". translated from Polish (1957) Nat. Sci. Found. and U.S. Dept. of Int. Washington D.C.

Jeffreys, H. (1929) "On the transport of sediment by streams." Proc. Cambridge Phil. Soc. XXV.

Johnston, G.S. (1966) British Regional Geology. "The Grampian Highlands" HMSO. Edinburgh.

Kalinske, A.A. (1947) "Movement of sediment at the bed in rivers". Trans. Am. Geophys. Union 28 615.

Kennedy, J.F. (1963) "The mechanics of dunes and anti-dunes in erodible-bed channels". J.F.M. 16 Pt. 4. 521.

Kennedy, J.F. (1966) Chmn "Nomenclature for bed forms in alluvial channels". Proc. A.S.C.E. 92 No. HY3.

Kitchener, J.A. (1969) "Colloidal minerals: chemical aspects of their dispersion, flocculation and filtration". Proc Filtration Society.

Klebanoff,P.S. (1954) "Characteristics of turbulence in a boundary layer with zero pressure gradient". NACA TN 3178.

Kline, S.J., Reynolds, W.C., Schraub, F.A. and Runstadler, P.E.(1967). "The structure of turbulent boundary layers". J.F.M. 30 741.

Klug, H.P. and Alexander, L.E. (1954) "X-Ray diffraction procedures for Polycrystalline and amorphous Materials." Wiley, New York.

Kolbuszwski, J. (1950) "Notes on the deposition of sands". Research 3 478-483.

Kondrat'ev, N.E. (1962) in "River flow and river channel formation". Translated by the National Science Foundation. Washington D.C.

Kramer, H. (1935) "Sand mixtures and sand movements in fluvial models". Trans. A.S.C.E. 100 798.

Lane, E.W. (1953) "Progress report on studies on the design of stable channels of the Bureau or Reclamation". Proc. A.S.C.E. 79.

Laufer, J. (1954) "The structure of fully developed pipe flow". NACA. Report 1174.

Le Feuvre, A.R., Altenbilck, H.D., Carstens, M.R. (1970) "Sediment - pick up function". Proc. A.S.C.E. 96. No.HY10.

Liu, H.K. (1957) "Mechanics of sediment ripple formation". Proc. A.S.C.E. 83 No. HY2.

Macrae, J.C. and Gray, W.A. (1961) "Significance of the properties of materials on the packing of real spherical particles". British Jo. Applied Physics. 12 164-172.

Manegold, E. and von Engelhardt, W. (1933) Kolloid Zeitschrift. 62 285, 63 12 and 149.

Marshall and Orr (1965) J.Mar.Biol. Ass. U.K. 44 285.

Mavis, F.J. and Laushy, L.M. (1948) "A re-appraisal of the beginning of bed movement-competent velocity". IAHR. 2nd Meeting. Stokholm.

Mercer, A.G. (1964) Disc. of Raudkivi, A.J. "Study of sediment-ripple formation". Proc. A.S.C.E. 90 HY4. p.289-292.

Mercer, A.G. (1971) "Analysis of alluvial bed forms" in River Mechanics Vol.1 Ed. Shen, H.W. Fort Collins, Colorado, U.S.A.

Miller, R.L. and Byrne, R.J. "The angle of repose for a single grain on a fixed rough bed". Sedimentology 6 303.

Nagy, V., Karadi, G. and Kalmar, G. (1959) "A study into the incipient stage of bed-load movement". Convegnio di Idraulica i Construzione Idrauliche A.18. Padova.

Nikuradse, J. (1933) "Laws of flow in rough pipes". Forschungshift 361 VDI Berlin.

Neill, C.R. (1967) "Mean-velocity criterion for scour of coarse uniform bed-material". Proc. 12th congress I.A.H.R. Fort Collins 3

Neill, C.R. (1968) "A re-examination of the beginning of movement for coarse granular bed materials". Internal Report No.68. Hydraulic Research Station, Wallingform, England.

Neill, C.R. and Yalin, M.S. (1969) Technical Note. Proc. A.S.C.E.No.HY1.

Offen, G.R. and Kline, S.J. (1974) "Combined dye-streak and hydrogen-bubble visual observations of a turbulent boundary layer". J.F.M. 62 pt. 2. 223-239.

Oseen, C.W. (1913) Ark. Mąt.Astrom. Fys. 9. Nr.16.

Pang, Y.H. (1939) "Abhangigkeit der Geshiebebewegung von der Kornform und der Temperatur". Mitteil. Preuss. Versuchsanst. Wasser, Erd. Schiffsbau. Berlin Heft.37.

Paintal, A.S. (1971) "Concept of critical shear stress in loose boundary open channels". Jo. Hyd. Res. 9 No.1.

Partheniades, E. (1965) "Erosion and deposition of cohesive soils." Proc. A.S.C.E. HY.1. 105.

Raichlen, F. and Kennedy,J.F. (1965) "The growth of sedimentary bed forms from an initially flattened bed". I.A.H.R. 11th Congress Leningrad.

Raudkivi, A.J. (1963) "Study of sediment ripple formation". Proc. A.S.C.E. 89 HY6 15-33.

Raudkivi, A.J. (1967) "Loose boundary hydraulics". Pergamon. Oxford.

Rees, A.J. (1961) "The effect of water currents on the magnetic remanence and ansitropy of susceptibility of some sediments." Geophys. Jo. 5 235-251.

Rees, A.J. (1966) "Some flume experiments with fine silt". Sedimentology. 6 209.

Richards, J.C. (1966) "The storage and recovery of particulate solids". Inst. Chem.Engrs. London.

Rottner, J. (1959) "A formula for bed-load transportation". La Houille Blanche. No.3.

Rouse, H. (1939) "An analysis of sediment transportation in the light of fluid turbulence". Soil Conservation Service Report No.SCS-TP-25. U.S.Dept. Agric.Washington D.C. July.

Rubey, W.W. (1938) The force required to move particles on a stream bed. U.S. Dept. Interior. Prof. papers. 189E.121

Rusnak, G.A. (1957) "The orientation of sand grains under conditions of unidirectional fluid flow". Jo.Geol. 65 384-409.

Runstadler, P.W. Kline, S.J. and Reynolds, W.C. (1963) "An investigation of the flow structure of the turbulent boundary layer". Report MD-8. Thermosciences division, Stanford University.

Saffman, P.G. (1965) "The lift on a small sphere in a slow shear flow". J.F.M. 22 Pt.2. 385.

Schoklitsch, A. (1914) "Uber Schleppkraft und Geschiebebewigung." Engelmann, Leipzig.

Schlichting, (1968) "Boundary Layer Theory". 5th ed. McGraw-Hill.

Schraub, F.A. and Kline, S.J. (1965) "A study of the structure of turbulent boundary layers with and without longitudinal pressure gradients". Report MD.12.Dept. of Mech.Eng. Stanford University.

Schumm, S.A. (1960) "The shape of alluvial channels in ralation to sediment type". U.S. Geol. Survey. PP. 351-8.

Schumm, S.A. (1968) "River adjustment to altered hydrologic regimen-Murrumbidgee River and palaeochannels, Australia, U.S. Geol.Survey. P.P. 598.

Segre, G. and Silberberg, A. (1961) "Radial particle displacements in Poiseuille flow of suspensions". Nature 189 209.

Shaw, D.J. (1970) "Introduction to colloid and surface chemistry" Butterworths, London.

Shields, A. (1936) "Anwendung der Aenlichkeitsmechanik und der Turbulentzforschung auf die Geshiebebeweging". Mitteil. der Preuss. Versusch. fur Wasserbau und Schiffbau. Berlin 1936.

Simons, D.B. and Richardson, F.V. (1971) "Flow in alluvial sand channels". in 'River Mechanics' Vol.1 Ed. by Shen, H.W. Fort Collins, Colorado.

Simons, D.B. (1971) "River and Canal morphology" in River Mechanics"1 Ed. by Shen, H.W. Fort Collins, Colorado, U.S.A.

Sorby, H.C. (1859) "On the structures produced by the currents present during the deposition of stratified rocks." Geologists 2 137-147.

St. Anthony Falls (1957) Report No.12. "Some fundamentals of Particle size Analysis". Published at St.Anthony Falls Hydraulics Lab. Minneapolis, Minnesota. December.

Stokes, W.L. (1947) "Primary lineation in fluvial sandstones a criterion of current direction". J.Geol. 55 52-54.

Straub, L.G. (1953) "Dredge-fill closure of Missouri river at Fort Randall". Proc. Minnesota Int. Hyd. Convention. IAHR/A.S.C.E.

Sundborg, A. (1956) "Astudy of fluvial processes". Geogr.Ann.Arg.37 132

Taylor, B.D. and Vanoni, V.A. (1972) "Temperature effects in low-transport flat-bed flows". Proc. A.S.C.E. 98 no.HY8.

Tison, L.J. (1949) Int.Ass. for Hydr. structures Res. 3rd Meeting. Grenoble, France.

Townsend, A.A. (1957) Symp.Int. Union of Theoretical and Applied Mechanics. Springer.

Tracy, H.J. and Lester, C.M. (1961) "Resistance coefficients and velocity distribution smooth rectangular channel". Geol. Survey Water-Supply Paper 1592-A.

Uno, S. and Kintner, R.C. (1956) J.Amer. Inst.Chem.Engineers. 2 420.

U.S.W.E.S. (1935) "Studies of river bed material and their movement with special reference to the lower Mississippi River". Paper No. 17. U.S. Waterways Experiment Station. Vicksburg, Mississippi.

Van Burkalow, A. (1945) "Angle of repose and angle of sliding friction: an experimental study". Bull.Geol.Soc. America. 56 669-708.

Vanoni, V.A. (1946) "Transport of suspended sediment by water". Trans. A.S.C.E. 111 67-102.

Vanoni, V.A. and Brooks, N.H. (1957) "Laboratory studies of the roughness and suspended load of alluvial streams". Pasadena. Calif.. Calif. Inst. Tech. Report E-68.

Vanoni, V.A. (1966) Sediment transportations mechanics: "Initiation of motion" (Progress report of Task Committee). Proc.A.S.C.E. 92 NO. HY2.

Velikanov, M.A. (1936) "Formation of sand ripples on the stream bottom". Commission de Potamologie. Sec. 3. Rapport 13. Int. Ass. of Scientific Hydrology.

Verwey, E.J.W. and Overbeck, J.T.G. (1948) "Theory of the stability of Lyophobic Colloids ". Elsevier.

Williams, P.B. and Kemp, P.H. (1971) "Initiation of ripples on flat sediment beds". Proc. A.S.C.E. 97 HY4.

White, C.M. (1940) "The equilibrium of grains on the bed of a stream". Proc. Roy. Soc. London 174A.

White, S.J. (1970) "Plane bed thresholds of fine sediments". Nature 228 152. Oct. 10th.

White, S.J. (1970) "The plane bed thresholds of movement of fine grained sediments under liquid flow". Unpublished Ph.D. thesis. University of Southampton, England.

Yalin, M.S. (1963) "An expression for bed-load transportation". Proc. A.S.C.E. 89 No.HY5.

Yalin, M.S. (1972) "Mechanics of sediment transport". Pergamon. Oxford.

Yang, C.J. (1973) "Incipient motion and sediment transport". Proc. A.S.C.E. 99 No.HY10.

NOMENCLATURE

The Nomenclature convention proposed by Bagnold (1954) of associating capital script with the mineral solid quantities and small script with the fluid quantities has been adopted herein as closely as possible.

A scale area ($>>D^2$) of a flat bed.

A_1 normalised bed area capable of being detached.

A_2 normalised applied stress area capable of detaching.

B_F bed form type.

C packing coefficient of a sedimentary bed = ratio of solid volume to total volume.

C_- packing coefficient of a coplanar surface grain layer of thickness D.

C_I initial volumetric concentration of sediment suspension.

C_S packing coefficient of a grain layer = ratio of integral solids volume to total volume.

D_{50} median solid diameter from a cumulative size distribution curve.

D_c critical diameter of a moving solid for which inertial forces are balanced by fluid drag forces.

D_G geometric flake face diameter = $(F_a F_i)^{1/2}$

D_F standard fall diameter = the diameter of a sphere of S.G. 2.65, which has the same terminal fall velocity in still water at $24^\circ C$, as the solid.

D_N nominal diameter of a solid = the diameter of a sphere that has the same volume as the solid.

D_V viscous standard fall diameter = the diameter of a sphere of S.G. 2.65, which has the same terminal fall velocity during viscous settling, as the solid.

F_1 centrifugal force on a solid moving in the rotor of an aerodynamic classifier.

F_2 Oseen corrected drag force on a steadily sedimenting solid.

F_a maximum flake face geometric diameter.

F_i minimum flake face geometric diameter.

Fr Froude number of flow = $\bar{u}_m/(g\bar{d})^{1/2}$

G weight of a single solid.

G_I rate of the dry weight of sediment introduction to the flume.

G_o dimensionless flat-bed sediment transport rate = $\dfrac{\bar{Q}_{so}}{gD(\bar{\tau}_o/\rho)^{1/2}}$

I intensity of deposition = mass of solids deposited at a sedimentary bed per unit time and bed area.

K^{-1} electrical double layer thickness.

L length scale representing the roughness of a flakey bed.

L_E equivalent grain critical roughness length.

P or P_{Au*} number of moving solids over a flat-bed area, A.

P_A number of solids detached from a flat-bed area, A.

P_{AT} number of solids detached from a flat-bed area, A, in time T.

$\bar{Q}_{so}$ flat-bed sediment transport rate = submerged weight of transported solids per unit bed-width and time.

R centripetal drag force on a solid moving in the rotor of an aerodynamic classifier.

$\bar{R}e$ Reynolds number for two dimensional flow = $\bar{u}_m\bar{d}/\nu$.

$\bar{R}e_m$ Reynolds number for open-channel flow = $\bar{u}_a m/\nu$.

$\bar{R}o$ boundary Reynolds number = $(\bar{\tau}_o/\rho)^{1/2} D\nu^{-1}$

So Trask geometric quartile sorting coefficient = $(D_{75}/D_{25})^{1/2}$

T thickness of a flakey solid.

$\bar{U}$ average longitudinal velocity of a transported solid.

V volume of a single solid.

V_D impact velocity of a sedimenting solid with the bed.

V_g terminal fall velocity of a solid in a still fluid.

V_R surface repelling interaction energy between two equal spheres immersed in an electrolyte.

W dry weight of solids introduced to the flume during bed laying.

a_o multiplicative factor applied to the standard deviation, σ_o

a_R multiplicative factor applied to the standard deviation, σ_R

c concentration of salts in an electrolyte.

$\bar{d}$ average flow depth.

e dielectric constant of a fluid medium.

f D'arcy Weisbach friction factor for open channel flows = $8gm\bar{i}/\bar{u}_a^2$

f_d D'arcy Weisbach friction factor for two-dimensional flows = $8g\bar{d}\bar{i}/\bar{u}_m^2$

g acceleration due to gravity = 981 cm/s^2.

$\bar{i}$ average water surface gradient.

l_o fluid lift pressure at a sedimentary bed.

l fluid lift force on a bed solid.

m hydraulic radius of an open channel flow = $w\bar{d}/(2\bar{d} + w)$

n number of sediment suspension transits along the flume channel.

o flume overall length = 13m.

r radius of the rotor of an aerodynamic classifier.

s fraction of remaining dry weight of sediment suspension after one channel transit.

$\overline{\delta t}$ average time taken for a solid detachment from a flat bed.

$\bar{u}$ average longitudinal flow velocity at a normal distance, y, above a bed.

$\bar{u}_a$ average longitudinal flow velocity across the transverse section of open channel flow.

$\bar{u}_b$ average longitudinal flow velocity near to the bed.

$\bar{u}_m$ average longitudinal flow velocity for two dimensional flow.

$\bar{u}_{mb}$ average longitudinal flow velocity, for two dimensional flow, during bed laying.

$\bar{u}$ average longitudinal water surface velocity.

u_θ, u_r tangential and radial velocity components of a solid moving in the rotor of an aerodynamic classifier.

u_* velocity scale for two dimensional flow = $(\bar{\tau}_o/\rho)^{1/2}$

w width of flume = 30cm.

y the co-ordinate normal to a bed.

y^+ dimensionless y co-ordinate = $y(\nu/u_*)^{-1}$.

z charge number of the salts in an electrolyte.

α angle of repose of a pile of solids.

α_F limiting coefficient of sliding friction between solids.

α_L angle of rolling detachment.

α_P angle of the plane of contact between two solids with the horizontal.

α_R limiting static angle of repose.

α_- static coefficient of resistance between a surface and adjacent grain layer.

β angle of a flat bed surface with the horizontal.

γ volumetric shape factor for a solid.

$\bar{\lambda}$ initial average linear separation between grains in a suspension, in D units.

λ_d dune wavelength.

λ_l transverse separation distance between a current primary lineation.

λ_r ripple wavelength

λ_s scale spacing of turbulent-smooth boundary layer streaks.

μ abbreviation for a micron = 10^{-6}m.

μ_a dynamic viscosity coefficient of air.

μ_w dynamic viscosity coefficient of water.

ν fluid kinematic viscosity coefficient.

ρ water density.

ρ_a air density.

ρ_s solid density.

ρ' submerged density of a solid in a fluid = $(\rho_s - \rho)$ for water.

σ_l standard deviation of applied fluid lift pressure distribution to bed.

σ_o standard deviation of applied fluid stress distribution to bed.

σ_R standard deviation of bed shear resistance distribution.

ϕ angle of rolling.

τ_o applied fluid shear stress tangential to a flat bed.

$\tilde{\tau}_o$ spatially averaged value of τ_o.

$\bar{\tau}_o$ time and spatially averaged value of τ_o.

τ_R solid resistive stress tangential to a flat bed.

τ_{ob} applied fluid shear stress tangential to a flat bed during bed laying.

$\bar{\theta}_o$ dimensionless applied fluid shear stress tangential to a flat bed = $\bar{\tau}_o / \rho' g D$.

$\tilde{\theta}_{oc}$ critical detachment dimensionless stress = spatially averaged value of θ_o for which $P_A D^2/A \longrightarrow 0$.

$\bar{\theta}_{oc}$ critical low transport dimensionless stress = time and spatially averaged values of θ_o for which $\bar{G}_o \longrightarrow 0$.

$\theta_{\bar{u}_c}$, $\theta_{\bar{u}_{mc}}$ critical drag coefficients for incipient motion = $\rho \bar{u}^2_c / \rho' g D$ $\quad \bar{u}^2_{mc} / g D$